Tissue resident macrophage STING signaling is a central safeguard against decline with age

A thesis submitted by

Katherine Sulka

in partial fulfillment of the requirements for the degree of

PhD

in

Immunology

Tufts University

Graduate School of Biomedical Sciences

April 16, 2025

Advisors: Shruti Sharma, PhD and Philip Haydon, PhD

ABSTRACT

Aging is a highly complex, progressive process that is influenced by a multitude of interdependent factors that, when compounded, results in the decline of the organism. At the forefront, unchecked inflammation is a hallmark of nearly all age-related diseases and neurodegenerative diseases, known as inflammaging. Chronic inflammation is increasingly described as a combination of DNA damage responses (DDRs), senescence, type-I interferon (IFN-I), and proinflammatory transcriptional signatures. Yet the identity of immune pathways responsible for these signatures and cell-types through which they modulate aging-associated inflammation remain hotly debated. However, the pathways regulating the same inflammatory processes that maintain homeostasis remain understudied. The cyclic GMP-AMP synthase (cGAS)-Stimulator of interferon genes (STING) pathway has garnered significant attention in age-associated inflammation and neuroinflammation, given its role in sensing damaged DNA and modulation of cellular senescence. Despite intense interest, research into the role of the STING-pathway has primarily focused on small molecule therapeutics, gain-of-function, and accelerated models of aging. Thus, the role of the STING-pathway in physiological aging processes remains understudied and critical to ascertain given the impact of multiple loss-of-function polymorphic alleles of *STING* widely expressed (≥40%) in the human population. In this dissertation, I hypothesize that tissue resident macrophages (TRMs) within their respective organ systems perform a protective and necessary function mediated through STING-signaling to prolong longevity and preserve tissue and overall health. Here, we used physiologically aged mice to uncover a vital role for STING in preserving longevity, tissue health, and brain function with age by protecting against widespread DNA damage. We found that STING-deficiency exacerbates neurological decline during aging through blood brain barrier breakdown, microhemorrhages, and neuromotor deficits. We revealed that STING-deficiency leads to an accrual of neuronal

DNA damage, which in turn correlates with exacerbated inflammation with age. Further, STING-signaling modulates the innate immune landscape in the CNS by altering proinflammatory transcriptional profiles, type I interferon (IFN-I) signaling and senescence in microglia, altering their phenotypic landscapes. Finally, microglial STING is both necessary and sufficient for protection against age-associated changes in the CNS. Importantly, these findings highlight a protective role of microglial STING-signaling within the aging brain (**Chapter 3.1**). Next, we characterized the role of IFN-I within the microglia population and transcriptional changes that are dependent on age and STING-signaling (**Chapter 3.2**). Lastly, we investigated highly vascular and interdependent organs vital for organismal heath: the heart, kidney, and liver. Together, these organs ensure that the blood is providing necessary nutrients, properly filtered, and clean of toxins to support overall health and prevent complex health issues commonly associated with age. In addition to CNS finding, we observed that STING-deficiency exacerbates systemic inflammation in the serum of physiologically aged mice. STING also appears to protect against tissue degeneration and dysregulation in old mice. Also, STING-deficient TRMs compared to bone marrow derived macrophages (BMDMs) are more susceptible to cell death and mice lacking STING in TRM populations have a shortened lifespan (**Chapter 3.3**). Together, these findings challenge the prevailing paradigm that TRM-STING signaling drives age-associated inflammation, instead revealing a protective role for long-term TRM STING signaling during aging.

DEDICATION

I would like to dedicate this work to my family and friends who have supported me during these years. I would not be the person I am without each one of you.

ACKNOWLEDGEMENTS

I am honored to acknowledge the people that helped me through this journey. You all helped me make this body of work possible and the words I use here cannot express the gratitude I feel. I wish to acknowledge the people that have supported my growth as a scientist and in becoming a good human during this long journey.

I would first like to thank my mentor, Dr. Shruti Sharma, for her role in shaping me into the scientist I am today. I would not be as resilient and strong without your mentorship. I thank you for your openness to investigating age-dependent mechanisms within the brain and for creating an environment that allows students to have ownership over their own projects. Secondly, I would like to thank my co-mentor Dr. Philip Haydon. You constantly reminded me to put one foot in front of the other during some of the hardest days of this process. Thank you for helping me check off even the most mundane tasks and holding me to a high standard. I am a more thoughtful scientist because of your combined mentorship. I appreciate your dedication towards my growth as a scientist and as a person.

I would also like to thank my committee members, who served on my committee these many years. I am honored to have learned from you during committee meetings and one-on-one conversations. Dr. Pilar Alcaide, thank you for serving as my committee chair and for pushing me towards success. Dr. Alexander Poltorak, thank you for your constant support and I will always appreciate the help you provided. Dr. Pedram Hamrah, thank for your guidance in shaping my projects and providing perspective that always pushed it towards a more complete story. Thank you all for your kindness and support during some particularly difficult times; and there were a few.

I am grateful to Dr. Allen Steere and Dr. Klemen Strle for nurturing my love for science and immunology. I truly would not be defending a PhD in Immunology without the

support from everyone in the Steere lab at MGH. I would also like to thank my professors at PC for their continued guidance and support Thank you, Pam and Vikki. There are many past and current Tufts' students I am honored to call a close friend, and I am forever grateful to know that we have forged these beautiful and supportive lifelong friendships. I hope everyone has the kind of luck that I had. Sasha, Zoie, Bennett, David, Abe, Mike, Kimberly, Machlan, James, Morgan, Allie, Hymlaire, and Urmila thank you for being there for me. Thank you for being my friends and always being available for a sad hug, a rant, a coffee, a happy hug, a sweet treat, a run, a high five, a chat, or just a hug. I am fortunate to still have the support my Hilltop and PC friends, Haley, Jess, Shannon*, Emily, Natalie, Lindsay, Bess, Irma, Sam, and Erin. Thank you for always being there and I love you all so much. I would be remiss not to thank all the other people who helped shape me every minute of every day at Tufts. I loved learning with you and became better because of you.

I would also like to acknowledge my most essential support system: my family. Thank you for all the dinners, rides to/from the train, drinks, business meetings, movies, drives, calls, facetimes, and just for simply showing up for me when I needed you most. Mom, Dad, Maggie, Steve, and Russell, you are the best family, and I am lucky to have your support during this journey. I am also lucky to have an incredible extended family. My Gramma, aunts, uncles, cousins fill my heart. Madelyn Grace and Suz, thank you for all the phone calls. Brandon, you have made this past year easier and filled with more love than I expected. Thank you for your endless support.

I am excited to see what is next. Thank you all again for your support.

*Thank you, Shannon and Jillian, for reading and providing feedback.

BIG HUGS!

TABLE OF CONTENTS

LIST OF TABLES

LIST OF FIGURES

LIST OF COPYRIGHTED MATERIAL USED

Adapted with permission from:

Sulka KB, Carroll KA, Sawden M, Hopkins JW, Smolgovsky SA, Bayer AL, Reed E, Tai A, Alcaide PA, Haydon P, Sharma S. Microglial STING is a central safeguard against neurological decline with age. (*Accepted*, *Cell Reports*).

From Cell reports Website to be used upon final submission of the paper: *Microglial STING is a central safeguard against neurological decline with age.*

Creative Commons Attribution License 4.0 International License (CC BY 4.0). This license allows users to alter and build upon the article and then distribute the resulting work, even commercially, and thus encourages maximum use and redistribution.

LIST OF ABBREVIATIONS

Abbreviation	word/s
AD	Alzheimer's disease
AGS	Aicardi-Goutières syndrome
AIM2	absent in melanoma-2
AKI	acute kidney injury
ALE	systemic lupus erythematosus
ALR	absent in melanoma-2 (AIM2)-like receptors
ALS	amyotrophic lateral sclerosis
BBB	blood-brain barrier
BCR	B-cell receptor
Ca^{2+}	calcium
CCL	C-C motif ligand
CD	cluster of differentiation
cGAMP	2’3’ cyclic GMP-AMP
cGAS	cyclic-GMP-AMP (cGAMP) synthase
CKD	chronic kidney disease
CLDN1	claudin 1
CLR	C-type lectin receptors
CNS	central nervous system
COPII	coatomer protein complex II
CPEpiC	choroid plexus epithelial cells
CXCL	chemokine (C-X-C motif)
DAI	DNA-dependent activator of IFN-regulatory factors
DAMPs	damage-associated molecular pattern
DC	dendritic cells
DDR	DNA damage response
DKD	diabetic kidney disease
ds	double stranded
DSBs	Double-stranded DNA breaks
E	embryonic day
EF	ejection fraction
EJ	ejection fraction
EndoC	endothelial cells
Eng	Endoglin
ER	endoplasmic reticulum
ERGIC	ER-Golgi intermediate compartment
G-CSF	granulocyte colony-stimulating factor
GFR	glomerular filtration rate
GM-CSF	granulocyte-macrophage colony-stimulating factor
GO	gene ontology
GPCR	G-protein coupled receptors

Hb-EndoC	hemoglobin-associated endothelial cells
HCC	hepatocellular carcinoma
HF	heart failure
HFpEF	heart failure with preserved ejection fraction
HSC	hematopoietic stem cell
IFN	interferons
IFN-I	type I interferon
IFN-II	type II inteferon
IFN-III	type III interferon
IFNAR	IFN-α receptor
IFNα	interferon alpha
IFNβ	interferon beta
IFNγ	interferon gamma
IFNγR	IFNγ receptor
IFNλ	intereferon lambda
IL	interleukin
IRF	interferon regulatory factors
IRM	interferon responsive microglia
ISGF3	interferon stimulated gene factor 3
ISGs	interferon responsive genes
IκB	NF-κB inhibitor alpha
JAK1	tyrosine kinases Janus 1
LBD	ligand-binding domain
LOF	loss of function
LPS	lipopolysaccharide
LS	lifespan
LV	left ventricular
M-CSF	macrophage colony-stimulating factor
MAPK	mitogen-activated protein kinase
MAVS	mitochondrial antiviral sensing protein
MG	microglia
MHC	major histocompatibility complex
MMP	matrix metalloprotease
MoMac	monocyte-derived macrophages
MS	multiple sclerosis
mtDNA	mitochondrial DNA
NAFLD	non-alcoholic fatty liver disease
NASH	nonalcoholic steatohepatitis
NF-κB	nuclear factor kappa-light-chain-enhancer of activated B cells
NHEJ	non-homologous end joining
NK	natural killer
NLR	nucleotide oligomerization domain (NOD)-like receptor
NOD	nucleotide oligomerization domain

NOD1	NOD-containing protein 1
NOD2	NOD-containing protein 2
OA	osteoarthritis
PAMPs	pathogen-associated molecular pattern
PD	Parkinson’s disease
PEC	parietal epithelial cell
PPR	Pattern recognition receptor
RIG-I	retinoic acid-inducible gene-I
RLR	retinoic acid-inducible gene-I (RIG-I)-like receptors
SA-β-Gal	senescence-associated β-galactosidase
SASP	senescence-associated secretory phenotype
SASP	senescence-associated secretory phenotypes
SNPs	single nucleotide polymorphisms
SOCS	suppressor of cytokine signaling (
ss	single stranded
STAT1	signaling transducer and activator of transcription 1
STING-/-	STING knock-out
TBI	traumatic brain injury
TBK1	TANK binding kinase 1
TCR	T-cell receptor
Tgfb1	Transforming growth factor beta 1
TLR	Toll-like receptors
TLTs	tertiary lymphoid tissues
TNFα	tumor necrosis factor alpha
TRM	tissue-resident macrophage
TYK2	tyrosine kinase 2
USP18	ubiquitin carboxy-terminal hydrolase 18 (
VDJ	diversity, joining, recombination
WT	wild type / C57BL/6
ZBP1	Z-DNA binding protein 1
γH2A.X	phosphorylatedH2A.X

CHAPTER 1: **INTRODUCTION**

1.1. THE IMMUNE SYSTEM

The immune system was originally described as the body's way of protecting the host against infections, injury, and disease. Our understanding has expanded to include the importance of the immune system in development, homeostasis, sterile inflammation, diseases, and infections[1]. The immune system is comprised of the innate immune system and the adaptative immune system. The two arms work together to either effectively rid the body of infections or mount a specific response that directly attacks the current infection or damaged site. The innate immune system is defined by three features: (1) a fast response time that is (2) non-specific responses, and cells express (3) germline encoded receptors primed for activation. The adaptive immune system is defined by a learned responsiveness to highly specific pathogens, allergens, or damage. The innate immune system is required for activation of the adaptive immune system and the combined responses result in a resolution of the infection or injury and decrease of innate and adaptive immune responses (**Figure 1.1.1**).

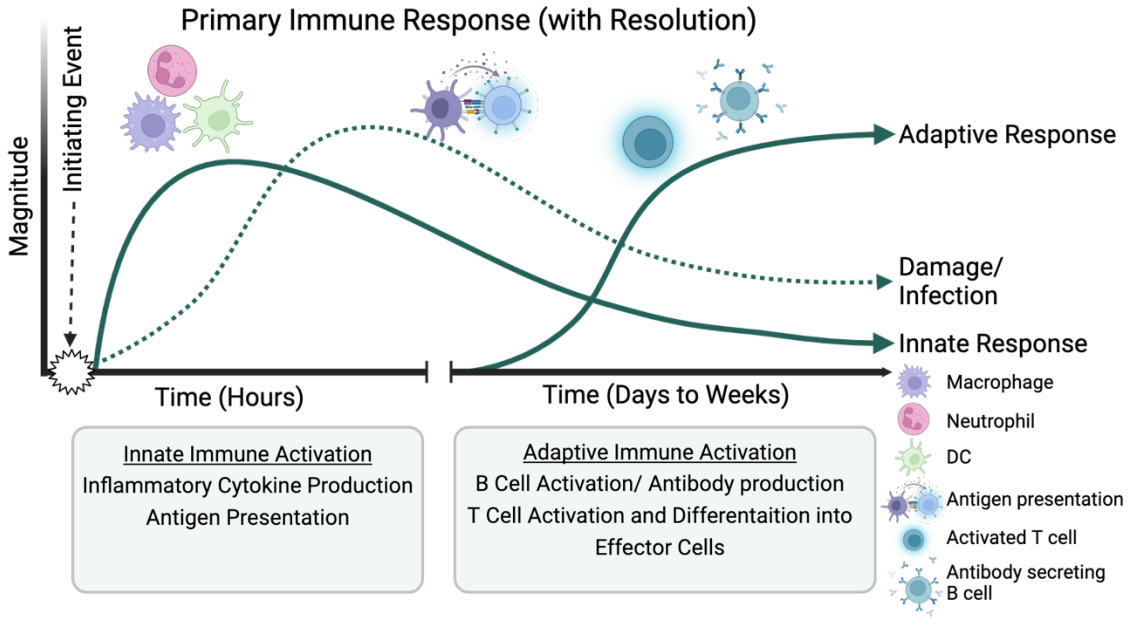

Figure 1.1.1. Innate and adaptive immune magnitude response to damage or infection and time to resolution.

Upon infection or injury (initiating event), the innate immune response is rapidly infection by release of pathogen-associated molecular pattern (PAMPS) or damage-associated molecular pattern (DAMPs). This process occurs within minutes to hours and releases a large number of cytokines to begin suppressing the infection/damage by innate immune cells (macrophages, neutrophils, dendritic cells (DCs). After initial activation, innate immune cell numbers decrease continually through resolution. Within days, the adaptive immune responses are activated through antigen presentation. During this time T cells are activated and differentiated for specific purposes and B cells are activated and begin secreting antibodies specific to the pathogen. During this time (days-weeks) the organism resolves the infection or injury through killing and/or debris removal. At the same time, adaptive immune cells reduce in numbers. *(Created with Biorender.com).*

Both arms of immune systems are found systemically, or within the circulation, in lymphoid organs, such as the bone marrow, or within the tissues. Circulating immune cells are critical for surveillance by traveling in the bloodstream throughout the body to provide protection from foreign pathogens[2,3].

While studying the blood has been readily available, the study of the immune system within tissues is a relatively new area of research[4-6]. Studying the immune system within tissue has been made accessible due to medical advances that require removal of organs or biopsies, however, in humans, these are commonly associated with disease states [4,5]. Both arms of the immune system have been shown to play critical roles within tissues and moreover, these cells are programmed for specific functions within tissues to support the organ's health and promote homeostasis.

1.1.1. **Innate Immune System**

The innate immune system is the host's first line of defense against foreign substances, pathogens, and injuries. It responds to all molecular patterns or antigens using the same basic mechanisms and is therefore referred to as non-specific immunity. The host utilizes innate immunity at two levels: first, the skin, mucosal tissues, blood-brain barrier, and chemical barriers are used as evasion tactics; second, the host uses surveillance of innate immune cells to mount curated responses[3,7,8]. Innate immune cells consist of mast cells, neutrophils, basophils, eosinophils, dendritic cells (DCs), macrophages, and

natural killer (NK) cells (**Figure 1.1.2**). These cells express pattern recognition receptors (PRRs), which aid in the recognition of common pathogen-associated molecular patterns (PAMPs) or damage-associated molecular patterns (DAMPs).

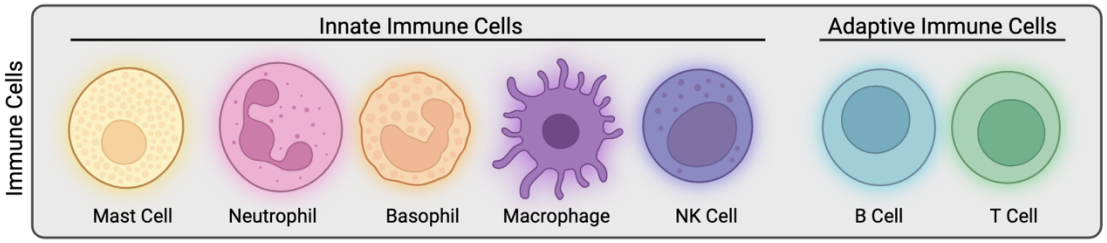

Figure 1.1.2. Basic immune cells of the immune system.
Immune cells are broken up into innate immune cells and adaptative immune cells. Innate immune cells are primarily made up of mast cells, neutrophils, basophils, macrophages, and NK cells. Adaptive immune cells are made up of B and T cells. These are the broad characterizations of immune cells. most cell populations have differential states or differentiate into subsets of the primary cell type. The functions are related within the cell populations. *(Created with Biorender.com).*

Work done in Drosophila identified Toll-like Receptors (TLRs) as PRRs[9,10]. Lemaitre et al. in 1996 mutated *Toll* and showed that Drosophila were not protected against fungal infections because they lacked the necessary activation of an inflammatory cascade through TLR signaling[11]. PRRs are found on the extracellular membrane, in intracellular compartments, such as the endosome, or within the cytosol. PRRs are currently divided into six categories: TLRs, nucleotide oligomerization domain (NOD)-like receptor (NLRs), retinoic acid-inducible gene-I (RIG-I)-like receptors (RLRs), C-type lectin receptors (CLRs), absent in melanoma-2 (AIM2)-like receptors (ALRs) and intracellular DNA sensors (e.g. cyclic-GMP-AMP (cGAMP) synthase (cGAS) and Stimulator of interferon

genes (STING))[8,12] (**Figure 1.1.3**).

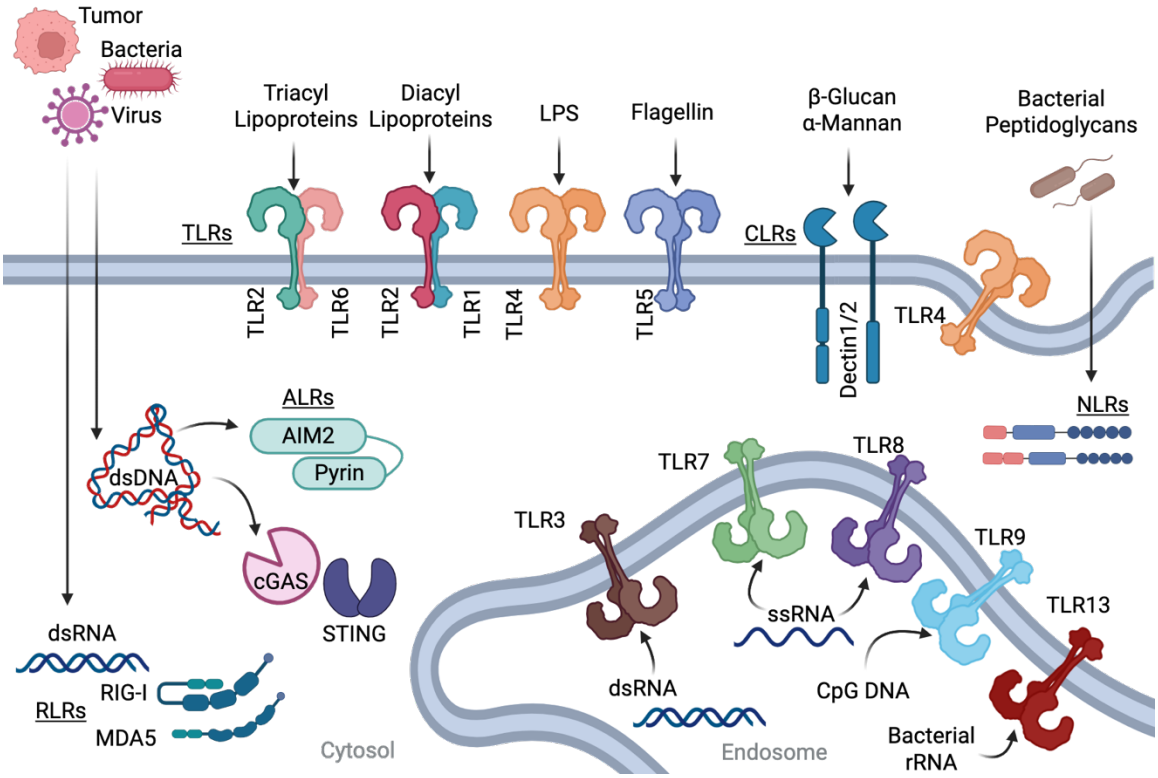

Figure 1.1.3. Pattern Recognition Receptors on cells.
Pattern recognition receptors (PRRs) are found on most cells in the body but are primarily expressed on innate immune cells. Toll-like receptors (TLR) are found on the cell membrane or endosomal membrane, whereas alternative PRRs, such as NOD-like receptors (NLRs), RIG-I-like receptor (RLRs), AIM2-like receptors (ALRs), and the DNA sensors cGAS and STING are found within the cytosol. C-type lectin receptors (CLRs) are similar found on the cell membrane with TLR2, TLR6, TLR1, TLR4, TLR5. The heterodimer TLR1/2 senses pathogenic components: diacyl lipoproteins. The heterodimer TLR2/6 senses pathogenic components: triacyl lipoproteins. The homodimer TLR4 recognized the pathogenic component: lipopolysaccharide (LPS). The homodimer TLR5 recognized flagellin. Endosomal TLRs recognize nucleic acids from host or pathogen. Specifically, TLR3 senses double stranded (ds)RNA, TLR7 and TLR8 sense single stranded (ss)RNA, TLR9 senses CpG DNA, and TLR13, which is only found in mice, recognizes bacterial ribosomal RNA (rRNA). Not pictured is the recently described TLR10, which is only found in humans and the ligand is unknown. RLRs recognize dsRNA in short (RIG-I) or long (MDA5) form from host or pathogens. Similarly, cGAS/STING and ALRs recognizes the dsDNA from host or pathogens. CLRs recognize β-Glucans (Dectin1) and α-Mannan (Dectin2). NLRs recognize pathogen (bacterial peptidoglycans) as well as regulate specific PRRs. *(Created with Biorender.com).*

Human cloning and discovery of TLR4[9] activation in 1997 proved innate immunity was necessary step for recognition of PAMPs, such as lipopolysaccharide (LPS)[13], and the

subsequent activation of downstream mediators promoted inflammation. Therefore, PAMPs are associated with microbial patterns, whereas DAMPs are associated with tissue damage or injury. Both DAMPs and PAMPs drive inflammation that either aides in the resolution of the infection or clearance of the damage, or it orchestrates activation of the adaptive immune response.

TLRs are signaling receptors that activate the immune response by secreting cytokines and antiviral factors downstream of activation[2,8]. Each TLR recognizes unique molecular patterns that are specific to the microbe or host cell. TLRs on the extracellular membrane detect microbial components, such as TLR4 (LPS), TLR5 (flagellin), TLR 1, 2, and 6 (bacterial lipoproteins), TLR 11 and 12 (*Taxoplasma gondii*). TLRs found within the endosome detect nucleic acids, such as TLR3 (double-stranded (ds)DNA), TLRs 7 and 8 (single-stranded(ss)RNA)), TLR9 (unmethylated CpG containing ssDNA), and TLR13 (bacterial ribosomal RNA). As previously mentioned, there are other PRRs found intracellularly, such as RLRs which consist of RIG-I (short chain dsRNA), MDA5 (long-chain dsRNA), and LPG2 (dsRNA). CLRs are made up of Dectin-1 and -2, which recognizes β-Glucan and α-Mannan, respectively. Lastly, both ALRs and cGAS recognize dsDNA, though activation of these receptors triggers different downstream immune response. STING recognizes cGAMP downstream of cGAS, but as also been shown to be alternatively activated[14]. Currently, some TLRs have no known ligand, such as human TLR10, though it has been shown to possibly provide inflammatory and anti-inflammatory effects[15].

PRRs are activated by a specific ligand prior to signal transduction. There are four common innate immune mechanisms of transduction that follow ligand recognition: nuclear factor kappa-light-chain-enhancer of activated B cells (NF-κB) signaling, TANK binding kinase 1 (TBK1)- interferon regulatory factor (IRF)-3 signaling, mitogen-activated protein kinase (MAPK) signaling, and inflammasome activation. The transcription factor,

NF-κB, is composed of a heterodimer of two molecules, p50 and p65, and is inactive when bound to NF-κB inhibitor (IκB). Upon phosphorylation, IκB degrades through ubiquitination, which in turn releases NF-κB for translocation into the nucleus for transcription of proinflammatory cytokines, such as TNF-α and IL-6. Antiviral immunity is an important response during innate immune activation and is primarily driven through activation of the transcription factor IRF3. Upon phosphorylation and dimerization of IRF3, the complex enters the nucleus for transcription of interferons (IFNs) and interferon responsive genes (ISGs). A common intersection of signaling transduction pathways are MAPKs as they are capable of transmitting signals from the cell surface to the nucleus. Extracellular signal-regulated kinase (ERK), c-Jun N-terminal kinase (JNK), and p38 make up the three major groups of MAPKs which drive proinflammatory cytokines and other genes to support cell function. ERKs modulate cell proliferation and control the cell cycle by driving the phosphorylation of the Activator Protein-1 (AP1) by stabilizing and supporting the complex formation of c-Jun and c-Fos prior to transcription[16]. Lastly, the inflammasome is assembled in the cytoplasm by PRRs such as NLRs and ALRS in the cytoplasm following ligand recognition, which recruits and activates Caspase-1. Once activated, Caspase-1 cleaves pro-IL-1β and pro-IL18 into their active forms, IL-1β and IL-18, which are important proinflammatory cytokines that are secreted from the cell.

The cytokines produced during the innate immune response primarily function to contain and control treat to the host, but they also act as initiators for the adaptive immune system, which is the second line of defense if the innate immune system is unable to control the infection or threat. In addition to cytokines, innate immune cells express co-stimulatory factors, such as CD80 and CD86. In addition to co-stimulatory factors, professional antigen presenting cells (APCs) present major histocompatibility complex

(MHC)-I or MHC-II molecules with antigen to adaptative immune cells. This occurs after acidification of antigen peptides within the endosome are loaded into the MHC complex.

1.1.2. **Adaptive immune system**

The adaptive immune system is the second line of defense. It is induced by the innate immune system and produces cytokines to drive migration, differentiation, and proliferation of B and T cells. These cells provide curated responses specific to self- or non-self-antigens presented by innate immune cells. Naïve B and T cells are created within the bone marrow as common lymphoid progenitors during a process called hematopoiesis. Both cell types mature and develop a primary immune response, which can take weeks to establish and strengthen. During a secondary exposure, also known as a secondary immune response, to a previously encountered antigen, activation and immune responses occur much more efficiently.

B cell commitment is controlled by transcription factors and maturation occurs within the bone marrow. The cells develop antigen specificity in the bone marrow through an antigen-independent process, given a successful combination of heavy chain and light chain heterodimer formation I successful and results in a functional pre-B cells receptor (BCR) on the cells. At this point, the cells are IgM^+ and ready to leave bone marrow and are capable of secreting IgM. The second phase of development occurs when the B cells interact with antigen and are activated. After this, the B cells either become memory cells or short-lived plasma cells and produce large amounts of antibodies. During a process called variable (V), diversity (D), joining (J) recombination, VDJ segments are randomly sliced together and dictate the binding specificity of the receptor. Memory B cells undergo class switching, also known as somatic hypermutation, from IgM^+IgD^+ cells to IgG^+, IgA^+, or IgE^+ cells through the VDJ region of BCR. Class switching is partially dependent on cytokine availability and supports development of

higher affinity antibodies. Antibody production is time-dependent, and antibody specificity increases during class switching towards high affinity antibodies, such as IgG, IgA, and IgE.

Lymphoid progenitor cells seeded in the thymus undergo rapid expansion and are committed to T cell lineage due to environmental signals and transcription factors that induce genes critical for the development of the T-cell receptor (TCR) assembly. TCRs are defining features of T cells and determine their identity. Like B cells, T cells undergo VDJ recombination to increase receptor specificity. After two productive and sequential TCR rearrangements, the cell expresses two TCR chains and a CD3 complex. These double positive T cells undergo positive and negative selection processes involving APCs. Positive selection occurs with low avidity binding to self-MHC to ensure the double positive T cells recognizes self-MHC. In contrast, negative selection occurs when double positive T cells experience a high avidity binding to self-MHC, thus curating a selective but non-self-reactive subset of T cells. As a result, only T cells with appropriate affinity for self-MHC remain, while those with too strong or weak binding are removed. Single positive, CD4+ or CD8+ T cells are selected within the thymus, specifically the thymic epithelial, and after they have established their phenotype, single-positive cells are prepared for circulation as antigen-naïve T cells. These cells interact with the peptides complexed within the MHC molecules on APCs and become activated by TCR signaling. $CD8^+$ T cells engage with MHC-I expressing cells, such as on NK cells, and $CD4^+$ cells engage with MHC-II expressing cells, such as DCs or other cells that present antigen peptides.

T cells finish developing and mature in the thymus during negative and positive selection events. Adaptive immune cells are activated in lymphoid tissues, such of lymph nodes or the spleen, via MHC-I, found on all nucleated cells, or MHC-II, found on APCs, to drive immune effector pathways and establish immunological memory to the antigen

presented. Immune memory allows for the host to quickly recognize the antigen and mount a faster and more effective immune adaptive immune response. The adaptive immune system develops over time alongside the organism, building a diverse repertoire based on previous exposures encountered throughout the lifespan.

1.1.3. **Hematopoiesis**

The immune system is primarily supported by immune organs, such as the bone marrow, spleen, lymph nodes, and thymus. The immune system protects the organism against pathogens after birth, when the major structures of the immune system are in place. However, the initial formation of the immune system starts during embryogenesis after the generation of the three germ layers, ectoderm, endoderm, and mesoderm. There are timed waves of hematopoietic stem cell dissemination (HSCs) and hematopoietic progenitors which are produced during embryogenesis to support the growth of the fetus[17-20]. During the first wave of hematopoiesis occurs in the mesoderm of the yolk sac where granulomacrophage progenitors are produced, termed primitive hematopoiesis (**Figure 1.1.4**). During the second wave of hematopoietic development, cells migrate to the fetal liver where HSCs are fully developed and expand, called definitive hematopoiesis. The final wave sends the HSCs to colonizes the bone marrow and the spleen, which provide immune cells to the organism that are continuously replenished throughout life[21,22].

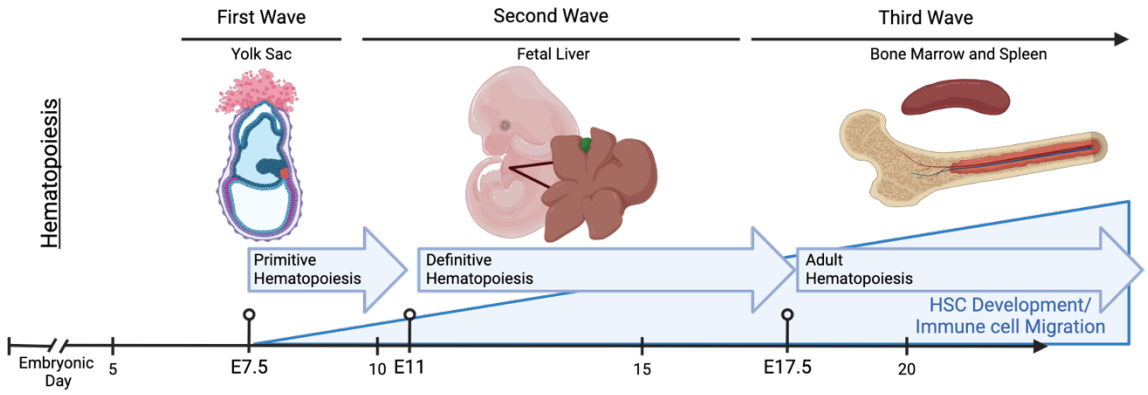

Figure 1.1.4. Hematopoiesis timeline during embryogenesis.
The first wave of hematopoiesis begins during yolk sac development and the mesoderm produces granulomacrophages; primitive hematopoiesis and migrate to sites of organ development. This occurs between embryonic day (E)7.5-9.5. During the second wave cells migrate to the fetal liver and hematopoietic stem cells (HSC) develop and expand. They migrate to tissues. This second wave occurs between E11-17.5. HSCs colonize the bone marrow niche and spleen to develop immune cells throughout the lifespan of the organism beginning at E17.5. *(Created with Biorender.com)*.

1.1.4. **Tissue-Resident Macrophages**

During this critical developmental period, progenitor cells seed individual tissues during to establish a tissue-resident macrophage (TRM) niche that supports tissue development. TRMs are seeded during the first wave of hematopoiesis and monocytes and monocyte-derived macrophages (MoMacs) are differentiated during the third wave of hematopoiesis. The TRMs are specific to the tissue and have unique transcriptional landscapes that are shaped by the tissue microenvironment[23]. TRMs are long-lived and have proliferative self-renewing capabilities[24], while MoMacs are short-lived and are replenished by the bone marrow progenitors that differentiate into macrophages[25]. TRMs orchestrate and tune homeostatic, inflammation, and repair processes, therefore, they are highly plastic, and their identity is shaped by their local microenvironment.

TRM development is critical for the tissue niche and the precise tissue function. For vital organs, such as the heart, kidney, and liver, which all play a critical role in maintaining an operational system and are highly dependent on each other, TRM populations are

especially necessary for supporting homeostatic functions within these tissues (**Figure 1.1.5**).

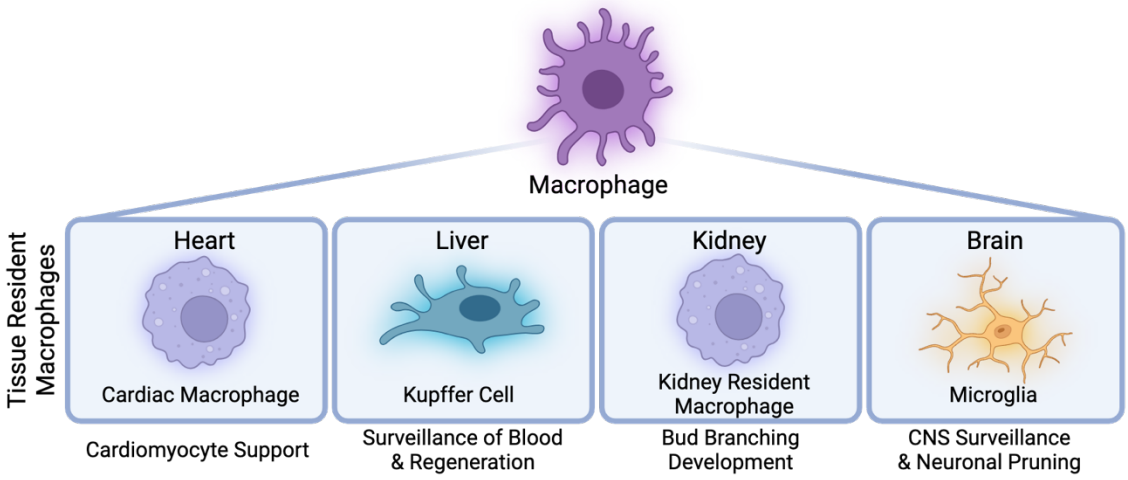

Figure 1.1.5. Tissue resident macrophage populations within each organ. Tissue resident macrophages are unique to each tissue and provide specific functions to support development and maintenance of the organ. Cardiac macrophages reside in the heart and provide cardiomyocyte support during stress or injury in order to return to homeostasis. Kupffer cells reside in the liver and are positioned to survey the blood to microorganisms and support in regenerative properties of the liver. Resident kidney macrophages reside in the kidney and have been shown to support bud branching development during kidney development. Microglia reside in the brain and survey the CNS for injury and perform neuronal pruning and engulfment to support a functioning neuronal network. *(Created with Biorender.com).*

The heart pumps the blood to the remaining organs, the liver filters the blood and senses for pathogens, while the kidney excretes the toxins found from in the blood. Typically, failure of one of these organs leads to the inevitable decline of the others and systemic degeneration[26-29]. The central nervous system (CNS) is made up of the brain and spinal cord which is used for managing information sensing and processing from the peripheral nervous system and autonomic nervous system. The autonomic nervous system regulates homeostasis by operating and regulating organ systems without having to think about the function. Without the CNS, the body is not able to function.

TRMs are seeded around E9.5, and therefore, position them as a necessary cell population that supports the function of the tissue[24]. Each of the organs above have a

transcriptionally unique TRM population (Figure 1.1.5). Within the heart, cardiac macrophages are mostly derived from the fetal yolk sac and fetal liver and characterized by their lack of CCR2 expression. These cells also support cardiomyocyte function during stress and injury[30]. However, precise mechanisms that dictate function are still not well understood. There are fewer studies on kidney resident macrophages, however they are yolk sac and fetal liver derived and seed during embryogenesis in small numbers[31] and expand to multiple resident populations[32]. Studies support that resident kidney macrophages uphold a similar homeostatic function and further highlight their importance in stimulating bud branching during development[33], during a time when they are plentiful. Kupffer cells, the liver resident macrophage population, support liver function by screening the blood flowing for toxins. During a resting state, they are located near portal veins during in healthy individuals[34], supportive of their known surveillance function. They are also critical for liver regeneration and resuming health after injury and metabolism. Changes to the Kupffer cell niche results in multiple liver diseases[34]. Microglia, the tissue resident populations, settle the brain and survey, prune processes within the brain that support neural networks, and support injury repair[35,36]. Microglia play a role in all stages of development, age, and neurodegeneration[36-38]. With such specialized functions and niche-dependent transcriptional signatures, TRMs are likely organized specifically within the tissue. In tissues, TRMs can eventually be replaced by MoMacs that adopt certain transcriptional profiles similar to TRMs, but are never fully functionally/ transcriptionally like TRMs[23]. These infiltrating cells are linked through a potentially conserved transcription specific the heart, kidney, and liver. MoMacs that express CCR2 share the ability to induce fibrosis at the site of injury in the heart, liver, kidney[39,40]. Thus, linking these organs and requiring a more in-depth understanding into how MoMacs and TRMs are organized within the tissue, and which pathways regulate specific functions through transcriptional programing.

1.2. HALLMARKS OF AGING AND INFLAMMATION

Aging is a complex process defined as the progressive functional decline of tissues and increased risk of chronic diseases. Aging itself is not a disease, but rather a compilation of alterations to normal functions that result in decline of the organism. Aging, and age-associated diseases are well studied, however, there are many aspects that are unclear. For example, the primary initiators, underlaying mechanisms, consequences, and cellular changes during aging remain open questions in the field[41]. Although many disease states are well studied and have targeted interventions, the initiating factors of aging and strategies to mitigate against the negative effects of healthy aging remain unclear. On a similar note, the homeostatic mechanisms that protect against organismal decline are still poorly understood.

1.2.1. Twelve Hallmarks of Aging

Aging is a complex process. The current processes that lead to degeneration of the organism have expanded to twelve hallmarks of aging[27,42]. The hallmarks of aging consist of: (1) genomic instability, (2) telomere attrition, (3) epigenetic alterations, (4) loss of proteostasis, (5) disabled macroautophagy, (6) deregulated nutrient sensing, (7) mitochondrial dysfunction, (8) cellular senescence, (9) stem cell exhaustion, (10) altered intercellular communication, (11) chronic inflammation, and (12) dysbiosis[27]. The hallmarks of aging are interconnected and progressive, and hyper-dependent on each other. Hallmarks of aging must be considered individually and as a whole to determine the full impact of the aging process and implications for anti-aging treatments. Aging research is largely focused on the negative consequences of common pathways, but research addressing necessary inflammatory components that support healthy aging is lacking.

1.2.2. **Hallmark of Aging: Genomic instability and DNA damage**

Genomic instability arises from DNA damage and is a central hallmark of aging as it is found in all age-associated phenotypes and diseases[43]. Functional DNA repair mechanisms are necessary for health and function of the organism and are known to decline with age. Further, there are complex repair and maintenance mechanisms that protect chromosomal architecture failures and telomere shortening. DNA damage can also occur from endogenous and exogeneous stimuli, which induces senescence and DNA damage response (DDR) pathways, ultimately driving the age-associated pathology noted in failing organs and disease states. Double-stranded breaks (DSBs) in DNA is marked by the phosphorylated histone H2A.X (γH2A.X), and the detection of damaged DNA ends is highly specific to DNA damage initiation and resolution[44]. γH2A.X is used as a recruitment tool for DDR proteins, and subsequent loss of γH2A.X suggest repaired DNA breaks[45]. Other markers, such as 53PB1, are used along with γH2A.X to mark sites of DDR pathways. DSBs are essential steps in multiple cellular process, such as VDJ recombination, but as unprogrammed processes, they severely compromise genomic stability as the original genetic is lost and accurate chromosomal DNA is not passed along[46]. Downstream effects also include transcription blocking, alterations in proteostatic pathways, mitochondrial dysfunction, and cell fate decisions[43].

As mentioned above, age is associated with impaired repair mechanisms, which results in the accumulation of genomic DNA and mitochondrial DNA (mtDNA)[27,42]. The role for mtDNA in aging is very complex. For instance, it is proposed that mutations in mtDNA, rather than intact mtDNA, increases in the cytosol with age and that aged cell accumulate mutated mtDNA. More recently, lesser-known hypotheses suggest that damaged nuclear DNA is a trigger for subsequent mtDNA mutations, deletions and thus accumulation of the altered mtDNA that may activate DDR pathways[47]. Finally, feedback

mechanisms between mitochondrial stability and genomic stress are well established and recent studies further elucidate these feedback loops[48,49].

1.2.3. **Hallmark of Aging: Senescence**

Cellular senescence is when a cell enters an irreversible cell cycle arrest state that leaves the cell still viable, though the exact function of senescent cells remains unknown. Senescent cells are found in a variety of settings, such as aging tissues, disease states, cancer settings, or required physiological functions, such as wound healing and embryonic development. Thus, seemingly contradictory effects of senescence, as deleterious or beneficial effects, are dependent on the context. Senescence occurs in response to stress, such as persistent DNA damage, telomere shortening, and oncogene activation. It also occurs as a controlled program during biological processes like cancer, wound healing, and embryonic development. Several types of senescence have been described during the lifespan of an organism. When a cell enters an irreversible state of cell cycle arrest it is referred to as replicative senescence[50]. A second type of senescence is known as oncogenn-induced senescence, which triggers senescence after oncogene activation or loss of tumor suppression/ proliferative arrest and supports the development of cancers. The last type of senescence is associated with telomere attrition and stress, which triggers the DDR as the ends begin to resemble DSBs[51]. All these pathways ultimately engage the DDR pathway and are known to be associated with negative consequences. However, senescence is a stress response and performs necessary and beneficial functions. Cellular senescence occurs during embryonic development and wound healing; these functions support homeostasis and normal tissue development and function. It has been shown that during early stages of acute kidney injury, cellular senescence is protective

and necessary for resolution, but if there is no resolution and DDR pathways are prolonged, there are pathological effects[52,53].

Markers of senescence were identified to detect cells within tissues and are extensively used in cancer and aging reach. Increases of cell cycle-inhibitory proteins are used to identify cells that have entered cell cycle arrest. These proteins, known as cyclin-dependent kinase inhibitors, consist of p16 (*Cdkn2a*) and p21 (*Cdkn1a*) and are critical for maintaining a state of arrest at different timepoints of senescence[54]. These genes are upregulated as a cell enters senescence (p16) and then as the senescent state is maintained (p21)[55]. Senescent cells also increase in size, granularity, changes to nuclear proteins (e.g. reduced lamin B1, increased telomere shortening, and transcript changes), increase senescence-associated-β-galactosidase (SA-β-Gal), and have an increase of lipofuscin found within the lysosome[54]. SA-β-Gal is a canonical marker of senescent cells and is widely used to label senescent cells. However, within the aging brain, lipofuscin-like particle (LLPs) have been used to label senescence cells within the white matter[56].

These cells produce a plethora of proinflammatory cytokines and other factors, collectively known as senescence-associated secretory phenotype (SASP). The inflammatory gene expression and production of proinflammatory cytokines of senescent cells leads them to change the microenvironment of their immediate surroundings and the tissue at large, impacting overall function and homeostasis. This change may lead to degenerative states of the tissue[57,58]. Though SASP is associated with proinflammatory cytokines, it is also associated with the chemokines that recruit immune cells to tissues to deal with the senescent and damaged cells. Senescence is a critical checkpoint mechanism for proliferating cells to ensure that cells with dysfunctional telomeres, due to repeated DNA replication that causes telomere shortening, are withdrawn from the cell cycle. Cells that avoid senescence drive malignant transformations[59], and therefore

senescence acts as a beneficial anti-cancer mechanism[58]. These mechanisms were shown to be necessary within functional and renewable tissues, but as tissues aged, their capacity to renew decreases and senescent cells are found and accumulate within aged tissues and age-associated diseases, such as atherosclerosis and osteoarthritis[60]. Therefore, the outcomes associated with senescent cells are tightly linked to age. Since senescent cells increase with age and in pathological conditions, they are the target for a class of therapeutics, known as senolytics, to remove senescent cells[61].

There are multiple triggers for senescence and with age, the most accepted hypotheses are telomere shortening and subsequent stresses or other forms of genomic stress resulting in DNA damage and activated DDR pathways. Recent reports link senescence, SASP, DNA damage to the dsDNA sensor, cGAS, located in the cytosol[62], thus, highlighting the importance of PRRs and the innate immune system within age-associated senescence. Further, senescence has been reported to be highly heterogeneous at the single-cell level and therefore more research is needed to understand senescence in specific cell types and if there are tissue-specific differences depending on the organ[54].

1.2.4. **Hallmark of Aging: Inflammation**

One of the largest consequences of aging is a decline in immune function. The innate and adaptive immune systems evolve independently of each other with age, regardless of their close interaction and dependencies on one another. Nearly all components of the immune system from the innate to adaptative immune systems are impacted. For example, elderly populations are more at risk for infections as their immune system is not capable of recognizing novel or foreign antigens effectively. This is exemplified by the fact that people over 70 years-old are more at risk for influenza, regardless of

vaccination status[63]. Vaccinations are also shown to be less effective in the elderly populations because of an ineffective immune system[64].

Immune cell distributions are severely impacted with age. Fundamental changes occur within the HSC and progenitor compartment impacting the immune system during aging. HSCs have a reduced capacity to regenerate and proliferate into lymphoid and myeloid progenitor cells[65]. There are numerous cytokines and growth factors, such as interleukin (IL)-1α/β, IL-6, TNF-α, interferons (IFNs), macrophage colony-stimulating factor (M-CSF), granulocyte colony-stimulating factor (G-CSF), and granulocyte-macrophage colony-stimulating factor (GM-CSF), that are increased with age and skew HSC differentiation towards myelopoiesis[66]. Studies have shown that inhibition of TNF-α[67], IL-6[68] rescued effects of age-associated HSC bias differentiation towards myelopoiesis. Therefore, myeloid-biased HSC and myeloid cells increase with age, while lymphopoiesis decreases with age[66,69,70]. Consequently, the cytokines associated with age directly impact the niche that is responsible for making new immune cells.

These cytokines impact hematopoiesis which results in a decrease of B and T cells and increase of macrophages, such as neutrophils, macrophages, and NK cells with age, and most importantly, the functions of all immune cells are severely impacted[71]. Generally, thymic selection of T cells decreases and the involution of the thymus, which impairs adaptive immune responses. Systemic markers, such as IL-6 and TNF-α, are well characterized as proinflammatory cytokines that increase with age and are used as biomarkers for mortality in humans[72]. Proinflammatory cytokines increase with age systemically, but with each decade of life in humans the risk for chronic diseases within specific organs increases.

1.2.5. **The cGAS-STING Pathway**

DNA damage is a critical defining feature of aging. DNA can be recognized by multiple PRRs found in the endosomal compartment or the cytosol. Multiple sources of dsDNA activate cGAS, such as microbial DNA, mtDNA, extracellular 'self' DNA, or intracellular 'self' DNA as micronuclei. The ubiquitously expressed cGAS[73]-STING[74,75] signaling pathway is tightly linked to sensing dsDNA from aberrant 'self' DNA within the cytosol. After DNA is sensed by cGAS, the complex is rearranged to produce the secondary messenger, 2'3' cyclic GMP-AMP (cGAMP)[76]. cGAMP is a potent activator of the endoplasmic reticulum (ER) bound protein, stimulator of interferon genes (STING). STING is composed of a four short span transmembrane domains, a connector region, and cytosolic ligand-binding domain (LBD), which forms a domain swapped homodimer[77]. Once activated, STING untwists the LBD to change the conformation of its state to a side-by-side oligomerization of STING dimers supported by spanning the dimers by disulfide bridges and palmitoylation of cysteine residues, C88 and C91. In this formation, activated STING is released from the ER membrane into coatomer protein complex II (COPII) vesicles and trafficked though the ER-Golgi intermediate compartment (ERGIC) bound for the Golgi. Here, STING recruits TBK1, promoting autophosphorylation of TBK1. Subsequent STING phosphorylation at human-Ser366 or mouse-Ser365 results in the recruitment of IRF3[78]. STING activation and recruitment of TBK1 and subsequent phosphorylation of IRF3, supports IRF3 dimerization and its translocation into the nucleus and transcription of ISGs. STING also activates IKK, which in turn phosphorylates IκB[78]. Upon phosphorylated, IκB proteins are polyubiquitinated and then degraded by the ubiquitin-proteosome pathway. Thus, resulting in the translocation of NF-κB into the nucleus and transcription of pro-inflammatory genes,

such TNFα and IL-6 (**Figure 1.2.1**).

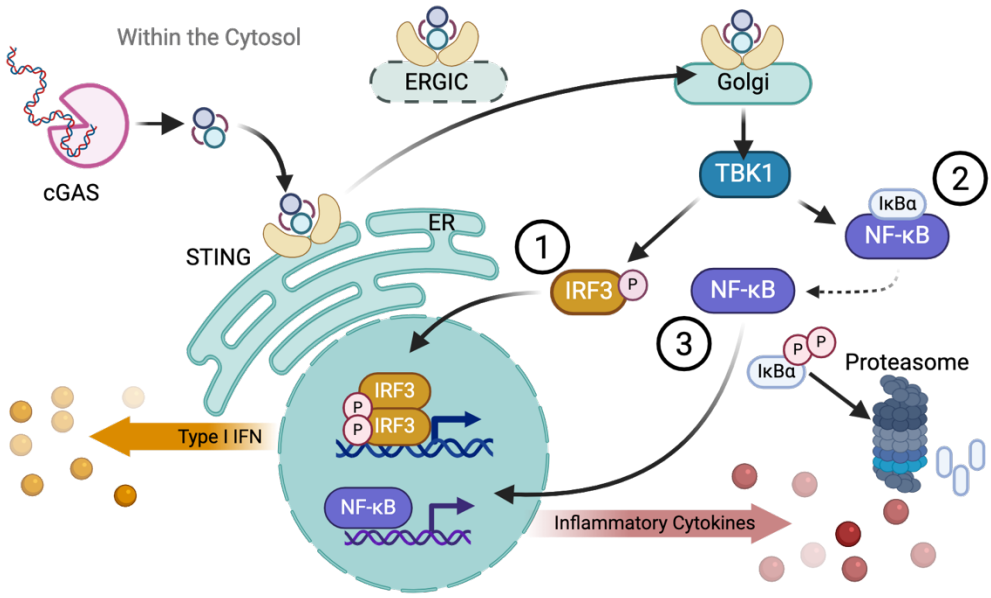

Figure 1.2.1. Activation of cGAS-STING signaling pathway.
Cyclic-GMP-AMP (cGAMP) synthase (cGAS) senses double stranded (ds)DNA and rearranges it into a secondary messenger (cyclic GMP-AMP (cGAMP). cGAMP activates the endoplasmic reticulum (ER) bound protein, stimulator of interferon genes (STING), which is trafficked to the Golgi upon activation and conformational changes occur. STING recruits TANK-binding kinase (TBK1) promoting (1) IRF3 phosphorylation and dimerization or IRF3. IRF3 is translocated into the nucleus to induce interferon stimulated genes (ISGs). (2) At the same time, STING stimulates the inhibitor of nuclear factor-κB (NF-κB) (IκBα). IκB proteins are polyubiquitinated and degraded by the ubiquitin-proteosome pathway. During this time, (3) IκB releases NF-κB for translocation into the nucleus for induction of proinflammatory genes (e.g. TNF-α and IL-6). *(Created with Biorender.com).*

STING expression and activation often have contrasting outcomes that are dependent of context. During human colon and breast cancer studies, STING expression is often associated with positive outcomes that result in reduced tumor growth, regulation of vasculature, and better survival. Activation of STING in these models by STING agonist renormalized the tumor vessels to support T cell infiltration and enhance anti-tumor immunity[79]. Overall, STING expression is associated with clinical positive outcomes, it is the activation of STING that triggers immune responses, including the production of IFN-

I and proinflammatory cytokines resulting in antitumor T cell responses, cell death, and autophagy.

The cGAS-STING pathway is a critical antiviral response pathway responsible for producing IFN-I and pro-inflammatory cytokines that protect against viral attacks. Beyond its original function, STING also plays a role in controlling autophagy, cell death, metabolic modulation, and endoplasmic reticulum (ER) stress responses[80]. In humans, there are multiple single nucleotide polymorphisms (SNPs) that have been shown to impact innate immune signaling. The human population is mostly heterozygous for SNPs in *TMEM173*[81] and the SNPs result in either the lack of functional STING protein or dysfunctional STING responses. There are four loss-of-function (LOF) SNPs that impact nearly 40% of the human populations: R71H-G230A-R293Q (HAQ) occurs in 20.4%, R232H in 13.7%, G230A-R293Q (AQ) in 5.2% , and R293Q in 1.5% of the population[82]. The most common human *TMEM173* allele has an Arginine at the amino acid 232 (*R232*) and only ~45% of the population is *R323/R323.* A homozygous substitution to histidine at position 232 (H232/H232) on both the major and minor alleles results in a defective and near complete loss of STING-mediated immune responses, a genotype that is extremely rare in the human population. In comparison, the heterozygous SNPs HAQ and R232H are relatively common, with approximately 30% of East Asian and 10% of European individuals carrying HAQ, HAQ/H232, or H232/H232 genotypes[81]. These LOF SNPs result in a decreased activation ability or redcued ability to produce IFN-β or NF-κB promotors, but each polymorphism does not respond to ligands the same way or has the exact same outcome. The R232H SNP impacts IFNα production[83]. Gain-of-Function (GOF) STING polymorphisms are the cause of severe interferonopathies, such as STING-associated vascular disease (SAVI)[83]. Interestingly, it was shown that introduction of the HAQ LOF mutation to the mutation associated with SAVI corrected localization of STING to the ER and corrected immune responses[84]. These works

highlight the importance of STING in regulating immune responses in humans, underscoring the need to study the role of STING signaling during aging.

1.2.6. **Interferons**

IFNs and interferon stimulated genes (ISGs) are necessary for antiviral immune responses and are produced through multiple pathways, a prominent pathway being cGAS-STING. Most cells have IFN mechanisms to either produce or respond to IFN signaling as they are important regulators for innate immune responses. There are three distinct families of IFNs: type I interferon (IFN-I), type II interferons (IFN-II), and type III interferons (IFN-III). IFN-I is made up of 13 subtypes of IFNα gene products in humans (14 subtypes in mice) and one IFN-β gene product. Most cells can produce IFN-β, whereas hematopoietic cells are the primary producers of IFN-α[85]. IFN-II only product is IFN-γ, which is mainly produced by NK cells and T cells and acts on any cells that expresses the IFNγ receptor (IFNγR). IFN-III are made up of multiple IFN-λs and acts primarily on epithelial cell surfaces[85].

1.2.7. **Activation and Control of IFN-I**

IFNs play a critical role in various disease states and immune responses during infections, IFN-I have been implicated in a complex relationship with age[86-92]. There are multiple studies that have shown increased levels of IFN-I during age-associated diseases[86,89,92].

Along with the cytosolic dsDNA sensor, cGAS, alternative PRRs and pathways drive IFN-I production and ISG activation. However, activation of PRRs are context specific. On the surface of the cell, TLR4 is a potent activator of IFN-I through the TIR-domain during microbial infections. RIG-I and MDA5 are cytosolic RNA sensors that induce large amounts of IFN-I and proinflammatory cytokines in response to viral infections[93]. DNA-dependent activator of IFN-regulatory factors (DAI, also known as Z-DNA binding protein

1(ZBP1))[94] and DEAD box and DEAH box (DEXD/H box)[95] recognize DNA motifs within the cytosol to produce IFN-I as well as driving inflammation and mediating cell death mechanisms. Lastly, the NOD-containing protein 1 (NOD1) and NOD2 recognize DAMPs and PAMPs within the cytosol that protect the cells from pathogens that replicate intracellularly[96].

After IFN-α and IFN-β are produced, they can act in an autocrine manner or paracrine manner through IFNα receptor (IFNAR), which is found on the cell membrane. Engagement of IFNAR activates the receptor-associated proteins tyrosine kinases Janus 1 (JAK1) and tyrosine kinase 2 (TYK2), which phosphorylate transcription factors found in the cytoplasm, signaling transducer and activator of transcription 1 (STAT1) and STAT2. When these factors dimerize and translocate into the nucleus, they assemble with IRF9 to form a trimolecular complex known as stimulated gene factor 3 (ISGF3) (**Figure 1.2.2**).

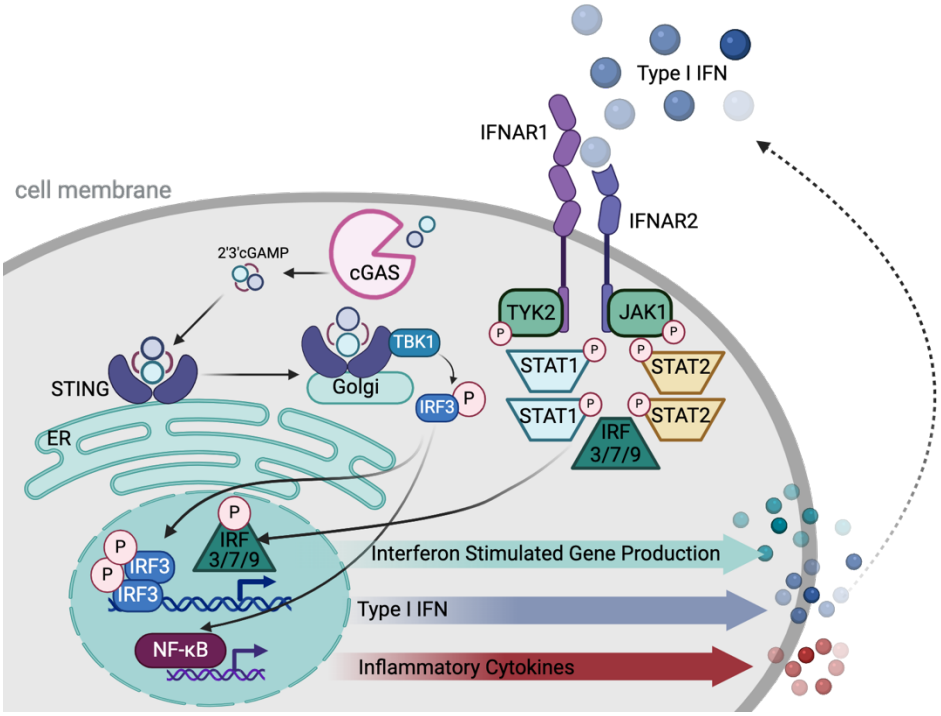

Figure 1.2.2. cGAS-STING-IFNAR signaling pathway.

The cGAS-STING signaling produces ISGs, which include type I interferons (IFN-I) along with other interferon stimulated genes (ISGs) and proinflammatory cytokines. IFN-I bind to interferon alpha/beta receptor (IFNAR1/2) to activate the tyrosine kinases, Janus 1 (JAK1) and tyrosine kinase 2 (TYK2). Theses kinases phosphorylate the transcription factors signaling transducer and activator of transcription 1/2 (STAT1/2). Upon dimerization of STAT1/2, these factors assemble with interferon regulator factor (IRF)9 and translocate to the nucleus as the stimulated gene factor (ISGF)3 factor complex. ISGF3 produces hundreds of ISGs that up and downregulate the interferon response and microenvironment. *(Created with Biorender.com).*

This pathway activates hundreds of ISGs that drive finely tuned antiviral immune responses. The activation of ISGs is dependent on cell type and the surrounding microenvironment. ISGs can drive a positive feedback loop to drive more production of IFN-I or a negative feedback loop to suppress the response[89]. These cells drive IFN-I and produce ISGs to suppress antiviral responses in order to protect the organism against toxic levels of IFN-I[85]. Factors, such as suppressor of cytokine signaling (SOCS) and ubiquitin carboxy-terminal hydrolase 18 (USP18), and miRNAs mediate and suppress IFN-I responses by downregulating IFNAR expression on the cell surface. Many viruses and tumor cells use IFNAR internalization to stop IFN-I mediated antiviral responses and antitumor effects. Other immune cells similarly utilize IFN-I suppression mechanisms to control cell functions, such as $CD8^+$ T cells, which use miRNAs to suppress the IFNAR-JAK-STAT pathway to drive $CD8^+$ T cell proliferation and memory formation during infections[97].

1.3. AGE-ASSOCIATED INFLAMMATION AND THE CNS

1.3.1. The Central Nervous and the Immune System

The blood brain barrier (BBB) is a critical barrier mechanism that is central to the innate immune system as the brain's first line of defense. For years the brain has been described as an immune privileged site, which was originally taken to mean that the brain was separate from the rest of the body. However, we know now that although the

brain is separated from the periphery by the BBB, it is capable of sending select chemokines and cytokines through a one-way interface and while restricting other signaling. The cytokines and chemokines that are transported through the BBB play important roles in delivering signals to the CNS. It is now accepted that the brain is tightly intertwined with the immune system and is dependent on it for homeostasis, development, normal physiology, and neurodegeneration[98,99]. Specialized immune cells reside at border interfaces and provide specialized functions to support the brain niche. Inflammation is strongly associated with diseases states, infections, or injury and compromises normal function[100,101]. Though inflammation is normally associated as a negative consequence, it also has been reported as critical for supporting CNS health[102]. There are many examples of the complex interactions between the immune system and the CNS. First, complement proteins are reported in synapses during development and are important for synaptic pruning, to support normal healthy functions[103]. TLRs are expressed on neurons and have been reported to regulate neuroplasticity during development and adulthood, such as during learning[104]. TNF-α is an activator of NF-κB signaling during traumatic brain injury (TBI) and mediated synaptic plasticity regulation in the hippocampus[105]. TNF-α has also been shown to be protective against neurodegeneration in mouse models of TBI and Alzheimer's disease (AD)[106,107]. Thus, importantly defining canonical inflammatory immune response as homeostatic mediators which support necessary and normal functions, such as memory formation[108] and cortical development[109], as well as during diseases states.

Adaptive immune responses have also been reported to be important for healthy and disease states. Activated $CD4^+$ T cells are pro-inflammatory and signs of disease within the CNS. However, it has also recently been reported that resident CD69+ $CD4^+$ T cells are found within the healthy brain and necessary for microglia maturation and synaptic pruning[110]. Importantly, the cells of the CNS are all capable of responding to and

conducting immune responses themselves. To support the tissue niche, there is a specialized immune cell within the brain called microglia. These cells perform necessary function, and studies have shown that without microglia the brain is susceptible to dysfunction and exacerbated pathology[111], which highlight necessary immune functions within the CNS. With age, there are signs of pathological immune responses that require more research in order to parse out the protective immune responses from the detrimental immune responses.

1.3.2. **The Role of Neurons, Glia, and Stroma**

The major cell types found within the brain are as follows: neurons, glia, and stroma cells. Neurons are made up of glutamatergic neurons and GABAergic neurons, respectively, which result in excitatory post-synaptic effects and inhibitory post-synaptic effects after activation potential is reached. Action potential is when a rapid change in voltage results in the depolarization of the cell membrane because of an exchange of sodium ions and potassium ions[112]. These neuronal signals are transported quickly as electrical impulses, which result in encoded information sent through the cell and results in immediate physiological changes. After activation, neurons return to resting potential. Glial cells, called oligodendrocytes, support this process through quickening signal transduction by insulating nerves with myelin sheaths. Oligodendrocytes support conduction of the electrical signaling being sent down the axon of the neuron[113]. At the synapse, astrocytes, another glial cell type, support and modulate neurotransmission at the tripartite synapse through internal calcium regulation that releases modulatory transmitters into the synapse[114]. Stromal cells within the brain consist of endothelial cells, vascular- associated endothelial cells, ependymal cells, choroid plexus epithelial cells, all of which protect as a barrier site or make-up the BBB[115].

1.3.3. **The Role of Microglia**

Microglia are the resident immune population found within the CNS and are seeding early in embryonic development. During embryogenesis, yolk-sac derived macrophages are seeded in the brain at embryonic day (E) 9.5, prior to hematopoiesis and development of the immune system. As critical homeostatic mediators, they perform a multitude of functions[116]. As the TRM population, microglia, carries out surveillance, support CNS cell fates, neurogenesis, and neuronal survival through multiple processes. The primary function of microglia is to phagocytose cellular debris, regulated synapse formation, and modulate soluble factors, such a growth factors, cytokines, and reactive oxygen species[35,117]. Microglia are seeded in the brain on E9.5, the cells differentiate into immature microglia at the same time as neuronal genesis occurs and before other glial cells differentiate. They are a highly adaptable and responsive cell type, making them difficult to study *in vitro* because of their plasticity. Microglia alter their transcriptional landscape and morphology in response to environmental cues, health, and disease states[36,116,118]. Though they are critical for homeostasis, microglia also regulate neuroinflammatory pathways found in neurodegenerative states. However, their homeostatic role in controlling neuroinflammation remains understudied.

1.3.4. **The Aging Brain and Neurodegenerative Diseases**

Inflammation is a defining feature of aging and other neurodegenerative diseases. The brain is susceptible to function decline associated with age and positions the organism at high risk for age-associated neurodegenerative diseases. With age, there are multitudes of behaviors that decline such as memory, attention, decision-making processes, perception, and lastly motor coordination[119]. Critically, the structure of the brain is an indication of function and health[120]. The structure(s) and dynamic neural networks must be supported and maintained for healthy functions to continue. With age, the

connections, structure, and neural connections are reduced and any alteration in the cellular network and overall structure renders the brain vulnerable to degeneration or age-associated diseases[102]. Studies show that atrophy can predict the brain age and likelihood for a patient with mild cognitive impairment to transition to AD[121]. Glial cells are chronically activated in neurodegenerative states, based on morphology of the cells and proinflammatory cytokine production, such TNF-α, IL-6, IFN-I[37,86,100,122,123]. Though microglia are primarily the target of neuroinflammatory research, astrocytes have also been shown to enter into a reactive and stress-related states. The most common age-associated neurodegenerative diseases and pathologies are AD, Parkinson's disease (PD) and stroke[124].

1.3.5. **IFN-I and the Brain**

Interestingly, it has been shown that DSBs accumulate in the cytosol of the cells where PRRs activate proinflammatory immune response[125,126]. The cGAS-STING signaling pathway is activated by genomic DNA[127] and mtDNA[128]. As previously described, once STING activates to induce multiple downstream mediators that results in proinflammatory cytokines and IFN-I production through NF-κB and IRF3 activation, respectively. Inflammation during aging is unsurprising, but recently IFN-I have been implicated in multiple processes during brain function, maintenance, and disease progression[88,115]. Overall, IFN-I is important for basic surveillance of immune cells and priming immune responses to threats[89,129]. At basal levels, IFN-I are important for supporting autophagy, synaptic plasticity, spatial learning, and memory formation[129]. IFN-I, specifically IFN-β, is used to treat multiple forms of MS[130] and low doses of IFN-β supported autophagy fluxes and clearance of α-synuclein in *in vitro* neuronal cultures[131]. Moreover, cell specific effects in neurons showed IFN-β signaling was necessary for controlling protein aggregation because of the deficits in autophagy and resulting

neuronal loss[131]. Furthermore, Hosseini et al. highlighted the importance of cell-specific responses and productive of IFN-I. They ablated *Ifnar1* in astrocytes to show that is an essential signaling component for normal hippocampal function[132].

However, IFN-I also play a negative role in neurodegeneration. Specific regions appear to have prominent IFN-I signatures, such as the choroid plexus, which is a critical barrier structure that is responsible for cerebrospinal fluid (CSF). By blocking IFNAR signaling, cognition and memory deficits were recovered[133]. In models AD, transgenic amyloid precursor proteins (APP) mouse models, accumulate amyloid-beta (Aβ) plaques, which is a hallmark of AD. These plaques contain nucleic acids which activate microglia to induce ISG expression and become hyper phagocytic and excessively remove neuronal synapses[134]. Exogeneous treatments of IFN-I worsened tau aggregation in *in vitro* mixed neuronal culture[135]. Therefore, excessive IFN-I may be detrimental, however IFN-I are still utilized to maintain homeostasis. Combined these data highlight the dual functions of IFN-I and the important of regulating amounts of IFN-I for specific functions.

1.4. SYSTEMIC INFLAMMATION AND SENESCENCE

Inflammation is central to aging and is often the target of anti-aging strategies. Systemic chronic inflammation is linked to age-associated diseases, such as AD, osteoarthritis (OA), heart failure (HF), chronic kidney disease (CKD), non-alcoholic fatty liver disease (NAFLD), and cancers. These diseases are linked to organ failure. It has been shown that after the 6th decade of life the likelihood of comorbidities and multi-morbidities dramatically increases[136]. Immune, stress, and defense responses are central to many aging studies[137]. DNA damage drives these systemic effects by activating inflammatory responses during DDR pathways, which can activate senescence in cell populations. Mitotic cells typically become senescent, however, recently research has shown that

postmitotic cells, or terminally differentiate cells, such as neurons, mature adipocytes, osteocytes can also become senescent[138].

These cells secrete proinflammatory chemokines and cytokines known as senescence-associated secretory phenotype (SASP), which change the tissue landscape surround the senescent cells. On the other hand, inflammation can also cause immunosenescence, which results in more inflammation through SASP production. Therefore, there is a tightly regulated network between inflammation and senescence. The prevailing theory regarding the role senescence plays during aging is that cells progressively lose their ability to proliferate, and the accumulation of non-dividing, SASP-secreting cells causes age-associated tissue damage and dysfunction. Though senescence is known to play a beneficial role in wound healing and other basic functions and how senescence may be provided necessary support during aging has not been addressed.

1.4.1. **cGAS-STING Drive Senescence and Inflammation**

NF-κB and IFN-I responses are tightly linked to models of premature aging and show that importance of DNA damage and senescence in influencing the inflammatory environment. Studies link premature aging and DNA damage to immune dysregulation through cytosolic DNA sensing pathways, such as the cGAS-STING signaling pathway. In 2015, researchers first showed that DNA damage can stimulate IFN-β *in vitro*[139] beyond what was already known in that DNA damage causing agents could stimulate IFN-I, excitingly in microglial cultures[140]. In a 2015 study by Yu et al.[139], researchers were able to attenuate DDR-induced senescence in stem cells by blocking IFN-β receptor or by neutralizing IFN-β. Then, showed that damaged DNA signaled through the known DNA sensor, cGAS, in response to the DNA damaging agents, etoposide and ionizing irradiation[62]. Furthermore, in 2023 Gulen et al., showed that microglial cGAS-

STING-signaling was driving age-dependent neuroinflammation and neuronal decline using a small molecule STING inhibitor[126]. This study highlights the importance of inflammation regulation and control with age, but more is needed to understand the homeostatic properties of the cGAS-STING pathway with age.

1.4.2. **Aging Heart and Age-Associated Inflammation**

The heart is important for pumping blood through an organism and providing the necessary nutrients and oxygen to organ systems. Age-associated deterioration of the heart is a major risk factor for cardiovascular disease, particularly heart failure (HF). Longitudinal studies highlight that HF during healthy aging is the result of multiple factors such as in an increased prevalence of left ventricular (LV) hypertrophy, increased prevalence of atrial fibrillation, decreases diastolic function, and preserved systolic function measured by ejection fraction (EF). The most common form of HF that is linked with aging is heart failure with preserved ejection fraction (HFpEF), as diastolic function is exacerbated in the absence of systolic heart failure[26,141].

Chronic inflammation is implicated as one of the primary mechanisms of cardiovascular aging, along with excessive oxidative stress and limited regenerative capacity of the heart[142]. Chronic inflammation drives cardiac and vascular fibrosis through mechanisms associated with senescence, genomic instability, and inflammation with age[28]. At homeostasis, the TRM population, cardiac macrophages, clear senescent and dying cells. However, with age, there is an increase of infiltrating macrophages that exhibit a more proinflammatory phenotype through the production of TNF-α, IL-6, matrix metalloprotease (MMP) 9 and C-C motif ligand (CCL) 2, which correlate with increased LV, a common feature of the aged heart[143]. Macrophages are linked to remodeling and the inhibition of myeloid extravasation into the heart by silencing endothelial cell adhesion molecules, resulting in improved cardiac function in models of HF[144].

Endothelial cells play a critical role in angiogenesis, or the development of blood vessels, and have been implicated as senescent cells that are driving decrease in adhesion, migration, and proliferation associated with age[142]. Additional age-associated mechanisms that are associated with cardiac function are dependent on stress. Thus, reducing stress on the heart such as through regular exercise[142] or caloric restriction[26], is used to prevent age-associated decline and impaired function. Studies have also investigated reducing age-associated phenotypes mitochondrial dysfunction intervention through redox active compounds[145], mTOR intervention through rapamycin treatments[146], inhibition of angiotensin II signaling[147], as well as other targeted therapies[26] to stall or reverse detrimental effects on the heart.

1.4.3. **Aging Liver and Age-Associated Inflammation**

The liver is important for detoxifying the blood by removing harmful substances before the blood is sent to the kidney for filtration. Unlike, the brain, heart, and kidney, the liver is a highly regenerative tissue. A unique consequence of age in the liver is the decreased ability to regenerate[148], resulting in liver fibrosis and eventually cirrhosis, or the permanent liver damage by severe fibrosis[149]. Chronic liver diseases, such as NAFLD and nonalcoholic steatohepatitis (NASH), are accompanied by chronic inflammation and fibrosis, along with increased prevalence with age[150]. Age-related changes to senescence and genomic instability in the Kupffer cells, stellate cells, and HSCs, but not in hepatocytes[151] are linked to tissue dysfunction, injury susceptibility and disease[149]. Inflammation and recruitment of immune cells contribute to age-dependent fibrosis[66,149]. Within the liver, senescence induces SASP factors and limits growth of potentially harmful cells before the liver is irreversibly damaged. The complexity of senescence is likely compounded because of the regenerative nature of the liver. Specifically, senescence is a critical cellular response in hepatocytes because it limits

the growth of DNA damaged hepatocytes during regenerative states. If the DNA damaged hepatocytes remain in the liver and regenerate, the damaged cells can turn into hepatocellular carcinoma (HCC)[152]. The senescent hepatocytes release of SASP factors recruit immune cells for removal of senescent cells. Similarly, the recruitment of immune cells, such as macrophages, also increase inflammation and contribute to liver disease by causing fibrosis and impairing the function of neighboring cells[153]. Thus, it is critical to understand the impact of senescence and inflammation with the liver and at what stage inflammatory and senescence processes are beneficial and when they can drive tissue degeneration.

1.4.4. **Aging Kidney and Age-Associated Inflammation**

The kidney is important for filtering blood and removing toxins. Age-associated decline of the kidney is a major risk factor for acute kidney injury (AKI) and CKD. Conversely, CKD is a risk factor for systemic inflammation and premature and accelerated aging[154]. An aged kidney is characterized by a loss of nephrons, which results in a progressive decline of renal flow and vascular function impacting the structure and function of the kidney. More structural changes include thickening of the glomerular basement membrane and enlargement of the mesangial compartment, resulting in glomerular swelling and hyperfiltration. When paired with glomerulosclerosis, or the progressive accumulation of extracellular matrix, age can also result in decrease in glomerular filtration rate (GFR)[29,154]. Both outcomes impair the kidney's ability to filter waste and excess fluid from the blood. A high GFR is associated with cardiovascular disease because the kidneys are filtering too much blood. Alternatively, a low GFR is when the blood is not filtered as quickly as it should be and results in CKD and kidney failure[155]. Several hallmarks of aging are linked to age-associated kidney decline such as inflammation, genomic instability, and senescence. DNA damage responses that trigger

inflammation and cell death pathways are known to drive CKD progression and alter genes associated with kidney function and age-driven fibrosis (mTOR, insulin/insulin-like growth factors, and sirtuin activity)[156]. An increase of senescent cells in the kidney, as well as other organs, is associated with decreased functional capacity[29,157]. Senescence is also known to alter NF-κB transcription and production of proinflammatory cytokines. These cytokines contribute to kidney decline through promotion of glomerulosclerosis and support leukocyte trafficking into the kidney via tertiary lymphoid tissues (TLTs) near glomeruli[158]. In this study, along with NF-κB signaling, IFN-I- signaling is activated and drives fibrosis and inflammation impacting cell-cell communication between proximal tubules leukocytes[158]. Thus, TLTs amplify and drive inflammation. Recent studies have linked CKD as a consequence of age, but CKD is also a risk factor for aging of distant organs such as the heart or the brain[159], therefore, implicating systemic inflammation as an increased risk for age-associated kidney dysfunction and central to the organism's aging process. Though kidney resident macrophages have been shown for necessary development, their role during aging is less defined and therefore, requires more work to understand the homeostatic contribution to protecting against decline.

1.5. **STING-DEFICIENCY DURING PHYSIOLOGICAL AGING**

This dissertation aims to address two critical gaps in knowledge: whether microglial-STING activation plays protective role in physiological aging in the CNS, and if STING modulates a similar age-dependent response within vital peripheral organs; the heart, the liver, and the kidney. We first use physiologically aged wild type (WT) and STING-deficient mice ($STING^{-/-}$) compared to young controls to determine functional impacts of long-term STING-deficiency. Using single-cell RNA sequencing (scRNA-seq), flow cytometry, and imaging techniques, we characterize key STING-dependent immune landscapes and cell populations that are central to age-associated inflammation and

tissue decline. To determine STING- and age- dependent changes to interferon responsive microglia (IRM), we utilized 12-mo cohort scRNA-seq dataset to characterize transcriptional changes and conducted functional assays with IFNAR$^{-/-}$ animals to determine benefits of IFN-I signaling with age. After investigating age-dependent changes in the CNS, we sought to understand if STING-signaling was protective for tissue health within vital organ systems (heart, liver, kidney) with age, systemic changes of inflammation, and lifespan and specifically driven by tissue resident macrophages (TRMs).

CHAPTER 2: **METHODS**

2.1. EXPERIMENTAL MODEL AND STUDY DETAILS

2.1.1. Mice

Male and female wild type (WT, C57BL/6 background) and STING$^{-/-}$ (Tmem173$^{-/-}$, C57BL/6 background) mice were used for all aging and *ex vivo* experiments. Aged experiments were organized into 3-months-old (mo) WT mice, 12-mo WT mice, 18-mo WT mice, 24-mo WT mice, and lifespan (Tufts University School of Medicine). STING$^{-/-}$ mice (G. Barber, U Miami) were set up to match WT ages: 3-, 12-, 18-, 24-mo and lifespan experimental groups (Tufts University School of Medicine). To control for sex-specific differences males and females were used for 2-and 24-mo sequencing dataset and flow cytometry experiments. Initial 3- and 12-mo sequencing dataset and imaging studies used males only because of longevity studies [160]. STING^{flox} animals were gifted from J. Cambrier (University of Colorado School of Medicine) and Csf1r-Cre (stock# 029206) were purchased from Jackson Laboratories. For frailty and longevity studies of MG$^{STING-/-}$ males and females were used to determine sex-specific differences and males were used for LLL and western blot assays. All mouse strains were bred and maintained by Tufts Rodent Breeding Services (RBS) in accordance with the Institutional Animal Care and Use Committee (IACUC) and guidelines set by Tufts University School of Medicine. Mice were housed under specific pathogen-free conditions in a 12-hour light-dark cycle. Mice were randomly distributed to aged groups and maintained with regular chow and water *ad libitum* unless euthanasia was required prior to the designated age per Tufts DLAM recommendations and requirements. Mouse cages were changed weekly. Images of mice next to a ruler were collected from different ages (3-mo, 12-mo, 18-m0, 24-mo, and LS timepoints) from WT, STING$^{-/-}$, cGAS$^{-/-}$, and IFNAR$^{-/-}$ mice.

,

2.2. **METHOD DETAILS**

2.2.1. **Survival Analysis**

Healthy WT and STING$^{-/-}$ mice of varying ages were designated for survival analysis. Mice were monitored weekly by the Division of Laboratory Animal Management (DLAM) for outward signs of disease, including daily body condition scores (BSC)[161]. BCS was only noted if mice progressed +/- 0.5 relative unit and in accordance with BCS conditions, which is based on vertebra prominence and overall condition (Figure 5.1.2). Animals were not always assigned a BCS upon required euthanasia. Date was recorded upon natural death or required euthanasia per DLAM instruction for animal welfare. Birth, death date, body weight, and BCS (if applicable) were recorded. Individual lifespan calculations were graphed in GraphPad Prism, statistical testing was performed using the Mantel-Cox Log rank test. Statistical significance of survival analysis testing was considered at p-value < 0.05.

2.2.2. **Serum Cytokine/Chemokine Multiplex ELISA**

Two mouse multiplex cytokine array panels generated by Eve technologies (Calgary, AB) were included to test serum for protein levels of the following chemokines/cytokines from young, 12mo, 18mo, 24mo WT and STING$^{-/-}$ mice (n=4-5): Eotaxin, G-CSF, GM-CSF, IFNγ, IL-1α, IL-1β, IL-2, IL-3, IL-4, IL-5, IL-6, IL-7, IL-9, IL-10, IL-12 (p40), IL-12 (p70), IL-13, IL-15, IL-17A, IP-10, KC, LIF, LIX, MCP-1, M-CSF, MIG, MIP-1α, MIP-1β, MIP-2, RANTES, TNFα, VEGF, (LIX results also included but not validated), EPO, 6Ckine, Fractalkine, IFNB1, IL-11, IL-16, IL-20, MDC, MCP-5, MIP-3a, MIP-3B, TARC, TIMP-1. Analysis was conducted using GraphPad Prism.

2.2.3. **Immunohistochemistry**

Mice were euthanized by CO_2 administration (4.5L/min) per IACUC regulations. Brains were extracted and placed in optimum cutting temperature medium (Tissue-Tek). OCT samples were flash frozen in dry ice and ethanol bath and stored in -80°C freezer. Tissues were sectioned manually on a cryostat (ThermoFisher Shandon Cryotome). Brains were sectioned serially at 10-15μm and flat mounted on slides (Fisherbrand Premium Superfrost™ Microscope Slides).

Prior to staining, slides were allowed to thaw to room temperature, and then OCT was removed with PBS. Tissues were fixed with cold 4% paraformaldehyde (PFA) (Fisher Scientific, PI28908) for 30 minutes and washed two times. Fixed tissues were blocked and permeabilized in PBS with 5% donkey serum and 0.3% Triton X-100 for two hours at room temperature. Tissues were incubated with primary antibodies diluted in PBS with 5% donkey serum and 0.3% Triton X-100 at 4°C. Tissues were washed for 5 minutes two times and incubated in secondary antibodies diluted in PBS with 5% donkey serum and 0.3% Triton X-100 for 2 hours at room temperature. Tissues were washed twice for 5 minutes. In most cases, sections were then treated with TrueBlack® Autofluorescence Quencher (Biotium). Samples were then stained with Hoechst in PBS for 5 minutes. Hoechst was removed and slides were coverslipped with Fluoromount (SouthernBiotech, OB10001).

The following primary antibodies were used: Anti-phospho-Histone H2A.X (Cell Signaling Technologies, Ser139, 20E3, 1:500); Mouse monoclonal anti-CD68 (clone FA-31) (Invitrogen, 14-0681-82, 1:1000); chicken polyclonal anti-GFAP (Invitrogen, PA1-10004, 1:1000); goat polyclonal anti-Neun (Invitrogen, PA5-143586, 1:400) ; rabbit polyclonal anti-beta Galactosidase (Proteintech, 15518-1-AP, 1:500) for stains.

The following secondary antibodies were used: Donkey anti-rat IgG (H+L) cross absorbed secondary antibody, Alexa Fluor 488 (Thermo Fisher Scientific, A21208,

1:1000); Donkey anti-chicken IgY (H+L) cross absorbed secondary antibody Alexa Fluor 555 (Thermo Fisher Scientific, A78949, 1:500); Donkey anti-rabbit IgG (H+L) Alexa Fluor 647 (SouthernBiotech, 6440-31, 1:500). Images were collected with a Leica Sp8 confocal microscope with a 63x objective lens and analyzed with FIJI software (v2.3.0). For γH2A.X and SA-β-Gal staining, the hippocampal region was imaged.

For visualization of lipofuscin-like particles, slides were not treated with any primary or secondary antibodies. The slides were incubated with blocking buffer or TrueBlack® at 1X in 70% ethanol from 20X stock for 30 seconds. The slides were dipped in water and then rinsed in PBS multiple times. The TrueBlack® is used as a control for a lipofuscin autofluorescent signature prior to staining with Hoechst for 5 minutes at room temperature. Slides were coverslipped and images were acquired with a Nikon Ti inverted fluorescent microscope with a 20x objective lens and analyzed with FIJI (v2.3.0). Three brain regions were collected from each mouse for analysis (hippocampus, cortex, thalamus).

For hematoxylin and eosin (H&E) staining of the brain sections, the Tufts histology core stained according to established protocols. Images were collected on the DMi8 epifluorescence microscope. Heart, liver, and kidney sections were stained at iHisto and in accordance with iHisto protocols and image acquisition was performed on Lionheart FX Automated Microscope (Tufts University).

2.2.4. **Confocal Image Analysis**

To quantify γH2AX, the total number of nuclei were counted based on Hoechst channel and a mask was applied. Then, a mask was applied to the γH2AX channel. The Image Calculator function was used to create a new image that included the overlapping binary mask of the two channels. Measurements were taken of γH2AX within Hoechst. For co-localization of γH2A.X to CD68, GFAP, or NeuN, QuPath[162] was used.

2.2.5. **Tissue Collection and Processing**

Mice were euthanized by CO_2 administration (4.5L/min) per IACUC regulations. Brains were dissected into DMEM and transferred into C tubes (Miltenyi, 130-093-237) containing digestion media (1mg/mL of Collagenase D (Sigma Aldrich, 1108866001), 1mg/mL of Dnase I (Sigma Aldrich, DN25-1G), and 2% fetal bovine serum(FBA) (R&D Sytems, S11550) in DMEM) for 30 minutes at 37 °C for mechanical digestion in a GentleMACS Tissue Dissociator (Miltenyi). Samples were passed through a 70µm strainer, brought up to 10mL in 2% DMEM, and centrifuged for 5 minutes at 500g at 4°C. Debris was removed from samples using Debris Removal (Miltenyi, 130-109-398) and after cells were pelleted, samples were lysed by resuspension in 1mL ACK lysis buffer (Fisher Scientific, NC0829166) for 1 minute at room temperature, followed by the addition of 9mL of 2% DMEM. Samples were pelleted, resuspended in PBS, and kept cold. Cells were counted (Countessa, Thermo, with Trypan Blue viability stain) and aliquoted for experimental use.

2.2.6. **Single-cell Isolations for Flow Cytometry**

All steps were performed on ice at 4ºC. After generating single cell suspensions as described above, cells were washed with 1X Phosphate Buffered Saline (PBS, Corning) and resuspended in 100µl of serum-free PBS with Zombie NIR (ZombieNIR anti-mouse Live/Dead) for 15-30 minutes. Cells were washed (5min, 400rpm 2x with 2mL FACS buffer (2% FBS in PBS)) and resuspend in 50µl of PBS with FC block (anti-mouse CD16/32; clone 2.4G2) for 15 minutes and incubated with a master mix of antibody cocktail (for 30 minutes (total of 100µl/ $2x10^6$ cells). Cells were then washed, centrifuged, and resuspended for analysis on the Cytek Aurora spectral flow cytometer (Cytek; Tufts Medical School). Single color controls were used on cells or beads

depending on the prevalence of the marker on target cell types. Unmixing was conducted using SpectroFlo (Cytek) and data was analyzed with Omiq (Dotmatics). The following antibodies were used:

eFluor 450 Anti-Mouse Ly6G (BD Biosciences, 741587), Anti-Mouse MerTK SuperBright 436 (Invitrogen, 62-5751-82), eFluor 506 Anti-Mouse CD11b (Invitrogen, 69-0112-82), BV510 Anti-Mouse CD11b (Biolegend, 107635), Anti-Mouse Ly6C BV570 (Biolegend, 128030), Anti-Mouse CSF1R (CD115) BV605 (BD Biosciences, 743640), Anti-Mouse CD200L BV650 (BD Biosciences, 745402), Anti-Mouse CD64 BV711(Biolegend, 139311), Anti-Mouse CD11c BV750 (Biolegend, 117357), Anti-Mouse CX3CR1 BV785 (Biolegend, BL149029), Anti-Mouse CD171 Vio-Bright FITC (Miltenyi, 130-106-105), Anti-Mouse CD45 AF532 (Invitrogen, 58-0451-80), Anti-Mouse CD19 PerCP (Biolegend, 115531), Anti-Mouse CD3 Complex PerCP (R&D Systems, Fab4841C), Anti-Mouse Ter119 PE (Biolegend, 116207), Anti-Mouse P2X7R PerCP-Cy5.5 (Biolegend, 148709), Anti-Mouse CD200R PerCP-eFluor710 (ThermoFisher Scientific, 46-5201-82), Anti-Mouse P2RY12 PE (Biolegend, 848004), Anti-Mouse F4/80 PE-Cy7 (BIolegend, 123114), Anti-Mouse ACSA-2 APC (Miltenyi, 130-116-245), Anti-Mouse Siglec-H (Biolegend, B271030), Anti-Mouse O4 AF700 (R&D Systems, FAB1326N-100G), Anti-Mouse CD68 APC-Cy7 (Biolegend, 137023), Anti-Mouse Live/Dead Zombie NIR (Biolegend, 423106) at their recommended dilutions.

2.2.7. **Fluorescence-Activated Cell Sorting (FACS)**

For fluorescence-activated cell sorting surface staining was performed as described. Cells were stained with Zombie viability dye and surface markers for anti-mouse Ter119 (Biolegend, 116207) and PI (), cells were sorted with the Legacy MoFlo (Cytomation; Tufts Medical School) into 1% BSA-PBS in 1.5mL Eppendorf tubes. Samples were used for Chromium Single Cell Gene Expression sequencing analysis.

2.2.8. **Prussian Blue Staining**

Slides were warmed up to room temperature for 20 minutes and then fixed in 37% formaldehyde for 1 minute or 10% neutral buffered formalin (NFB) for 5 minutes. Then slides were rinsed with tap water and placed into deionized water (DI). The slides were placed in equal parts 2% potassium ferrocyanide (Sigma Aldrich, P3289-100G) and 2% hydrochloric acid solution for 20 minutes at 60°C. After, slides were washed with DI water for several changes. Slides were counter stained with Nuclear-Fast Red Solution (Rowley Bio-Chemical, SO-130) for 5 minutes and rinsed under tap water for 2 minutes. Slides were dehydrated to xylene and cover slipped. Images were collected on a Leica DMi8 epifluorescence microscope with a 4x objective lens and processed within the LAS X Navigator program for positive stain via masking thresholding.

2.2.9. **Western Blotting**

Brain tissue were snap frozen from the midbrain/hippocampal regions and lysed on ice with RIPA buffer (150 mM NaCl, 50 mM Tris [pH 7.4], 1% NP-40, 0.1% SDS 5 mM EDTA, 0.1% sodium deoxycholate, 1 mM DTT) containing proteinase inhibitors (Roche, 04693159001) and phosphatase inhibitors (Roche PHOSS-RO), and quantified using DC protein assay (Bio-Rad, 5000112). Proteins were separated using SDS-PAGE on 10% gels, then transferred to PVDF membranes. Blots were blocked for 1 hour with 5% BSA (p-STING and vinculin) or nonfat milk (total STING, b-Actin, GAPPDH), in Tris-buffered saline plus 0.1% Tween-20. Incubation in primary antibodies diluted 1:1,000 (Rabbit IgG, Cell Signaling Technology, 2729S) in respective blocking buffer was conducted overnight at 4°C, except for GAPDH (Cell Signaling Technology, 2118), which was incubated at 1:2000. Blots were then incubated with secondary antibody conjugated to HRP (1:2,000; anti-rabbit, Cell Signaling Technology, 7074) at room temperature for 1 hour. West Pico or West Atto detection reagents were used (Thermo Fisher Scientific,

34580 and A38555, respectively) and imaged on a Bio-Rad ChemiDoc MP imager. Band intensity was quantified using ImageJ (NIH).

2.2.10. **Grip Strength**

Grip strength was used to assess muscular strength of the mice [163]. The mice were placed on a digital grip strength meter to test forelimb and total grip strength. For the test, mice were grasped by the tail and allowed to have their forelimbs grabs the meter, or all four of their paws were placed on the meter and the mice were gently pulled backwards in a straight line. The test lasts until the force of the pull exceeds the mouse's grip strength and the mouse releases the meter. The meter records the maximum force and displays the value on the screen. Each animal was tested three times in a row for each forelimb and the combined forelimb and hindlimb measurements were combined for a total of 6 trials combined. The three trial strength readouts were combined for one grip strength assessment.

2.2.11. **Hindlimb Clasping Assessment**

Mice were hung by the tail for 20 seconds three times in a row and the clasping score was estimated based on the observations made over a 30 second period. The scores are set to test quality of clasping behavior (0-3) and time to clasping (score 0-5). Briefly, for the quality of clasping scores: 0, wide splaying behavior; 1, One hind-limb retracted towards the abdomen (50% of the time); 2, both hind-limbs retracted towards the abdomen (50% of the time); 3, both hind-limbs entirely retracted and touching the abdomen. The timing to clasping score was assigned as follows: 0, no clasping; 1, clasping within 31-60 seconds; 2, within 16-30 seconds; 3, within 11-15 seconds, 4, within 6-10 seconds; 5, within 1-5 seconds. Genotypes and ages were blinded to the person administering the tests.

2.2.12. **Open Field Assay**

This assay assessed general locomotor activity by recording movements and locations around the open maze. It was performed by allowing mice to explore a grey square (40 x 40 cm) with 16 x 16 photocells equally spaced for 10 minutes (in core). Speed and time spent in the maze were recorded using EthoVision XT by Noldus. All mice were acclimated to the testing room 1 hour prior to testing. Animals were place in the maze for the duration of the recording and removed after 10 mins. After each run the maze was wiped with 70% ethanol and allowed to air dry for 1-2 minutes before next use. For analysis, the first 5 mins of collected times was used. Two separate experiments were conducted for each 12-mo cohort, 18-mo cohort, and 24-mo cohorts with young controls matched (sex and genotype).

2.2.13. **Novel Object Recognition**

Mice will spend more time exploring a novel object compared to a familiar one[164]. To assess recognition memory, mice were placed in a grey square box (40 x40 x 40 cm) with objects as visual cues. There were two days of training and habituation; during the first habituation, mice explored the area without objects for 10 minutes. During the second habituation, two identical objects were added and the mice explored for another 10 minutes. Then, on an experimental day, one of the objects was replaced with a new object of similar volume but with different shape, color, texture. After each run the maze was wiped with 70% ethanol and allowed to air dry for 1-2 minutes before the next use. Two separate experiments were conducted for each 12-mo, 18-mo, and 24-mo cohort with young controls matched (sex and genotype).

2.2.14. **Spontaneous Alternation (Y maze)**

Mice were first placed in the center of a maze and allowed to move down any of the arms. The test ran for an 8-minute period. The percent of alternation was determined by

the number of turns into each goal arm through a mathematical equation that determine the number of "correct" turns compared to incorrect turns[164].

$$\%\ Spontaneous\ Alternation = \frac{\#\ spontaneous\ altnernations}{total\ number\ of\ arm\ entries\ -\ 2} \times 100$$

Mice show a preference to the less recently visited arm which was calculated as percent alternation. Please note that no habituation was required because the novelty of the space drove the behavior, but animals were acclimated to the testing room for 1 hour prior to the test. After each run the maze was wiped with 70% ethanol and allowed to air dry for 1-2 minutes before the next use. Two separate experiments were conducted for each 12-mo cohort, 18-mo cohort, and 24-mo cohorts with young controls matched (sex and genotype).

2.3. SINGLE CELL RNA SEQUENCING

2.3.1. Single-cell RNA sequencing preparation

Single cell preparations were resuspended into enriched PBS (0.5% BSA). Approximately 9,000 cells were loaded into each well of the Chromium Chip A/B (10x Genomics v2 and v3, respectively), depending on the run, and then run on the Chromium controller. GEM formation quality was visualized manually before GEMs were transferred to a thermal cycler. GEM-RT cleanup and cDNA amplification steps were completed, and quantification was run in-house. 3’ gene expression library as constructed and post-library construction quality control was completed in-house as described in 10x Manual. Samples were sequenced on Illumina NextSeq 550 (Tufts Medical School) targeting a depth of 75,000 reads pe cells.

Sequenced samples were processed using Cell Ranger (v3.0.2) mkfastq pipeline. FASTQ files were assigned to the mm10 transcriptome, filters, and quantified.

Clustering analysis of scRNA-seq data

The Seurat package (v4.1.1.) was utilized to perform unsupervised clustering and differential gene expression analysis. Briefly, data was filtered for gene counts that passed specified QC thresholds (percent mitochondrial content < 15, nFeature_RNA < 3000, nFeature_RNA > 200) were normalized and log-transformed via SCTransform in Seurat. Principal component analysis (PCA) was conducted on the top 40 PCs, scaled data was utilized in the unsupervised cluster analysis of the single cells using k-nearest neighbor cluster calculations. The results were visualized using a low-dimension projection of Uniform manifold Approximation and Projection (UMAP). PCA, nearest neighbor, and UMAP was conducted on subsetted microglia population in later analysis to identified unique populations within the microglia.

The 3- and 12-mo dataset resulted in the analysis of 12,390 cells (3-mo (n=2 combined prior to sequencing; 3876 cells), 3-mo (n=2 combined prior to sequencing; 2929 cells), 12-mo WT (n=2 combined prior to sequencing; 3243 cells), 12-mo STING$^{-/-}$ (n=2 combined prior to sequencing; 2351 cells)). The 2- and 24-mo dataset resulted in the analysis of 11,496 cells (2-mo WT (n=2 (1 male and 1 female) combined prior to sequencing; 4152 cells), 24-mo WT (n=2 (1 male and 1 female) combined prior to sequencing; 2026 cells), 2-mo STING$^{-/-}$ (n=2 (1 male and 1 female) combined prior to sequencing; 3644cells), and), 24-mo STING$^{-/-}$ (n=2 (1 male and 1 female) combined prior to sequencing; 1674 cells))

2.3.2. **Clustering and cell type identification**

To identify differentially expressed genes (DEGs) within an individual cluster, we utilized the Seurat FindAllMarkers function to determine genes unique to one cluster when compared to the rest of the clusters. We used the Wilcoxon Rank Sum test with min.pct = 0.25 and logfc.thredhold = 0.25 as the settings. DEGs were also used later in identifying unique genes to microglia specific populations in the same way.

Clusters were identified based on known markers of cell populations: neutrophils (*S100a8*, *S100a9*), B cells (*Cd79a*, *Cd19*), T cells (*Thy1*, *Cd3g*), NKT (*Prf1*, *Nkg7*), ILC (T cell markers and *Il7r*), monocytes (*Lyz2*, *Cx3cr1*), border associated macrophages (BAMs)(*Pf4*, *Mrc1*), microglia (*Tmem119*, *Cx3cr1*), OPC (*Olig1*, *Pdgfra*), oligodendrocytes (*Cldn11*), immature neurons (*Sox4*, *Sox11*), endothelial cells (*Ly6c1*, *Cldn5*), vascular endothelial cells (*Hbb-bt*, *Alas2*),choroid plexus epithelial cells (*Enpp2*, *Chchd10*), neurons (*Snap25*, *Syt1*), excitatory neurons (*Grin2c*), inhibitory neurons (*Gad2*, *Gad1*), astrocytes (*Slc1a3*, *Aldoc*), pericytes (*Vtn*, *Higd1b*), ependymocytes (*Rarres*) (Figure S3).

2.3.3. **Volcano Plots and Gene Ontology Pathway Analysis**

DEG analysis was conducted between genotypes at each age with min.pct 0.1 and using model-based Analysis of Single Cell Transcriptomics (MAST) statistical test for volcano plots. Volcano plots were generated using the EnhancedVolcano() Package in R. Violin plots were generated using the Seurat VlnPlot() function in R.
DEGs were calculated using the Seurat function FindMarkers() to compared aged (12-mo or 24-mo, separately) WT and STING$^{-/-}$ samples or compare young (2- and 3-mo WT or STING$^{-/-}$) to age-matched (WT or STING$^{-/-}$) samples. DEGs were sorted by log2 fold change to select the top 50 genes for GO analysis. GO analysis was conducted using the Metascape webpage (www.metascape.org). Zip files were saved of the results webpage.

2.3.4. **RNAMagnet Analysis**

Single cell interactions were predicted using the RNAMagnet [165] package in R. Cell populations were subsetted based on age and/or genotype as demarcated. Each subset was evaluated individually using functions provided by the computational package. “RNAMagnetAnchors” was used to identify physical interactions by anchoring epithelial,

endothelial and vascular cell populations to query against all other cell populations by relative expression of receptor:ligand pairs. Heatmaps were generated using the strength of each interaction and plotted using ggplot2. “GetLigandReceptors” was used to identify distinct signaling axes between two specified populations based on the enrichment of cognate receptors and ligands in each respective cell population. Population comparisons were made quantitatively within ages and genotypes and compared qualitatively following complete analysis.

2.4. **QUANTIFCATION AND STATISTICAL ANALYSIS**

2.4.1. **Statistical Analysis**

GraphPad Prism was used for all statistical analyses of imaging, flow cytometry and behavior data. Statistical tests run and the number of n replicates and p-values are described in the text, figures, and/or figure legends. Statistical tests were run on the means of replicates per genotypes and the age of the animals, unless otherwise stated in the figure legends. For comparisons of two groups, student’s t-tests were run, and error bars represent the standard error of the mean (SEM). For multiple group comparisons, one-way or two-way analysis of variance (ANOVA) were run, followed up a Bonferroni correction factor applied. All bar graphs represent data by mean ± SEM and dots represent individual mice.

Statistics run unique to the test will be included in the specific section (e.g. lifespan analysis).

For statistical tests shown: ns is not significant, *p<0.05, **p<0.01, ***p<0.001, **** p< 0.0001.

CHAPTER 3: **RESULTS**

3.1. MICROGLIAL STING IS A CENTRAL SAFEGUARD AGAINST NEUROLOGICAL DECLINE WITH AGE.

Aging is a complex process associated with progressive functional decline of tissues and increased risk of chronic diseases. Age-associated increase in inflammation, a result of failures in proinflammatory checkpoints, is now considered a primary hallmark and central driver of aging[27]. Chronic, unresolved inflammation of the CNS, or neuroinflammation has been implicated in neurological decline during a myriad of diseases including AD and PD but also during physiological aging[100,123,166]. Chronic neuroinflammation is increasingly described as a combination of senescent, IFN-I, and proinflammatory transcriptional signatures[27,86]. Yet the identity of innate pathways responsible for these signatures and cell-types through which they modulate aging associated neuroinflammation remains hotly debated.

Recognition of DNA damage, a hallmark of aging, by myeloid cells has been shown to rely on several DNA-sensing mechanisms, key among them being the cytosolic DNA sensor, cGAS and its critical ER-associated signaling adaptor, STING[126,167]. Downstream of DNA sensing, STING signaling activates IRF3 and NF-κB to induce IFN-I, proinflammatory cytokines and also drive senescence in key cell types[92,126,168]. In recent studies, STING inhibition has been shown to be beneficial in decreasing the burden of proinflammatory responses in several diseases, including in models of accelerated aging[139,169,170]. However, there is only one study that specifically queried the role of STING-signaling in age-associated neuroinflammation[126], but they and others tested STING-antagonists and gain-of-function cGAS mutations, useful in rodent models of disease but less physiologically relevant for ascertaining the basis of healthy aging[171,172]. Thus, the long-term consequences of STING signaling or its loss, on health and lifespan during physiological aging have not fully been investigated. Indisputable incentive to study the long-standing impact of STING deficiency exists in the multiple

loss-of-function polymorphic alleles of STING that are widely expressed (≥40%) in the human population[82,83] which remains poorly characterized. Thus, a role for the STING-pathway in modulating CNS function during physiological aging requires urgent clarification for understanding the process of CNS aging. On the same note, these studies are equally important to fully understanding the impact of small-molecule STING-therapeutics during aging and other diseases.

Recent studies have highlighted the critical role of microglia, the resident effector immune cells, in shaping age-dependent changes in the CNS[173]. The complexity of microglia functions in the CNS have implicated them in opposing processes during aging[35,36,174]. Indeed, while microglia are critical in the clearance of damaged neurons and in the prevention of pathological changes in the brain[109,175], they have also been implicated as key drivers of pathological neuroinflammatory responses during aging[86,126,176]. How microglia may balance clearance of cellular damage with the induction of local inflammatory responses during aging, remains unstudied.

Here, we asked if the STING-pathway modulates distinct functions of microglia to mediate CNS homeostasis, resolve local damage and promote a protective, pro-inflammatory responses[109,126]. In support of this we reveal a critical, microglia-dependent role for STING-signaling in balancing homeostatic and inflammatory landscapes within the aging brain. We show that while STING-deficiency leads to lower levels of cellular senescence, it also results in a greater accumulation of damaged DNA and subsequent induction of inflammatory genes and pathways. Finally, deletion of global or microglial STING signaling results in significantly worsened neuromotor deficits, compromised blood-brain-barrier integrity and an increased prevalence of microhemorrhages. Together, our observations reveal a novel protective role for microglial STING in age-associated senescence and inflammation. Thus, we propose that microglial specific STING-function is necessary and beneficial for overall CNS health with age.

3.1.1. **STING-signaling restricts accumulation of DNA damage while driving senescence in aging brains**

To understand how long-term STING-deficiency shapes neurological processes during physiological aging, we first investigated how STING-deficiency impacts two core elements of aging: DNA damage and senescence in the brain. Brain tissue from WT and STING$^{-/-}$ mice at several timepoints; 2- 3mo (young adults), 12-14mo (middle aged), 18-24mo (healthy age), and 17-40mo (lifespan (LS) or end-of-life time points) were collected and processed (**Figure 3.1.1A-B**).

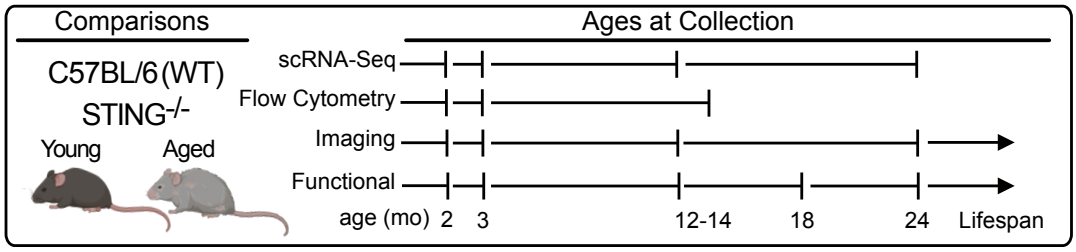

Figure 3.1.1. Experimental Design.
Diagram of ages of mice used for experiments throughout the paper. These include 3-mo, 12-14-mo, 18-24-mo (healthy), and lifespan (LS) animals (17-mo-40-mo) that required euthanasia WT and STING$^{-/-}$ mice.

We visualized damaged DNA in the brain utilizing confocal microscopy. Specifically, we measured numbers of cells with DSBs by assessing levels of γH2A.X, known to bind damaged-DNA ends[177]. We imaged several key regions of the CNS impacted with age including the hippocampus, thalamus, and cortex, important for cognitive processes, learning, and memory, respectively (**Figure 3.1.2A-B**) [176,178].

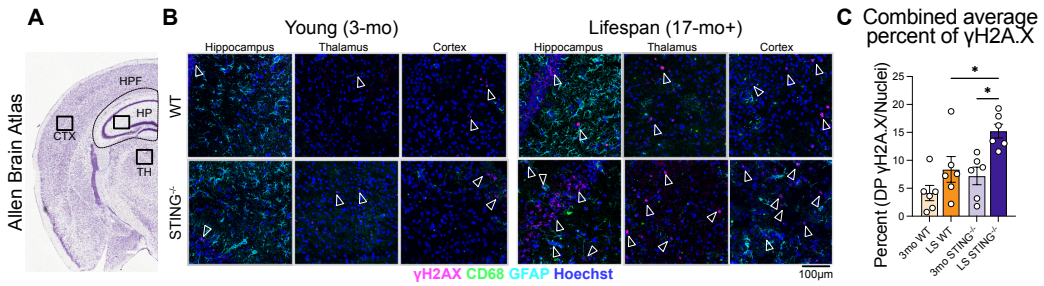

Figure 3.1.2. Immunofluorescence of DNA damage (γH2A.X) in the hippocampus. (A) Diagram of regions imaged and used for analysis: HPF, hippocampal formation; HP, hippocampus; TH, thalamus; CTX, cortex. B) Representative immunofluorescent images for γH2A.X (magenta), CD68 (green), glial fibrillary acidic protein (GFAP) (cyan), and Hoechst (blue) in the hippocampal region from 3-mo (n=) and LS (n=) WT and 3-mo (n=) and LS (n=6) STING$^{-/-}$ mice. Scale bars 100μm. The arrows highlight positive γH2A.X. (C) Bar graphs depict quantification of γH2AX expression across the hippocampal region.

Previous studies suggest that DSBs are notable during both, a) DNA damage responses noted in neurons critical for learning and memory formation, as well as b) a measure of apoptotic neuronal cell death[108,177]. Consistent with these studies, we observed that the expression of γH2A.X in both 3-mo WT and STING$^{-/-}$ brains was present at low levels, with around 5% of nucleated cells expressing γH2A.X in the three regions of interest (**Figure 3.1.2B-C**). As mice, the levels of γH2A.X increased and was primarily found in neuronal populations based on significant colocalization of γH2A.X and a neuronal marker (NeuN) compared to astrocytes (GFAP) and myeloid (CD68) in the hippocampus and thalamus. While similar colocalization is notable within the neurons of the cortex, the

differences between neuron, astrocyte or myeloid cells did not achieve significance (**Figure 3.1.3A-B**).

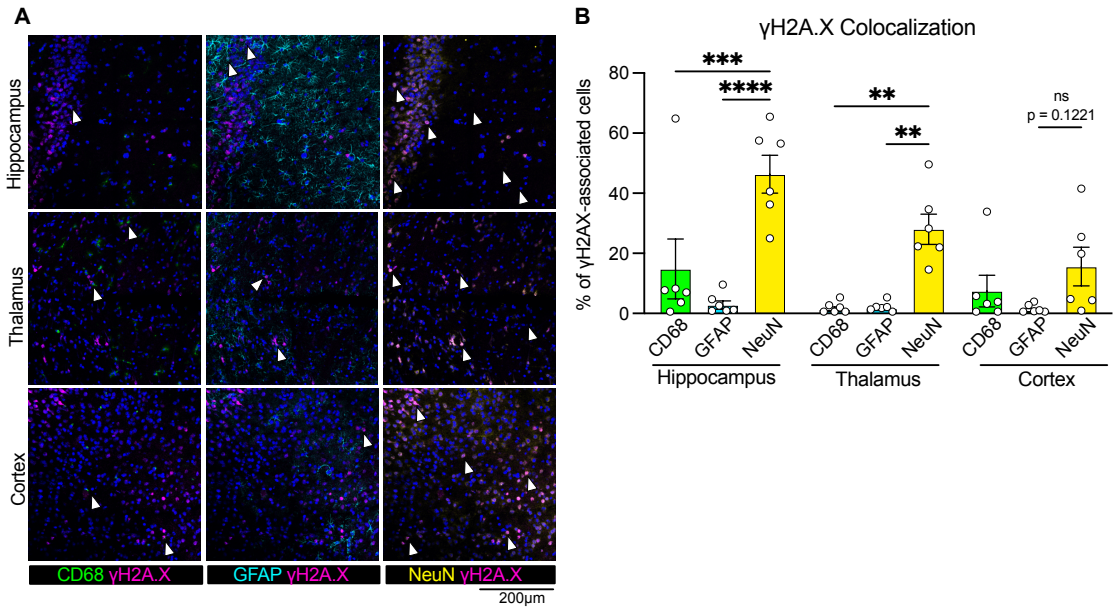

Figure 3.1.3. γH2A.X colocalizes with neurons with age.
(A)Representative immunofluorescent images for γH2AX (magenta), CD68 (green), glial fibrillary acidic protein (GFAP) (cyan), neurons (NeuN), and Hoechst (blue) in the hippocampal region from combined 3-mo WT and STING$^{-/-}$ (n=6) and combined LS WT and STING$^{-/-}$ (n=6) hippocampus, thalamus, and cortex regions. Scale bars are 200μm. (B) Bar graphs depict quantification of γH2A.X co-localization with CD68 (green), GFAP (cyan), NeuN (yellow) respectively from the hippocampus, thalamus, and cortex. Error bars represent mean ±SEM. Two-way ANOVA with with Tukey's multiple comparisons test was run. **** p< 0.0001, ***p<0.001, **p<0.01, ns = not significant

STING$^{-/-}$ brains also reveal an overall, significant increase in γH2A.X levels in neurons with age, which has linked to neurodegeneration[179], compared to their young controls. Critically aged STING$^{-/-}$ brains reveal a significant increase in DNA-damage marked by γH2A.X levels, in comparison to age-matched older WT (**Figure 3.1.2B-C**), suggesting aberrant accrual of damaged DNA with age and STING-deficiency.

The increased presence of damaged DNA is often considered a salient initiator of senescence and has recently been implicated as a trigger for DNA damage response (DDR) pathways that is induced in a cGAS/STING dependent manner[126,180]. Given the

increase of γH2A.X in the aged STING$^{-/-}$ brains, we investigated if there was a connection between the abundance of γH2AX and an age-dependent increase in senescent markers. To this end we utilized the auto-fluorescent (AF) properties of the senescent cells to determine changes with age in the brain in WT and STING$^{-/-}$ mice. The largest source of AF is lipofuscin, a mixture of metals, misfolded proteins, and oxidized lipids, which accumulates within the lysosome and is increased specifically in aged tissue[181,182]. All young brains contain very few lipofuscin-like particles (LLPs) that were small is size (~1 μm^2) in all regions imaged (**Figure 3.1.4A-B** and **Figure 3.1.5A-F**). Notably, we saw a significant age-dependent increase in the hippocampal LLP density and size in 12mo WT brain samples. The number and size of deposits continue to increase in the hippocampi through the lifespan of WT animals (**Figure 3.1.4A-C**).

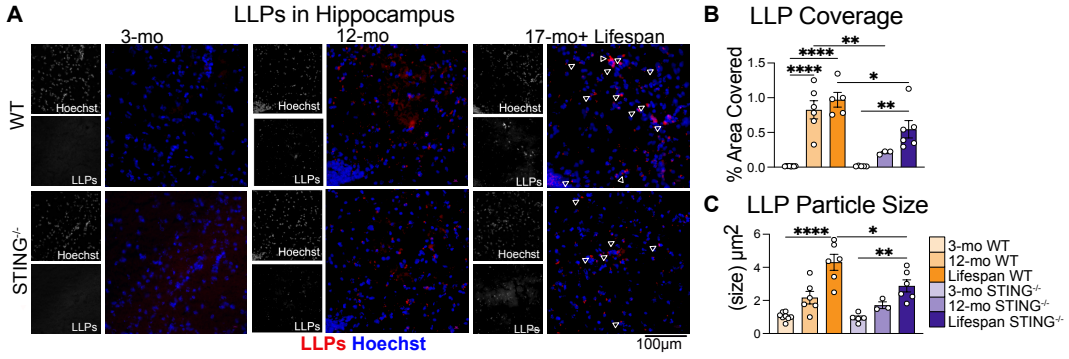

Figure 3.1.4. STING-signaling drives LLPs accumulation in the hippocampus. (A) Representative immunofluorescent images of autofluorescent signature from TxRed channel (excitation peak at 596nm and emission peak at 615nm) to label LLPs and with Hoechst of 3-mo WT (n = 8), LS WT (n = 6), young STING$^{-/-}$ (n = 5), and LS STING$^{-/-}$ (n = 6) hippocampal formation region (HP). Scale bars 100μm. The arrows highlight LLPs. (F) Bar graphs depict quantification of LLPs coverage in HP from young, 12mo and LS WT and STING$^{-/-}$ animals. (B) Bar graphs depict the quantification of LLPs particle size.

Similarly, LLP density and size significantly increased in the thalamus and cortex of WT animals with age (**Figure 3.1.5A-F**). We do not note any differences in the size or quantity of LLPs in the cortex and thalamus at 3-mo, 12-mo or LS timepoints between

the STING$^{-/-}$ and WT brains (**Figure 3.1.5A-F**).

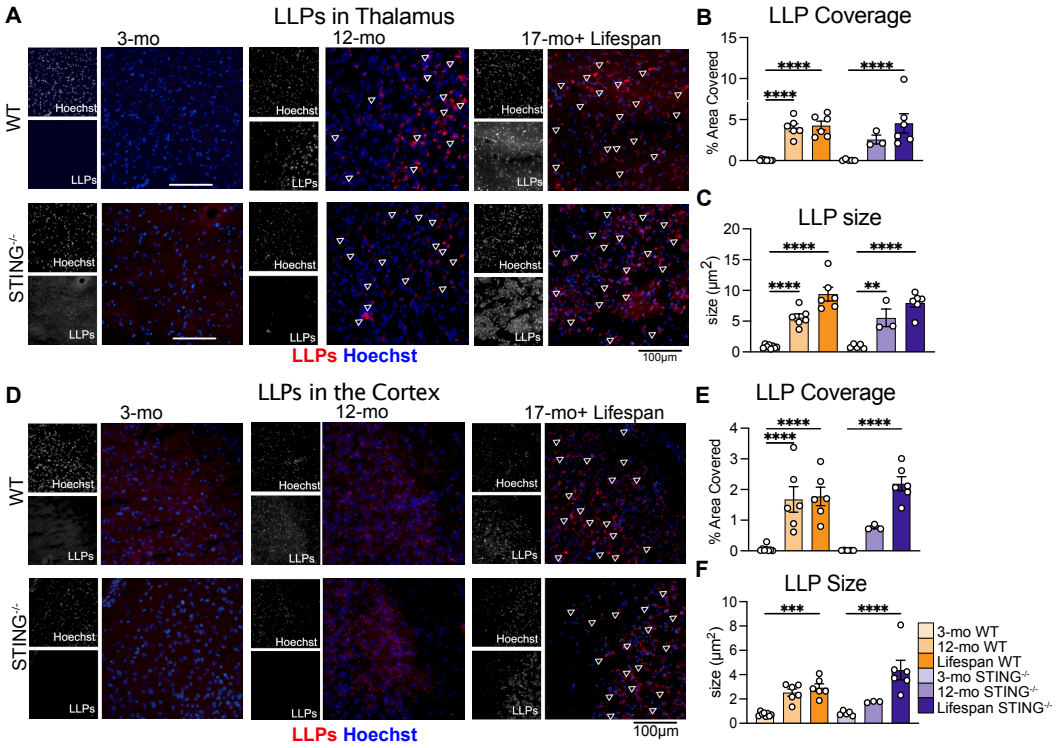

Figure 3.1.5. Lipofuscin-like particles (LLPs) increase in the thalamus and cortex with age in WT and STING$^{-/-}$ brains.
(A) Representative immunofluorescent images of autofluorescent signature from TxRed channel (excitation peak at 596nm and emission peak at 615nm) to label LLPs and with Hoechst of 3mo WT (n = 8), 12-mo WT (n = 6), LS WT (n = 6), young STING$^{-/-}$ (n = 5), 12-mo STING$^{-/-}$ (n = 3), and LS STING$^{-/-}$ (n = 6) thalamus. Scale bar is 100μm. (B) Bar graphs depict quantification of LLPs coverage in thalamus from young, 12mo and LS WT and STING$^{-/-}$ animals. One-way ANOVA with Tukey's multiple comparisons test. ns: not significant. Error bars represent mean ±SEM. (C) Bar graphs depict the quantification of LLPs particle size in the thalamus. One-way ANOVA with Tukey's multiple comparisons test. Error bars represent mean ±SEM. (D) Representative immunofluorescent images of autofluorescent signature from TxRed channel (excitation peak at 596nm and emission peak at 615nm) to label LLPs and with Hoechst of 3mo WT (n = 8), 12-mo WT (n = 6), LS WT (n = 6), young STING$^{-/-}$ (n = 5), 12-mo STING$^{-/-}$ (n = 3), and LS STING$^{-/-}$ (n = 6) cortex. Scale bar is 100μm. (E) Bar graphs depict quantification of LLPs coverage in cortex from young, 12mo and LS WT and STING$^{-/-}$ animals. One-way ANOVA with Tukey's multiple comparisons test. Error bars represent mean ±SEM. (F) Bar graphs depict the quantification of LLPs particle size in the cortex. One-way ANOVA with Tukey's multiple comparisons test. ns: not significant. Error bars represent mean ±SEM.

However, at end of the lifespan, we see a significant decrease in LLPs in the STING$^{-/-}$

hippocampus compared to their age-matched WT controls (**Figure 3.1.4A-C**). This data

emphasizes the impact of STING-deficiency on senescence marker density in key CNS regions. To confirm these data, we stained for a canonical marker of senescence, senescence-associated β-galactosidase (SA-β-gal)[54], in young, 12mo, and LS hippocampal regions from WT and STING$^{-/-}$ mice. SA-β-gal extracellular staining increased in an age-dependent manner in both the WT and STING$^{-/-}$, however, LS STING$^{-/-}$ animals had a significantly less SA-β-Gal compared to LS WT brains (**Figure 3.1.6A-B**).

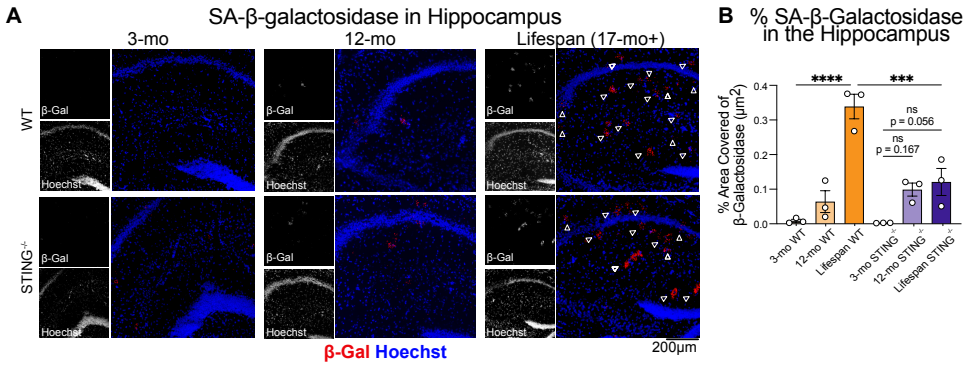

Figure 3.1.6. STING-signaling drives SA-β-Gal in the hippocampus.
(A) Representative immunofluorescent images of SA-β-Gal (red) in the hippocampus of young 3-mo WT, 3-mo STING$^{-/-}$, LS WT, LS STING$^{-/-}$. Data from 3 biological replicates and scale bars 200μm. The arrows highlight positive SA-β-Gal stain. (B) Bar graphs depict quantification of the percent area coverage of SA-β-Gal in the hippocampus.

Similar to LLP distribution, SA-β-Gal staining was significantly decreased in the of LS STING$^{-/-}$ hippocampus. Surprisingly, regardless of genotype, cells expressing GFAP (astrocytes) and CD31 (endothelial cells), which collectively make up part of the BBB microvascular[183], are the primary expressors of age-associated SA-β-Gal when

compared to CD68+ cells (myeloid/microglia) (**Figure 3.1.7A-B**).

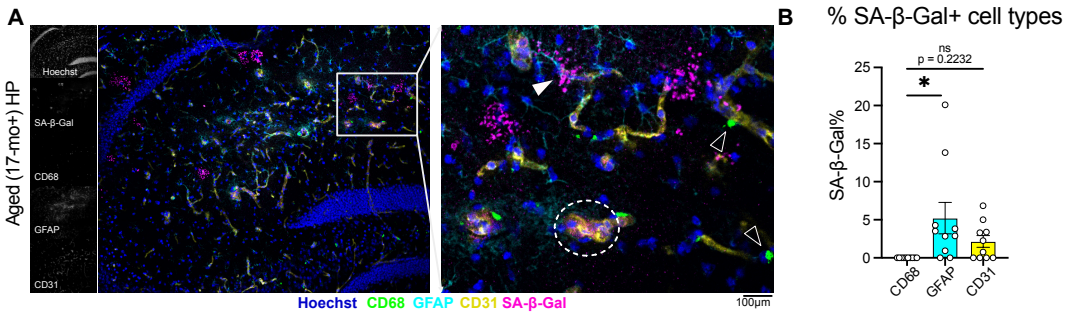

Figure 3.1.7. SA-β-Gal+ colocalizes with astrocytes and endothelial cells.
(A) Representative immunofluorescent images for SA-β-Gal (magenta), CD68 (green), glial fibrillary acidic protein (GFAP) (cyan), endothelial cells (CD31), and Hoechst (blue) in the hippocampal region from 6 biological replicates (n=3 WT and n=3 STING$^{-/-}$). Scale bars are 100μm. (B) Bar graphs depict quantification of γH2A.X co-localization with CD68 (green), GFAP (cyan), NeuN (yellow) respectively from the hippocampus, thalamus, and cortex from 6 biological replicates from all three regions (n=3 WT and n=3 STING$^{-/-}$). Error bars represent mean ±SEM. One-way ANOVA with Tukey's multiple comparisons test was run. **p<0.05, ns = not significant

These data emphasize that the cellular sources of secreted senescence markers like SA-β-Gal are unchanged in STING$^{-/-}$ brains. However, these data suggest that STING-signaling may connect sensing of DNA damage with the presence of senescent markers with age.

3.1.2. **STING-signaling regulates the inflammatory and senescent landscape of aging brains.**

Given that senescence and inflammation are considered coordinated processes[27,54,119], the reduction of senescent markers with age in the STING$^{-/-}$ brains suggests a likely decreased expression of inflammatory signatures as well. To assess the inflammatory landscape in an unbiased manner, we leveraged single-cell RNA sequencing (scRNA-seq) analysis of immune enriched single cells from young (3-mo) and middle-aged (12-mo) WT and STING$^{-/-}$ brains (12-mo dataset) (**Figure 3.1.8A**).

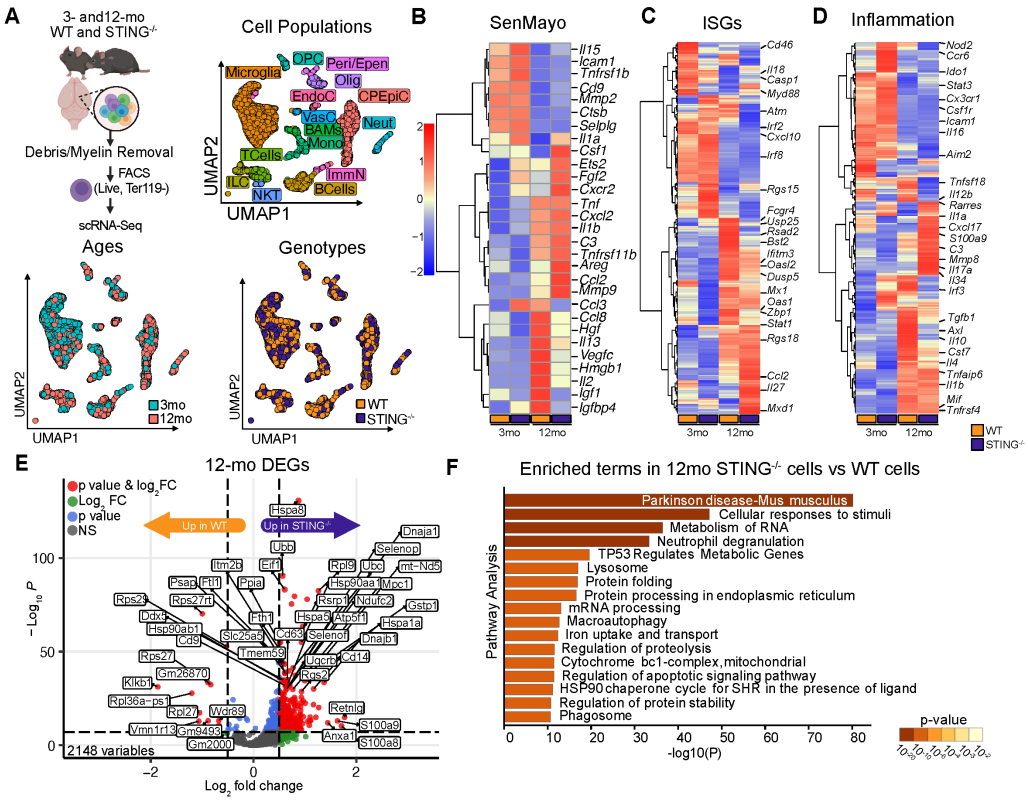

Figure 3.1.8. STING-signaling restricts accumulation of DNA damage while driving senescence transcriptional landscape in 12-mo brains

(A) Schematic of FACS-sorting live nucleated cell (PI-, Ter119-) preparation for scRNA-seq analysis from a total of 12,390 cells (3-mo (n=2 combined prior to sequencing; 3876 cells), 3-mo (n=2 combined prior to sequencing; 2929 cells), 12-mo WT (n=2 combined prior to sequencing; 3243 cells), 12-mo STING$^{-/-}$ (n=2 combined prior to sequencing; 2351 cells)). Representative UMAP(s) of ages independent of genotype (3-mo = teal; 12-mo = coral), genotypes independent of age (WT = gold; STING$^{-/-}$ = purple), and neuroimmune enriched cells clustered and identified as 15 distinct cell types by specific markers (ImmN., Immature Neurons, CPEpiC; Choroid Plexus Epithelial Cells, OPCs; Oligodendrocyte Precursor Cell, Olig; Oligodendrocytes, BAMs; Border-Associated macrophages, Peri/Epen.; Pericytes and Ependymocytes, EndoC.; Endothelial Cells, VasC.; Vascular Cells, Microglia, Mono; Monocytes, Neut; Neutrophils, B Cells, T Cells, NKT Cells; Natural Killer T Cells, (in clockwise order). (B) Heatmap of pseudo-bulk analysis of SenMayo genes from 3-mo WT, 3-mo STING$^{-/-}$, 12-mo WT, 12-mo STING$^{-/-}$ sequenced samples. (C) Heatmap of pseudo-bulk analysis of ISGs from 3-mo WT, 3-mo STING$^{-/-}$, 12-mo WT, 12-mo STING$^{-/-}$ sequenced samples. (D) Heatmap of pseudo-bulk analysis of inflammatory genes from inflammatory response GO term (GO:0006954). Gene expression scaled for row maximum. (WT = gold; STING$^{-/-}$ = purple). (E) Volcano plot of genes differentially expression in 12-mo STING$^{-/-}$ microglia relative to 12-mo WT. Dots: Red; p value and log2FC, green; Log2FC, blue; p value, grey; not significant (ns). (F) Metascape bar graph to visualize the top non-redundant enriched terms based on GO terms, KEGG pathways, Reactome, and CORUM in 12-mo STING$^{-/-}$ cells compared to 12-mo WT cells. Scale represents statistical significance.

Transcriptionally similar cells were clustered and identified based on their distinct transcriptional landscapes. Of the 25 transcriptionally distinct clusters identified, we were able to identify 15 cell populations (**Figure 3.1.9A**). We saw that numbers of conventional peripheral immune cell populations (ILCs, monocytes, neutrophils, NKT cells, B cells, T cells) increase in the 12-mo dataset independent of genotype, suggesting an influx of immune cells with age (**Figure 3.1.9A-B**). Shifts in immune cells suggested connected changes in the immunologic profile of the aging CNS.

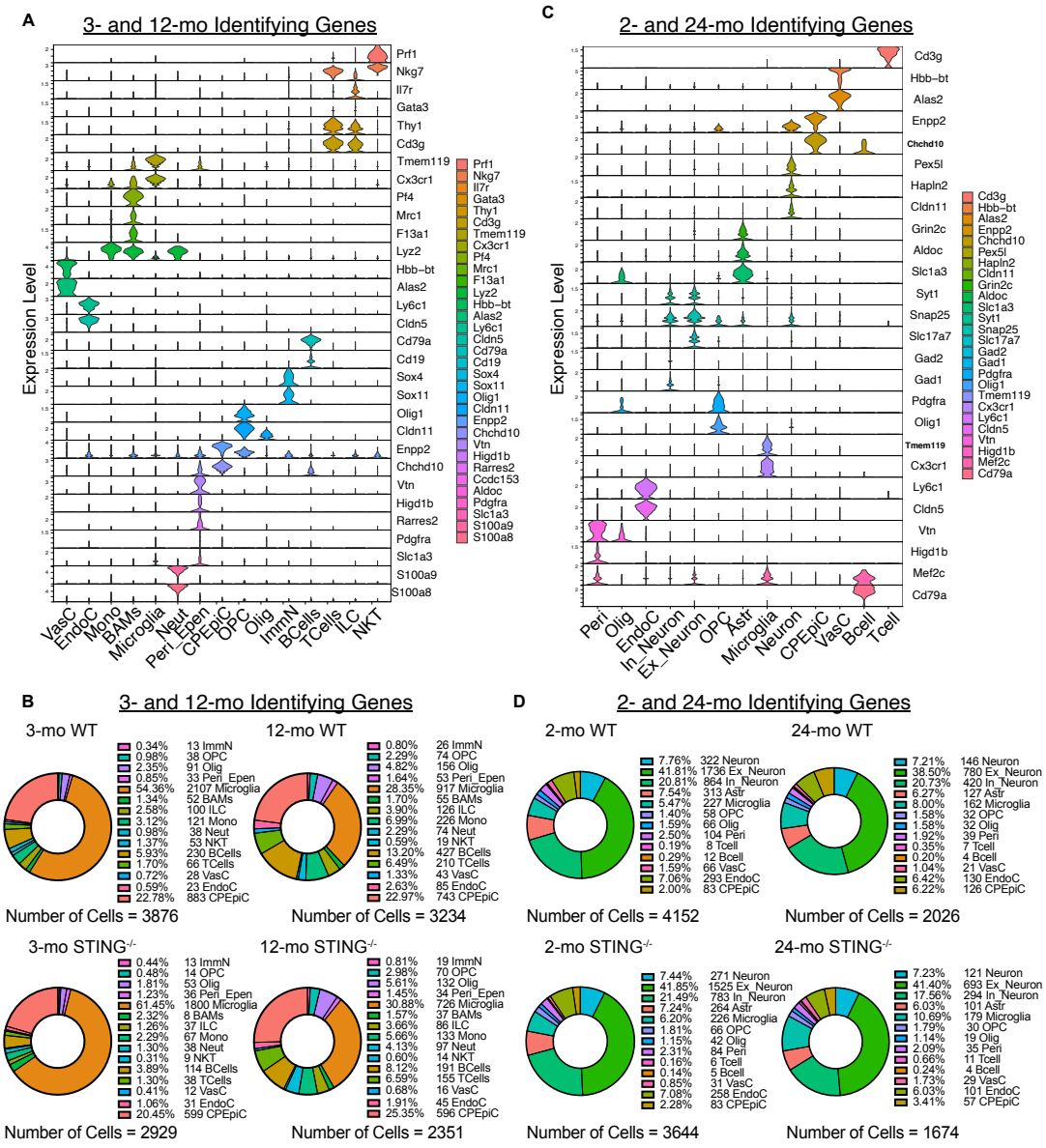

Figure 3.1.9. Cluster identification and cellular composition of 3-and 12-mo and 2- and 24-mo scRNAseq datasets.

(A) Stacked violin plot showing specific upregulation of select genes for each cluster identified in 3-mo and 12-mo dataset from FACS sorted single brain suspension. Violin plot shows expression of each gene on a scale based on the SCT normalized data. Single cells are not depicted with dots on Vlnplot. (B) Donut charts of 3-mo WT (3876 cells), 12-mo WT (3234 cells), 3-mo STING$^{-/-}$ (2929 cells), 12-mo STING$^{-/-}$ (2351 cells) single cells. Each section represents the proportion of cells within the identified cluster. Frequency and number of cells are shown next to corresponding donut chart. (C) Stacked violin plot showing specific upregulation of select genes for each cluster identified in 2-mo and 24-mo dataset from single brain suspension. Vlnplot shows expression of each gene on a scale based on the SCT normalized data. Single cells are not depicted with dots on Vlnplot. (D) Donut charts of 2-mo WT (4152 cells), 24-mo WT (2026 cells), 2-mo STING$^{-/-}$ (3644 cells), 24-mo STING$^{-/-}$ (1674 cells) single cells. Each

section represents the proportion of cells within the identified cluster. Frequency and number of cells are shown next to corresponding donut chart.

We conducted pseudo-bulk analysis of the aggregated single-cell data to create a dataset amenable for comparisons of inflammatory signatures between ages and genotypes. Overall, differentially expressed gene (DEG) analysis of WT and STING$^{-/-}$ brains indicates a discrete set of genes unique to each age (3-mo and 12-mo) as well as genotype (**Figure 3.1.8B-D**). Curated gene lists derived from the SenMayo datasets[184] were overlaid on the single-cell transcriptomes to determine the STING-dependent shifts in gene expression profiles with age (**Figure 3.1.8B**). While cells both from 12-mo WT and STING$^{-/-}$ express higher SenMayo genes, the WT CNS upregulate a distinct set of senescent genes (*Hmgb1*, *Igf1*, and *Igfbp4*) compared to STING$^{-/-}$ CNS (*Areg*, *Mmp9*, *Il1a*, and *Csf1*) (**Figure 3.1.8B**), indicating a differential regulation or nature of senescence between the genotypes. This altered profile also correlates with downregulation of myriad senescence genes in the aged STING$^{-/-}$ aged samples in comparison to WTs, further in line with the reduction of LLPs and SA-β-Gal, noted above in the aged STING$^{-/-}$ brains

To carefully evaluate the nature of inflammatory changes, we next queried the expression of 985 pan-IFN-I stimulated genes (ISGs)[168,185] in the CNS to determine age- and STING-dependent expression patterns. Several canonical ISGs (*Mx1*, *Oas1*, *Ifitm3*, and *Bst2*) were upregulated at 12-mo compared to the 3-mo WT datasets and were decreased in both 3- and 12-mo STING$^{-/-}$ samples (**Figure 3.1.8C**). Importantly, ISGs with known proinflammatory roles, such as *Ccl2*, *Il27* and *Mxd1*[80], are uniquely increased only in the 12-mo STING$^{-/-}$ samples compared to age-matched WT controls (**Figure 3.1.8C**). Next, expression of key immune response genes part of pro-inflammatory responses (GO:0006954) were assessed, genes indicative of predominantly homeostatic or regulatory functions (*Cx3cr1*, *Csf1r*, and *Icam1)* were

equivalently expressed in 3-mo WT and STING$^{-/-}$ brains. Aged WT CNS cells express genes canonically associated with neuroinflammation (*Axl*, *Cst7*, *Tgfb1*). In contrast, STING$^{-/-}$ brain cells express markers often seen in neurodegenerative diseases (*Mmp8*, *S100a8*, *Il34, Csf1*)[166,186] (**Figure 3.1.8D)** and were overall more transcriptionally active compared to 12-mo WT cells (**Figure 3.1.8E**).

To determine the nature of the immune response specifically enriched in the STING-/- CNS, we conducted an unbiased Metascape pathway analysis[187] on DEGs in CNS cells from young/old WT and STING$^{-/-}$ mice. 3-mo STING$^{-/-}$ CNS cells were more transcriptionally active compared to 3-mo WT (**Figure 3.1.10A**), but similarly expressed

known homeostatic[188] immune markers(*Tmem119* and *P2ry12*)[189] (**Figure 3.1.10B**) showed no significant differences.

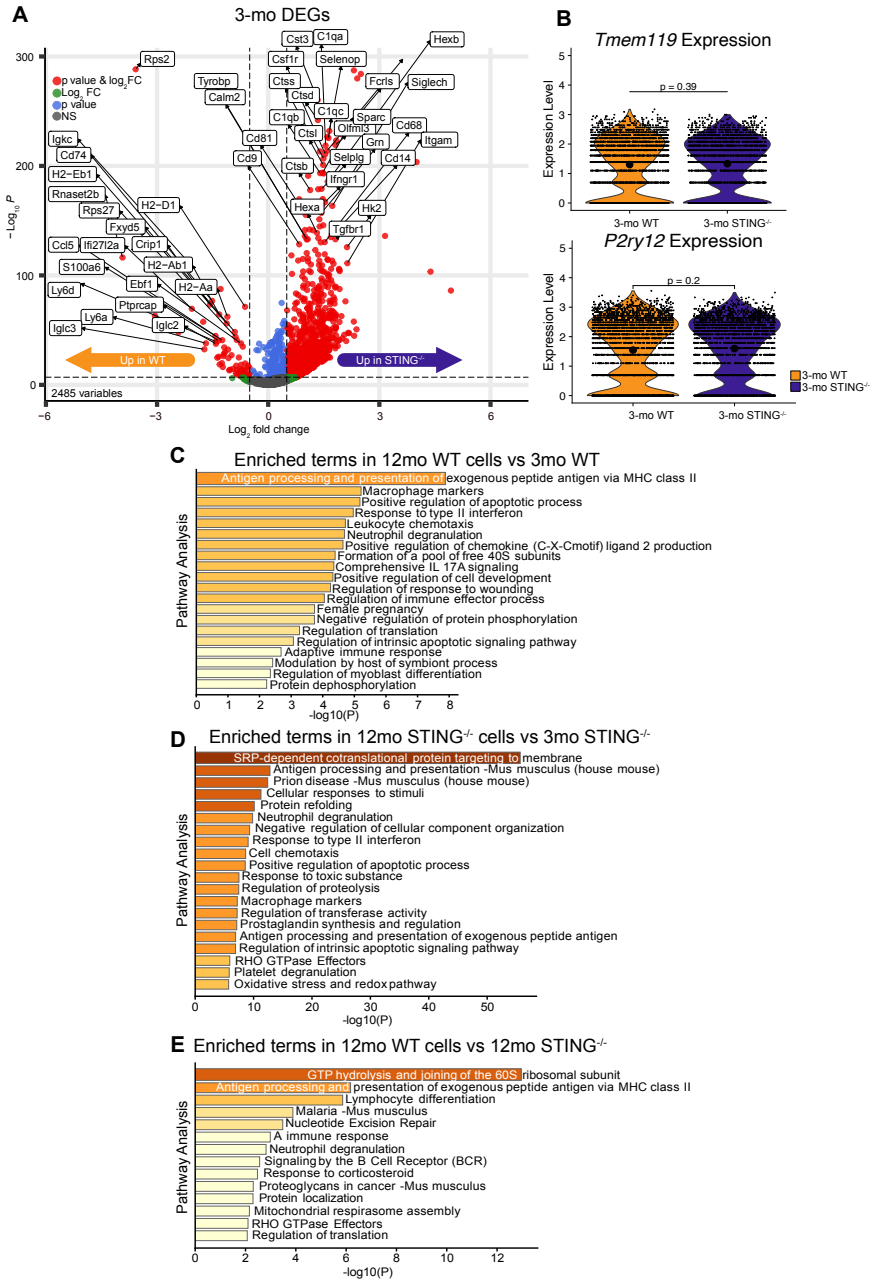

Figure 3.1.10. scRNA-Seq differentially expressed genes and pathway analysis of 12-mo dataset.
(A) Volcano plot of genes differentially expression in 3-mo STING$^{-/-}$ microglia relative to 3-mo WT. Dots: Red; p value and log2FC, green; Log2FC, blue; p value, grey; not significant (ns). (B) Violin plots of homeostatic genes associated with microglia: *Tmem119* and *P2ry12*. my_comparisons() passes statistical tests for t-tests or ANOVA depending on the number of comparisons defined. Therefore, t.test or wilcox.test were

used accordingly. Gold = WT and purple = STING$^{-/-}$. (C) Metascape bar graph to visualize the top non-redundant enriched terms based on GO terms, KEGG pathways, Reactome, and CORUM in 12-mo WT cells vs 3-mo STING$^{-/-}$. Scale represents statistical significance. (D) Metascape bar graph to visualize the top non-redundant enriched terms based on GO terms, KEGG pathways, Reactome, and CORUM in 12-mo STING$^{-/-}$ cells vs 3-mo STING$^{-/-}$. Scale represents statistical significance. (E) Metascape bar graph to visualize the top non-redundant enriched terms based on GO terms, KEGG pathways, Reactome, and CORUM in 12-mo WT cells vs 12-mo STING$^{-/-}$. Scale represents statistical significance.

Pathway analysis showed an expected increase in inflammation[27] related pathways in WT animals with age (**Figure 3.1.10C**). An increase in inflammatory pathways was also seen in the STING$^{-/-}$ samples, although the quality of the pathways was distinct from WT samples (**Figure 3.1.10D**). When 12-mo STING$^{-/-}$ and WT cells were directly compared, pathway analysis revealed an upregulation of pro-inflammatory networks in the aged STING$^{-/-}$ compared to WT (i.e. Parkinson disease, Regulation of apoptotic signaling pathways, response to oxidative stress, etc.) (**Figure 3.1.8F**), which were not seen in positive DEGs of 12-mo WT compared to 12-mo STING$^{-/-}$ (**Figure 3.1.10E**). Of note, pathways linked to DNA damage response (DDR) pathways are upregulated in STING$^{-/-}$ (i.e. (TP53 regulates metabolic genes, HSP90 chaperone cycle for Steroid Hormone Receptors (SHR) in the presence of a ligand, regulation of protein stability), which highlight changes associated with significant DNA damage, as we note in Figure 1D. Genes associated with DDR and stress responses (*Cdkn1a*, *Trp53*, *Egr1*, *Rbm7*, *Ubb*, *Hspa8*) were also trending or significantly increased in the 12-mo STING$^{-/-}$ brains

compared to age-matched WT (**Figure 3.1.11A**), further supporting STING's role in controlling DNA damage with age.

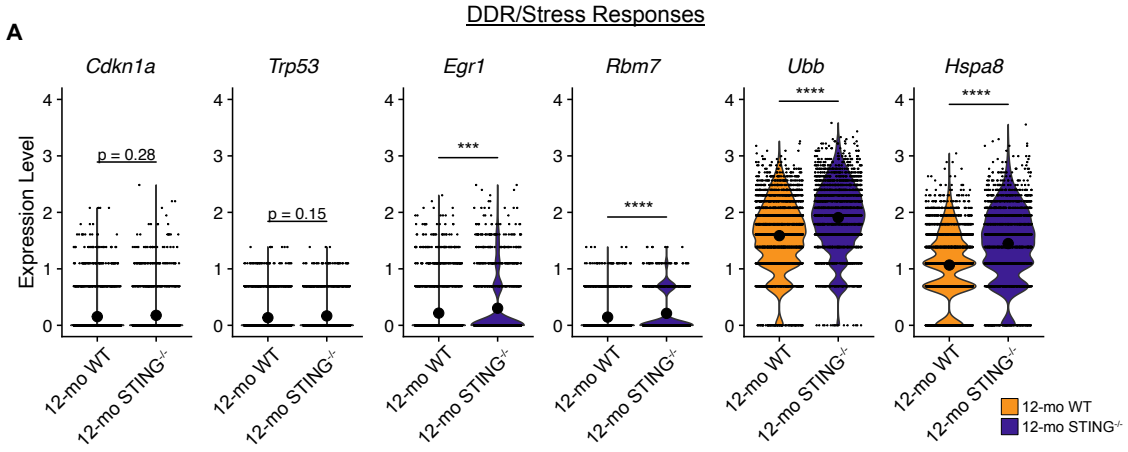

Figure 3.1.11.STING suppresses DNA damage response-associated genes at 12-mo.
(A) Violin plots of DNA damage response genes *Apoe*, *Junb*, *Nfkbia*, *Fos* from 12-mo WT and STING$^{-/-}$ single cells.

Furthermore, transcriptional drivers of inflammation, cellular stress, and senescence (*Apoe*, *Nfkbia*, *Junb, Fos*)[190-192] were increased significantly in 12-mo STING$^{-/-}$ aged CNS cells compared to young and WT controls (**Figure 3.1.12A**).

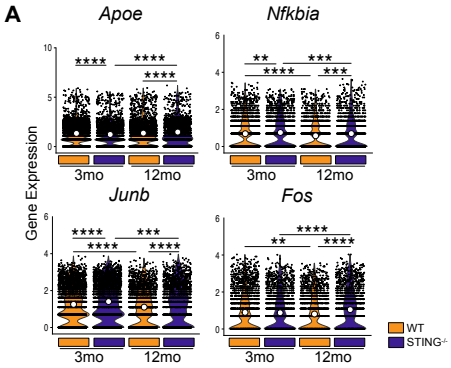

Figure 3.1.12. NF-κB and AP1 associated genes are increase in 12-mo STING$^{-/-}$ cells.
(A) Violin plots of disease/age-associated inflammatory genes *Apoe*, *Junb*, *Nfkbia*, *Fos* from 3-mo and12-mo WT and STING$^{-/-}$ single cells.

These data showcase a potential change in inflammatory pathways that are dependent on STING-signaling. The signatures are generally restrained in the aging process through STING-dependent signals. The presence of these proinflammatory signatures with potentially pathological roles in the STING$^{-/-}$ CNS, suggest presence of these atypical pro-inflammatory signatures in the STING$^{-/-}$ CNS suggest that these that these signatures are generally restrained in the aging process through STING-dependent signals.

Given the overall increase in a proinflammatory immune profile in the mature STING-deficient (12-mo) CNS, we next sought to understand if these changes were persistent with advanced age (24-mo) and furthermore, if there were any notable shifts in the CNS-resident cell types. Compared to the 12-mo dataset, we included all cells for sequencing from single cell suspensions for 2-mo and 24-mo WT and STING$^{-/-}$ brains to determine chronic changes in neural populations and other cell types that might occur after the 12-mo timepoint. To control for discrepancies between the quality and cellular heterogeneity in the 3- and 12-mo samples compared to 2- and 24-mo samples (**Appendix Figure 5.1.1**), the 2- and 24-mo WT and STING$^{-/-}$ scRNA-seq samples were investigated as an independent dataset (24-mo dataset) (**Figure 3.1.13C-D**). UMAP of cell distribution reveal that in addition to the prototypical immune clusters identified in our 12-mo dataset, we also found populations of resident glia (microglia, oligodendrocyte precursor cells (OPCs), oligodendrocytes, etc.) in the 24-mo dataset. Importantly, we identified key cell populations exclusively enriched in the 2- and 24-mo datasets i.e., astrocytes, excitatory and inhibitory neurons, in substantial numbers (**Figure 3.1.9C-D** and **Figure 3.1.13D**). Overall, the 24-mo dataset exhibited an accurate representation of the CNS composition with 60-70% neuronal populations and ~20% glia with 5-10% of the total CNS makeup being the resident microglia. We similarly conducted a pseudo-bulk analysis of the 24-mo cohort of the previous gene lists. Similar to the 12-mo cohort, 24-mo STING$^{-/-}$

animals upregulated pro-inflammatory genes (*Mmp9*, *Il1a*, *Tnf*, *Ccl5*), while 24-mo WT upregulated distinct senescence genes (*Hmgb1*, *C3*, *Igfbp6*) (**Figure 3.1.13C**), suggesting an altered functional inflammatory capacity. We next investigated the ISG panel, where STING$^{-/-}$ 24-mo cells upregulated a unique proinflammatory signature (*Cxcl10*, *Irf8*, *Il27*, *Ifng*), whereas 24-mo WT samples expressed many canonical ISGs (*Mx1*, *Ifitm3*, *Isg15*) (**Figure 3.1.13D**). We queried a broader array of inflammatory genes and saw that 24-mo STING$^{-/-}$ cells were enriched in genes described as DAMs (*Cst7*, *Apoe*, *Ctsc*, *Axl*) (**Figure 3.1.13E**), some of these genes were also upregulated at 12-mo. WT animals were downregulated in all of these genes when compared to age-matched STING$^{-/-}$, but some of these genes such as *Apoe* and *S100a9* were upregulated in both WT and STING$^{-/-}$ samples compared to young controls. Age-associated inflammation and senescence has been shown to be regulated by AP1 transcription[190], which require the expression of constituent transcription factor subunits, *Junb* and *Fos*. The expression of *Apoe* and *Junb* were significantly upregulated when comparing ages independent of genotypes, the aged STING$^{-/-}$ samples were only trending significantly compared to the aged WT (**Figure 3.1.13F**). *Nfkbia* and *Fos* expression was trending significantly in the 24-mo STING$^{-/-}$ compared to the 24-mo WT. The overall expression of these genes appears lower likely due to increased cellular diversity in the 24mo dataset.

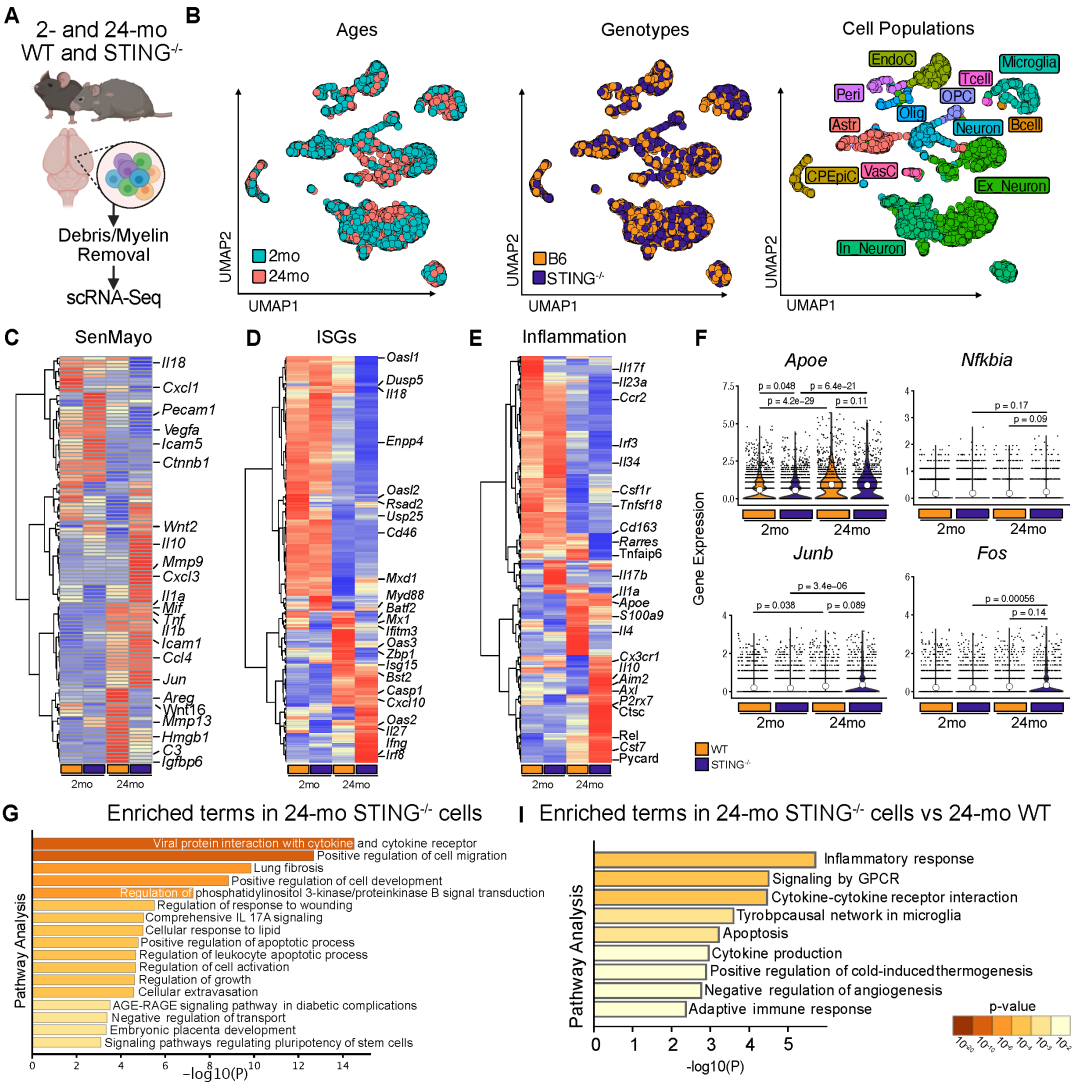

Figure 3.1.13. 24mo STING$^{-/-}$ cells exhibit proinflammatory responses.
(A) Schematic of live nucleated cell preparation for scRNA-seq analysis from a total of 11,496 cells (2-mo WT (n=2 (1 male and 1 female) combined prior to sequencing; 4152 cells), 24-mo WT (n=2 (1 male and 1 female) combined prior to sequencing; 2026 cells), 2-mo STING$^{-/-}$ (n=2 (1 male and 1 female) combined prior to sequencing; 3644 cells), and), 24-mo STING$^{-/-}$ (n=2 (1 male and 1 female) combined prior to sequencing; 1674 cells)). (B) Representative UMAP Representative UMAP(s) of ages independent of genotype (2-mo = teal; 24-mo = coral), genotypes independent of age (WT = gold; STING$^{-/-}$ = purple), and neuro/immune enriched cells clustered into 13 distinct cell types by specific markers (Neurons, Ex_Neuron., Excitatory Neurons, In_Neuron., Inhibitory Neurons, Astr (Astrocytes), OPCs; Oligodendrocyte Precursor Cell, Olig; Oligodendrocytes, Peri.; Pericytes, CPEpiC; Choroid Plexus Epithelial Cells, EndoC.; Endothelial Cells, Hb-EndoC.; Hemoglobin-associated endothelial cells, Microglia, B Cells, T Cells, (left to right as shown). (C) Heatmap of pseudo-bulk analysis of SenMayo genes from 3-mo WT, 3-mo STING$^{-/-}$, 12-mo WT, 12-mo STING$^{-/-}$ sequenced samples. (D) Heatmap of pseudo-bulk analysis of ISGs from 3-mo WT, 3-mo STING$^{-/-}$, 12-mo WT, 12-mo STING$^{-/-}$ sequenced samples. (E) Heatmap of pseudo-bulk analysis of

inflammatory genes from inflammatory response GO term (GO:0006954). Gene expression scaled for row maximum. (WT = gold; STING$^{-/-}$ = purple). (F) Violin plots of disease/age-associated inflammatory genes *Apoe*, *Junb*, *Nfkbia*, *Fos* from 2-mo and 24-mo WT and STING$^{-/-}$ single cells. (G) Metascape bar graph to visualize the top non-redundant enriched terms based on GO terms, KEGG pathways, Reactome, and CORUM in 24-mo STING$^{-/-}$ cells compared to all combined 3-mo WT, 3-mo STING$^{-/-}$, and 24-mo WT. Scale represents statistical significance. (I) Metascape bar graph to visualize the top non-redundant enriched terms based on GO terms, KEGG pathways, Reactome, and CORUM in 24-mo STING$^{-/-}$ cells vs 24-mo WT. Scale represents statistical significance.

Cells such as neurons and astrocytes, which are the predominant cells populations collected in the 24-mo dataset, do not highly express these genes compared to the microglia populations, which are 5-10% of the cells collected (**Figure 3.1.14**). This is compared to the 50-60% collected in the 12-mo cohort.

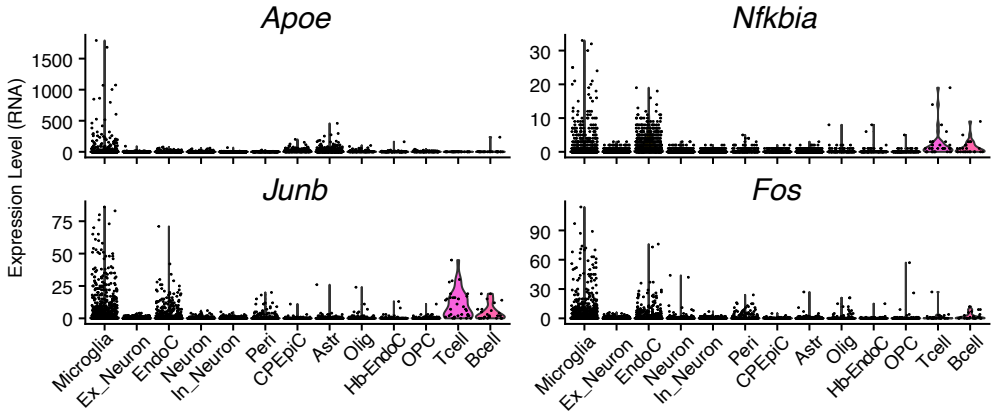

Figure 3.1.14. *Apoe*, *Nfkbia*, *Junb*, and *Fos* RNA expression levels.
Violin plots of RNA expression levels of *Apoe*, *Nfkbia*, *Junb*, *Fos* in cell populations collected from 24-mo cohort.

Next, we ascertained basic inflammatory states in the 24-mo dataset to understand how the longer lifespan of the aging mice impacts trends seen at 12-mo. Metascape pathway analysis[187] was performed on DEGs from 24-mo STING$^{-/-}$ against young controls and aged WT to determine age and genotype type specific DEGs. This analysis reveals an upregulation of pro-inflammatory networks in the aged STING$^{-/-}$ (i.e. viral responses, fibrosis, responses to wounding, regulation of apoptotic processes, etc.) (**Figure**

3.1.13G). Directed pathway analysis comparing 24-mo STING$^{-/-}$ and 24-mo WT genes similarly show a specific increase of terms of inflammatory responses identifying cell death pathways, such as GPCR-signaling downstream of cytokine signaling. (**Figure 3.1.13I**).

Age-associated inflammation and senescence has been shown to be regulated by AP1 transcription, which require the expression of constituent transcription factor subunits, *Junb* and *Fos*[190]. These genes similarly showed a trending increase in the STING$^{-/-}$ samples as in the 12-mo dataset (**Figure 3.1.13F**). Taken together, these data suggest that the STING$^{-/-}$ brain has a highly pro-inflammatory gene expression profile at both 12-mo and 24-mo compared to age-matched WT controls indicating a progressively more proinflammatory CNS with age.

3.1.3. **Loss of STING leads to blood brain barrier (BBB) breakdown and cognitive decline.**

During age-associated neurodegenerative disease states, inflammatory gene expression has been directly correlated to altered brain function[166,193,194]. To ascertain the functional impact of the notable changes in the inflammatory and immune landscape of the STING-deficient CNS, we conducted multi-pronged functional and behavioral assays to characterize neuro-motor capacity, locomotion, and memory with age. In contrast to previous studies[164], we noted non-significant but trending deficits in memory readouts in the aged STING$^{-/-}$ mice across lifespan when compared to age-matched WT mice (**Figure 3.1.15A-C**).

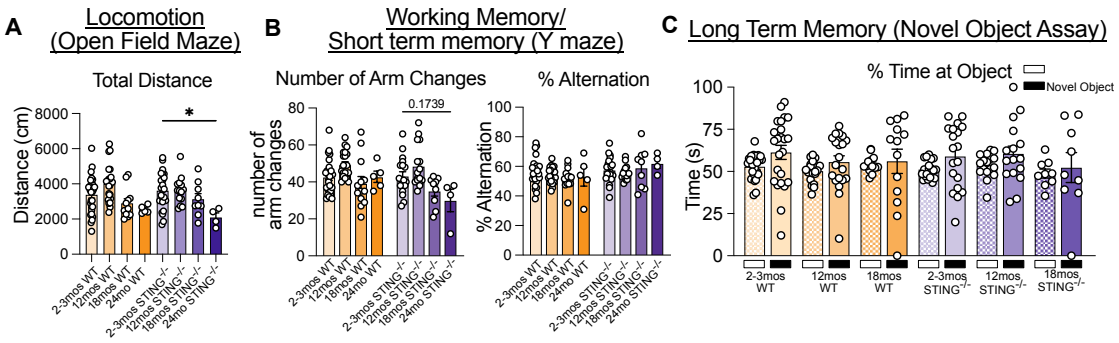

Figure 3.1.15. There are no major functional changes in memory functions of STING$^{-/-}$ mice with age.
(A) Bar graph depicts distance traveled during the full 10 minute period during open field maze from 3-mo WT (n = 29), 12-mo WT (n = 22), 18-mo (n = 12), 24-mo WT (n = 5), 3-mo STING$^{-/-}$ (n = 24), 12-mo STING$^{-/-}$ (n = 14), 18-mo STING$^{-/-}$ (n = 9), and 24-mo STING$^{-/-}$ (n = 4) mice. Data from 5 independent experiments. Each aged group (12-mo, 18-mo, 24-mo) contained 3-mo and genotype matched controls during 2 independent experiments. 24-mo group contained 3-mo and genotype matched controls. One-way ANOVA with Tukey's multiple comparisons test. ns: not significant. Error bars represent mean +/- SEM. (B) Bar graphs depict percent alternation during Y maze assay testing working and short-term memory. 3-mo WT (n = 27), 12-mo WT (n = 22), 18-mo (n = 13), 24-mo WT (n = 5) ,3-mo STING$^{-/-}$ (n = 21), 12-mo STING$^{-/-}$ (n = 16), 18-mo STING$^{-/-}$ (n = 9), and 24-mo STING$^{-/-}$ (n = 4) mice as above. Data from 5 independent experiments. Each aged group (12-mo, 18-mo) contained 3-mo and genotype matched controls during 2 independent experiments per aged group. 24-mo group contained 3-mo and genotype matched controls. First graph: number of arm changes made. Second graph: Percent alteration was calculated by dividing the number of alternations by the number of arm entries multiplied by 100. (C) Bar graphs depict the amount of time spent at the familiar object during the training day (checked bars) and the amount of time spent of the replaced novel object in the same position (solid bars) for 3-mo WT (n = 24), 12-mo WT (n = 20), 18-mo (n = 13),3-mo STING$^{-/-}$ (n = 19), 12-mo STING$^{-/-}$ (n = 16), and 18-mo STING$^{-/-}$ (n = 9). Data from 4 independent experiments. Each aged group (12-mo, 18-mo) contained 3-mo and genotype matched controls during 2 independent experiments per aged group. One-way ANOVA with Tukey's multiple comparisons test. **** p< 0.0001, ***p<0.001, **p<0.01, *p<0.05, ns = not significant. Error bars represent mean +/- SEM.

An early marker of neurodegeneration and neuromotor deficits is hindleg clasping[195]. Typically, rodents extend their limbs (splay) when anticipating contact with the ground, but when this reflex is decreased, clasping behavior increases[164,196]. The clasping score is based on two scales of a) 0-3 for quality of clasping and b) 0-5 for time to clasping, with higher numbers reflecting increased dysfunction (**Appendix Figure 5.1.3**). The 3-mo WT and STING$^{-/-}$ mice have an average score of 0, indicating an appropriate splay-

reflex of hindlimbs. However, clasping score significantly increased with age in the WT animals (**Figure 3.1.16A-C**). This impaired motor response was exacerbated in aged STING$^{-/-}$ mice (**Figure 3.1.16A-C**). To rule out the impact of muscular changes with age, we measured grip strength and found WT and STING$^{-/-}$ mice have similarly reduced muscle strength with age (**Figure 3.1.16D**).

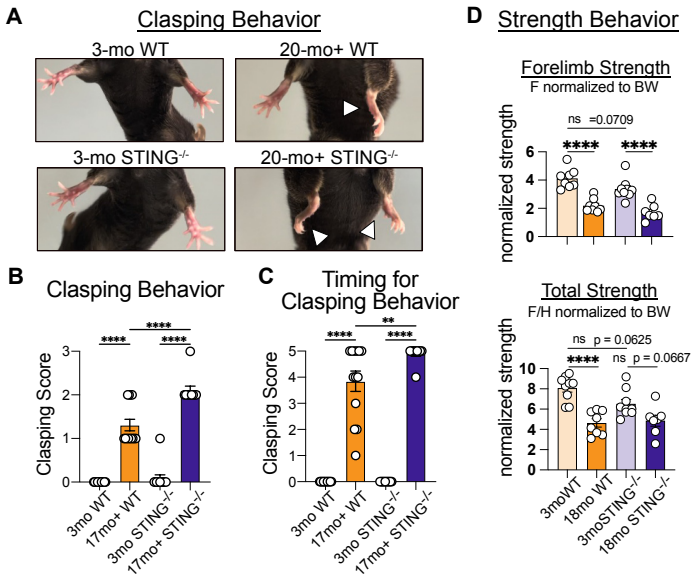

Figure 3.1.16. Neuromotor deficits are safeguarded by STING-signaling.
(A-C) Clasping behavior with age in WT and STING$^{-/-}$ mice. (A) Representative clasping behaviors of aged (20mo+) WT and STING$^{-/-}$ animals. White arrows represent clasping behavior. (B) Bar graphs depict the clasping behavior 0-3 scoring system representative of the amount of time hindlegs are retracted or splayed by a single leg or both legs (0 = hindlegs splayed away from abdomen, 1 = one hindleg retracted towards abdomen for 50% of the time, 2 = both hindlegs retracted towards abdomen for 50% of the time, 3 = hindlegs entirely retracted). (C) Bar graphs depict the clasping behavior 0-5 scoring system representative of the amount of time to retract hindleg(s). (0 = no clasping, 1 = in 31-60 seconds, 2 = in 16-30 seconds, 3 = in 11-15 seconds, 4 = in 10-6 seconds, 5 = in 1-5 seconds). Data are representative of biological replicates (n=10-13) and bar graphs show mean ± SEM and dots represent individual mice. (D) Bar graphs depict forelimb (F) grip strength normalized to body weight (BW). One-way ANOVA with Tukey's multiple comparisons test. Bar graphs depict the combined forelimb and hindlimb (F/H) grip strength normalized to body weight (BW). Error bars represent mean +/- SEM. One-way ANOVA with Tukey's multiple comparisons test. **** p< 0.0001, **p<0.01, ns = not significant.

Therefore, the clasping deficit in STING$^{-/-}$ mice supports specific neuromotor dysfunction with age, as an indication of neurological decline[195]. To determine if the observed neuro-

motor deficits were associated with impaired locomotion, we conducted an open field test measuring the total distance traveled. There was no age-dependent change in locomotion within WT controls. However, in contrast there was a significant age dependent decline in locomotion in STING$^{-/-}$ mice as well as a genotype dependent reduction in 24-mo old mice when STING-/- were compared to WT mice (Figure 3.1.17A-B). Combined, these data reveal how STING-deficiency promotes accelerated neuromotor decline with age.

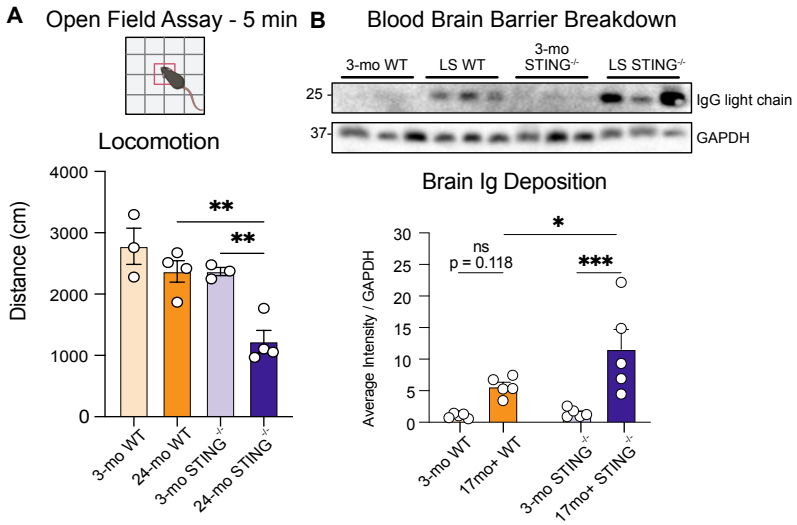

Figure 3.1.17. STING is essential for blood brain barrier integrity and locomotion with age.
(A) Graphic of open field maze with time used for analysis. Bar graph depicts the distance traveled during open field behavioral assay from 3-mo and 24mo WT and STING$^{-/-}$ mice during the first 5 minutes of the video collection. Measurement in cm (E). Data represents ±SEM from 3-4 biological replicates with error bars and dots representing individual mice. (B) IgG light chain and GAPDH western blot from 3-mo and LS) WT and STING$^{-/-}$ brain lysates. Bar graphs depict quantification of WB IgG light chain normalized to GAPDH. Data represents ±SEM from 5 biological replicates with error bars and dots representing individual mice.

Cognitive and locomotive deficits commonly seen with age and age-associated neurodegenerative diseases, such as Alzheimer's disease are often linked to a compromised blood-brain-barrier (BBB) and microhemorrhages[195,197,198]. The BBB is critical for maintaining brain homeostasis and is disrupted during aging and

neurodegenerative diseases states[199]. BBB integrity is often tested by the increased permissiveness of the CNS barrier to peripheral immune components such as re-circulating IgG[200]. We thus measured IgG levels by western blotting lysates of brains from STING$^{-/-}$ and WT 3-mo and LS (17-mo+) brains. Importantly, while very little IgG was detected in WT and STING$^{-/-}$ 3-mo mice, we note a significant increase of IgG light chain in the LS STING$^{-/-}$ brain lysate compared to LS WT (**Figure 3.1.17B**). Compromised BBB can be associated with microhemorrhages which have direct correlations to cognitive deterioration, dementia, and other neurovascular outcomes such as ischemic or hemorrhagic stroke[201]. To identify any incidence of microhemorrhages and evidence of bleeding, we measured iron deposits in the brain by Prussian blue staining, which directly binds iron in tissue sections. We noted accumulation of iron deposits within deep subcortical locations, such as the

hippocampus and thalamus, and ventricle spaces at the end of life (LS) in WT and STING$^{-/-}$ brains (**Figure 3.1.18A**).

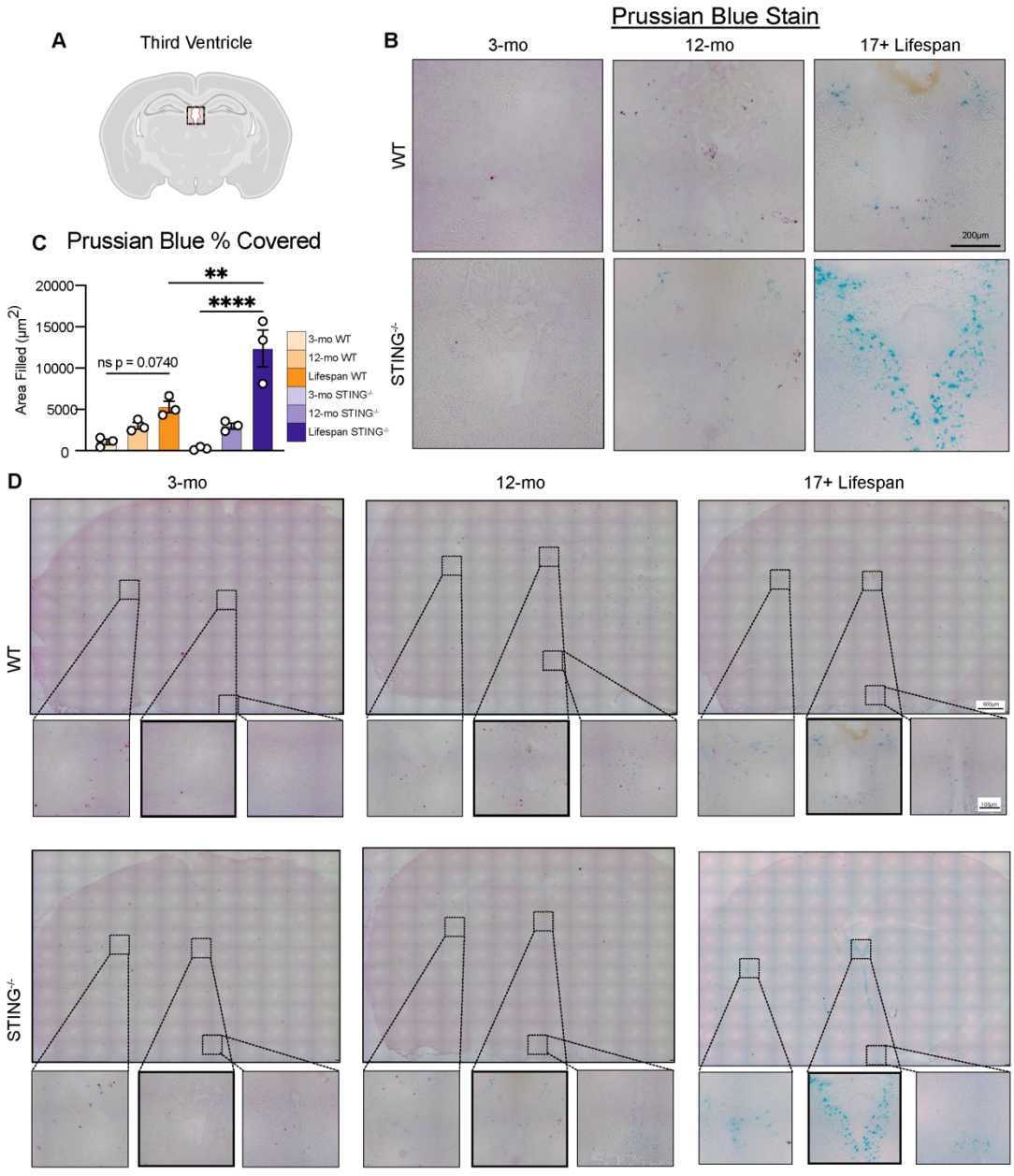

Figure 3.1.18. STING is essential for protection against microhemorrhages seen with age.
(A)Schematic showing third ventricle to show where representative images are focused. (B) Representative Prussian Blue staining of 3-mo (n = 3) and LS (n = 3) WT and STING$^{-/-}$ in the third ventricle. (C) The bar graph depicts quantification of Prussian Blue staining. Data from 3 biological replicates and scale bars 200µm. (D) Representative images of Prussian Blue stain from whole brains. Scale bars at 600µm. Below whole brain images are three zoomed in representative images from the ventricle spaces seen

in (B) and scales bars are 100μm. Black box indicates which figures were used in (B) 3-mo WT (n = 3), 12-mo WT (n = 3), LS WT (n = 3), 3-mo STING$^{-/-}$ (n = 3), 12-mo STING$^{-/-}$ (n = 3), and LS STING$^{-/-}$ (n = 3) were stained and imaged. Graph graphs represent data by mean ±SEM and dots represent individual mice. One-way ANOVA followed by Bonferroni correction factor. **** p< 0.0001, **p<0.01.

Iron deposition increased with age in WT, indicating microbleeds or microhemorrhages, with age (**Figure 3.1.18B-C).** Although 12-mo STING$^{-/-}$ and WT brains had similar levels of iron deposits, at LS, STING$^{-/-}$ brains displayed a significantly increased incidence of iron deposition specifically near the third ventricle, lateral ventricle, and choroid plexus regions compared to aged-matched LS WT (**Figure 3.1.18D**). Ventricle spaces border areas in contact with the cerebrospinal fluid (CSF) vasculature[202] and are thought to be anatomically related to the hippocampus[203], where we saw a decrease of senescent markers (**Figure 3.1.6**). Overall, we note that cognitive impairments in the STING$^{-/-}$ animals are associated with increased BBB permeability and evidence of microhemorrhages demonstrating that STING-activity protects against a multimodal, accelerated functional decline in aging mice.

3.1.4. **STING-deficiency modulates populations, inflammatory markers and transcriptional landscapes of homeostatic and precursor microglia.**

The breakdown of the BBB suggests that several key stromal populations such as endothelial cells or pericytes alongside microglia and astrocytes are likely impacted. We thus, leveraged unbiased predictive physical interactions (receptor-ligand interactions) and immune signaling components (chemokine-chemokine receptor interactions) by RNAMagnet[165] between stromal populations (choroid plexus epithelial cells (CPEpiC), endothelial cells (EndoC), and previously identified hemoglobin-associated endothelial cells[204] (Hb-EndoC)) and remaining CNS cell populations in our scRNA-seq dataset. Importantly, microglia emerge as the key population that experience any significant changes in cell-cell interactions with age. Microglia are a critical cell type for maintained

BBB integrity and their interaction is imperative for their function[205]. In line with this, we note that microglia likely interact with all three stromal populations (CPEpiC, EndoC, and Hb-EndoC) at 3-mo and with age shift to interact primarily with hemoglobin-associated endothelial cells in 12-mo WT and STING$^{-/-}$ brains (**Figure 3.1.19A-B**).

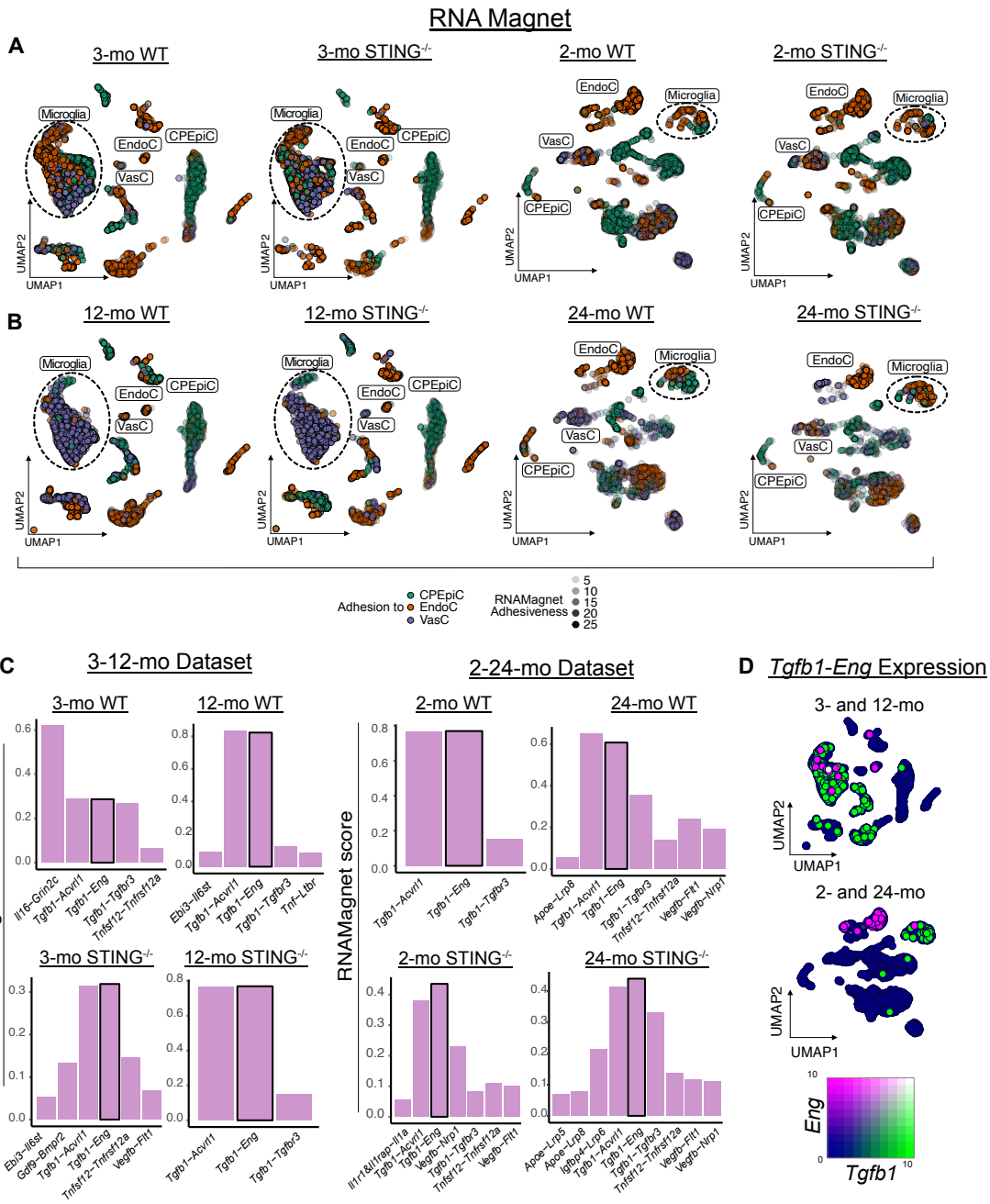

Figure 3.1.19. RNAMagnet interactions of microglia and endothelial cell populations.

(A) UMAP visualization of stromal, glial, and neuronal populations based on predicted adhesiveness of stromal populations using RNAMagnet of 3-mo WT, 3-mo STING$^{-/-}$, 12-mo WT, 12-mo STING$^{-/-}$, 2-mo WT, and 2-mo STING$^{-/-}$ cells, 24-mo WT, and 24-mo STING$^{-/-}$ cells, respectively. Colors represent anchored populations (CPEpiC (Choroid plexus epithelial cells): green, EndoC (Endothelial cells): orange, VasC (vascular cells): purple) and opacity represents strength of adhesion 5 through 25 with increased intensity. (C) RNAMagnet significant receptor ligand pairs from 3- and 12-mo dataset and 2- and 24-mo full datasets based on the RNAMagnet score. *Tgfb1-Eng* pairing highlighted by black outline on bar graph. (D) Feature plot of significant interactions from RNA Magnet analysis; Endoglin (*Eng*) (magenta) and Transforming growth factor beta 1 (*Tgfb1*) (green). Top UMAP is 3-12-mo dataset and bottom UMAP is the 2-24-mo dataset.

In contrast, at 24-mo, WT microglia primarily interact with the CPEpiC population, but STING$^{-/-}$ microglia populations further shift their interaction to EndoCs (**Figure 3.1.19A-B**). These cumulative shifts indicate that preferential interactions of microglia with vascular cells may be central in driving BBB dysfunction during aging, especially through cues typically moderated by STING-signaling and in the absence of STING, these interactions turn increasingly more pathological resulting in heightened BBB breakdown. In both 12-mo and 24-mo datasets, receptor-ligand pairs for Endoglin (*Eng*) and Transforming growth factor beta 1 (*Tgfb1*) emerge as the most significant pairings between EndoCs and microglia in STING$^{-/-}$ and WT brains, further supporting the importance of these interactions (**Figure 3.1.19C-D**). Endoglin and TGF-β are essential during angiogenesis and microvascular health in the brain[206-208] and thus changes in their interactions implicate microglia as critical arbiters of STING-dependent changes in CNS vascular health and neuromotor function. We next evaluated if there were visible changes in the ability of microglia to interact with endothelial cells with age and STING deficiency *in situ*. Though subtle, we noted overall decreases in numbers of CD31+ cells

and their colocalization with CD68+ cells in the aged STING$^{-/-}$ from all regions compared to aged WT regions (**Figure 3.1.20A-B**).

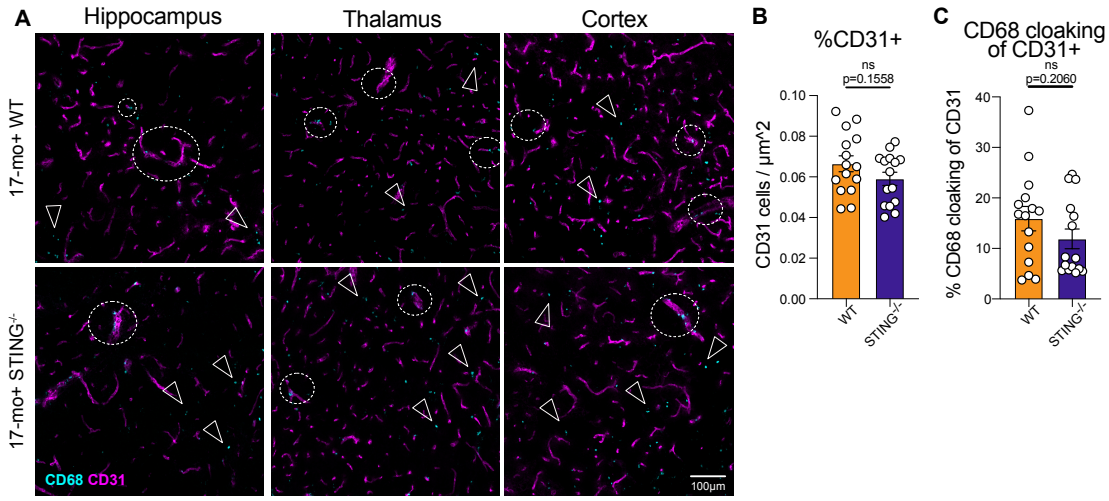

Figure 3.1.20. Endothelial and microglia interactions with hippocampus, thalamus, and cortex.
(A) Representative immunofluorescent images for CD68 (cyan) and CD31 (magenta) in the hippocampus, thalamus, and cortex regions from combined LS WT and STING$^{-/-}$ (n=6) Scale bars are 100µm scale bars. Circles highlight CD68 cloaking CD31 or colocalization, arrows highlight CD68 single stain or no colocalization. (B) Bar graphs depict quantification of percent (%) of CD31+ cells and (C) %CD68 colocalized with CD31, referred to as cloaking. Error bars represent mean ±SEM. Student's t test was run with Welch's correction. ns = not significant.

Thus, as endothelial cells and microglia localization are marginally disrupted in STING$^{-/-}$ brains compared to WT, it is likely that paracrine signals between these cells or altered cell-cell interactions, as well as the inflammatory milieu may play a more important role in shaping BBB integrity.

To reliably quantitate changes in microglia populations themselves with aging, we sought to immunophenotype microglia populations by multiparameter spectral flow cytometry (24 parameters) of CNS single-cell suspensions from WT and STING$^{-/-}$ mice at 3- and 14-mo of age (**Figure 3.1.21A**). CD45 and CD11b expression of singlets are used to differentiate lymphocytes (CD45^{hi}CD11b^{-}), infiltrating monocytes

(CD45^{hi}CD11b^{hi}), and microglia (CD45^{int}CD11b^{+}) (**Appendix Figure 5.1.4** and **Figure 3.1.21B-C**).

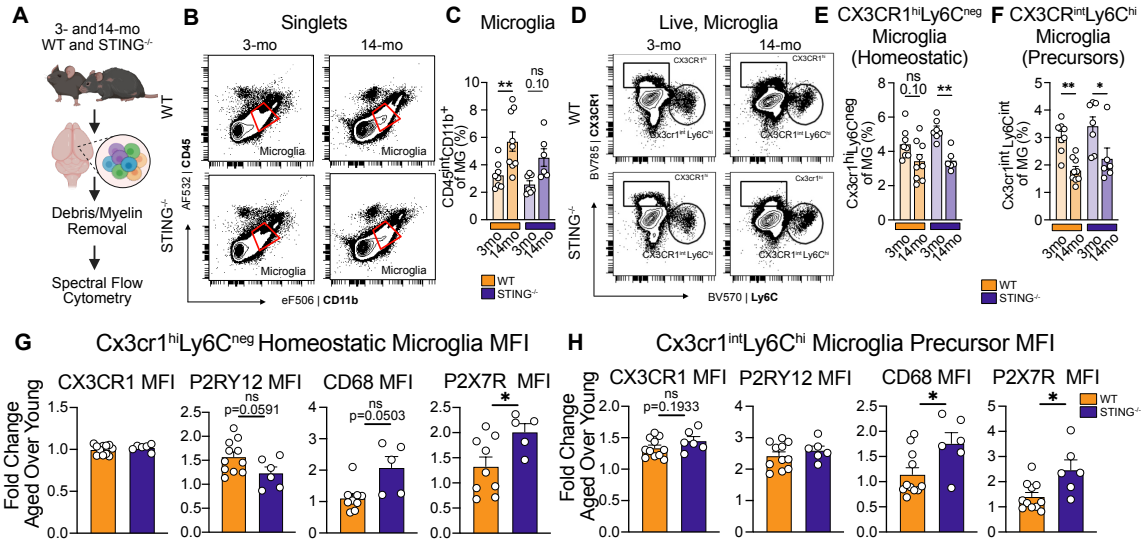

Figure 3.1.21. Microglia populations increase with age and inflammatory profiles are stifled by STING-signaling with age.
(A) Schematic of live nucleated cell preparation for of 3- and 14-mo WT and STING$^{-/-}$ brains processed through debris removal steps and prepared for flow cytometry. (B) Flow cytometry graphs of CD45 and CD11b from singlets to identify microglia. (C) Bar graphs depict microglia percentage quantification from singlets and lymphocytes (3mo WT; n = 8, 14mo WT; n = 9, 3mo STING$^{-/-}$; n = 7, 14mo STING$^{-/-}$; n = 6). Orange box with black outline = WT mice; Purple box with black outline = STING$^{-/-}$ mice. Ages are based on increased intensity of corresponding colors. Bar graphs represent data by mean ±SEM and dots represent individual mice. One-way ANOVA followed by Bonferroni correction factor. **p<0.01, *p<0.05, ns: not significant. (D) Flow cytometry graphs of microglia expressing CX3CR1 and Ly6C. Graphs are representative of each group. (E) Bar graphs depict percentage of CX3CR1 ^{hi}, Ly6C^{neg} microglia (homeostatic) population from young and aged WT and STING$^{-/-}$ brains. (F) Bar graphs depict the percentage of CX3CR1 ^{int}, Ly6C^{hi} microglia (precursor) population from young and aged WT and STING$^{-/-}$ brains. Bar graphs represent data by mean ±SEM and dots represent individual mice. One-way ANOVA followed by Bonferroni correction factor. **p<0.01, *p<0.05, ns is not significant. (G) Bar graphs depict fold change (FC) in MFI of markers in individual aged mice over the geometric mean MFI of young mice from CX3CR1^{hi}Ly6C^{neg} microglial populations MFI of CX3CR1, P2RY12, CD68, P2X7R, respectively. (H) Bar graphs depict FC of aged animals over young geometric mean from Cx3cr1^{int}Ly6C^{hi} microglia populations MFI of CX3CR1, P2RY12, CD68, P2X7R, respectively. Bar graphs represent data by FC ±SEM and dots represent individual mice. Student's t-test was run. *p<0.05, ns is not significant.

This broad category of microglia undergoes an age-dependent increase that only reaches significance in WT but not STING$^{-/-}$ brains even when powered to reveal shifts

(**Figure 3.1.21C**). These data support previous descriptions of age-associated microgliosis, i.e. a proliferation of microglia in response to accumulating damage during aging[37] and further suggest that microgliosis is at least in part STING-dependent.

Recent studies reveal significant heterogeneity in the CNS microglia populations in heathy and diseased states[173,174,188,209]. To evaluate subset specific changes within the microglia population with age that may explain the overall changes in the microglia populations, we expanded the identification and annotation of microglia to include CX3CR1 and Ly6C (**Appendix Figure 5.1.4**). CX3CR1 and Ly6C expression can be reliably used to delineate homeostatic microglia and precursor microglia as described previously[210,211]. Importantly, we note a specific and significant decrease in homeostatic microglia ($CX3CR1^{hi}Ly6C^{neg}$) with age in $STING^{-/-}$ brains at 14-mo compared to age matched WT and young controls (**Figure 3.1.21D-E** and **Figure 3.1.22B-E**). In addition to this, we evaluated precursor microglia, which are proposed to repopulate a depleted microglial niche over time ($CX3CR1^{int}Ly6C^{hi}$)[210,211]. Intriguingly, both the WT and $STING^{-/-}$ CNS reveal a significant decrease in this population with age, although there are equivalent numbers of these precursors at 3-mo in both genotypes (**Figure 3.1.21F**). These data suggest that the aging $STING^{-/-}$ CNS is unable to support the renewal of homeostatic microglia or their repopulation from circulating precursors. Moreover, it is reasonable to speculate that this process at least partially, if not wholly, impacts microgliosis in the $STING^{-/-}$ brains as well, potentially restraining these protective microglia transition to rein-in accumulating damage. Lack of consistent replenishment with precursors with age likely shifts the subset distribution of microglia in the CNS and explain the age-dependent phenotypes we outline thus far.

We next investigated relative expression levels of known homeostatic and inflammatory cell surface markers. In the total microglia ($CD45^{int}/CD11b^{+}$) population, we saw no changes in the mean fluorescent intensity (MFI) of the homeostatic markers CX3CR1

and a significant increase in the other homeostatic marker, P2RY12 in WT animals (**Figure 3.1.22F**). In contrast, expression of proinflammatory markers (P2X7R and CD68) in the total microglia populations were significantly increased in the STING$^{-/-}$ microglia population, suggesting that STING$^{-/-}$ microglia display higher levels of proinflammatory cell surface markers with age that may skew their functional responses (**Figure 3.1.22G**).

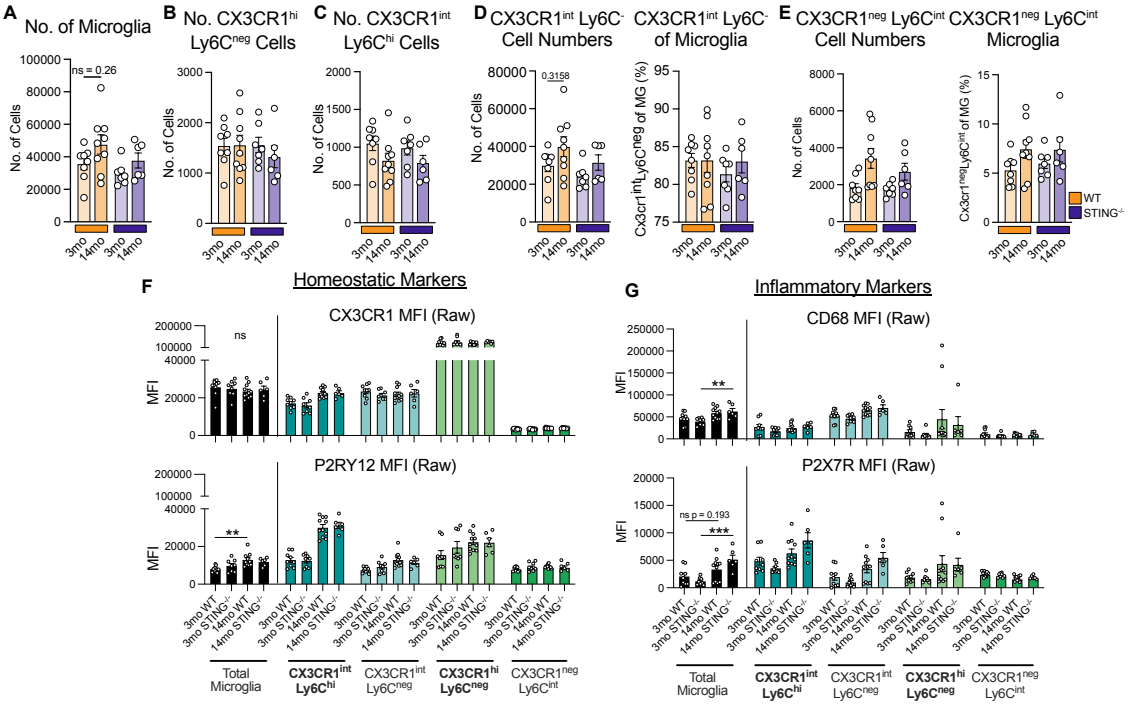

Figure 3.1.22. Microglia populations based on CX3CR1 and Ly6C expression with age.
(A) Quantification of number of microglia (3mo WT; n=8, 14mo WT; n=9, 3mo STING$^{-/-}$; n=7, 14mo STING$^{-/-}$; n=6. (B) Quantification of number of CX3CR1^{hi}Ly6C^{neg} microglia (3mo WT; n = 8, 14mo WT; n=9, 3mo STING$^{-/-}$; n=7, 14mo STING$^{-/-}$; n=6). (C) Quantification of number of CX3CR1^{int}, Ly6C^{hi} microglia (3mo WT; n=8, 14mo WT; n=9, 3mo STING$^{-/-}$; n=7, 14mo STING$^{-/-}$; n=6). (D) Quantification of number of CX3CR1^{int}, Ly6C^{neg} microglia (3mo WT; n=8, 14mo WT; n=9, 3mo STING$^{-/-}$; n=7, 14mo STING$^{-/-}$; n=6) followed by quantification of percentage of CX3CR1^{int}, Ly6C^{neg} from total microglia (3mo WT; n=8, 14mo WT; n=9, 3mo STING$^{-/-}$; n=7, 14mo STING$^{-/-}$; n=6). (E) Quantification of number of CX3CR1^{neg}, Ly6C^{int} microglia (3mo WT; n=8, 14mo WT; n=9, 3mo STING$^{-/-}$; n=7, 14mo STING$^{-/-}$; n=6) followed by quantification of percentage of CX3CR1^{neg}, Ly6C^{int} from total microglia (3mo WT; n = 8, 14mo WT; n = 9, 3mo STING$^{-/-}$; n = 7, 14mo STING$^{-/-}$; n = 6). (F) Raw MFI values of homeostatic markers: CX3CR1and P2RY12, respectively, from total microglia (black), CX3CR1^{int}, Ly6C^{hi} (dark teal), CX3CR1, Ly6C^{neg} (light teal), CX3CR1^{hi}Ly6C^{neg} (light green), CX3CR1^{neg}, Ly6C^{int} (dark green). Bar graphs represent data by mean ± SEM and dots represent individual mice.

One-way ANOVA followed by Bonferroni correction factor for total microglia only. (G) Raw MFI values of inflammatory markers: CD68 and P2X7R, respectively, from total microglia (black), CX3CR1^{int}, Ly6C^{hi} (dark teal), CX3CR1^{int}, Ly6C^{neg} (light teal), CX3CR1^{hi}Ly6C^{neg} (light green), CX3CR1^{neg}, Ly6C^{int} (dark green). Bar graphs represent data by mean ± SEM and dots represent individual mice. One-way ANOVA followed by Bonferroni correction factor for total microglia only. ***p<0.001, **p<0.01, ns = not significant. Raw MFI values of inflammatory markers: CD68 and P2X7R, respectively, from total microglia (black), CX3CR1^{int}, Ly6C^{hi} (dark teal), CX3CR1^{int}, Ly6C^{neg} (light teal), CX3CR1^{hi}Ly6C^{neg} (light green), CX3CR1^{neg}, Ly6C^{int} (dark green). Bar graphs represent data by mean ± SEM and dots represent individual mice. One-way ANOVA followed by Bonferroni correction factor for total microglia only.

We further ascertained how these markers change with age in the specific microglia populations altered in the aging STING$^{-/-}$ CNS. Specifically, the canonically homeostatic microglia populations (CX3CR1^{hi}Ly6C^{neg}) saw an overall decrease of P2RY12 MFI in the aged STING$^{-/-}$ animals compared to WT controls. This same population exhibited a significant increase in MFI of P2X7R and trending increase of CD68 in the STING$^{-/-}$ cells (**Figure 3.1.21G**), demonstrating that with age, STING-deficiency impacts overall function of homeostatic microglia and shapes them into a more inflammatory subset. Further, the precursor microglia (CX3CR1^{int}Ly6C^{hi}) show no changes in the expression of cell-surface CX3CR1 and P2RY12 but significantly increase the expression of inflammatory markers P2X7R and CD68 with age, selectively in the STING$^{-/-}$ microglia (**Figure 3.1.21H**). Thus, STING-signaling uniquely shapes the inflammatory landscapes of key subsets of the microglia populations that remain with age.

To further understand the impact of STING-expression in shaping microglia transcriptomes with age, we investigated the microglia population within the scRNA-Seq dataset. First, we note that, within the CNS populations collected from both the 12-mo and 24-mo dataset, STING (*Tmem173*) is predominantly expressed in the microglia in

agreement with previous studies[126,212,213] (**Figure 3.1.23A-B**).

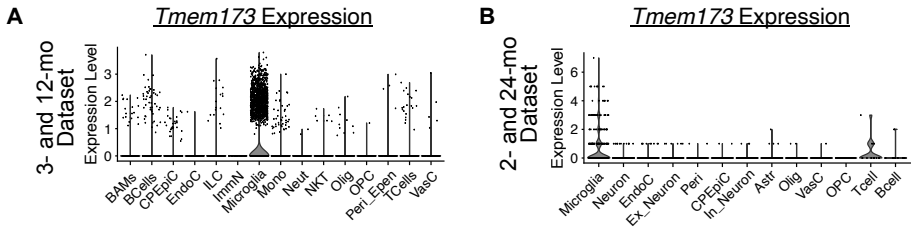

Figure 3.1.23 *Tmem173* expression level in scRNA-Seq identified clusters.
(A) Violin plot of the expression level of *Tmem173* in 12-mo dataset based on cell type in WT samples. (B) Violin plot of the expression level of *Tmem173* in 24-mo dataset based on cell type in WT samples.

Thus, with quantitative differences in microglia subsets and the propensity of STING to signal predominantly in this glial population, we next determined changes in the transcriptional landscape of the microglia population (**Figure 3.1.24A**).

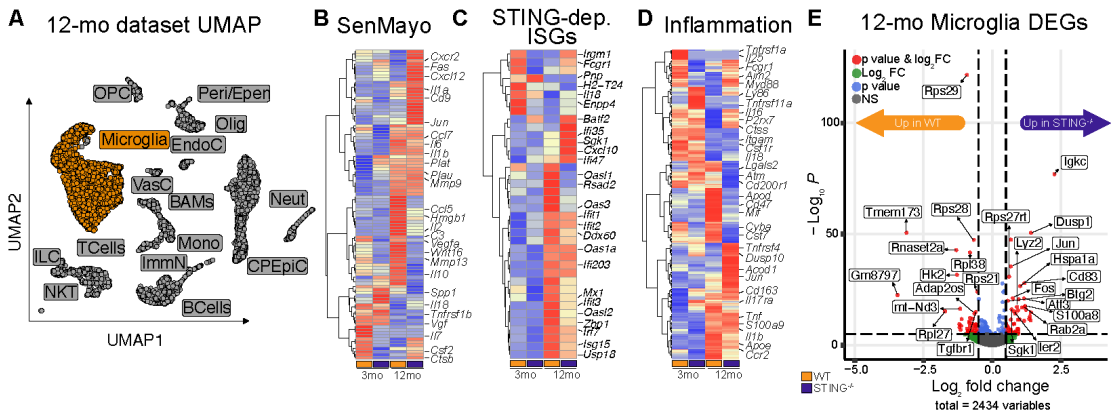

Figure 3.1.24. Proinflammation transcriptional landscape are stifled by STING-signaling with age.
(A) Representative UMAP from combined 3- and 12-mo cells and both genotypes (WT and STING$^{-/-}$) highlighting the microglia population in orange that were subsetted for the following analyses. Other cells identified are grey. (B) Heatmap of pseudo-bulk analysis of SenMayo genes from 3-mo and 12-mo WT and STING$^{-/-}$ samples. (C) Heatmap of pseudo-bulk analysis of ISGs from 3-mo and 12-mo WT and STING$^{-/-}$ samples. (D) Heatmap of pseudo-bulk analysis of inflammatory genes from inflammatory response GO term (GO:0006954) from 3-mo and 12-mo WT and STING$^{-/-}$. Gene expression scaled for row maximum. Gold=WT, purple=STING$^{-/-}$. (E) Volcano plot of genes differentially expression in 12-mo STING$^{-/-}$ microglia relative to 12-mo WT. Dots: Red; p value and log2FC, green; Log2FC, blue; p value, grey; not significant (ns).

For this we leveraged initial pseudo-bulk sequencing analysis of microglia in our 12-mo dataset, to determine specific changes in the senescence, IFN-I, and inflammatory signatures (**Figure 3.1.24B-D**). Critically, aged STING$^{-/-}$ microglia exhibit increased expression of inflammation-associated senescence genes (senescence associated secretory proteome; SASP) (*Il1a*, *Cxcr2, Cxcl12),* compared to young control and WT samples. Further, aged STING$^{-/-}$ microglia show decreased expression of genes that induce senescence (*Hmgb1, Vegfa*, *Wnt16*) compared to 12-mo WT microglia (**Figure 3.1.24B**). This expression profile suggests that microglia with STING-deficiency favor an elevated inflammatory state *in lieu* of decreased classical senescent markers like *Cdkn1a/2a, Hmgb1* and *C3*[119,139] compared to age-matched WT microglia.

We next queried the expression of a curated list of STING-dependent ISGs generated from our dataset and others[214,215] to probe for changes in STING-dependent IFN-I responses. Aged WT microglia upregulate the largest number of the ISGs (*Ifit3*, *Isg15*, *Oas3*), while aged STING$^{-/-}$ microglia downregulate a number of these same ISGs (**Figure 3.1.24C**). Importantly, STING-deficient microglia specifically expressed a limited set of ISGs that have known proinflammatory roles (*Cxcl10*, *Ifi47, Batf2* and *Sgk1*)[188,216] (**Figure 3.1.24D**). Both the senescence and ISG landscape indicate a definitive molding of the STING$^{-/-}$ microglia towards a more pro-inflammatory signature. Thus, we directly queried the expression of canonical proinflammatory genes as above. Microglia from 12-mo WT CNS specifically express key genes that define a neuroinflammatory/disease-associated microglia (DAM) signature (*Cst7*, *Mif*, and *Apoe)*, compared to the other ages and genotypes (**Figure 3.1.24D**). Directed DEG analysis between 12-mo WT and STING$^{-/-}$ microglia highlighted a unique inflammatory gene signature enriched in the STING cells, specifically, *Jun*, *Fos*, *S100a8*, *Dusp1* as well other inflammatory, disease- and stress-associated genes (*Mapk3* and *Clu*)[166,173,217], that were selectively and significantly upregulated in STING$^{-/-}$ microglia (**Figure 3.1.24E**). These data highlight

several key takeaways, 1) microglia are the primary drivers of the inflammatory signature that was seen in the whole brain analysis. 2) We reveal that STING$^{-/-}$ microglia have a unique proinflammatory profile that differentiates them from their young and aged WT controls. Overall, these data suggest that STING-signaling is important for maintenance of homeostatic expression and function of microglia during physiological aging. Microglial STING-signaling is necessary to protect against neuromotor decline and BBB breakdown.

3.1.5. **Microglial STING-signaling is a gatekeeper of neuromotor function and BBB integrity**

Given these remarkable findings in microglia, we next wondered if the loss of STING in microglia is sufficient to drive neurodegenerative effects and the overall behavior with aging that we noted previous for the whole-body STING$^{-/-}$ mice. We thus generated and aged *Csf1r*-Cre^{POS} *Tmem173*$^{flox/flox}$ (MG$^{STING-/-}$) and littermate control *Csf1r*-Cre^{NEG}; *Tmem173*$^{flox/flox}$ (MG^{WT}) mice that would ablate STING expression specifically in microglia and other resident macrophage populations found in the brain, such as BAMs or perivascular macrophages. Neuro-motor functional assays reveal that MG$^{STING-/-}$ mice had similar significant neuromotor impairments as global STING$^{-/-}$ mice exhibited (**Figure 3.1.16**) and compared to MG^{WT} mice. The MG$^{STING-/-}$ mice showcase a severe decrease in splaying behavior compared to their aged- matched MG^{WT} and young controls (**Figure 3.1.25A-C**).

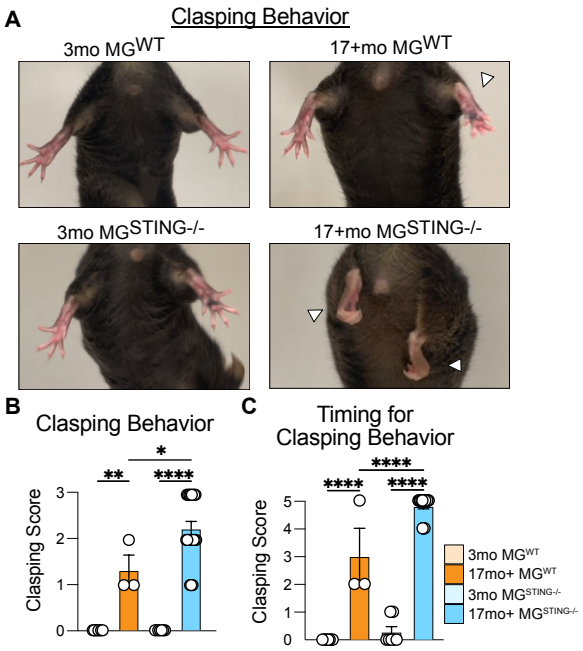

Figure 3.1.25. Clasping behavior is worse with age in MG$^{STING-/-}$ mice.
(A) Representative clasping behaviors of 2-3-mo MG^{WT}, (n=8), 2-3-mo MG$^{STING-/-}$ (n=7), 17-mo+ MG^{WT} (n=3) and 17-mo+ MG$^{STING-/-}$ (n=20) animals. White arrows represent clasping behavior. (B) Bar graphs depict the clasping behavior 0-3 scoring system representative of the amount of time hindlegs are retracted or splayed by a single leg or both legs (0 = hindlegs splayed away from abdomen, 1 = one hindleg retracted towards abdomen for 50% of the time, 2 = both hindlegs retracted towards abdomen for 50% of the time, 3 = hindlegs entirely retracted). (C) Bar graphs depict the clasping behavior 0-5 scoring system representative of the amount of time to retract hindleg(s). (0 = no clasping, 1 = in 31-60 seconds, 2 = in 16-30 seconds, 3 = in 11-15 seconds, 4 = in 10-6 seconds, 5 = in 1-5 seconds). Data represents ±SEM from 5 biological replicates with error bars and dots representing individual mice. . **** p< 0.0001, **p<0.01, *p<0.05, not significant (ns).

Critically, the MG$^{STING-/-}$ mice have a visually more pronounced retention of the hindlegs compared to STING$^{-/-}$ mice (**Figure 3.1.26A**), as is noted with the more retracted hindlegs towards the abdomen.

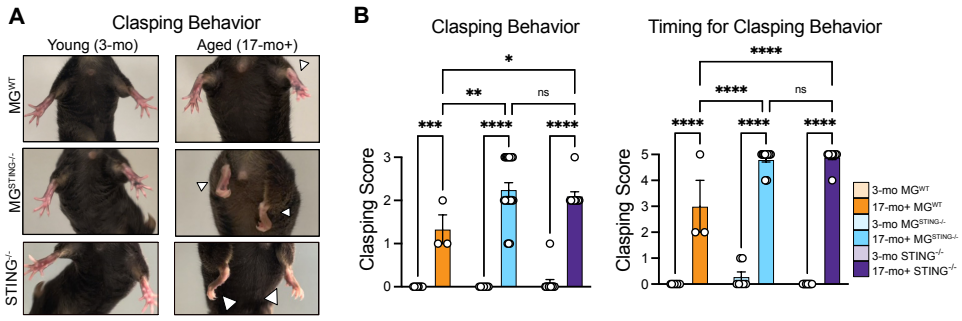

Figure 3.1.26. MG^{WT}, MG$^{STING-/-}$, and STING$^{-/-}$ clasping behavior.
(A) Representative clasping behaviors of aged (17mo+) MG^{WT}, MG$^{STING-/-}$, and STING$^{-/-}$ animals. White arrows represent clasping behavior. (B) Bar graphs depict the clasping behavior 0-3 scoring system representative of the amount of time hindlegs are retracted or splayed by a single leg or both legs (0 = hindlegs splayed away from abdomen, 1 = one hindleg retracted towards abdomen for 50% of the time, 2 = both hindlegs retracted towards abdomen for 50% of the time, 3 = hindlegs entirely retracted). Second bar graphs depict the clasping behavior 0-5 scoring system representative of the amount of time to retract hindleg(s). (0 = no clasping, 1 = in 31-60 seconds, 2 = in 16-30 seconds, 3 = in 11-15 seconds, 4 = in 10-6 seconds, 5 = in 1-5 seconds). Data are representative of biological replicates (n=10-13) and bar graphs show mean ± SEM and dots represent individual mice. Two-way ANOVA with Tukey's correction factor.

To determine the if the neuromotor deficits corresponded with the declining BBB integrity, as was seen with global STING$^{-/-}$ brains, we measured IgG abundance in the brain. We note a significant increase in IgG within the brain of aged (17-mo+) MG$^{STING-/-}$ compared to aged WT brains and their young controls (**Figure 3.1.27A-B**).

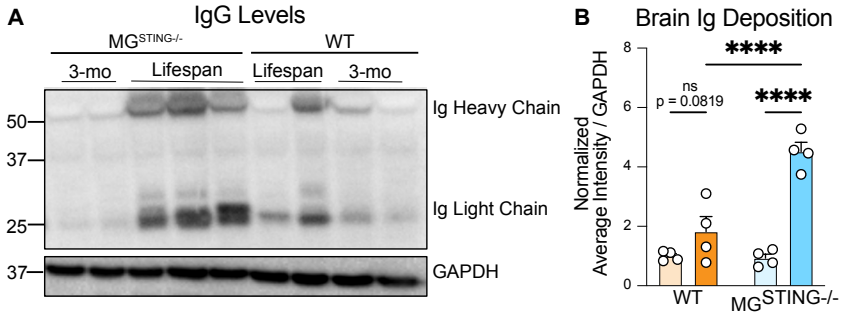

Figure 3.1.27. BBB dysfunction is prominent in MG$^{STING-/-}$ brains.
(A) IgG light and heavy chain and GAPDH western blot from 3-mo and LS WT and MG$^{STING-/-}$ brain lysates. (B) Bar graphs depict quantification of WB IgG light chain normalized to GAPDH(n=4/group). Data are representative of biological replicates and bar graphs show mean ±SEM. One-way ANOVA with Bonferroni correction factor. *p<0.05, not significant (ns).

To correlate these changes with senescence, we quantitated LLPs from aged WT and MG$^{STING-/-}$ brains. LLPs were significantly decreased in the aged MG$^{STING-/-}$ hippocampi compared to age-matched MG^{WT} (**Figure 3.1.28A-B**).

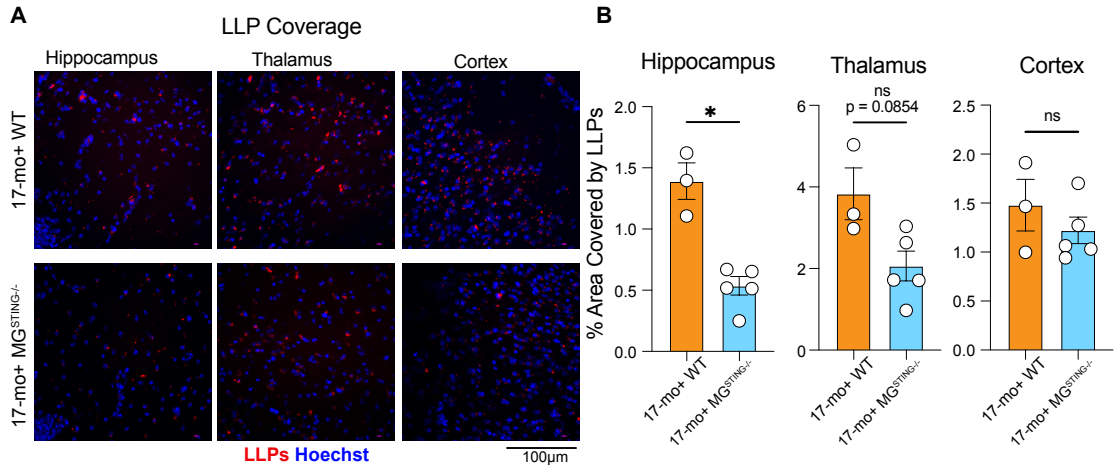

Figure 3.1.28. Microglial-STING increases LLPs accumulation in the hippocampus of aged brains.
(A) Representative immunofluorescent images of autofluorescent signature from TxRed channel (excitation peak at 596nm and emission peak at 615nm) to label LLPs and with Hoechst of LS WT (n=3), LS MG$^{STING-/-}$ (n=5) in hippocampus, thalamus, cortex. Scale bars 100µm. The arrows highlight LLPs. (F) Bar graphs depict quantification of LLPs coverage from LS WT and STING$^{-/-}$ animals. Data are representative of biological replicates and bar graphs show mean ±SEM. One-way ANOVA with Bonferroni correction factor. *p<0.05, not significant (ns).

However, LLP levels showed subtle decreases in the thalamus and no differences in the cortex of aged MG$^{STING-/-}$ compared to controls (**Figure 3.1.28B**). These data underscore a region-specific impact of microglial STING-signaling with age, similar to the global STING$^{-/-}$ brains, with some differences. Levels of LLPs were unremarkable in the young MG$^{STING-/-}$ and age-dependent changes like WT and STING$^{-/-}$ brains described before (**Figure 3.1.29A-C**).

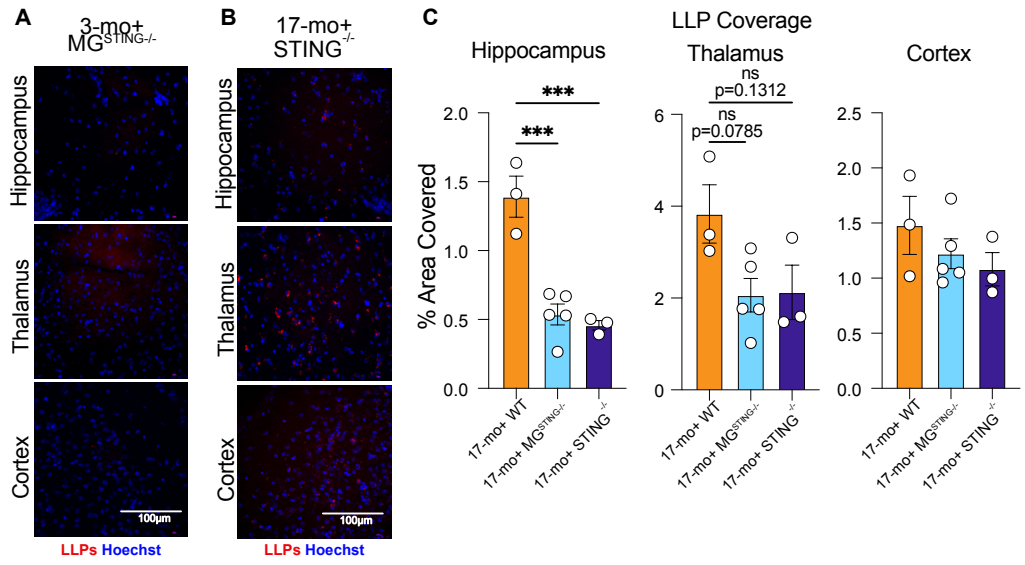

Figure 3.1.29. MG$^{STING-/-}$ recapitulates the decrease of LLPs seen in the global STING$^{-/-}$ compared to MG^{WT} brains.
(A) Representative immunofluorescent images of autofluorescent signature from TxRed channel (excitation peak at 596nm and emission peak at 615nm) to label LLPs and with Hoechst of 3-mo MG$^{STING-/-}$ mice and (B) non-required euthanasia aged (17-mo+) STING$^{-/-}$ brains in hippocampus, thalamus, cortex as experimental control. Scale bars 100μm. (C) Bar graphs depict quantification of LLPs coverage from non-required euthanasia aged (17-mo+) WT, MG$^{STING-/-}$, and STING$^{-/-}$ brains. Data are representative of biological replicates and bar graphs show mean ±SEM. One-way ANOVA with Bonferroni correction factor. ***p<0.001, not significant (ns).

The parity in data thus suggests that the functional outcomes seen due to STING-deficiency in the CNS during aging, are largely attributable to the loss of STING in the microglia populations with age.

Collectively our data support a novel paradigm whereby, STING directs what is ultimately a beneficial immune response with age through its action in microglia. Our results offer a highly salient, alternative perspective to age-associated changes in microglia behavior. By identifying neuroprotective mechanisms mediated by microglia STING-signaling with age, we reveal that well described age-associated changes in microglia (microgliosis and quality of inflammation) may be a beneficial physiological response to damage accrual. We reveal how a careful evaluation of physiological shifts

with aging uncovers an essential role for STING in shaping these beneficial roles of microglia and their overall advantage to CNS health and integrity.

All experiments and analysis within this section are my own. Exceptions to this statement are as follows: Kimberly Carroll conducted (1) RNAMagnet and (2) IF analysis utilizing QuPath. Grip strength assays were conducted with Kimberly Carroll. LLP image collection was conducted with Dr. Sasha Smolgovsky, PhD. Western blots were conducted by Dr. Abe Bayer, PhD.

3.2. **STING-SPECIFIC AGE-DEPENDENT CHANGES IN MICROGLIA**

In the previous section, I highlighted the importance of microglial-STING signaling as a safeguard against age-dependent pro-inflammatory pathways and mediator against neuromotor decline and BBB dysfunction. We highlighted specific changes within the microglia population based on flow cytometry and that STING$^{-/-}$ microglia were more proinflammatory. Recently, microglia nomenclature has been overhauled to identify a heterogeneous continuum of many microglia states defined by their distinct transcriptional landscape specific to disease states[36,166,173,188,218,219]. Microglia, play a large role in development, health, and disease progression and are shaped by their environment and interaction with surrounding cell types. The identification of the DAM population highlights the importance of the tissue microenvironment as drivers of inflammation. One of the primary functions of microglia is to survey the environment and response to signals, thus making them uniquely positioned to be potent responders of IFN-I and producers of downstream ISGs.

More recently, publications have identified a population of microglia important for responding to IFN-I, called interferon responsive microglia (IRMs). They were shown to be necessary for neuronal engulfment during development and critical pruning events[109]. Similarly, IRMs were spatially linked to CD8^{+} T cell immune responses within the white matter with age and necessary for a more beneficial aging response[220]. Though these mechanisms remain unclear. Alternatively, other previous studies have shown the importance of IFN-I in neurological decline[86]. By blocking IFNAR signaling to reduce IFN-I production, the researchers recovered memory deficits seen with age. Consequently, leaving us asking: what role are IFN-I playing throughout lifespan/disease states? More specifically, what homeostatic processes are they supporting within microglia and the CNS?

3.2.1. **Microglia heterogeneity is dependent on age and STING-signaling**

Originally identified as an antiviral response[221], IFN-I have since been shown to play a pivotal role in neuroinflammation[115,222]. IFN-I have also been shown to be detrimental in aging[4], AD[223,224], and murine prion disease. Conversely, they are necessary for maintaining neuronal health in models of PD and in mitigating neuroinflammation during MS[115,225] and neurodevelopment[109].

Within the CNS most cell types are capable of producing IFN-I upon activation during infections[91,115], diseases states[87,188,223,224], or injuries[226,227]. *In vitro* studies of age-associated telomeric dysregulation, impaired DNA-damage repair, and senescence[127,139,169,228], reveal that IFN-I is induced by the sensing of damaged DNA released into the cytosol[73]. Damaged DNA was shown to be sensed by microglial-cGAS to drive IFN-I and proinflammatory responses at early ages[126]. By blocking STING with a short-term use of small molecule agonist, Gulen et al. were able to decrease neuroinflammation and reverse neuronal loss[126]. However, the long-term consequences of the loss of STING-signaling and the impact on microglia heterogeneity remains unanswered. The complexity of IFN-I signaling is apparent, yet large gaps in knowledge remain, including: 1) the identity of the specific innate pathways that are paramount for IFN-I production in the CNS and 2) the cell-specific impact of IFN-I during aging. Clarification of these aspects will allow us to further explain and parse out negative and beneficial neuroinflammatory processes with age**.**

3.2.2. **STING-signaling regulates inflammatory and IFN-I landscape of aged microglia**

To address the impact of age and STING-deficiency with age in the microglia population we isolated the population and first identified the number of distinct states of microglia found at 3-mo and 12-mo in WT and STING$^{-/-}$ brains. We identified 11 distinct cluster of

microglia (**Figure 3.2.1A-B**) based on top 10 DEGs (**Table 5.1**). Based on the DEGs, we identified homeostatic microglia (MG1, MG2) (*Sall*, *Fcrls*, *Cx3cr1, P2ry13*), G-protein coupled receptors (GPCR) activated microglia (MG4, MG9 (*Gpr183, Gpr84)*, inflammatory microglia (MG5, MG6, MG7, MG10, MG11 (*Jun*, *Dusp1*, *Ccl4*, *Pf4*, *Cd74*, *H2*-Ab1), mitochondrial regulated microglia (mtMG) (MG3, MG8 (*mt-Atp6*, *mt-Cytb*, *Malat1*).

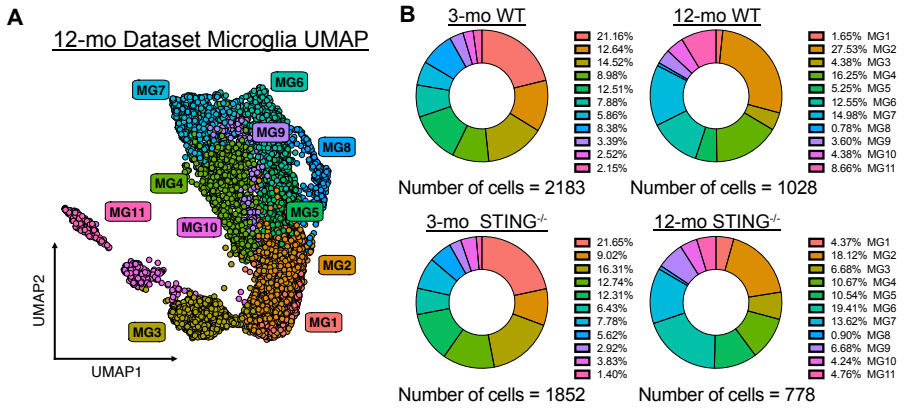

Figure 3.2.1. Microglia heterogeneity with age in WT and STING$^{-/-}$ mice.
(A) Representative UMAPs of microglia subsetted from scRNA-seq 12-mo cohort. (B) Donut plots of 3-mo WT, 3mo STING$^{-/-}$, 12-mo WT, and 12-mo STING$^{-/-}$ microglia with frequency of populations next to donut plot. Donut plots are percentages to make up 100.

MG1 decreases with age, while MG2 increases with age. The mtMG group decreases with age, which is unsurprising considering the genes encoding mtDNA decrease with age and possibly contribute to age-associated decline[229]. Of the inflammatory microglia, both 3-mo WT and STING$^{-/-}$ make up 30.92% and 31.75%, respectively, from the total microglia population collected. With age, STING$^{-/-}$ brains increase their inflammatory population and have more of these inflammatory microglia (52.57%) compared to the WT (45.82%). This data further supports the data from the previous section that STING$^{-/-}$ microglia are more pro-inflammatory compared to age-matched WT. We next looked at the distribution of collective homeostatic, inflammatory, activated, and ISG scores to

identify the cellular distribution of the transcriptional landscape between the aged WT and STING$^{-/-}$ (**Figure 3.2.2A-D**).

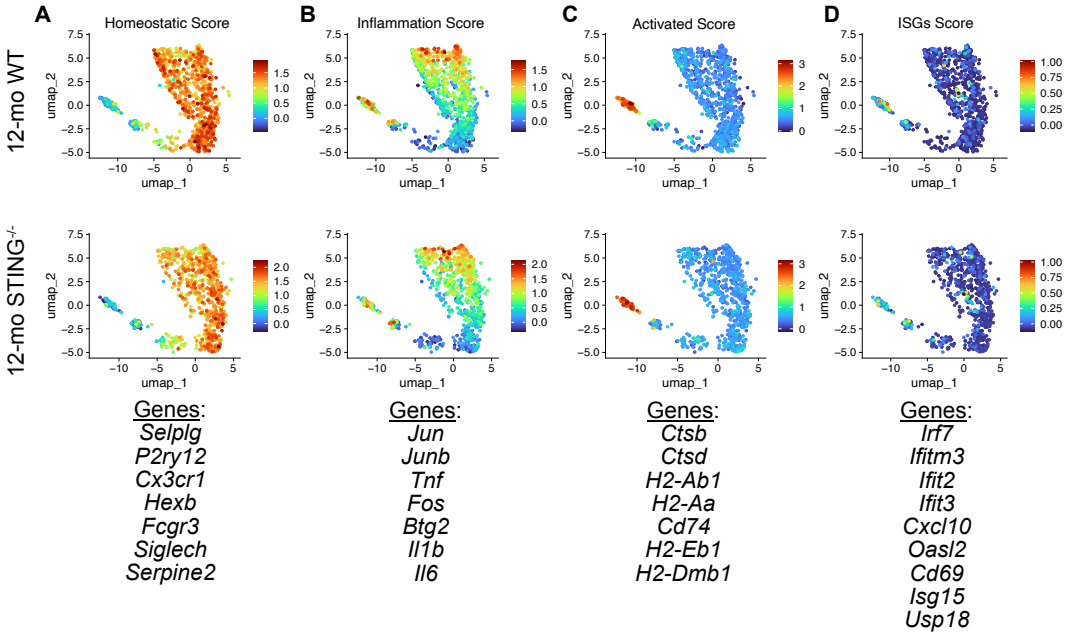

Figure 3.2.2. Transcriptional landscape module scores highlight ISG-specific microglia populations.
(A-D) Representative UMAPs of combined signatures from homeostatic genes, inflammations genes, activated genes, and interferon stimulated genes (ISGs) as a cumulative score within the microglia populations. Top panels are 12-mo WT and bottom panels are 12-mo STING$^{-/-}$ microglia.

There are slight differences in the cell populations within the UMAPs and the scale changes depending on the genotypes. Unsurprisingly, homeostatic genes are more widespread across the microglia populations (**Figure 3.2.2A**). We note that between the WT and STING$^{-/-}$ UMAPs of the inflammation score, the STING$^{-/-}$ UMAP has a higher scale further indicating higher inflammation based on these select genes (**Figure 3.2.2B**). The main activated population is similar between genotypes (**Figure 3.2.2C**). Lastly, there are select clusters of microglia that have a specific ISG signature. Though, it is difficult to see immediate difference in transcriptional levels between WT and STING$^{-/-}$ cells (**Figure 3.2.2D**). Therefore, to investigate the role of a novel IFN-I/ISG-dependent microglia population during healthy aging, such as was described at a single-cell level

during development[109] and disease models[188], we isolated MG9, M10, MG11 microglia clusters that showcased higher levels of ISGs in the combined UMAP of 12-mo WT and STING$^{-/-}$ microglia (**Figure 3.2.3A**). Similar to Hammond et al.[188], we identified that the combined clusters (MG9, MG10, MG 11) increased 2-fold. Thus, showcasing a progressive expansion of these microglia by 12-mo in WT and STING$^{-/-}$ (**Figure 3.2.1B**). After isolation and re-normalization of the ISG-high subset of microglia, we visualized 7 distinct clusters of IRMs (**Figure 3.2.3B**) based on the top 10 DEGs from the clusters (**Table 5.2**).

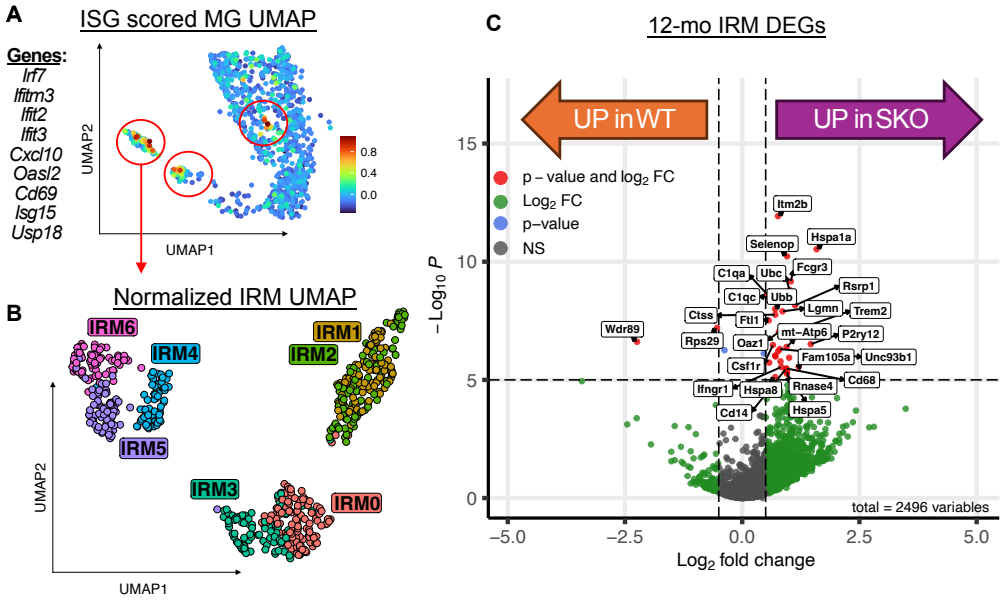

Figure 3.2.3. Heterogeneity of Interferon Responsive Microglia (IRM) and age-dependent DEGs.
(A) Representative UMAP of 12-mo cohort of microglia populations with a curated score of a combined ISG signature. The genes driving the signature are left of the UMAP. (B) Representative UMAP of normalized cell populations originally from MG9, MG10, and MG11 in (A) now called interferon responsive microglia (IRMs). (C) Enhanced volcano plot of differentially expressed genes in STING$^{-/-}$ relative to WT MG.

The STING$^{-/-}$ IRM populations appear to be more transcriptionally active compared to the 12-mo WT cells (**Figure 3.2.2C**). Further, STING$^{-/-}$ IRMs are statistically more significant in homeostatic genes (*P2ry12*, *Csf1r*) and pro-inflammatory markers (*Ctss*, *Ifngr1*, *CD68*). Other significantly upregulated genes in STING$^{-/-}$ IRMs suggest an increased risk

to neurodegenerative states in the brain, such as *Itm2b*, *Trem2*, *Hsp1a1*, *Selenop*[173,209,230,231]. Similar to previous reports[109,188], we have identified a bone fide IRM population, IRM4, that is the primary expressor of multiple canonical ISGs (*Isg15*, *Cxcl10*, *Usp18*, *Ifit3*, *Fcgr1*, *Ccl12*) (**Figure 3.2.4A**).

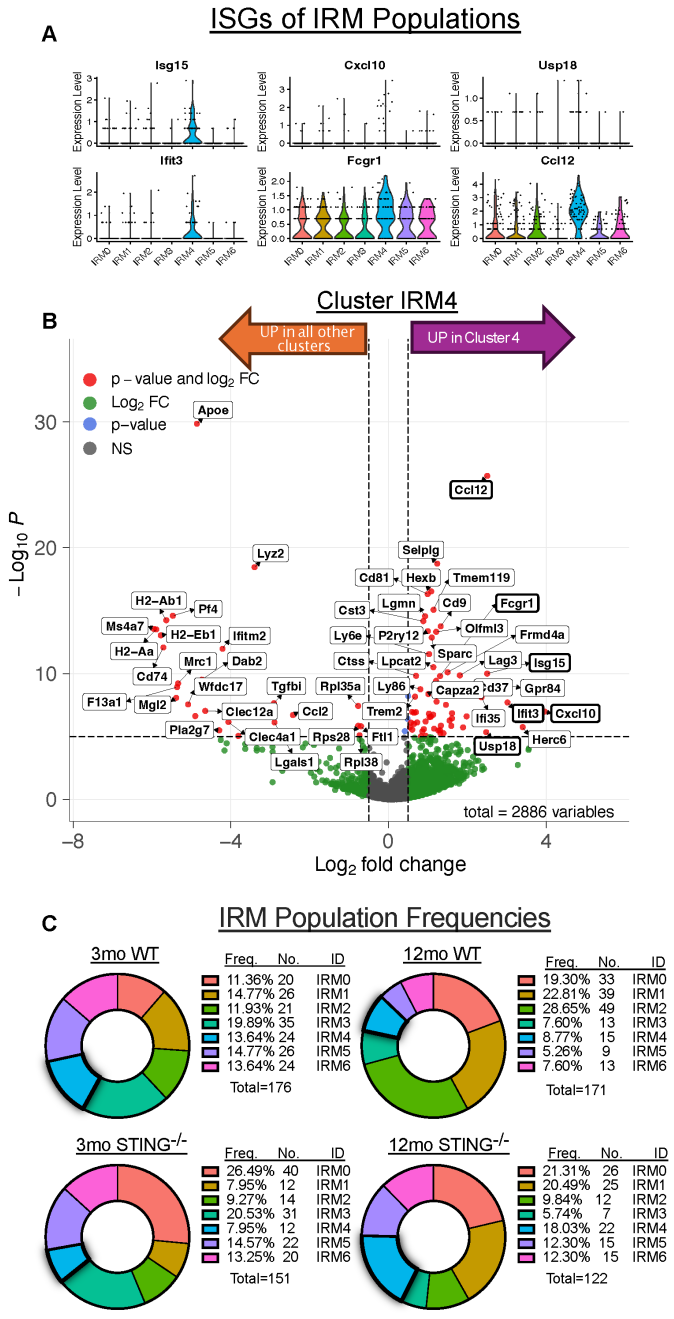

Figure 3.2.4. IRM changes with age.
(A) Violin plots of IRM populations showing SCT expression levels of *Isg15*, *Cxcl10*, *Usp18*, *Ifit3*, *Fcgr1*, and *Ccl12* ISGs from all 3-mo and 12-mo WT and STING$^{-/-}$ samples. (B) Volcano plot of IRM4 with upregulation of canonical ISGs in IRM4 compared to the rest IRM populations (C) Donut charts of IRM population frequencies and number of cells. Total number of IRMs from each sample: 3-mo WT = 176, 12-mo WT = 171, 3-mo STING$^{-/-}$ = 151, 12-mo STING$^{-/-}$ = 122.

Based on its transcriptional landscape, IRM4 is identified as the main IRM population that is the primary driver of ISGs based on significantly upregulated genes in the volcano plot (*Ccl12*, *Isg15*, *Ifit3*) (**Figure 3.2.4B**). The WT IRM4 frequency decreases with age and is increased in the 12-mo STING$^{-/-}$ compared to the 12-mo WT (**Figure 3.2.4C**). Age-related activation of ISGs and IFN-I have been reported in the choroid plexus[133], but our data highlights that some ISGs are not regulated by the STING-signaling pathway as they are upregulated in the STING$^{-/-}$ microglia population. As we have seen negative age-associated defects in the STING$^{-/-}$ brain in the previous section(**3.1.3**), we suggest that STING$^{-/-}$ animals produce a suboptimal range of IFN-I that are detrimental to neuromotor and BBB health and overall inflammatory responses. Thus, STING-dependent IRM populations may be providing the optimal level of IFN-I to protect against unhealthy aging.

To determine specific contributions of STING-dependent IFN-I, we investigated age-dependent neuromotor changes in IFNAR$^{-/-}$ mice. IFNAR is a downstream mediator of IFN-I upon binding of IFN-α or IFN-β. We noted an age-dependent neuromotor deficit in IFNAR$^{-/-}$ animals, but the 17-mo+ IFNAR$^{-/-}$ animals recapitulated WT clasping behavior and did not exhibit worsened neuromotor deficits that resembled STING$^{-/-}$ animals (**Figure 3.2.5A-B**).

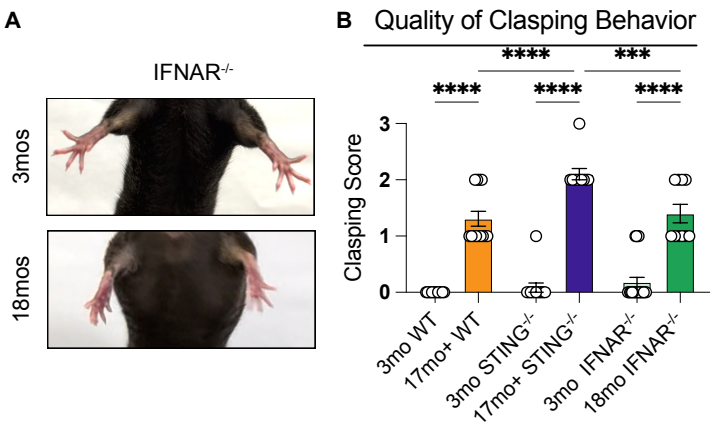

Figure 3.2.5. IFNAR-KO rescues neuromotor deficits seen with age compared to STING$^{-/-}$ mice.
(A) Representative image of IFNAR$^{-/-}$animals at 3-mo(n=8) and 18-mo (n=3). (B) Bar graphs depict the clasping behavior 0-3 scoring system representative of the quality of their clasping behavior of WT (3-mo and 17-mo+), STING$^{-/-}$ (3-mo and 17-mo+), and IFNAR$^{-/-}$ (3-mo and 17-mo+). The scoring system is explained in the methods. Bar graphs represent data by mean ±SEM and dots represent individual mice. The scoring system is explained in the methods. Two-way ANOVA with Tukey's correction factor was run; **** p< 0.0001, ***p<0.001.

Therefore, the pathological outcomes associated with age are dependent of STING-dependent IFN-I. We also looked at microglia numbers by flow cytometry in the IFNAR$^{-/-}$ brains to determine if there were changes to the number of microglia (**Figure 3.2.6A-C**).

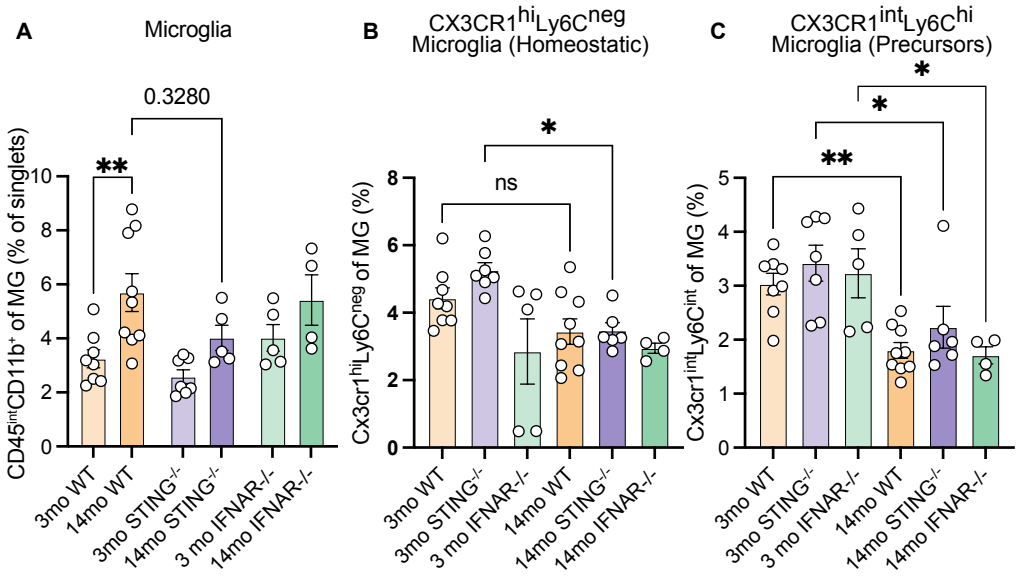

Figure 3.2.6. IFNAR$^{-/-}$ impairs microglia subsets with age.

(A) Bar graphs depict microglia percentage quantification from singlets and lymphocytes (3mo WT; n = 8, 14mo WT; n = 9, 3mo STING$^{-/-}$; n = 7, 14mo STING$^{-/-}$; n = 6, 3-mo IFNAR$^{-/-}$; n = 5, 14mo IFNAR$^{-/-}$; n = 4). Orange box with black outline = WT mice; Purple box with black outline = STING$^{-/-}$ mice; green box with black outline = IFNAR$^{-/-}$ mice. Ages are based on increased intensity of corresponding colors. (B) Bar graphs depict percentage of CX3CR1^{hi}, Ly6C^{neg} microglia (homeostatic) population from young and aged WT and STING$^{-/-}$ brains. (C) Bar graphs depict the percentage of CX3CR1 ^{int}, Ly6C^{hi} microglia (precursor) population from young and aged WT and STING$^{-/-}$ brains. Bar graphs represent data by mean ±SEM and dots represent individual mice. One-way ANOVA followed by Bonferroni correction factor. **p<0.01, *p<0.05, ns: not significant.

Preliminary data suggests that IFNAR$^{-/-}$ mice do not show any significant changes compared to WT and STING$^{-/-}$ mice. We do note that with age, precursor populations (CX3CR1^{int}Ly6C^{hi}) are similarly significantly decreased with age in IFNAR$^{-/-}$ brains (**Figure 3.2.6C**). It is worth further investigation to increase the number of IFNAR$^{-/-}$ mice used and to expand to 17-mo+ aged animals to determine further changes with age. However, based on this data, age seems to be the largest factor for driving changes in microglia populations. Based on the preliminary IFNAR$^{-/-}$ data, 3-mo IFNAR$^{-/-}$ animals may have more microglia to begin with, and therefore, will require further investigation is warranted.

With mounting evidence of microglial cGAS activation of STING to drive neuroinflammation[126], we investigated the neuromotor defects seen with age and expanded our study to determine if there were any links to senescence. First, we conducted the clasping behavior assay on cGAS$^{-/-}$ mice with WT, STING$^{-/-}$, and IFNAR$^{-/-}$ mice. cGAS$^{-/-}$ mice show a similar neuromotor decline with age as was shown in the WT, STING$^{-/-}$, and IFNAR$^{-/-}$ mice (**Figure 3.2.7A-B**).

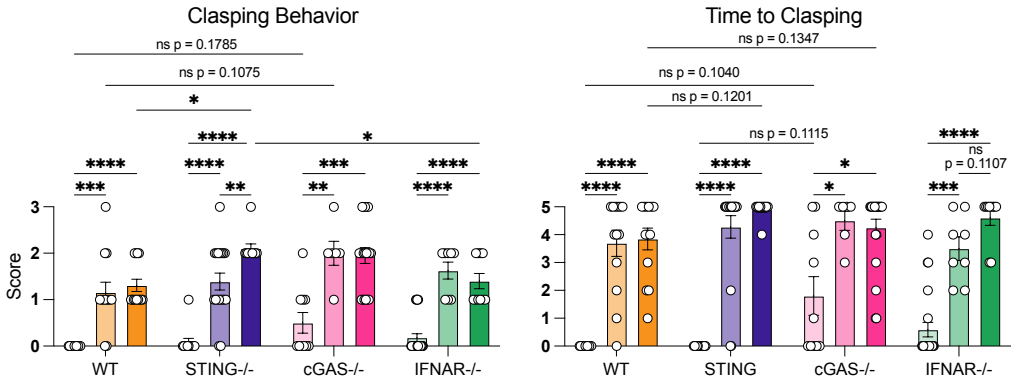

Figure 3.2.7. STING-deficiency drives the largest neuromotor defects seen with age compared to global cGAS$^{-/-}$ and IFNAR$^{-/-}$ mice.
(A) Bar graphs depict the clasping behavior 0-3 scoring system representative of the quality of their clasping behavior (3mo WT = 13, 12-mo WT = 13, 17-mo+ WT = 13, 3-mo STING$^{-/-}$ = 12, 12-mo STING$^{-/-}$ = 18, 17-mo+ STING$^{-/-}$ = 10, 3-mo cGAS$^{-/-}$ = 10, 12-mo cGAS$^{-/-}$ = 6, 17-mo+ cGAS$^{-/-}$ = 20, 3-mo IFNAR$^{-/-}$ = 22, 12-mo IFNAR$^{-/-}$ = 8, 17-mo+ IFNAR$^{-/-}$ = 10). (B) bar graphs depict 0-5 time to clasping behavior (3-mo WT = 13, 12-mo WT = 13, 17-mo+ WT = 13, 3-mo STING$^{-/-}$ = 12, 12-mo STING$^{-/-}$ = 18, 17-mo+ STING$^{-/-}$ = 10, 3-mo cGAS$^{-/-}$ = 10, 12-mo cGAS$^{-/-}$ = 6, 17-mo+ cGAS$^{-/-}$ = 20, 3-mo IFNAR$^{-/-}$ = 22, 12-mo IFNAR$^{-/-}$ = 8, 17-mo+ IFNAR$^{-/-}$ = 10). Data is a combination of 5 experiments. Bar graphs represent data by mean ±SEM and dots represent individual mice. The scoring system is explained in the methods. Two-way ANOVA with Tukeys correction factor was run; **** p< 0.0001, ***p<0.001.

The cGAS$^{-/-}$ mice at 17-mo+ have a larger standard deviation (SD = 0.759), which is more similar to the WT animals (SD = 0.48) (**Figure 3.2.7B)**, suggesting that the STING$^{-/-}$ phenotype may be independent of cGAS activation. In STING$^{-/-}$ animals, we saw a reduced level of senescence, by LLP accumulation, and exacerbated neuromotor function. Therefore, we looked for LLPs accumulation in IFNAR$^{-/-}$ and cGAS$^{-/-}$ mice in addition to WT and STING$^{-/-}$ mice (**Figure 3.2.8A-C**).

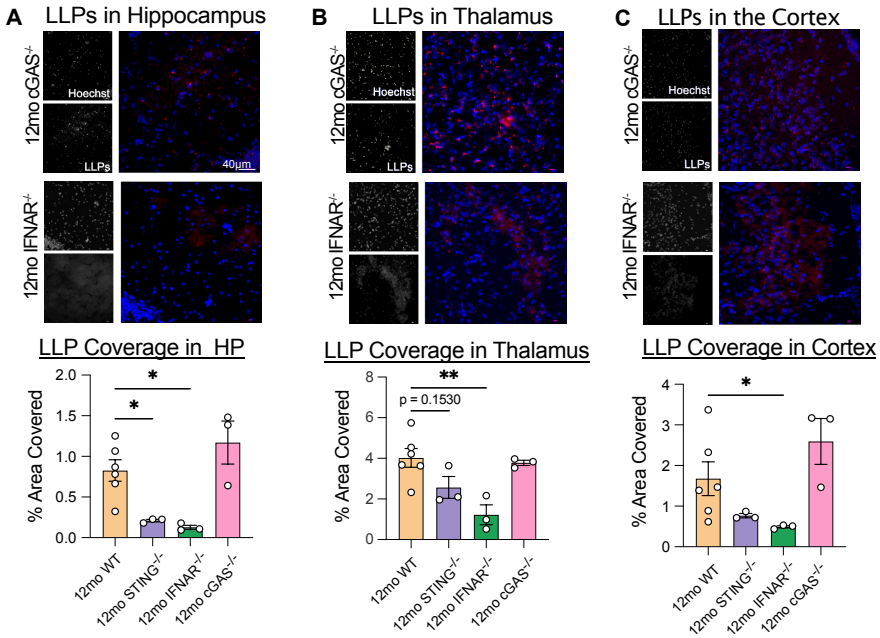

Figure 3.2.8. LLPs accumulation occurs independent of cGAS-signaling in hippocampus, thalamus, and cortex at 12-mo.
(A) Hippocampus representative immunofluorescent images of autofluorescent signature from TxRed channel (excitation peak at 596nm and emission peak at 615nm) to label LLPs (red) and with Hoechst (blue) of 12-mo WT (n = 6), 12-mo STING$^{-/-}$ (n = 3), 12-mo IFNAR$^{-/-}$ (n = 3), and 12-mo cGAS$^{-/-}$ (n = 3) hippocampal formation region (HP). Scale bars 40μm. Below; bar graphs depict quantification of LLPs coverage in HP. (B) Thalamus representative immunofluorescent images of autofluorescent signature from TxRed channel (to label LLPs (red) and with Hoechst (blue) of 12-mo WT (n = 6), 12-mo STING$^{-/-}$ (n = 3), 12-mo IFNAR$^{-/-}$ (n = 3), and 12-mo cGAS$^{-/-}$ (n = 3) hippocampal formation region (HP). Scale bars 40μm. Below; bar graphs depict quantification of LLPs coverage in thalamus. (B) Cortex representative immunofluorescent images of autofluorescent signature from TxRed channel (to label LLPs (red) and with Hoechst (blue) of 12-mo WT (n = 6), 12-mo STING$^{-/-}$ (n = 3), 12-mo IFNAR$^{-/-}$ (n = 3), and 12-mo cGAS$^{-/-}$ (n = 3) hippocampal formation region (HP). Scale bars 40μm. Below; bar graphs depict quantification of LLPs coverage in cortex.

The images highlight a significant difference in LLP accumulation between cGAS$^{-/-}$ and IFNAR$^{-/-}$ brain regions. We see a significant decrease in the IFNAR$^{-/-}$ animals compared to the WT and no changes between the cGAS$^{-/-}$ and the WT. The IFNAR$^{-/-}$ show a similar, but more significant decrease in the LLP accumulation. Thus, strengthening the hypothesis that STING-dependent IFN-I responses are mediating LLP accumulation and IFN-I production independent of cGAS activation.

All experiments and analysis within this section are my own. Exceptions to this statement are as follows: LLP image collection was conducted with Dr. Sasha Smolgovsky, PhD.

3.3. **STING PROMOTES TISSUE MAINTENANCE AND LONGEVITY WITH AGE.**

In the previous sections, the focus was on a notoriously immune privileged site: the CNS. Though it is clear that the CNS is not devoid of immune responses, we uniquely showed that microglia-dependent STING-signaling is necessary to protect against age-associated neurological decline and neuroinflammation. However, STING is ubiquitously expressed by most cell types[74,75] and central to host defenses against microbial DNA and host DNA in instances of damage or cancer and has recently been described in most organ systems and the blood[232]. STING activation is primarily associated with systemic and multi-organ inflammatory responses, such as is seen in mice deficient in three prime repair exonuclease 1 (TREX1)[233], which degrades DNA, or STING gain of function (GOF) mouse models which result in autoimmune responses[234,235]. In the different contexts, STING drove the inflammatory response from DCs or endothelial cells, respectively, to induce elevated interferon and proinflammatory cytokine levels. However, in contrast to these previous studies, STING was shown to suppress inflammation and reduce disease pathology in models or systemic lupus erythematosus (SLE)[236]. Sharma et al. showed that STING-deficient mice prone to SLE had significantly shorter lifespans and STING-deficient macrophages did not upregulate negative regulators of inflammation[237], thus, highlighting necessary functions of STING-signaling. Recently, STING's homeostatic role for immune cell development and function has been described[232]. Here the authors highlight a dynamic relationship between tightly regulated STING expression in various immune cells and tissue. The collected data highlights the need to critically investigate STING-signaling and with small molecule agonists of STING being tested, it is more crucial to understand long term consequences of suppressing STING-signaling. Therefore, we asked if STING-deficiency had negative consequences similar to these recent publications and impaired tissue health in the heart, kidney, and

liver. Further we investigated the systemic effects of long-term STING-deficiency and consequences on lifespan.

To understand the STING-dependent gross changes that occur within vital organs that are required for healthy aging; the heart, kidney, and liver serum analysis, histopathology, imaging, and in vitro functional assays were used. We used young (2-3mo), middle aged (12-14-mo), and aged (18-mo+), and lifespan (17-mo+ animals that were required to be euthanized for humane reasons) WT and STING$^{-/-}$ mice (Figure 3.3.1).

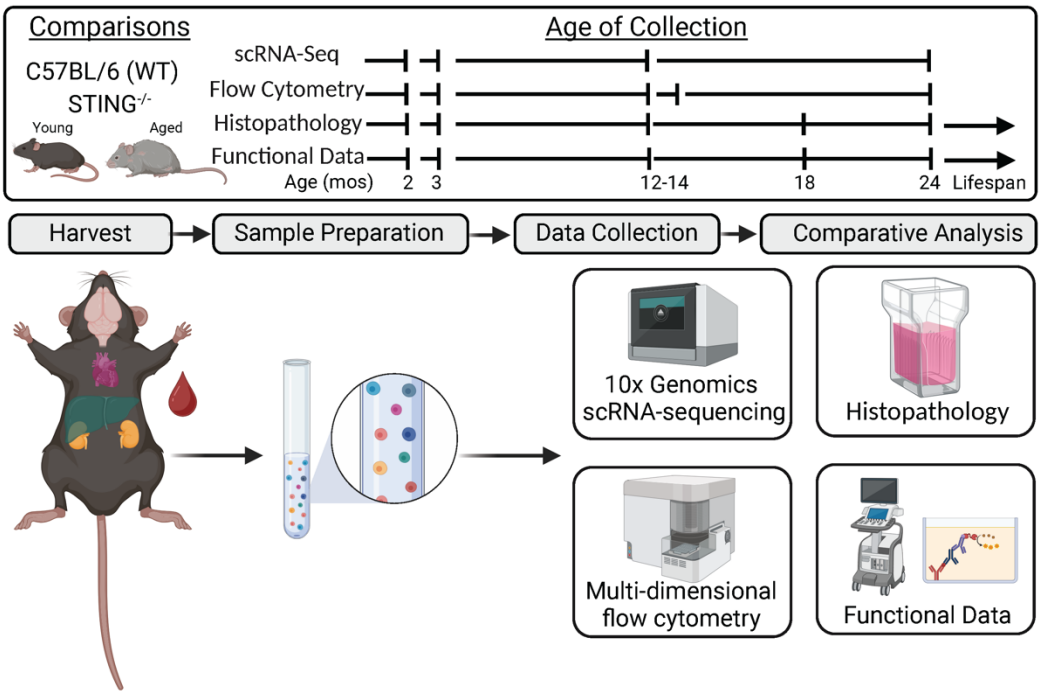

Figure 3.3.1. Experimental Design
Diagram of ages of mice used for experiments throughout the paper. These include 3-mo, 12-14-mo, 18-24-mo (healthy), and lifespan (LS) animals (17-mo-40-mo) that required euthanasia WT and STING$^{-/-}$ mice. Techniques used for analysis includes scRNA-seq, histopathology, flow cytometry, and functional readouts.

3.3.1. The Role of STING in Tissue Immunity

Inflammation is a central hallmark to aging. Therefore, to determine STING-dependent changes to systemic inflammation, we collected serum from 3-mo, 12-mo, 18-mo, and

24-mo WT and STING$^{-/-}$ animals and tested a 44 multi-plex panel of proinflammatory biomarkers. Unsurprisingly, we saw significant age-dependent changes to cytokines, such IL-10, EPO, and IL-20 in WT animals (**Figure 3.3.2A-D**).

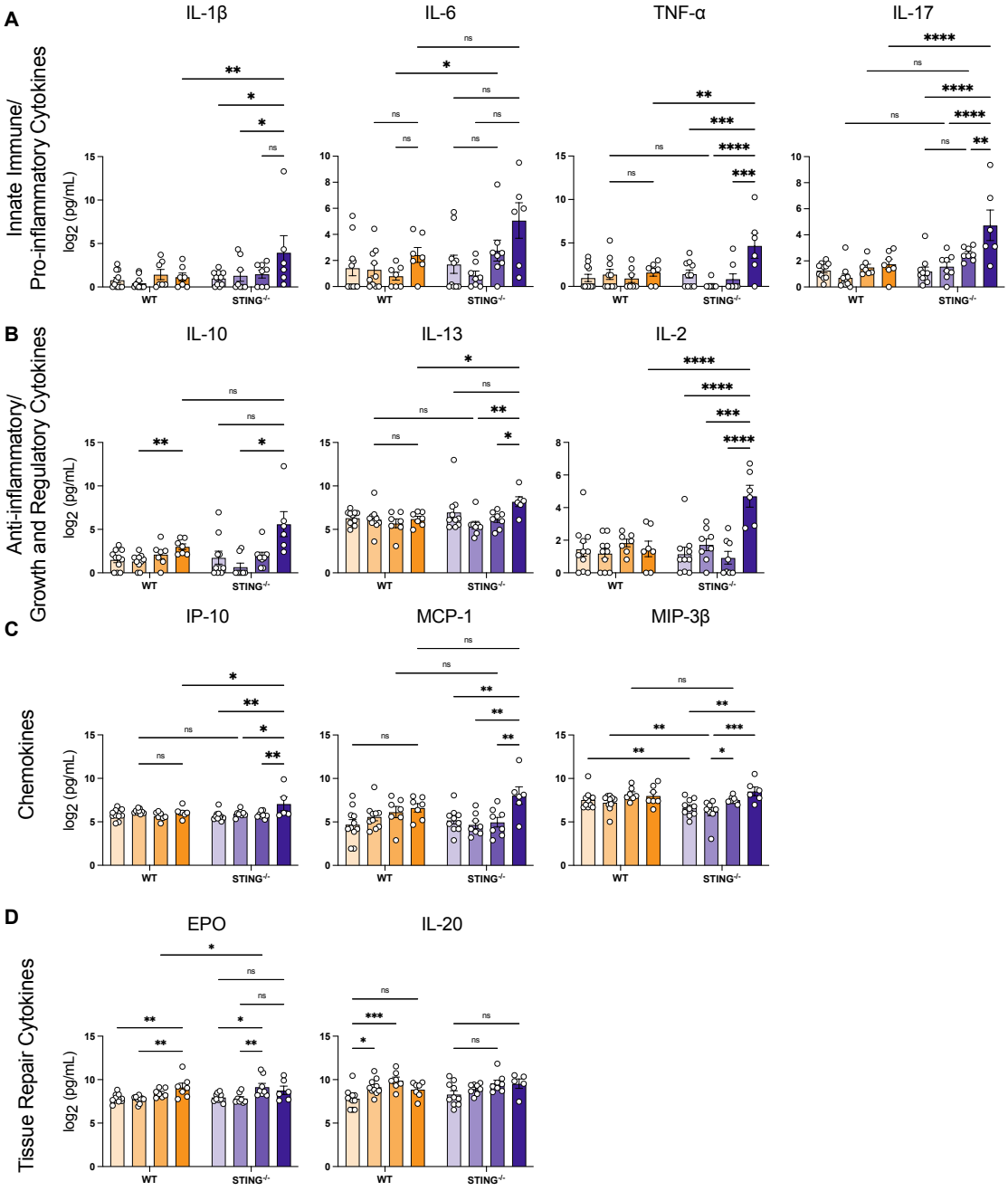

Figure 3.3.2. STING-signaling suppresses uncontrolled inflammation with age. (A) Bar graphs depict biomarker levels (log transformed pg/mL) of innate immune/pro-inflammatory cytokines (IL-1β, Il-6, TNF-α, Il-17), anti-inflammatory cytokines (IL-10, IL-13, IL-2), chemokines (IP-10, MCP-1, MIP-3β), and cytokines that are important for tissue repair (EPO, IL-20) from 3-mo, 12-mo, 18-mo, and 24-mo WT (gold) and STING$^{-/-}$

(purple). Color transparency indicates ages (25% transparency bars are 3-mo, 50% transparency are 12-mo, 75% transparency are 18-mo, and darkest color is 24-mo). Bar graphs represent data by mean ±SEM and dots represent individual mice. The scoring system is explained in the methods. Two-way ANOVA with Tukey's correction factor was run; **** p< 0.0001, ***p<0.001, **p<0.01, *p<0.05, numbers without star indicated p-value.

We also saw trending increases ($p < 0.2$) based on a two-way ANOVA analysis with Tukey's correction factor for TNF-α, IL-6, IL-13, IP-10 (CXCL10), and MCP- in the WT animals, supporting an increase of inflammation with age. The most significant differences between STING$^{-/-}$ and WT animals was seen in the innate/pro-inflammatory cytokines group, which mediate inflammatory responses[3] (**Figure 3.3.2A**). IL-10, IL-13 and IL-2 are important for anti-inflammatory regulatory responses and differentiation are seen to trend up in 24-mo STING$^{-/-}$ compared to WT (IL-10) or are significantly increased in 24-mo STING$^{-/-}$ compared to younger aged STING$^{-/-}$ mice or 24-mo WT mice (**Figure 3.3.2B**). Specific chemokines are increased with age, such as IP-10 or CXCL10 (**Figure 3.3.2C).** At 18-mo STING$^{-/-}$ mice have significantly more EPO compared to age-matched WT mice (**Figure 3.3.2D)**. In WT mice, there are significant increases with age that are not seen in STING$^{-/-}$ mice, even though there trending increases with age, but there are not differences seen between genotypes. Overall, in STING$^{-/-}$ aged groups there are significant increases in proinflammatory cytokines showcasing exaggerated inflammation with age. Therefore, STING-signaling is controlling inflammation with age and protecting against unrestrained inflammation.

Next, to visualize organ deterioration with age[27], we evaluated histopathological changes with age. We used H&E staining to visualize gross histological changes in 3-mo and LS (17-mo+) heart, kidney, and liver to determine the extent of decline at end-of-life points (**Figure 3.3.3A**).

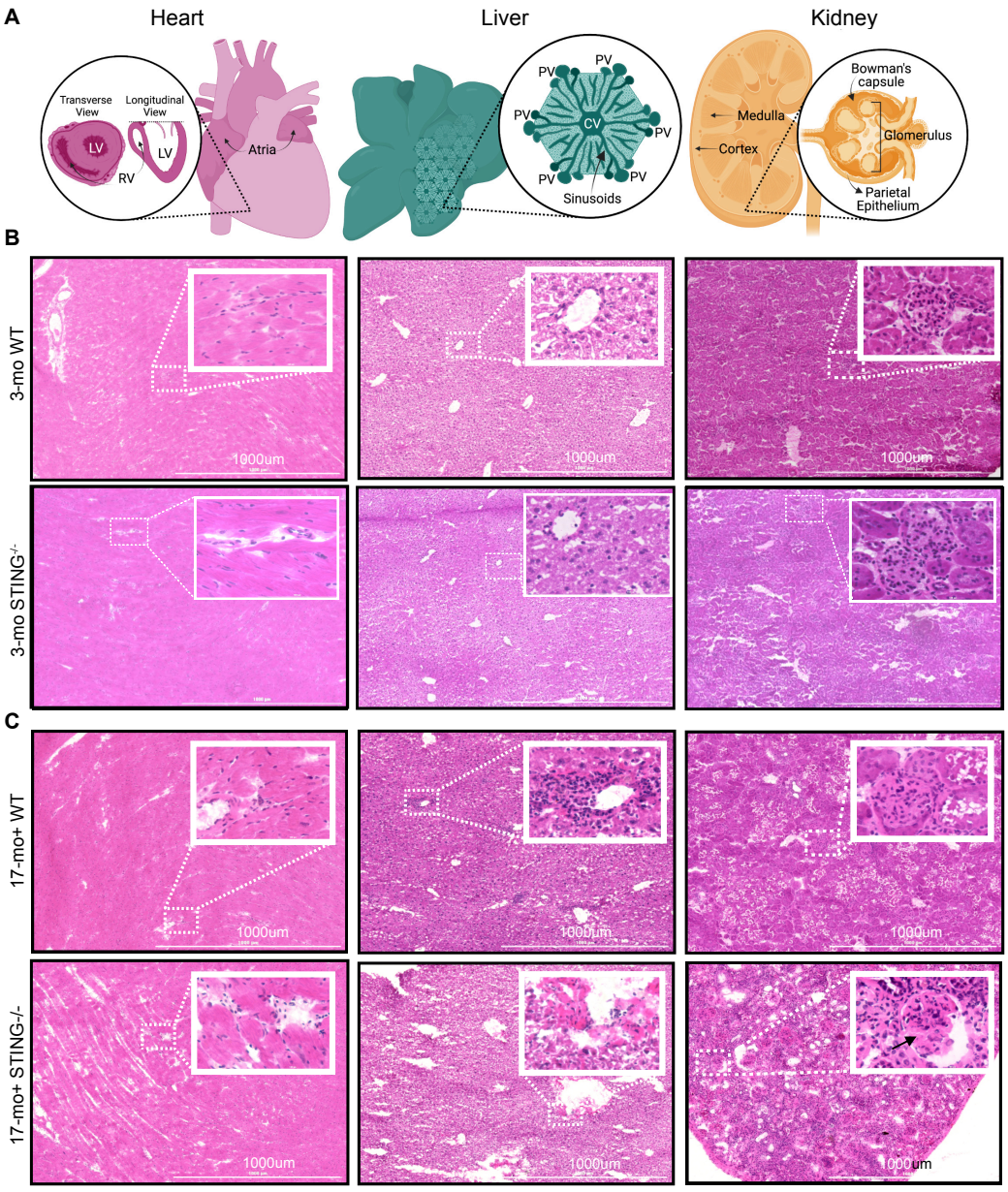

Figure 3.3.3. STING$^{-/-}$ animals heart, liver, and kidney show signs of exacerbated decline and inflammation.
(A) Representative images of hematoxylin and eosin (H&E) staining of heart, kidney, livers from WT and STING$^{-/-}$ 3-mo and LS (17-mo+) mice (n=5/group stained). Graphics above each staining showcase information of organ structure and/or orientation of sectioning. Black arrow highlights scarring. Scale bar represents 1000μm.

Routine histopathology visually reveals greater numbers of infiltrating cells in the heart, liver, and kidneys of both WT and STING$^{-/-}$ mice (**Figure 3.3.4A-C**), and further corresponds with increased systemic inflammation. Specifically, LS STING$^{-/-}$ hearts have

a larger number of infiltrates and increased numbers of cells around vasculature (**Figure 3.3.3B-C and Figure 3.3.4A**) compared to age-matched WT.

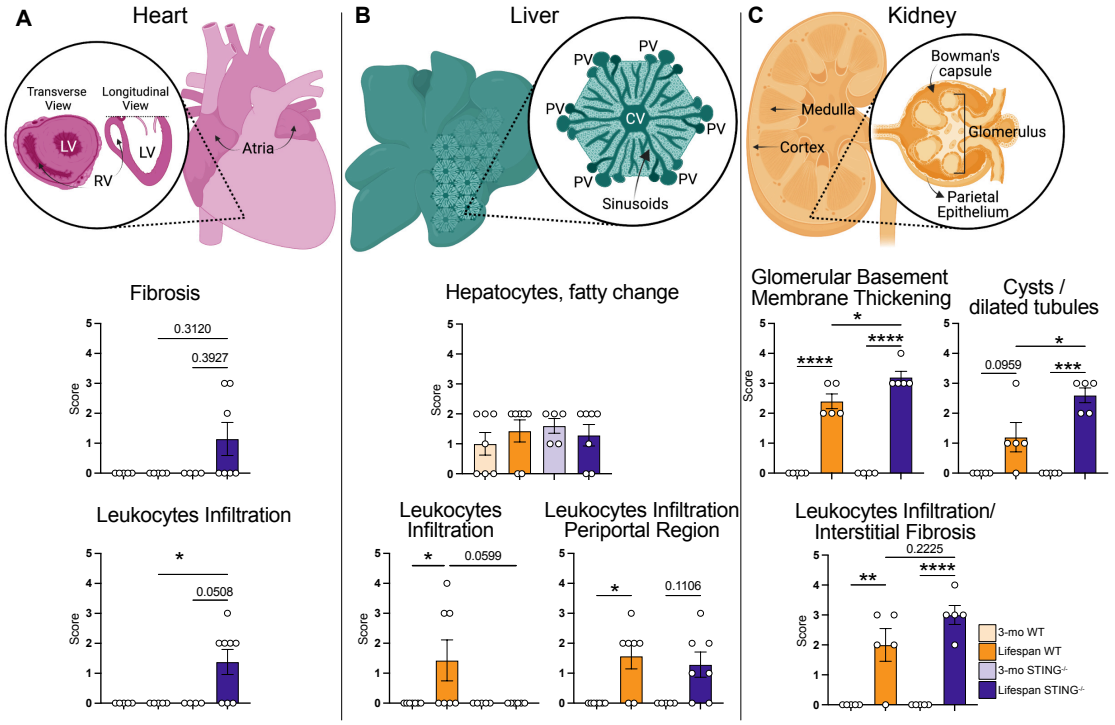

Figure 3.3.4. Histopathological scoring indicates overall organ deterioration in STING$^{-/-}$ hearts, liver, and kidneys.
(A) Graphic of a mouse heart; below graphs depict fibrosis and leukocyte infiltration scoring. (B) graphic of mouse liver; graphs below depict hepatocyte changes, general leukocyte infiltration, and leukocyte infiltration in the periportal region. (C) graphic of kidney, graphs below depict glomerular basement thickening, cysts/ dilated tubules, and leukocyte infiltrations/ interstitial fibrosis. Light gold = 3-mo WT, gold = LS WT, light purple = 3-mo STING$^{-/-}$, purple = LS STING$^{-/-}$. Bar graphs represent data by mean ±SEM and dots represent individual mice. One-way ANOVA followed by Bonferroni correction factor. **** p< 0.0001, **p<0.01, *p<0.05, numbers without star indicated p-value.

We also note enlarged striations found within the LS STING$^{-/-}$ heart tissue compared to age-matched WT. In the STING$^{-/-}$ LS livers, we note increased cellular infiltrates although many are interstitially localized and not proximal to the vasculature as in WT livers (**Figure 3.3.3B-C and Figure 3.3.4B**). Further, the endothelial cell layer around the portal veins and central veins are severely disrupted and has larger amounts of eosin staining without nuclei in the STING$^{-/-}$ compared to the WT. This altered

localization pattern of infiltrates is in part complicated by the high degree of stromal disorganization notable in aged STING$^{-/-}$ livers (**Figure 3.3.3B-C**). STING$^{-/-}$ kidneys present with remarkable histopathological changes that are represented by large increases in tubular infiltrates, the size of Bowman's capsules, and the thickening of parietal epithelial cell (PEC) layer surrounding the Bowman's capsules (**Figure 3.3.3B-C and Figure 3.3.4C**). There is also apparent loss of cells and scarring within glomeruli (**Figure 3.3.3C**, black arrows) in LS STING$^{-/-}$ mice, suggesting glomerulosclerosis. Though the increased interstitial infiltrates and fibrosis (**Figure 3.3.4C)** are strongly indictive of chronic inflammation and kidney disease, these features more pronounced in the STING$^{-/-}$ livers[29,154]. LS WT kidneys exhibit thickening of the glomerular basement, which was worse with the loss of STING. Importantly, changes impacting age-associated immune infiltrates and organ decline are dependent on STING. We next looked at functional readouts, using echocardiograms and ELISAs for markers of dysfunction (**Figure 3.3.5A-B**).

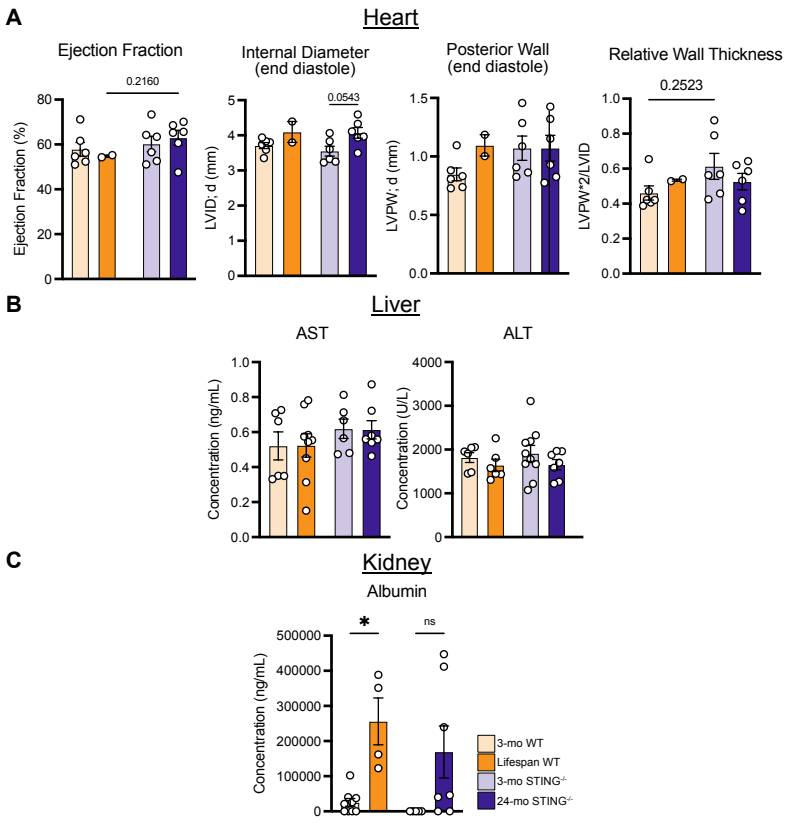

Figure 3.3.5. No major functional changes from Echocardiograms, albumin levels from urine, or AST/ALT/ levels from serum.
(A)Functional readout from echocardiograms in order; left ventricular (LV) wall thickness: (1) Internal diameter LV internal dimension (LVID) (mm), (2) posterior wall LV posterior wall (LVPW) (mm), (3) relative wall thickness (LVPW*2/LVID). (B) Aspartate aminotransferase (AST) (ng/mL) and alanine aminotransferase (ALT) (U/L) levels from serum. (C) Albumin levels from urine (ng/mL). Bar graphs represent data by mean ±SEM and dots represent individual mice. One-way ANOVA followed by Bonferroni correction factor. Numbers without star indicated p-value, ns; p values between 0.05-0.2.

To determine changes in the heart function, we performed echocardiograms on 3-mo and 24-mo WT and STING$^{-/-}$ animals. STING$^{-/-}$ and WT hearts showed no significant changes in ejection fraction though there was a trending increase in 24-mo STING$^{-/-}$ compared to WT (**Figure 3.3.5A)**. Overall there are no indications of heart failure[28] as the EFs are within the normal range. We saw significant increases in the internal diameter wall (LVID) in 24-mo STING$^{-/-}$ hearts compared to 3-mo STING$^{-/-}$ hearts, which is associated with LV dysfunction[238]. There were no significant changes in the posterior

wall thickness and LV relative wall thickness. We noted that the 3-mo STING$^{-/-}$ animals has a trending increase in LV relative wall thickness compared to 3-mo WT, suggesting base changes in LV function in STING$^{-/-}$ animals (**Figure 3.3.5A)**. Age-associated decline of liver function is often associated with an increase of protein aggregates because of the decline of macroautophagy and chaperone-mediated autophagy[239]. To test liver dysfunction, we measure levels of aspartate aminotransferase (AST) and alanine aminotransferase (ALT) in the serum of 3-mo and 24-mo+ mice. We saw no significant changes between young and aged WT and STING$^{-/-}$ mice (**Figure 3.3.5B**). With age and kidney failure, protein levels, such as albumin, increase in the urine because of glomerular basement membrane permeability[29]. In aged WT mice, we saw a significant increase of urine albumin levels and in 24-mo STING$^{-/-}$ urine showed an trending increase with age, to indicate kidney failure in both genotypes (**Figure 3.3.5C)**. Thus, indicating age-dependent changes in kidney functions, but no differences between genotypes. Based on the histopathological changes there are significant functional declines, however the functional readouts we tested did not indicate the same exacerbated decline in STING$^{-/-}$ compared to WT with age.

To determine age-dependent changes in body weight and organ weight, we measured body, heart, liver, kidney weights of WT and STING$^{-/-}$ animals throughout lifespan *ex vivo* (**Figure 3.3.6A-B**). Over time WT animals exhibit age-dependent changes in grooming habits and experience hair thinning, greying and other habits[240]. STING$^{-/-}$ animals also exhibited hair loss and greying at LS timepoints, but they also exhibited decline in wound healing capabilities which can be visualized in the male STING$^{-/-}$ mice image (**Figure 3.3.6A**).

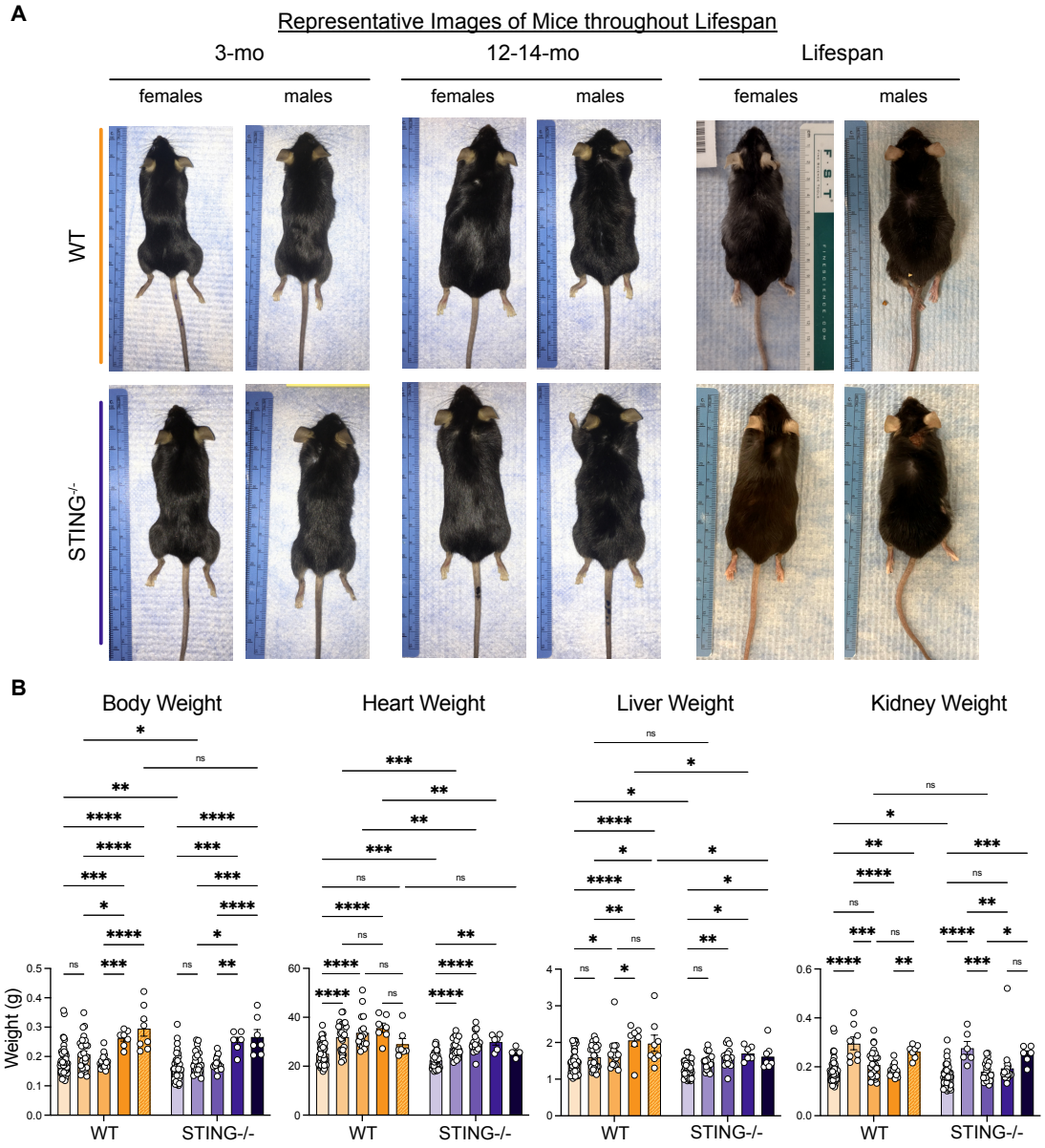

Figure 3.3.6 mouse images and body weights
(A) Representative images of female and male WT and STING$^{-/-}$ mice at 3-mo, 12-mo and lifespan timepoints. (B) bar graphs depict body, heart, liver, and kidney weights from 3-mo, 12-mo, 18-mo-24, mo, and lifespan (LS) (17-mo+) mice. 3-mo WT = 56, 3-mo STING-/- = 42, 12-mo WT = 30, 12-mo STING-/- = 23, 18-mo WT = 17, 18-mo STING-/- = 17, 24-mo WT = 7, 24-mo STING-/- = 6, LS WT = 8, LS STING-/- = 7; Bars that are 25% transparency are 3-mo, 50% transparency are 12-mo, 75% transparency are 18-mo, and darkest color is 24-mo. Bar graphs represent data by mean ±SEM and dots represent individual mice. The scoring system is explained in the methods. Two-way ANOVA with Tukey's correction factor was run; **** p< 0.0001, ***p<0.001, **p<0.01, *p<0.05, ns: p = 0.05-0.2, no value shown p>0.2.

With age, we see that body weights increase in both WT and STING$^{-/-}$ animals. 3-mo STING$^{-/-}$ body weights are significantly less compared to age-matched WT and remain significantly reduced or trending reduced wrights suggestive of reduced body condition[240,241]. Heart, liver and kidney weights were also reduced in STING$^{-/-}$ animals at 3-mo. In most instances, the organs weighed less in the STING$^{-/-}$ compared to age-matched WTs even though body weights increased. Most organ weights increase with age[241]. Typically decreased weight was only seen in very old mice and our data indicates that STING$^{-/-}$ mice, regardless of age, had a reduced organ weight, thus, suggesting uncommon aging effects and decrease in body condition.

To further identify changes in body condition, we utilized the animal health information to plot changes in body condition score (BSC) (**Figure 3.3.7A-B**).

A

Genotypes	Decreased BCS score	Dermatitis	Eye Abrasions	Abnormal Mass	Prolapse	Abdominal Distension
WT	0.65	0.47	0	0.06	0.47	0.2
STING$^{-/-}$	0.52	0.56	0.1	0.04	0.08	0.2

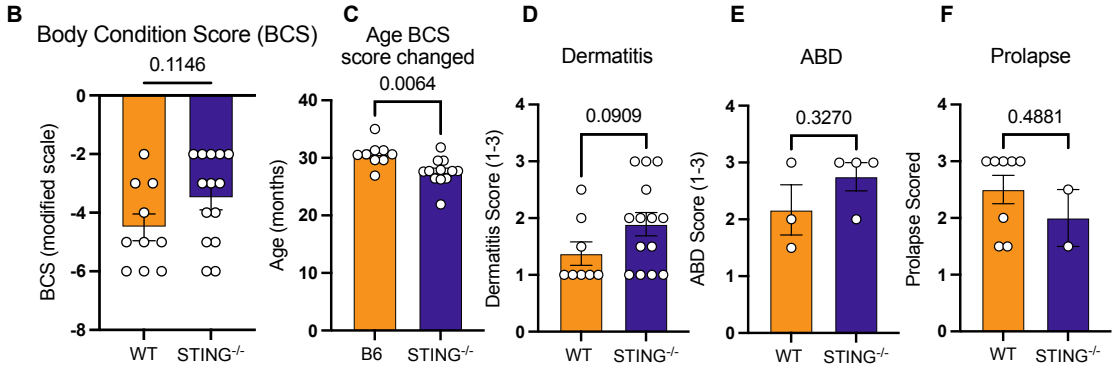

Figure 3.3.7. Body condition scores reveal reduced body conditions in STING$^{-/-}$ animals prior to euthanasia.
(A) Chart of percent (%) of animals with a decreased BCS score from total number of mice noted for required euthanasia followed by the reason for required euthanasia out of the total mice noted (% = #mice/total) of WT and STING$^{-/-}$ mice. (B) BCS (C) Bar graph depicts the age at which a mouse was at the time of euthanasia with a BCS score. (D) Bar graph depicts the score assigned to mice based on severeness from WT (gold) and STING$^{-/-}$ (purple). (E) Score assigned based on severeness of abdominal distension (ABD) from WT and STING$^{-/-}$. (F) Bar graph depicts the score assigned to mice based on severeness of prolapse from WT and STING$^{-/-}$. Student's t-test was run with Bonferroni correction factor. P values are shown not based on start values.

BCS scores were given to mice to assess overall health and were used to establish a standardized endpoint for euthanasia. The STING$^{-/-}$ mice did not received a worse BCS score (**Figure 3.3.7B**). Importantly, STING$^{-/-}$ mice were much younger when they were assigned a decreased BCS (**Figure 3.3.7C**). Though BSC scoring was assigned to more WT mice, STING$^{-/-}$ animals received worse scores for euthanasia in dermatitis, ABD, and prolapses (**Figure 3.3.7D-F)**. Given the increased inflammatory profile, worsened histopathology and overall degenerating health at time of euthanasia, we evaluated the role of STING-deficiency on lifespan. We note that STING$^{-/-}$ male mice showed a significant decrease in lifespan (**Figure 3.3.8**).

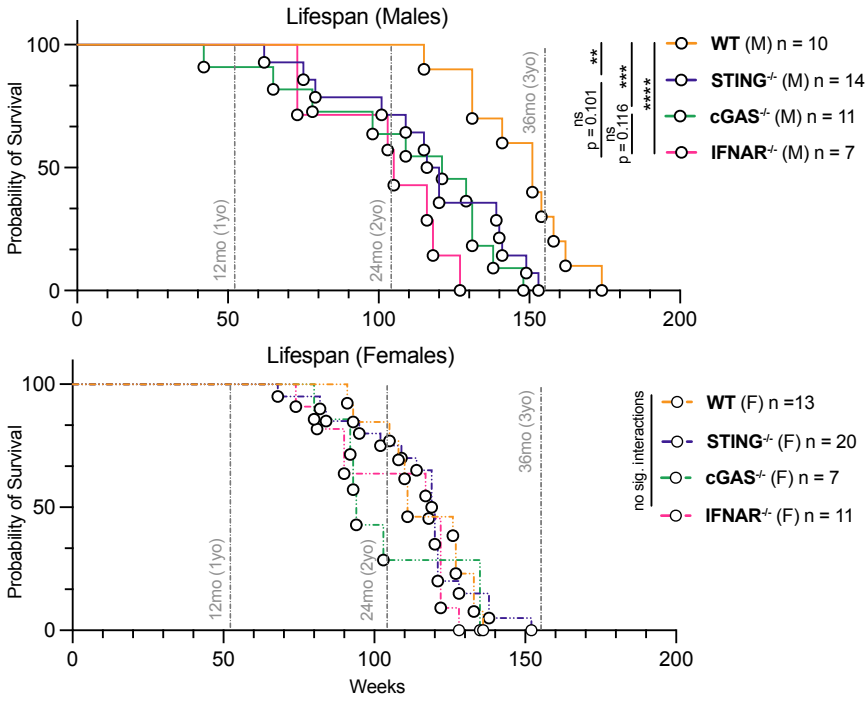

Figure 3.3.8. IFN-I-cGAS-STING-signaling pathway decreases lifespan in male mice.
(A) Top graph depicts lifespan survival data of male WT (gold), STING$^{-/-}$ (purple), cGAS$^{-/-}$ (green), IFNAR$^{-/-}$ (pink) mice. Bottom graph depicts lifespan survival data of female WT, STING$^{-/-}$, cGAS$^{-/-}$, IFNAR$^{-/-}$ mice. Data shows Kaplan-Meier survival probability curves with Mantal-Cox statistical significance test. **** p< 0.0001, ***p<0.001, **p<0.01, ns not significant.

Importantly, these changes were seen only in male STING$^{-/-}$, cGAS$^{-/-}$, IFNAR$^{-/-}$ mice, not females (**Figure 3.3.8**, bottom graph), suggesting that STING may influence the sexually dimorphic nature of longevity. Collectively, these data challenge current paradigms that place STING-signaling as a driver of chronic inflammation and shorter lifespans. Furthermore, our data underscore the importance of evaluating the role of STING and related molecules (cGAS and IFN-I) in physiologic aging to understand their role in homeostasis.

3.3.2. **The STING-signaling pathway encodes viability and vitality of TRMs and thereby accumulation of damaged DNA in tissue**

During pathway analysis within the brain 12-mo cohort, we saw upregulation of cell death regulating and response to stimuli pathways and we noted a decrease of key microglia populations in the STING$^{-/-}$ mice (**Figure 3.1.10** and **Figure 3.1.22**). Therefore, we investigated if TRM populations compared to bone marrow derived macrophages (BMDM) are more susceptible to forms of cell death (**Figure 3.3.9A-C**).

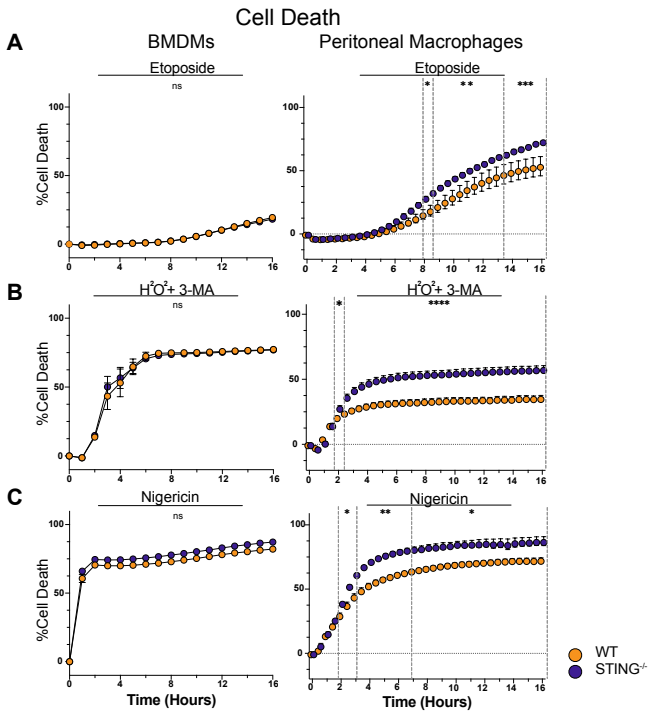

Figure 3.3.9. STING-deficiency drive TRM susceptibility to cell death mechanisms. (A) Graphs depict cell death curves of WT (gold) and STING$^{-/-}$ (purple) BMDMs and peritoneal macrophages with stimulation from Etoposide. (B) Graphs depict cell death curves of WT (gold) and STING$^{-/-}$ (purple) BMDMs and peritoneal macrophages with stimulation from hydrogen peroxide (H_2O_2) and 3-MA. (C) Graphs depict cell death curves of WT (gold) and STING$^{-/-}$ (purple) BMDMs and peritoneal macrophages with stimulation from nigericin. Student's t-test **** p< 0.0001, **p<0.01, *p<0.05, ns not significant.

We investigated cell death mechanisms associated with DNA damage induced cell death (etoposide), oxidative stress induced cell death (H_2O_2) and mediated by the autophagy inhibitor, 3-methyadenine (3-MA), and inflammasome-mediated cell death (nigericin). We compared BMDM to peritoneal macrophages as a proxy for TRM populations from 3-mo WT and STING$^{-/-}$. We note that STING$^{-/-}$ TRMs were more susceptible to multiple forms of cell death (**Figure 3.3.9A-C**).

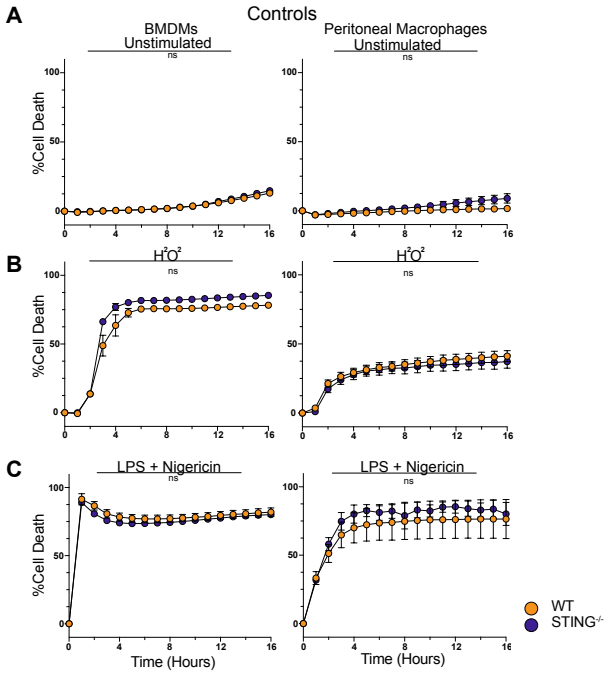

Figure 3.3.10. Controls for cell death comparing 3-mo WT and STING$^{-/-}$.
(A) Graphs depict cell death curves of WT (gold) and STING$^{-/-}$ (purple) BMDMs and peritoneal macrophages with stimulation from Etoposide. (B) Graphs depict cell death curves of unstimulated WT (gold) and STING$^{-/-}$ (purple) BMDMs and peritoneal macrophages. (C) Graphs depict cell death curves of WT (gold) and STING$^{-/-}$ (purple) BMDMs and peritoneal macrophages with stimulation from nigericin + LPS. Student's t-test

These data suggest that STING-signaling regulates responses to stimuli commonly seen with age that result in cell death. Overall, BMDMs from WT and STING$^{-/-}$ cells behave identically (**Figure 3.3.9** and **Figure 3.3.10**), supporting niche-specific contributions to cell-specific functions and sensitivity of TRM to cell-death stimuli. Collectively, these findings emphasize the responsiveness of TRMs to damaged DNA and stress responses, such as oxidative stress, which are common hallmarks are aging, and the critical role STING plays in tuning the responsiveness of TRMs to excessive DNA-damage and increased oxidative stress, both highly prevalent in aging tissue.

3.3.3. **TRM-dependent STING, a master regulator of tissue immune response, reinforces organismal longevity and homeostasis**

As STING is ubiquitously expressed, we utilized scRNA-seq data from heart, kidney, and liver datasets to determine *Tmem173* (STING) expression within cell populations. We saw that the cells resident to the tissue that express STING are primarily macrophages and stromal cells, such as endothelial cells (**Figure 3.3.11**).

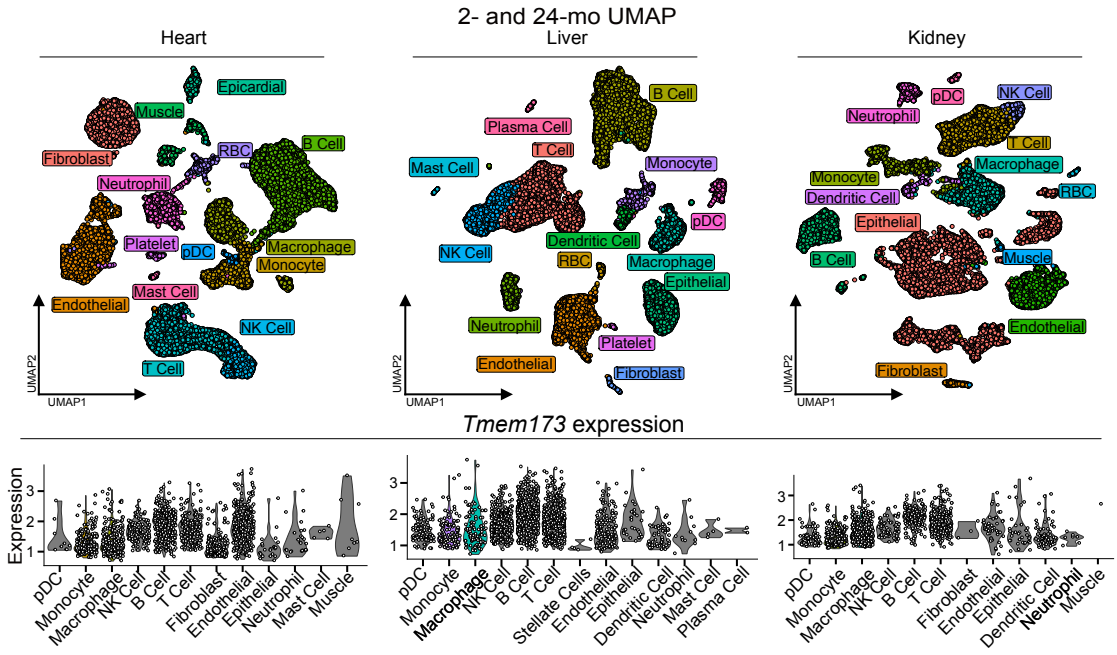

Figure 3.3.11. Macrophages and endothelial cells express *Tmem173*. Representative UMAP 24-mo cohort of heart, liver, and kidney single cells followed by violin plots of Tmem173 expression of identified cell populations by cluster from WT samples.

Adaptive immune cells also express levels of STING, but they are less likely to be resident to the tissue. In previous sections, we have noted the importance of STING-signaling in microglia population, the brain's TRM population. We showed how global STING-deficiency and STING-deficiency in *Csf1r* cells ($MG^{STING-/-}$ or $Csf1r^{STING-/-}$) contributed to exacerbated neuromotor functional decline (**Figure 3.1.16** and **Figure**

3.1.26). Therefore, we investigated the loss of STING-signaling within macrophage and more specific TRM populations reveals significant impacts on lifespan (**Figure 3.3.12**).

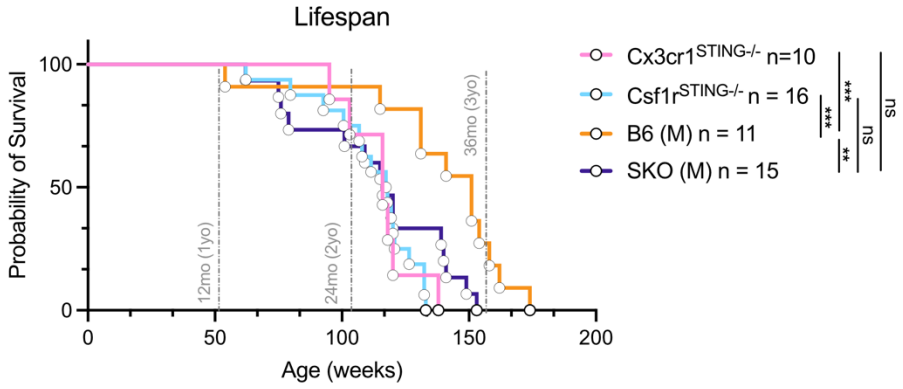

Figure 3.3.12. Loss of STING in TRM negatively impacts lifespan.
Graph depicts lifespan survival data of male WT (n = 11) and male STING$^{-/-}$ (n = 15) mice and female and male Cx3cr1$^{STING-/-}$ (n = 10) and female and male Csf1r$^{STING-/-}$ (n = 16) from both sexes. Ns are included within the figure. Data shows Kaplan-Meier survival probability curves with Mantal-Cox statistical significance test. ***p<0.001, **p<0.01, ns not significant.

We saw significant decreases in lifespan in both Cx3cr1$^{STING-/-}$ and Csf1r$^{STING-/-}$ mice compared to WT male mice. There were no significant differences in the cell-specific knockouts of STING compared to the global STING$^{-/-}$ mice. Preliminary data showed a general trending elevation of pro-inflammatory cytokines in Cx3cr1$^{STING-/-}$ and Csf1r$^{STING-/-}$ serum compared to their 3-mo and age-matched WT controls (Figure 3.3.13).

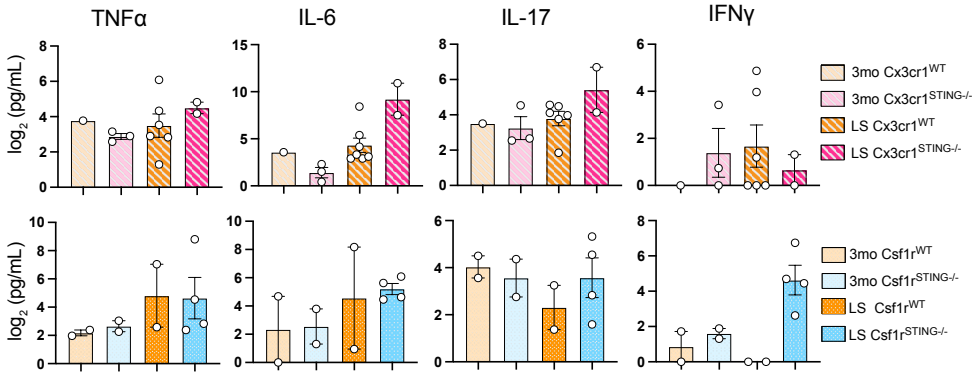

Figure 3.3.13. Pro-inflammatory cytokines in Cx3cr1$^{STING-/-}$ and Csf1r$^{STING-/-}$ serum.
(A) Bar graphs depict pro-inflammatory serum cytokines levels of 3-mo Cx3cr1^{WT} (n = 1) (orange) and 3-mo Cx3cr1$^{STING-/-}$ (n = 2) (pink) and Lifespan (LS) Cx3cr1^{WT} (n = 6)

(orange with fill pattern) and LS Cx3cr1$^{STING-/-}$ (n = 2) (pink with fill pattern) and (B) 3-mo (orange) and LS Csf1r^{WT} (orange with dotted fill pattern) (n=2/ group) and 3-mo Csf1r$^{STING-/-}$ (n = 2) (blue) and LS Csf1r$^{STING-/-}$ (n = 4) (blue with dotted fill pattern). No statistics was done due to number of mice –preliminary experiment.

These data suggest that macrophage-specific STING-signaling is an important inflammatory regulator protecting against age-associated pathologies and decline.

All experiments and analysis within this section are my own. Exceptions to this statement are as follows: Cell death assays were planned and completed with Machlan Sawden.

CHAPTER 4: **DISCUSSION**

4.1. OVERVIEW AND IMPACT

The compiled work in this thesis expands on the basis of aging and further describes the role of inflammation, senescence, and cell-specific contributions of innate immune pathways to age-associated pathologies. Further, this work highlights a beneficial role of TRM-specific STING signaling in preserving health and supporting longevity. Inflammation is a hallmark of aging and is commonly associated as a negative consequence to aging[27]. In the combined studies, we first describe STING as necessary in neuronal damaged DNA clearance, senescence signaling, and supportive of preserving neuromotor functions and BBB maintenance through microglia signaling. Next, we highlight the novel discovery of IRM populations during healthy aging and discover STING-independent IRM populations that expand with age. Next, we described the negative consequence of STING-deficiency in vital organs and circulating cytokines and chemokines. Overall, we have shown the importance and necessity of STING-signaling as a central safeguard against age-associated decline of multiple organ systems during physiological aging.

Previous studies defined STING as a pathological driver of age-associated inflammation; these studies inhibited STING with a small molecule in aged mice[126]. However, acute inhibition is not analogous to a constitutive, life-long deficiency in STING, which likely enforces numerous adaptive changes in the organism over its lifespan. The latter is more emblematic of the altered physiology in ~40% of humans with LOF variants of STING[83,242]. More than 40% of the human population have 4 major loss-of-function (LOF) single nucleotide polymorphisms (SNPs) in *TMEM173* or *STING1* (R232H, R293Q, HAQ, AQ)[82,83]. These SNPs all negatively affect innate immune signaling by impacting cell intrinsic signaling and resulting IFN-I and proinflammatory cytokine responses. Our studies underscore that STING inhibitors that are used haphazardly of existing LOF allelic variants of STING or for long periods of time may have unexpected

detrimental impact on neurological and systemic health-spans. In this work, STING-deficient mouse models were used to cover this critical gap, making this work directly relevant to a significant cross-section of the human population who possess a LOF STING variant.

Although most of our understanding of STING signaling is based on antiviral immune responses outside of the brain, there is a large amount of data that highlights the importance of this pathway in the CNS. IFN-I have a prominent role in neurodegenerative disease progression because of their ties to cellular stress which occurs during protein aggregation and cellular damage with age. Similar to IFN-I, STING plays dual roles in the CNS as a producer of IFN-I and proinflammatory cytokines. Hyperactivation of STING has been shown to play a role in AGS and PD. During AGS, damaged DNA triggers excessive IFN-I responses through STING signaling and results in elevated inflammation levels in the brain. In models of PD, STING expression increases, and cells are hyperactivated by α-synuclein aggregates, with microglia shown to be main drive of neuroinflammation in these models of α-synucleinopathies[243]. Our data suggest that STING is likely activated more with age because of the increased presence of damaged DNA in neuronal populations. However, in the absence of STING there is an increase of inflammation and more damaged DNA is present, which highlights a critical role of STING regulation of neuroinflammation and age-associated phenotypes. Therefore, it is possible that STING is activated to control inflammation and drive autophagy phenotypes, which are now known to be a basic function of STING[244,245]. TBI models similarly show that STING is important for autophagy and that STING contributes to neuroinflammatory environments through glial populations[246]. However, these TBI models are short-term studies that do not look at the overall impact STING-deficient animals beyond 24-hours post-TBI. In contrast to the detrimental effects of STING signaling, in MS models activation of STING was shown to reduce microglia

reactivity and inflammation[168]. We similarly saw that STING signaling was important for containing inflammation with extended aging. STING signaling is also important for antiviral responses and anti-tumor immunity[247]. The elderly populations are more susceptible to infections because of their impaired immune system. The activation of STING pathway is necessary for the recognition of viral DNA and activating immune protection[248], and could lead to detrimental outcomes if the already susceptible population has blocked this prominent antiviral pathway. Similarly, the prevalence of cancer is increased in the elderly population, and importantly, STING engagement promotes antitumor IFN-I and NF-κB-dependent cytokine production[249] and anti-proliferative[62] effects. These studies highlight the complexity of STING signaling and dual nature of STING. STING is important for driving IFN-I and proinflammatory cytokines, however this response may become detrimental after prolonged exposure. However, our data shows there are consequences to STING-deficiency during aging and the necessity of STING signaling may be more context and time dependent.

A question that remains unanswered in our studies is what ligands engage STING in these complex roles in the aging tissues. Though it is unclear how DNA damage is initiated with age, numerous studies continue to implicate damaged nuclear (genomic) DNA, marked by γH2A.X, (radiation damage, telomeric, mitotic chromatin breaks, etc.) and/or related sources of nuclear DNA (reactivated endogenous retroelements/viruses, micronuclei, microbes etc.) as persistent triggers of the cGAS-STING pathway[127]. To add further complexity, mitochondrial DNA (mtDNA) has recently been shown to activate cGAS[126]. It is also unclear whether it is mtDNA or DNA damage that drive STING signaling in our model, and contribute to feedback loops resulting in the accrual of mtDNA mutations to drive compounding mitochondrial instability and genomic stress[47,250,251]. Identifying what drives cGAS-STING activation remains an ongoing area of investigation.

4.2. MICROGLIAL STING IS A CENTRAL SAFEGUARD AGAINST AGE-ASSOCIATED NEUROLOGICAL DECLINE.

The role of innate immune pathways and cell types in neurological disease processes are increasingly well-described, however, the identity and role of innate pathways in maintaining homeostasis, especially with age, is poorly elucidated. Here, this work reports a role for the second-messenger sensor and ER-resident signaling adaptor, STING, in safeguarding neurological health, especially with age. First, we reveal STING is critical for the interrelated functions of neuronal DNA-damage clearance and the induction of senescence in non-neuronal cells. STING is critical in modulating cellular senescence with age[62,125,169,172], our data shows it may be a critical signaling component driving 'necessary' inflammation to protect against worsened damage. The overall protective role for STING in the CNS is further supported by our data that reveal that STING-signaling protects against detrimental changes in the immune transcriptomes and microglial populations with aging. In STING-deficient animals, homeostatic microglia population sizes decrease with age, with many of the microglia acquiring increasingly activated and proinflammatory signatures with age. Moreover, it is reasonable to speculate that this process at least partially, if not wholly, impacts microgliosis in the STING$^{-/-}$ brains as well. If microgliosis is a protective/appropriate response to damage in the brain, STING-deficiency is potentially restraining this transition, and fails to restrain accumulating damage with age.

Phenotypic and transcriptional changes within the aged STING$^{-/-}$ microglia populations and their physical proximity to endothelial cells suggest they drive accelerated BBB breakdown, increased incidence of microhemorrhages and aggravated neuromotor deficits. Importantly, we show evidence that microglial STING-signaling is critical for LLP accumulation, preventing BBB breakdown, and ensuing neuromotor deficits emblematic of aging in the full-body STING$^{-/-}$ mice. Collectively, our study represents a novel

paradigm shift revealing a protective role for the ubiquitous innate immune protein, STING, in neurological homeostasis with aging. Furthermore, we provide mechanistic insight into how *microglial* STING-signaling safeguards the trajectory of neurological aging by balancing senescence induction with damage-control and tissue repair, thereby mitigating archetypal age-associated neuropathology.

As the interface between the CNS and periphery, the BBB is essential for maintaining brain function[252]. Specifically, hippocampal BBB breakdown is an early event, directly linked to cognitive impairment with age in humans. How the BBB is maintained has yet to be fully elucidated[198], however, extrinsic inflammatory processes, such as a plethora of proinflammatory cytokines in the sera are directly implicated in BBB leakage during human patients with AD, PD, amyotrophic lateral sclerosis (ALS), MS[253]. The exact role and contribution of cell-intrinsic or CNS-restricted inflammatory components contributing to BBB breakdown is not well understood. Here we report the exacerbated disruption in the BBB in aged STING$^{-/-}$ brains compared to aged WT, which in turn correlates with the uniquely proinflammatory fingerprint of STING$^{-/-}$ CNS distinct from age-matched WT CNS. Our data thus indicate that the 'type' of inflammation may be a critical component of aging associated dysfunction, and in healthy aging, the type of CNS-intrinsic inflammation engaged presents as a critical and measured response to damage accrual, necessary for preserving BBB homeostasis.

The type of immune signature enriched in the STING$^{-/-}$ CNS is potentially insightful for characterizing the 'necessary' inflammatory responses that maintain homeostasis. While lacking key senescent, IFN-I stimulated and proinflammatory genes, STING-deficiency triggers the expression of other genes from these same pathways, prototypically associated with more pathological inflammation. In response to elevated levels of age-associated inflammation, Activator Protien-1 (AP1) complex members become transcriptionally more active across multiple mouse models of extended and shortened

lifespans[191]. We saw increased AP1 activation through the upregulation of AP1 family members (*Jun* and *Fos*) and inhibition of NF-κB (*Nfkbia)* which indicate preferential engagement of upstream pathways in the absence of STING. We note enriched transcriptional levels in both WT and STING$^{-/-}$ aged animals and show more specificity in microglia populations. Glial AP1 has been shown to be detrimental in the brain when chronically activated and becomes critical for sensing damaged neurons[254]. As AP1 has been defined as a driver of age-associated inflammation and neuroinflammation, our work contributes that without STING, there are heightened levels of pro-inflammatory cytokines, such as IL-6. Therefore, it is possible that STING mediates AP1 activation to tune inflammatory responses. Future studies will require more work to understand how STING suppresses inflammation via AP1. Overall, these data suggest that STING likely drives the induction of routine, “clearance-biased” inflammatory genes, critical in the sensing and removal damaged neurons. STING-deficiency, in contrast, instigates a pathological proinflammatory state indicative of unresolvable damage and increasing alarm.

Separately, Adaptor protein complex-1 (AP-1) (with a hyphen) is tightly linked to STING signaling. AP-1 sequesters phosphorylated STING into clathrin-coated vesicles to the lysosomes for degradation[255]. AP-1 was the first adaptor identified and it is most known for its capacity to transport cargo through clathrin-mediated trafficking[256]. Similar to STING[244,245], AP-1 complexes are evolutionarily conserved supporting a longstanding relationship to STING as part of its degradation system. Recently, it was shown that suppression of AP-1 mediated trafficking exacerbated STING-dependent responses[255]. It was reported that the hydrophobic residues on the cytosolic parts of STING were necessary for AP-1 trafficking and resulting in an increase of IFN-I if AP-1 was unable to bind to STING. It is unclear how STING-deficiency impacts these required processes

and if there are any unintended consequences to a dysregulated degradation pathway with age.

Our data extends our understanding of how STING-dependent senescence plays a role *in situ* and *in vivo* responses during aging. Indeed, the induction of senescence markers by STING-signaling may be a critical signaling intermediate in the resolution and clearance of on-going DNA damage in the CNS with age. Canonically, increased senescence is often considered another marker of age-associated loss-of-fidelity[119,257]. However, studies have also implicated senescence in critical pro-survival, anti-tumorigenic and wound-healing processes[119,257]. Intriguingly, recent studies suggest that outright removal of senescent cells from key tissues during aging may cause aggravated pathological outcomes[258]. The mechanistic basis for the latter studies remains unknown. Our findings may provide some insight into this observation. One possibility is that adequate cellular senescent remodels inflammatory signatures in cells that make up the BBB and subsequently recruits microglia in a STING-dependent fashion to silently clear and repair damage in the vasculature. The decrease in this signature or the decreased capacity of STING-deficient microglia to sense secreted signals, leads to pathological responses by the microglia likely promoting the disruption and damage of vasculature rather than repair.

Changes in microglia states, such as DAMs, have been shown to increase with age and in neurodegenerative diseases, such as AD, MS, ALS[166,173,188,209]. Researchers have found CLEC7A^{+} microglia surround amyloid-beta plaques in AD mouse models and human samples during neurodegenerative states. They go on to show that restoration of homeostatic microglia in mouse models protect against neurodegeneration[209,259]. Our data corroborates and extends these studies and implicates STING-dependent processes in preserving homeostatic microglia populations by enriching necessary inflammatory mechanisms that are functionally important for CNS maintenance. The

absence of STING attritions not just key populations of homeostatic microglia (Cx3cr1^{hi})[173] but also precursor microglia (Ly6C^{hi}) known to replenish depleted microglia niches in the CNS[210,211]. In addition to an increased loss in key microglia subsets, we show that the STING-deficient CNS acquires microglia with an exaggerated inflammatory signature, typified by upregulation of cellular-stress associated AP1 transcriptional module with concomitant increase in negative regulators of NF-κB, *Nfkbia*. Considering these data, it is likely that microglial-STING dependent induction of core protective inflammatory pathways routinely contribute to microglia-supported repair mechanisms.

With age, the brain is susceptible to DNA damage and senescence; classic hallmarks associated with age. DNA damage is directly linked to neurodegenerative diseases and is used as an early indicator of neuropathology[260]. Neurons are particularly in danger of accumulated damaged DNA as postmitotic cells. As postmitotic cells, neurons are unable to perform most DNA repair mechanisms beyond non-homologous end joining (NHEJ). The most common genomic stress that occurs is single-stranded breaks (SSBs), largely from reactive oxygen specifics (ROS) attacking DNA oxidized bases and abasic sites[261]. This is most prevalent in neurons because of the energy expenditure that is required for basic functions. DSBs occur in neurons through transcriptional activity rather than replication[260] and the only likely repair mechanism to repair DSBs is NHEJ. This process is error-prone and DSBs are marked by γH2A.X. Though these processes are found throughout the lifespan of the animals, DSBs are most prominent in aged populations due to reduced function of DNA repair mechanisms, thus securing damaged DNA as a hallmark of aging in the CNS. However, γH2A.X is also used to mark DSBs in neurons during memory formation, a basic cognitive function. It was shown that TLR9 sensing of DSBs drives inflammatory activation in hippocampal CA1 neurons and activation supports repair mechanisms necessary for memory formation. Furthermore,

neuronal-specific deletions of TLR9 resulted in impaired memory and alterations in the neurons transcriptional landscape[108]. DSBs appear to be a critical signaling component of the neuroimmune system that results in both positive and negative consequences. Unregulated DDR pathways drive cells to become senescent, undergo uncontrolled cell division, or apoptosis. DNA damage is a potent activator of senescence and multiple downstream proinflammatory pathways through DDR pathways or mis-localization of 'self'-DNA[260,262]. Cells that become senescent exert SASP profiles, which are made up of pro-inflammatory cytokine, chemokines, growth factors, and extracellular matrix proteases. It has been shown that full body removal of senescent cells has positive outcomes in mouse models of neurodegenerative diseases[263]. Intriguingly, recent studies suggest that outright removal of senescent cells from key tissues during aging may cause aggravated pathological outcomes[258]. In our work, we show correlations between increased neuronal DNA damage and BBB breakdown and the reduced levels of senescent cells in the brain. In mouse models of disease, senescent cells, commonly marked by p16 (*Cdkn2a*) or p21 (*Cdkn1a*), are reported in multiple cell types found within the brain such as neurons, microglia, astrocytes and stromal cells[264,265]. Importantly, SASP initially is beneficial to clear other senescent cells, but over time the chronic exposure results in more senescent cells[61]. It is important to decipher the positive contributions of senescence, such as wound healing and tissue repair, from the negative consequences that result in an unrestrained chronic inflammatory niche.

A contributing factor of the unrestrained activation of iinflammation is the engagement of the upstream cytosolic DNA sensor, cGAS. In 2023, Gulen et al.[126] showed that cGAS-specific engagement increased inflammatory genes and ISGs using a mouse model that activated cGAS in microglia in the absence of a ligand. These mice showed the importance of cGAS without a trigger and that STING antagonist reduce inflammation and reverse neurodegeneration[126]. In our hands, cGAS$^{-/-}$ mice showed age-dependent

neuromotor deficits similar to WT animals and compared to STING$^{-/-}$ and IFNAR$^{-/-}$ mice. They also had a significantly reduced lifespan similar to STING$^{-/-}$ mice. Therefore, lifespan and neuromotor deficits are likely dependent on cGAS-signaling. In opposition to our STING$^{-/-}$ data, LLP accumulation was not dependent on cGAS-signaling. Therefore, LLP accumulation during physiological aging is cGAS-independent. These data were surprising as we know that cGAS is necessary for senescence[62] and so more investigation into the purpose of LLPs is required. We suggest that there are cGAS-independent mechanisms that impact specific aspect of neurodegeneration, such as senescence.

The timeline associated with CNS age-associated decline mimics that of other organ systems[124]. Further, while the number of deaths attributed to heart disease, cancer, and stroke decreased in the last couple of decades, the number of deaths attributed to AD increased by 70% between the years 2000 and 2013[124]. These data suggest that while understanding how age impacts all organs, there is critical need to understand more about how age impacts brain function and the underlying immune mechanisms that drive age-related changes. Our study demonstrates that STING is a critical and necessary signaling component that preserves CNS health with age (**Figure 4.2.1**) and urges caution in indiscriminate inhibition of the STING-signaling pathway with age.

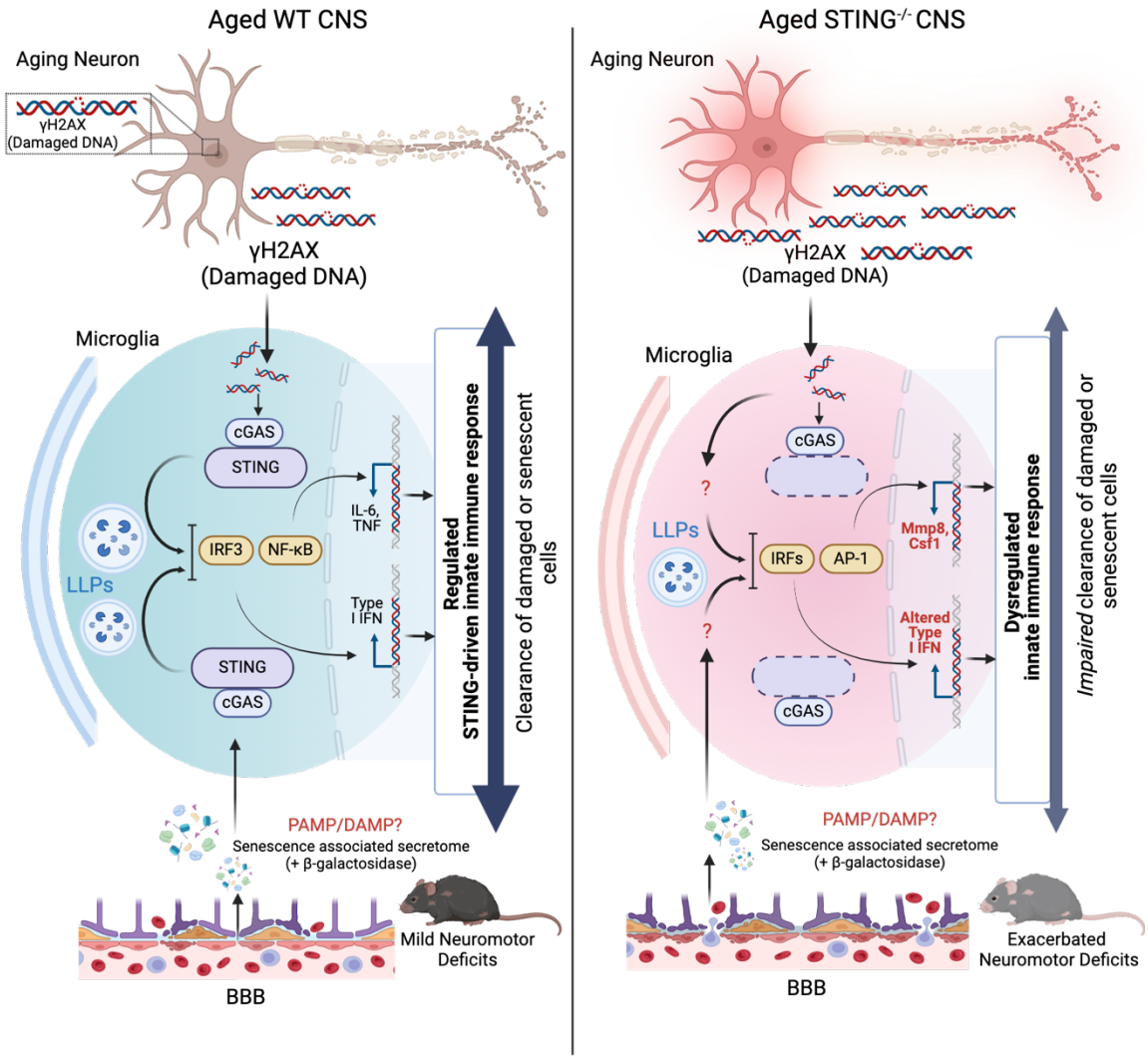

Figure 4.2.1. Graphical representation of the consequences of STING-deficient aging in the CNS.
During normal aging (WT) in the brain, damaged neuronal DNA, marked by phosphorylated H2AX (γH2A.X), accumulates with age and likely activates STING to upregulate IFN-I and inflammatory genes. Senescence increases in WT animals in an age-dependent manner and BBB integrity is compromised resulting in neuromotor deficits. During STING-deficient (STING$^{-/-}$) aging, the inflammatory components are altered and drive a more neurodegenerative inflammatory states that results in the accumulation of more damaged. The mice showed reduced cellular senescence marked by LLPs and senescence-associated beta galactosidase (SA-β-Gal). However, senescence associated secretory phenotype (SASP) and neurodegeneration-associated gene expression profiles were upregulated in STING$^{-/-}$ animals. STING$^{-/-}$ mice also had worsened functional outputs in all the following: neuromotor deficits, degradation of BBB integrity, and microhemorrhages in an age-dependent manner. Specifically, microglial-STING provides protective and necessary inflammatory components that keep progressive age-associated decline mechanisms, such as inflammation and structural deterioration in check, as these phenotypes are worse in STING$^{-/-}$ compared to WT. *(Created with Biorender.com)*

4.3. STING-DEPENDENT INTERFERON-RESPONSIVE MICROGLIA SUPPORT HOMEOSTATIC FUNCTIONS WITH AGE.

IFN-I are an important immune regulator for antiviral defenses, but their role within the CNS and physiology is unclear. First, IFN-β is one of the current treatments for multiple forms of MS as the first disease-modifying therapy. For MS treatments, the mechanism of action is not completely understood, but we do know that IFN-β regulates IFN-I signaling through IFNAR engagement, T cell activation, and drives anti-inflammatory cytokine production[130]. In instances of interferonopathies, such as SLE and Aicardi-Goutières syndrome (AGS), chronic production of IFN-I is a toxic feature of these disease states[266]. IFN-I are produced and regulated through a multitude of pathways further adding to the complexity of IFN-I[89]. Here, we highlight that STING-dependent mechanisms drive IFN-I responses within the aging brain and influence IRM populations. Similar to others, we identify a small IRM population[109] and show that specific ISG and proinflammatory transcriptional landscapes are dependent on age and STING-signaling. STING-dependent IFN-I transcription increases with age in our dataset, and it has been shown that IFN-I-dependent microglia populations are essential for cortical development underpinning a homeostatic function of IFN-I signaling in neuronal pruning[109]. Since pathways expressed during development may become re- or aberrantly expressed during disease[188], re-expression of a specific subset of IFN-I genes may be beneficial with age as they play homeostatic roles during development. Similarly, interferon responsive populations were found in the white matter of aging mice and shown to be moderated by adaptive immune responses[220]. Removal of $CD8^+$ T coincided with a reduction of IRMs and interferon-responsive oligodendrocytes (IROs), resulting in altered aging phenotypes within the white matter. However, the specific cellular mechanisms that dictate adaptive control of IRMs, IROs, and interferons and resulting impact on health unclear. These combined studies, highlight the complicated role of IFN-I signaling

and the related cell populations. Though it may prove to be beneficial, we suspect that experiments with re-expression of IFN-I will have a range of effects that are difficult to predict. Furthermore, the exact timing of administering a correct dose of IFN-I remains a challenge in physiologically aged animals. These data underscore that STING-deficiency leads to an overall poor performance of a key glial cell type, microglia, customarily responsible for homeostatic functions, such as neuronal corpse disposal. Therefore, if the population is performing neuronal engulfment functions[109], it may not be beneficial to have a larger frequency of this populations as is seen in the STING$^{-/-}$ brains. More work is necessary to elucidate specific roles of IFN-I the triggers for activation within the CNS. In injury models, researchers described high levels of dsRNA in neurons that require mitochondrial antiviral sensing protein (MAVS)-sensing for appropriate activation of IFN-I to support neuronal engulfment[109]. In the context of memory formation, neuronal dsDNA sensing through TLR9-specific engagement is critical for memory formation through DDR pathways[108]. This work identified NF-κB and not IFN-I as downstream mediators for the inflammatory responses that support neuron encoded memory. We noted changes of NF-κB signaling molecules (*Nfkbia*) within the transcriptional landscape of STING$^{-/-}$ microglia populations. Given that different triggers drive specific responses downstream of TLR9, we ask a similar question whether damage from specific cells or sources drive specific IFN-I or NF-κB pro-inflammatory responses from specific microglia populations. We ask if IRM populations are beneficial a support necessary inflammation, while other microglia populations become more inflammatory and skew towards an NF-κB signaling phenotype.

This data further suggests that the STING$^{-/-}$ brains are declining faster and begins to implicate a specific population of microglia. While there were many ISGs upregulated in the IRM4 cluster, there were also other genes upregulated that are associated with DAM signatures and neurodegeneration. One such gene is *Ctss*, which encodes for Cathepsin

S (CTSS) and is important for immune responses as a lysosomal cysteine protease. CTSS is activated by its pro-peptide within lysosomes and is important for antigen processing and presentation[267]. It has also been shown to increase in AD[268] and aging[269] and is found to be preferentially expressed in myeloid cells, such as microglia[270]. CTSS derived from CP-macrophages cleave tight junction components, claudin 1 (CLDN1), within the choroid plexus causing disruption to blood-CSF barrier functions with age[270] and blocking *Ctss* transcription was protective against brain damage after stroke[271]. Recently, it was shown that CTSS also dysregulates calcium (Ca^{2+}) fluxes, is necessary for action potential in neurons, and acts a secondary signal during immune signaling[272]. Therefore, continued research within the CNS is necessary to understand this critical intersection between the CNS and the immune system.

We showed that specific ISGs are up and downregulated in aged STING-deficient animals. Within the same IRM4 cluster, we saw *Ctss* was upregulated in the $STING^{-/-}$ scRNA-Seq datasets and therefore it is possible that key IFN-I production which is dependent STING-signaling is suppressing CTSS and potentially other cathepsin levels with age. Others have shown that IFN-β suppress cathepsin levels and impair immune cell migration[273]. This presents another avenue by which STING-dependent IFN-I may regulate inflammation and protect against BBB breakdown.

In summary, this data supports STING-dependent IRM populations as providing protective mechanisms with age (**Figure 4.3.1**) and demonstrates that more research is needed to fully understand the impact of this pathway with age.

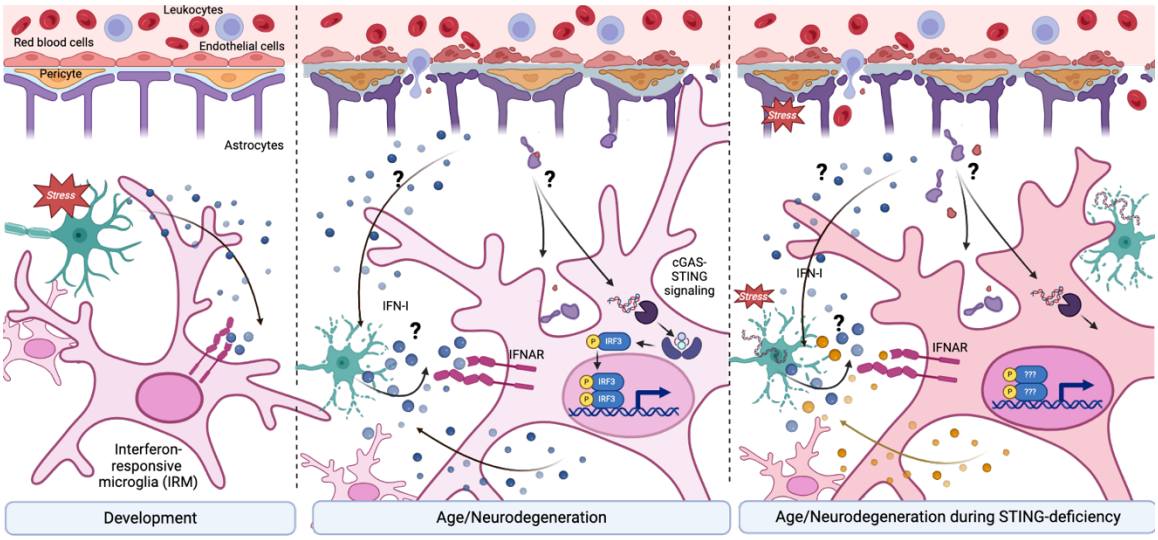

Figure 4.3.1. IRM behavior in development is mimicked with age and during neurodegenerative states.
Interferon responsive microglia (IRM) described during development, aging/ neurodegenerative states with and without STING. During development, IRMs drive phagocytic functions and inflammation to clean up debris and stressed/ damaged neurons. With age, STING-dependent signaling supports microglia homeostatic functions and provides protection against excessive inflammatory states and necessary and appropriate levels of IFN-I production. Similar to development stages, IRMs are critical for overall brain health with age. IRMs sense molecular patterns in the environment and respond through STING-dependent mechanism. Therefore, STING-deficiency aging and likely downstream alterations of IRM populations result in increased neurons with DNA damage, excessive inflammation, and worsened BBB breakdown as normal IRM populations are altered with age and not able to appropriately respond to the stressed or damage neurons that normally accumulate with age and increase even more with STING-deficiency. *(Created with Biorender.com)*

4.4. **STING** PROTECTS AGAINST SYSTEMIC DECLINE WITH AGE AND PRESERVES LONGEVITY.

The role of inflammation is well defined as a hallmark of aging[27]. However, which key innate immune pathways that drive the inflammatory signatures remains unclear. Similarly, the primary cell types which drive the responses remain poorly defined. The work here investigating vital organs (heart, liver, kidney) begins to address key cell types and pathways that are responsible for age-dependent inflammation. We investigated the impact of STING-deficiency on inflammatory serum signatures, tissue deterioration, and consequences on lifespan. STING is responsible for the production of IFN-I and pro-

inflammatory cytokines in viral[75], injury[226], and disease[171,235,253,274] settings. However, contrary to expectations, the data highlights a necessary and beneficial role for STING signaling in preserving tissue architecture and controlling systemic inflammation. We also highlight that long-term loss of STING signaling results in a shortened lifespan, revealing a critical need for STING-signaling. A recent study has comprehensively investigated STING expression and activation levels in tissue during development[232]. They highlight that STING is essential for homeostatic functions that regulate immune cell differentiation and functionality[232]. In concordance with this recent publication, we suggest a protective role of STING signaling with age.

The data presented in this thesis highlights the complexities of STING's role in regulating inflammatory profiles and homeostatic properties that protect the aging organism against uncontrollable inflammatory profiles. Our data calls for more in-depth research into the long-term loss of STING, which is found in ~40% of the human population[83,242]. These LOF polymorphisms generally show impaired DNA sensing and reduced innate immune responses, as well as reduced functionality in monocytes within human population[242]. Humans with LOF *Tmem173* develop autoimmunity and are more susceptible to viral infections. Our understanding of the benefits of STING have expanded dramatically in cancer research. In human acute myeloid leukemia cell lines, cancer cells directly silence STING to reduce IFN-I production, resulting in a protected tumor microenvironment[275]. Our lifespan data supports what is seen in the human population, that the loss of STING results in negative consequences. We show that the loss of STING in macrophages mimics the global STING$^{-/-}$ lifespan, suggesting that macrophage-specific STING-signaling is the critical mediator of inflammation and disease progression, similar to the human population. More research is required to identify specific triggers (i.e. cell types or types of damage) and the mechanisms that activate STING to control the downstream responses. The triggers can cause acute or

chronic STING-signaling, which have different durations and outcomes. Acute STING-signaling has a quick resolution period and is controlled by ISGs and removal of phosphorylated STING. Phosphorylated STING is removed through microautophagy from recycling endosomes. STING is brought into vesicles and encapsulated into lysosomes for degradation[255,276]. This process stops active signaling and disruption of the ESCRT pathway drives more cytokine production via active STING-signaling[276]. The lack of resolution after chronic inflammation may contribute the tissue degradation and of the dysregulation of tissue function and integrity seen in the heart, liver, and kidneys. Any process that prolongs STING-signaling may ultimately be detrimental. However, STING-signaling is still a necessary regulator of IFN-I and proinflammatory cytokines and caution should be used during STING-antagonist or agonist therapeutic studies. Though chronic activation of STING may lead to unresolved inflammation, the chronic loss of STING similarly results in an increase of damaged DNA and activation of different inflammatory signatures. The canonical activation is through cGAS and development of the secondary messenger cGAMP[73,76]. We see the presence of damaged DNA, imaged by γH2A.X, and know that a likely ligand is present. However, STING can be activated independently of cGAS[14] and the transcriptional responses are dependent on the mode of activation. More research will be required to understand the alternative inflammatory pathways that are driving the tissue degeneration, increased inflammation, and ultimately decreased lifespan.

Our work also notes sex differences in the lifespans of STING$^{-/-}$ mice. Though data from previous sections did not discriminate between sexes, it is possible that overall sex-specific differences controls protein patterns with age. In a study of diabetic kidney disease (DKD), researchers focused on sex differences and age-specific contributions resulting in DKD and saw significant differences in activity of cGAS/STING in male mice

compared to females[277]. Future studies to decipher specific differences between sexes with STING-signaling will aide in clarifying specific triggers and changes during aging. In summary, the data presented supports a beneficial role of TRM-STING signaling with age in the heart, liver, kidney, and bloodstream (**Figure 4.4.1**).

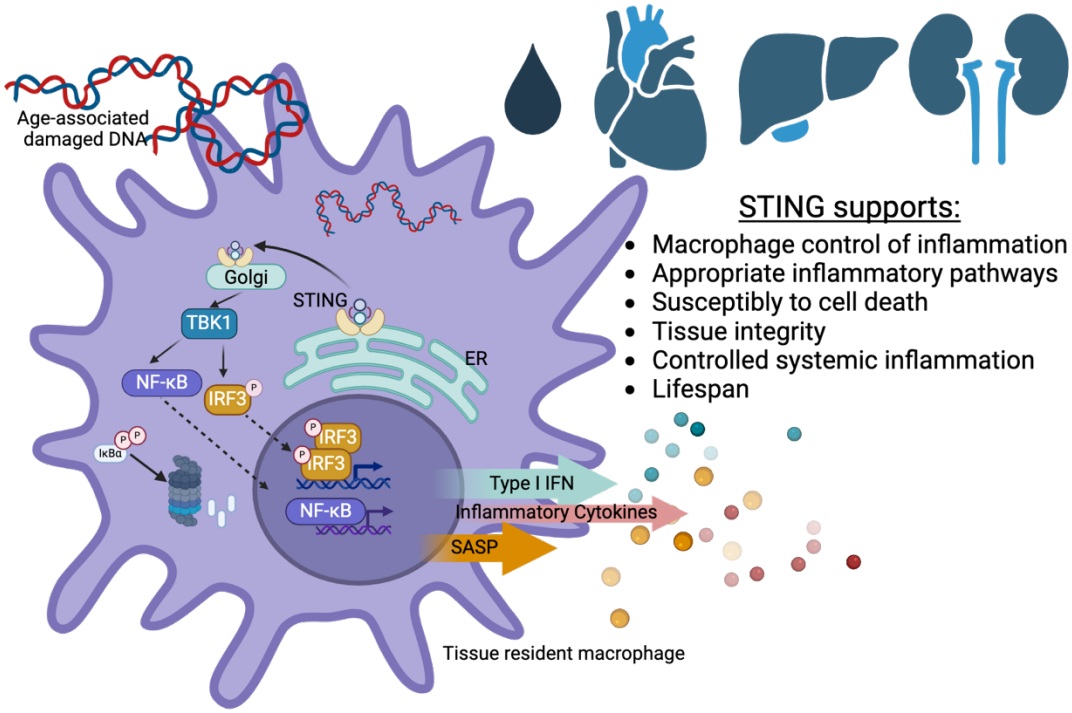

Figure 4.4.1. Tissue resident macrophage promotes homeostasis via STING-signaling with age.
Tissue resident macrophage (TRM)-specific STING-signaling preserves homeostasis during aging in the heart, liver, and kidney with age. TRMs sense damaged DNA within the tissues to activate the STING-signaling pathway and corresponding type I interferon (IFN-I), pro-inflammatory cytokines and associated senescence-associated secretory phenotype (SASP) cytokines. Macrophage-specific STING signaling suppresses exacerbated pro-inflammatory pathways, protects TRMs against susceptibility to multiple triggers of cell death, and protects against deteriorate and consequential dysfunction of all the tissues. Systemic inflammation is contained by STING-signaling and protects against shortened lifespan during physiological aging. *(Created with Biorender.com)*

4.5. Limitations and Future Directions

4.5.1. CNS and Microglia

While our study relies on comprehensive, complimentary, and rigorous approaches, some key limitations persist. First, we observe that STING-deficiency leads to a

reduction of senescence markers, LLPs and SA-β-Gal in the CNS, which coincides with an increase in neuronal DNA damage, suggesting that these processes are linked. However, we are only able to show correlation between these two pieces of data, as the molecular detail of this intersection likely requires in-depth inquiries into multiple cellular processes (e.g. *p53* signaling, mitochondria recycling, autophagy or lysosomal functions), potentially in a cell-specific manner. Further experiments are required to determine the specifics of glial senescence and if/how it is acting as a signal for clearance of degenerating neurons marked by DNA damage. Second, our work highlights a link between microglia and CNS vasculature that relies on STING. While we are able to show that STING in microglia determines this interaction, the molecular details of microglia-endothelial cell interaction remain untested and cell specific roles of STING during BBB maintenance remains unknown. Third, examination of other pattern recognition receptors (PRRs), including specific TLRs, are important for sensing damage DNA will be critical for fully understanding the source of proinflammatory signatures in the absence of STIING and the specific contribution of microglial STING-signaling with age. Fourth, which transcription factor/pathways downstream of STING determine its protective roles remain uncharacterized, although our study does implicate NF-κB and AP1 as key regulators of protection vs. pathology. Finally, future studies with spatial transcriptomic, proteomic, and imaging data, will exponentially enhance our understanding of STING's role in shaping location and function of key microglia subsets, especially those that localize proximal to endothelial cells and vasculature. These experiments will also further elucidate STING-dependent roles in other cell types of the brain, because STING is ubiquitously expressed (although enriched in microglia).

4.5.2. **Periphery and TRMs**

Our study identified major structural and health specific changes in the absence of STING signaling. Though the data highlights specific relevance to the human population there are key limitations that will need to be addressed in future work. First, our study briefly touches on the relevance of macrophage-specific STING signaling for lifespan. Future experiments would include a comprehensive immunophenotyping panel, scRNA-Seq of stromal and macrophage populations, and immunofluorescence to determine presence or alterations of ligand availability. Secondly, IFN-I drives B and T cell differentiation and maturation[89] and therefore, we further investigate into how STING-deficiency and changes in the IFN-I production impacts the adaptive immune responses. Similar to the above section, more research is needed to identify which transcription factors are downstream of STING and alter the signaling and inflammatory profiles.

4.6. **CONCLUDING REMARKS**

In summary, the work presented in this thesis reveals that (1) microglia-specific STING-signaling is a safeguard against neuromotor decline and BBB dysfunction, (2) STING-dependent IFN-I responses suppress detrimental microglia transcriptional landscapes, and (3) STING-deficiency in vital organs similarly results in worsened tissue architecture and macrophage-specific deletion of STING reduces lifespan similar to global STING$^{-/-}$ compared to WT mice. STING is implicated in many age-associated disease progressive states and more work will be necessary to determine critical times during healthy aging that makes these necessary immune responses detrimental. This work importantly identifies the critical innate immune signaling pathway, STING, as providing control of inflammatory networks and pathways and further identifies STING-dependent microglia-signaling as important for overall health-span.

CHAPTER 5: **APPENDIX**

5.1. SUPPLEMENTAL FIGURES

5.1.1. QC of 12-mo and 24-mo datasets for scRNA-Sequencing analysis.

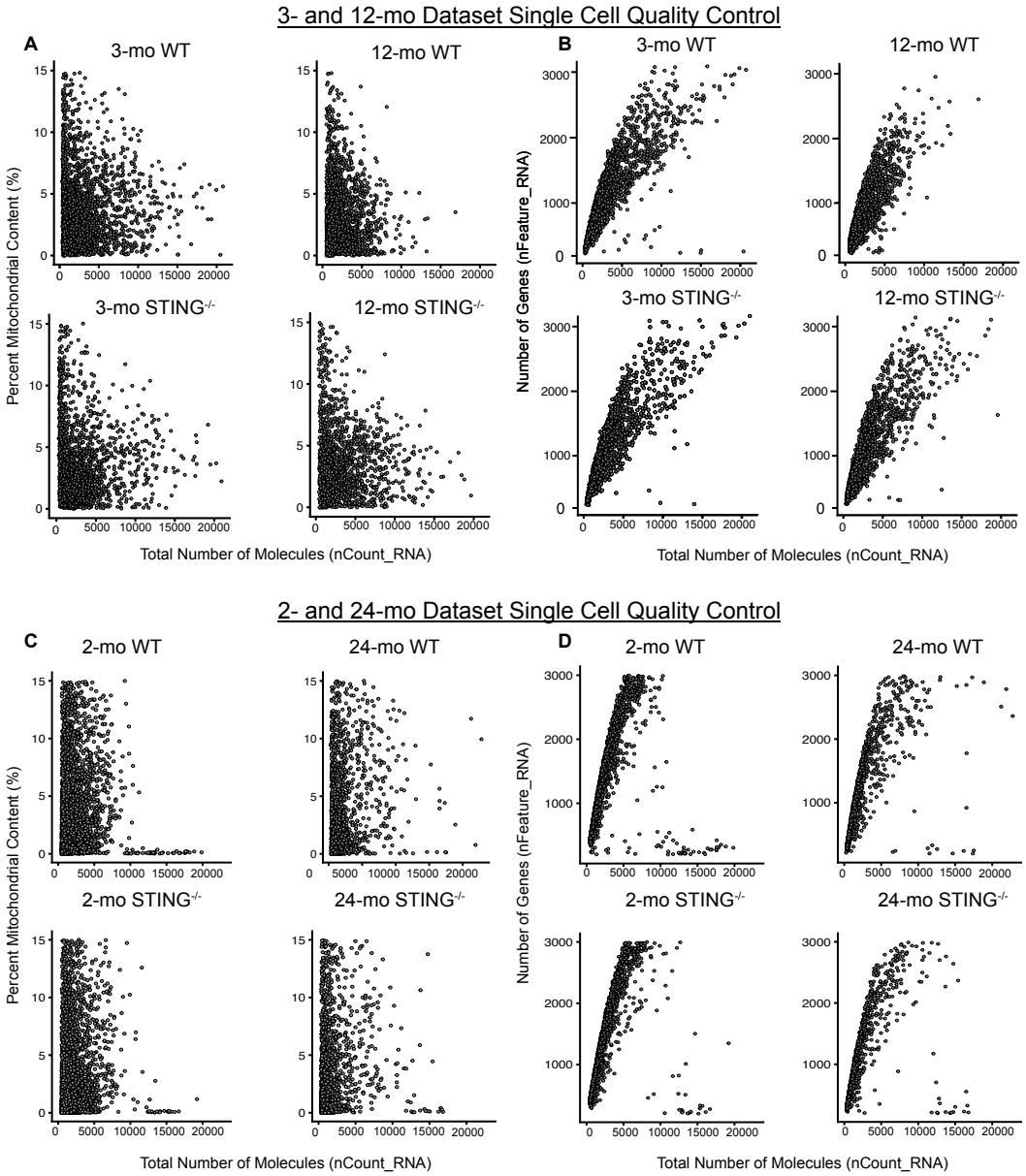

Figure 5.1.1. scRNA sequencing data QC.
(A) 3-mo and 12-mo scatter plots of total number of molecules vs. percent mitochondria of cells used during analysis for 3-mo WT, 12-mo WT, 3-mo STING$^{-/-}$, 12-mo STING$^{-/-}$. (B) 3-mo and 12-mo scatter plots of total number of molecules vs. number of genes of cells used during analysis for 3-mo WT, 12-mo WT, 3-mo STING$^{-/-}$, 12-mo STING$^{-/-}$. (C) 2-mo and 24-mo scatter plots of total number of molecules vs. percent mitochondria of cells used during analysis for 2-mo WT, 24-mo WT, 2-mo STING$^{-/-}$, 24-mo STING$^{-/-}$. (D)

2-mo and 24-mo scatter plots of total number of molecules vs. number of genes of cells used during analysis for 2-mo WT, 24-mo WT, 2-mo STING$^{-/-}$, 24-mo STING$^{-/-}$.

5.1.2. **Mouse BCS and Neurological Readouts**

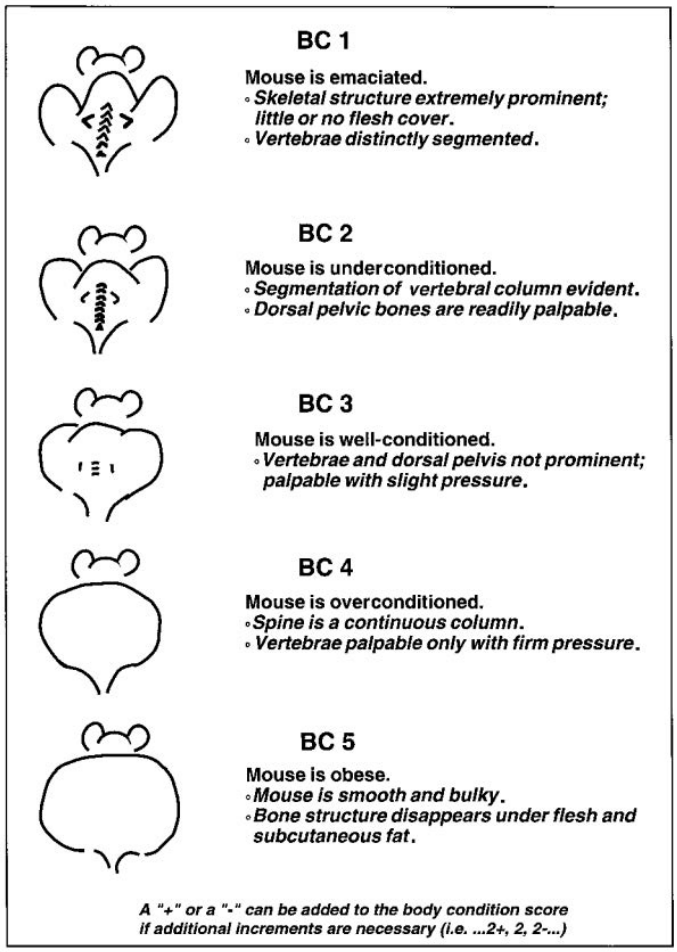

Figure 5.1.2. Body Condition Scores (BCS) diagram.
Diagram Figure1. from Ullman-Cullere and Foltz (1999) highlighting specifics to BCS scores used by DLAM to determine BCS.

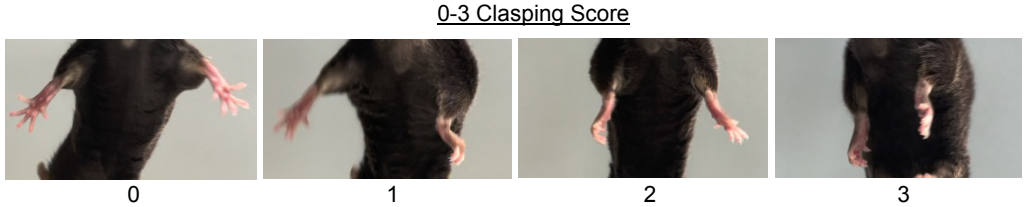

Figure 5.1.3. Scored 0-3 Clasping behavior.

(A) Representative images of splaying behaviors 0-3. Quality of clasping is represented (hindlegs are retracted or splayed by a single leg or both legs (0 = hindlegs splayed away from abdomen, 1 = one hindleg retracted towards abdomen for 50% of the time, 2 = both hindlegs retracted towards abdomen for 50% of the time, 3 = hindlegs entirely retracted)

5.1.3. **Gating for flow cytometry of middle-aged WT and STING$^{-/-}$ brains.**

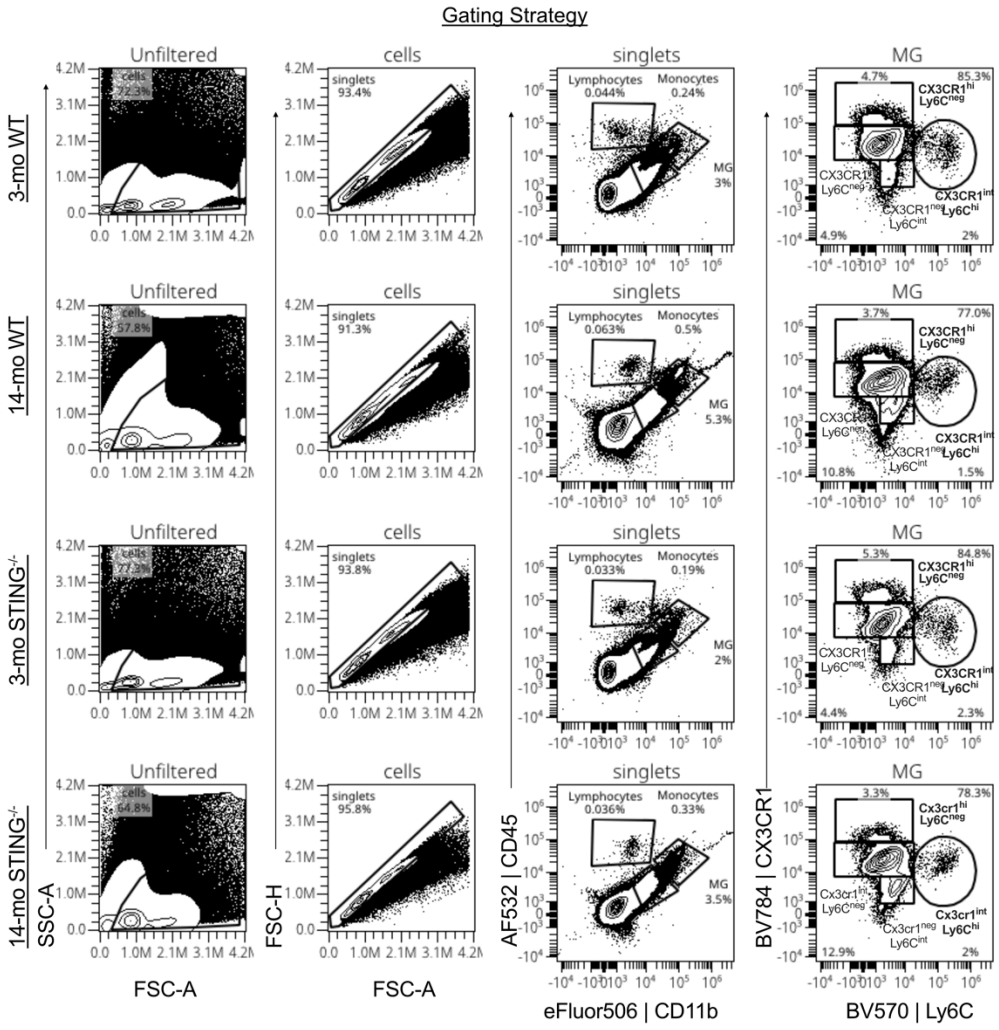

Figure 5.1.4. Flow cytometry gating strategy for microglia.
Representative gating strategy from 3-mo and 14-mo WT and STING$^{-/-}$.

5.1.4. **Top 10 DEGS from microglia populations.**

Table 5.1. Top 10 DEGs of microglia populations from all samples combined.

Microglia populations	Top DEGs	Metascape® Top Pathway Hits based on top 10 DEGs
MG1	*Fcrls, Ecscr, Adora3, Tspan4, Sall1, Herc2, Slc40a1, Thrsp, Tmem100, Gp9*	(1) tube morphogenesis
MG2	*Arhgap45, Cx3cr1, P2ry13, Vgll4, Pld1, Foxn3, Arhgap5, Rnaset2b*	(1) positive regulation of cell migration
MG3	*mt-Atp6, mt-Nd1, mt-Cytb, mt-Nd4, Cox4i1, Atp5l, Cox6c, Cox7c, Atp5j, 1500015O10Rik*	(1) Oxidative phosphorylation (2) oxidative phosphorylation (3) proton transmembrane transport
MG4	*Ccl3, Zfp36, Acox3, Rgs1, Slc15a3, Btg1, Ier5, Gpr183, Wbp2*	(1) Signaling by GPCR
MG5	*Jun, Hspa1a, Btg2, Hspa1b, Gem, Tmx4, B430010I23Rik, Hsp90aa1, Jund, Acox3*	(1) Attenuation phase (2) MAPK signaling pathway (3) IL-17 signaling pathway
MG6	*Fos, Nfkbia, Ier2, Egr1, Dusp1, Atf3, Ppp1r15a, Dnajb1, Nfkbiz, Fosb*	(1) skeletal muscle cell differentiation (2) IL-17 signaling pathway (3) positive regulation of apoptotic process
MG7	*Ccl4, Ccl3, Nfkbia, Atf3. Ier3, Nfkbiz, Cd83, Ppp1r15a, Ccrl2, Tnf*	(1) cytokine-mediated signaling pathway (2) regulation of inflammatory response (3) apoptotic signaling pathway
MG8	*Malat1, mt-Atp6, mt-Co3, Enpp2, mt-Cytb, mt-Nd1, mt-Nd2, mt-Nd4, 1500015O10Rik, Itgb5*	(1) Electron transport chain (2) aerobic electron transport chain (3) Oxidative phosphorylation
MG9	*Ccl2, Ccl12, Bst2, Lgals3bp, Ccrl2, Ier5, Rgs1, Nfkbid, Gpr84, Cd83*	(1) chemokine-mediated signaling pathway (2) Signaling by GPCR (3) Herpes simplex virus 1 infection
MG10	*Pf4, Ms4a7, F13a1, Cbr2, Folr2, Mrc1, Dab2, Apoe, Wfdc17, Lgals1*	(1) negative regulation of neuron projection development (2) negative regulation of cell activation
MG11	*H2-Eb1, H2-Aa, H2-Ab1, Clec12a, Plbd1, Klra2, Mgl2, Cybb, Ccr2, Cd74*	(1) antigen processing and presentation of exogenous peptide antigen via MHC class II (2) regulation of leukocyte differentiation (3) positive regulation of cytokine production

Table 5.2. Top 10 DEGs of IRM populations from all samples combined.

IRM populations	Top DEGs
IRM0	*Pf4, F13a1, Cbr2, Folr2, Clec4n, Lyve1, Mrc1, Ccl24, Cd209f, Clec10a*
IRM1	*H2-Eb1, H2-Aa, H2-Ab1, Cd74, Fxyd5, Ccr2, Plbd1, Gm34084, Mcub, Klra2*
IRM 2	*Crip1, S100a6, Vim, Mgl2, Ccnd2, Gm9493, Klra2, Plbd1, Pim1, Tmsb10*
IRM 3	*Cox8a, Ctsd, Enpp2, Cox6c, Atp5e, Atp6v1f, Tomm7, Dpm3, Atp5j, Pld3*
IRM 4	*Ccl12, Isg15, Ifit3, Lag3, Gpr84, Ifi35, Phf11b, Rtp4, Slc1a3, Irf7*
IRM 5	*Slc2a5, Frmd4a, Adgrg1, B430010I23Rik, Lrba, Insig2, Klk8, Usp2, Ints6l, Tmem63a*
IRM 6	*Ccl2, Sgk1, Mertk, Socs3, Pik3r1, Gem, Slc44a2, Upk1b, Il1a, Nav3*

5.1.5. **TRM and Brain Projects: Extended Data**

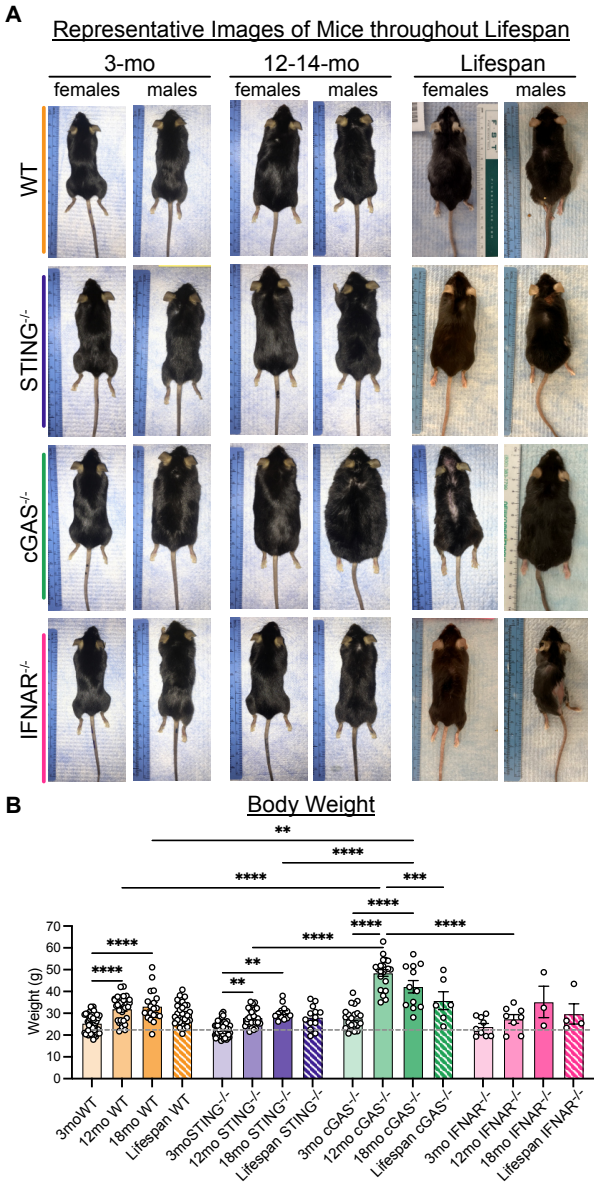

Figure 5.1.5. Representative images of WT, STING$^{-/-}$, cGAS$^{-/-}$, and IFNAR$^{-/-}$ mice and body weights.
(A) Representative images of WT, STING$^{-/-}$, cGAS$^{-/-}$, and IFNAR$^{-/-}$ mice at 3-mo, 12-mo and Lifespan time points. Both sexes are represented in the images. (B) Body weights (g) of 3-mo, 12-mo, 18-mo, lifespan WT, STING$^{-/-}$, cGAS$^{-/-}$, and IFNAR$^{-/-}$ mice. Two-way ANOVA with Tukey's multiple comparisons test was run. **** p< 0.0001, ***p<0.001, **p<0.01, ns = not significant.

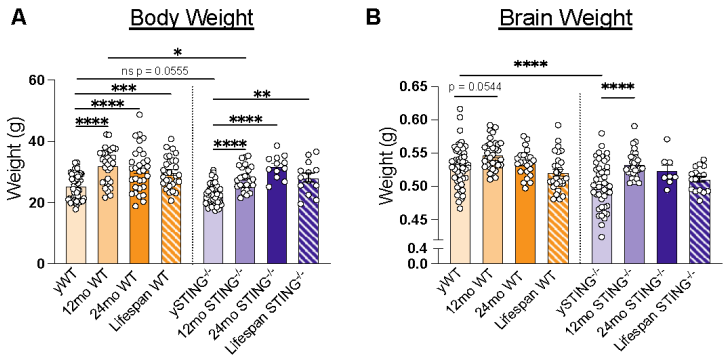

Figure 5.1.6. Body weight and brain weights of WT and STING$^{-/-}$ mice.
(A) Copy of body weight from previous figure. (B) brain weights of WT and STING$^{-/-}$ from 3-mo, 12-mo, 24-mo, and lifespan mice; Bars that are 25% transparency are 3-mo, 50% transparency are 12-mo, 75% transparency are 24-mo, and darkest color are Lifespan animals. Two-way ANOVA with Tukey's multiple comparisons test was run. **** p< 0.0001, ***p<0.001, **p<0.01, ns = not significant.

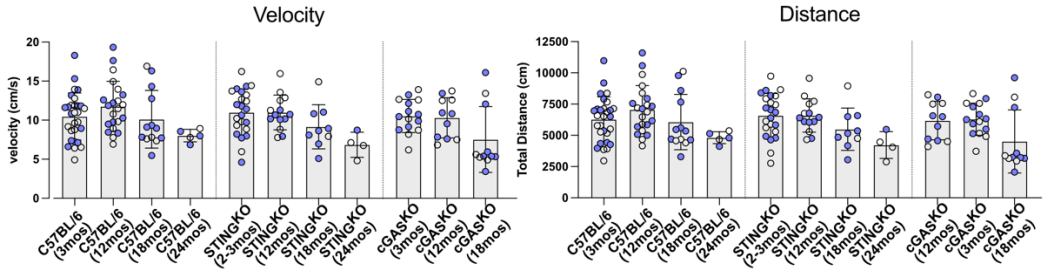

Figure 5.1.7. Extended open field data to include cGAS$^{-/-}$ ages.
First panel; quantification of velocity of 3-mo, 12-mo, 18-mo, and 24-mo WT, STING$^{-/-}$, and cGAS$^{-/-}$ mice. These are combined experiments; purple is experiment 1, green and clear dots are experiment 2. No statistics are shown in these data.

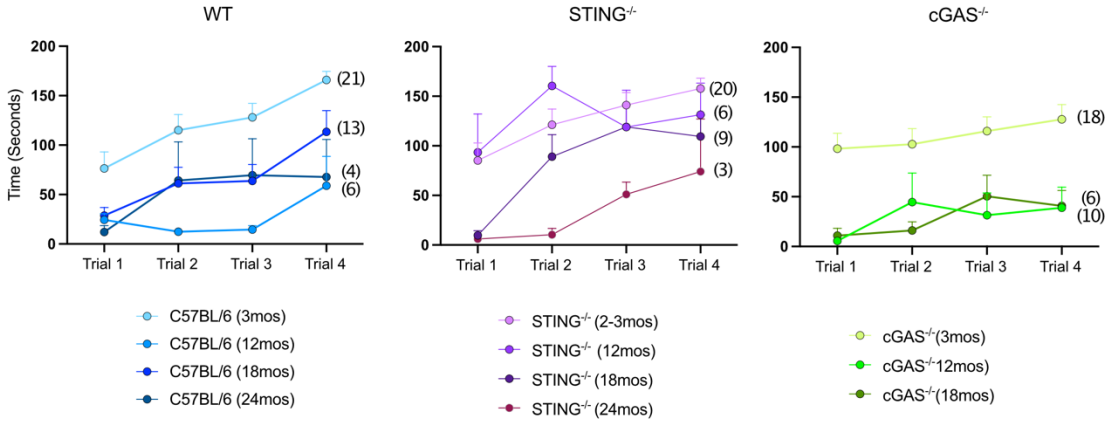

Figure 5.1.8. Rotarod assay to test balance.
First panel depicts WT learning curves on a rotarod apparatus with consistent speed. Second panel depicts WT learning curves on a rotarod apparatus with consistent speed. Third panel depicts WT learning curves on a rotarod apparatus with consistent speed.

The data above (**Figure 5.1.8**) show all WT have improved balance and coordination with practice, but with age the animals are not as coordinated. In the STING$^{-/-}$ animals, they are similarly able to practice coordination and improve over time. However, at 18-mo STING$^{-/-}$, balance plateaus compared to the WT. At 24-mo STING$^{-/-}$ mice show difficulty in staying on the beam compared to the WT suggesting motor impairments at this late age. Findings from the rotarod assay suggest major deficits within the cGAS$^{-/-}$ mice at 12-mo and 18-mo.

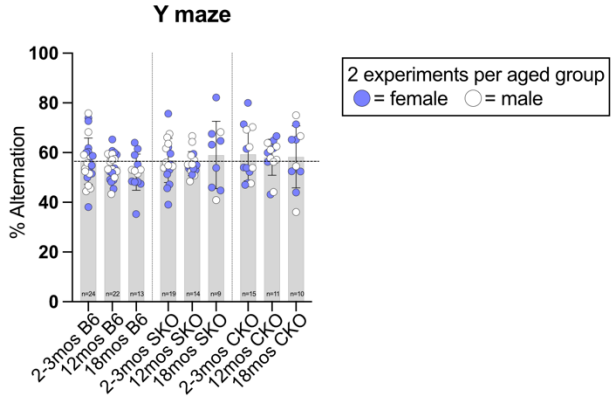

Figure 5.1.9. Y maze behavior assay.
Extended data from above (Figure 3.1.17) to incude 3-mo, 12-mo and 18-mo cGAS$^{-/-}$ mice. No statistics are shown in these data.

5.1.6. **Optimization Data**

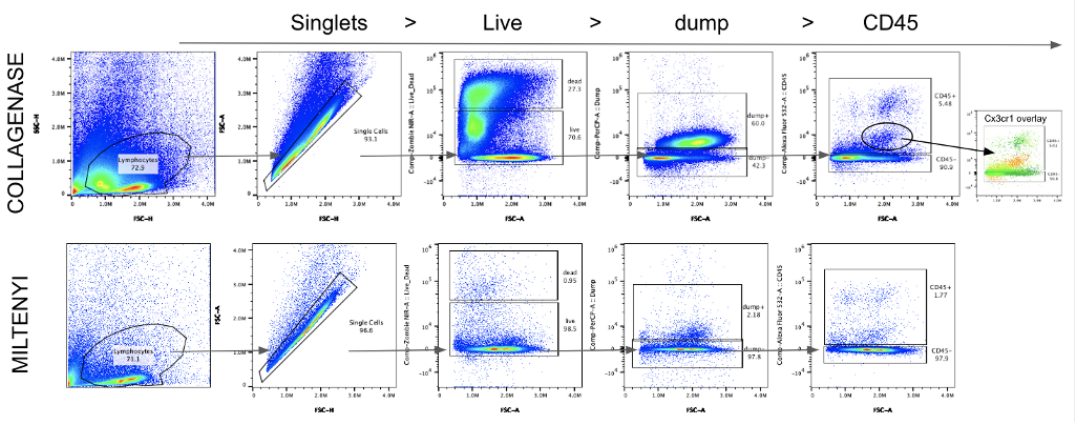

Figure 5.1.10. Optimization of dissociation of brain samples.
Top panels utilized the collagenase and DNaseII enzymatic digestion buffer within the Miltenyi octo-dissociator with to preserve more microglia when compared to the Miltenyi Brain Dissociation Kit within the Miltenyi octo-dissociator, as per the manufacturers protocol.

5.2. LIST OF PUBLICATIONS TO DATE

Sulka KB, *Carroll KA, Sawden M, Hopkins JW, Smolgovsky SA, Bayer AL, Reed E, Tai A, Alcaide PA, Haydon P, Sharma S. Microglial STING is a central safeguard against neurological decline with age. (Accepted, Cell Reports).*

Hopkins JW,* ***Sulka KB****, Sawden M, Carroll KA, Brown RD, Smolgovsky SA, Bunnell SC, Poltorak S, Alcaide PA, Tai A, Reed E, Sharma S. Homeostatic maintenance of tissues and longevity with aging rely on STING signaling. (In Review).*

Ehrbar D, Arvikar SL, **Sulka KB**, Chiumento G, Nelson NLJ, Hernandez SA, Williams MA, Strle F, Steere AC, Strle K. Variants in the Late Cornified Envelope Gene Locus Are Associated With Elevated T-helper 17 Responses in Patients With Postinfectious Lyme Arthritis. J Infect Dis. 2024 Aug 14;230(Supplement_1):S40-S50. doi: 10.1093/infdis/jiae164. PMID: 39140723; PMCID: PMC11322884.

Bayer AL, Smolgovsky S, Ngwenyama N, Hernández-Martínez A, Kaur K, **Sulka K**, Amrute J, Aronovitz M, Lavine K, Sharma S, Alcaide P. T-Cell MyD88 Is a Novel Regulator of Cardiac Fibrosis Through Modulation of T-Cell Activation. Circ Res. 2023 Aug 18;133(5):412-429. doi: 10.1161/CIRCRESAHA.123.323030. Epub 2023 Jul 26. PMID: 37492941; PMCID: PMC10529989.

Sulka KB, Strle K, Crowley JT, Lochhead RB, Anthony R, Steere AC. Correlation of Lyme Disease-Associated IgG4 Autoantibodies With Synovial Pathology in Antibiotic-Refractory Lyme Arthritis. Arthritis Rheumatol. 2018 Nov;70(11):1835-1846. doi: 10.1002/art.40566. Epub 2018 Sep 24. PMID: 29790305; PMCID: PMC6203610.

Arvikar SL, Crowley JT, **Sulka KB**, Steere AC. Autoimmune Arthritides, Rheumatoid Arthritis, Psoriatic Arthritis, or Peripheral Spondyloarthritis Following Lyme Disease. Arthritis Rheumatol. 2017 Jan;69(1):194-202. doi: 10.1002/art.39866. PMID: 27636905; PMCID: PMC5195856.

Strle K, **Sulka KB**, Pianta A, Crowley JT, Arvikar SL, Anselmo A, Sadreyev R, Steere AC. T-Helper 17 Cell Cytokine Responses in Lyme Disease Correlate With Borrelia burgdorferi Antibodies During Early Infection and With Autoantibodies Late in the Illness in Patients With Antibiotic-Refractory Lyme Arthritis. Clin Infect Dis. 2017 Apr 1;64(7):930-938. doi: 10.1093/cid/cix002. PMID: 28077518; PMCID: PMC5850331.

CHAPTER 6: **BIBLIOGRAPHY**

1. Bonilla, F. A., & Oettgen, H. C. (2010). Adaptive immunity. *J Allergy Clin Immunol*, *125*(2 Suppl 2), S33-40. https://doi.org/10.1016/j.jaci.2009.09.017
2. Fitzgerald, K. A., & Kagan, J. C. (2020). Toll-like Receptors and the Control of Immunity. *Cell*, *180*(6), 1044-1066. https://doi.org/10.1016/j.cell.2020.02.041
3. Riera Romo, M., Perez-Martinez, D., & Castillo Ferrer, C. (2016). Innate immunity in vertebrates: an overview. *Immunology*, *148*(2), 125-139. https://doi.org/10.1111/imm.12597
4. Dominguez Conde, C., Xu, C., Jarvis, L. B., Rainbow, D. B., Wells, S. B., Gomes, T., Howlett, S. K., Suchanek, O., Polanski, K., King, H. W., Mamanova, L., Huang, N., Szabo, P. A., Richardson, L., Bolt, L., Fasouli, E. S., Mahbubani, K. T., Prete, M., Tuck, L.,…Teichmann, S. A. (2022). Cross-tissue immune cell analysis reveals tissue-specific features in humans. *Science*, *376*(6594), eabl5197. https://doi.org/10.1126/science.abl5197
5. Poon, M. M. L., & Farber, D. L. (2020). The Whole Body as the System in Systems Immunology. *iScience*, *23*(9), 101509. https://doi.org/10.1016/j.isci.2020.101509
6. Weisberg, S. P., Ural, B. B., & Farber, D. L. (2021). Tissue-specific immunity for a changing world. *Cell*, *184*(6), 1517-1529. https://doi.org/10.1016/j.cell.2021.01.042
7. Thaiss, C. A., Zmora, N., Levy, M., & Elinav, E. (2016). The microbiome and innate immunity. *Nature*, *535*(7610), 65-74. https://doi.org/10.1038/nature18847
8. Li, D., & Wu, M. (2021). Pattern recognition receptors in health and diseases. *Signal Transduct Target Ther*, *6*(1), 291. https://doi.org/10.1038/s41392-021-00687-0
9. Medzhitov, R., Preston-Hurlburt, P., & Janeway, C. A., Jr. (1997). A human homologue of the Drosophila Toll protein signals activation of adaptive immunity. *Nature*, *388*(6640), 394-397. https://doi.org/10.1038/41131
10. Gay, N. J., & Keith, F. J. (1991). Drosophila Toll and IL-1 receptor. *Nature*, *351*(6325), 355-356. https://doi.org/10.1038/351355b0
11. Lemaitre, B., Nicolas, E., Michaut, L., Reichhart, J. M., & Hoffmann, J. A. (1996). The dorsoventral regulatory gene cassette spatzle/Toll/cactus controls the potent antifungal response in Drosophila adults. *Cell*, *86*(6), 973-983. https://doi.org/10.1016/s0092-8674(00)80172-5
12. Kawasaki, T., & Kawai, T. (2014). Toll-like receptor signaling pathways. *Front Immunol*, *5*, 461. https://doi.org/10.3389/fimmu.2014.00461
13. Poltorak, A., He, X., Smirnova, I., Liu, M. Y., Van Huffel, C., Du, X., Birdwell, D., Alejos, E., Silva, M., Galanos, C., Freudenberg, M., Ricciardi-Castagnoli, P., Layton, B., & Beutler, B. (1998). Defective LPS signaling in C3H/HeJ and C57BL/10ScCr mice: mutations in Tlr4 gene. *Science*, *282*(5396), 2085-2088. https://doi.org/10.1126/science.282.5396.2085
14. Dunphy, G., Flannery, S. M., Almine, J. F., Connolly, D. J., Paulus, C., Jonsson, K. L., Jakobsen, M. R., Nevels, M. M., Bowie, A. G., & Unterholzner, L. (2018). Non-canonical Activation of the DNA Sensing Adaptor STING by ATM and IFI16 Mediates NF-kappaB Signaling after Nuclear DNA Damage. *Mol Cell*, *71*(5), 745-760 e745. https://doi.org/10.1016/j.molcel.2018.07.034
15. Fore, F., Budipranama, M., & Destiawan, R. A. (2022). TLR10 and Its Role in Immunity. *Handb Exp Pharmacol*, *276*, 161-174. https://doi.org/10.1007/164_2021_541
16. Cargnello, M., & Roux, P. P. (2011). Activation and function of the MAPKs and their substrates, the MAPK-activated protein kinases. *Microbiol Mol Biol Rev*, *75*(1), 50-83. https://doi.org/10.1128/MMBR.00031-10

17. Christensen, J. L., Wright, D. E., Wagers, A. J., & Weissman, I. L. (2004). Circulation and chemotaxis of fetal hematopoietic stem cells. *PLoS Biol*, *2*(3), E75. https://doi.org/10.1371/journal.pbio.0020075
18. Gomez Perdiguero, E., Klapproth, K., Schulz, C., Busch, K., Azzoni, E., Crozet, L., Garner, H., Trouillet, C., de Bruijn, M. F., Geissmann, F., & Rodewald, H. R. (2015). Tissue-resident macrophages originate from yolk-sac-derived erythro-myeloid progenitors. *Nature*, *518*(7540), 547-551. https://doi.org/10.1038/nature13989
19. Hoeffel, G., Chen, J., Lavin, Y., Low, D., Almeida, F. F., See, P., Beaudin, A. E., Lum, J., Low, I., Forsberg, E. C., Poidinger, M., Zolezzi, F., Larbi, A., Ng, L. G., Chan, J. K., Greter, M., Becher, B., Samokhvalov, I. M., Merad, M., & Ginhoux, F. (2015). C-Myb(+) erythro-myeloid progenitor-derived fetal monocytes give rise to adult tissue-resident macrophages. *Immunity*, *42*(4), 665-678. https://doi.org/10.1016/j.immuni.2015.03.011
20. Hossain, Z., Reza, A., Qasem, W. A., Friel, J. K., & Omri, A. (2022). Development of the immune system in the human embryo. *Pediatr Res*, *92*(4), 951-955. https://doi.org/10.1038/s41390-022-01940-0
21. van de Laar, L., Saelens, W., De Prijck, S., Martens, L., Scott, C. L., Van Isterdael, G., Hoffmann, E., Beyaert, R., Saeys, Y., Lambrecht, B. N., & Guilliams, M. (2016). Yolk Sac Macrophages, Fetal Liver, and Adult Monocytes Can Colonize an Empty Niche and Develop into Functional Tissue-Resident Macrophages. *Immunity*, *44*(4), 755-768. https://doi.org/10.1016/j.immuni.2016.02.017
22. Orkin, S. H., & Zon, L. I. (2008). Hematopoiesis: an evolving paradigm for stem cell biology. *Cell*, *132*(4), 631-644. https://doi.org/10.1016/j.cell.2008.01.025
23. Lavin, Y., Winter, D., Blecher-Gonen, R., David, E., Keren-Shaul, H., Merad, M., Jung, S., & Amit, I. (2014). Tissue-resident macrophage enhancer landscapes are shaped by the local microenvironment. *Cell*, *159*(6), 1312-1326. https://doi.org/10.1016/j.cell.2014.11.018
24. Epelman, S., Lavine, K. J., & Randolph, G. J. (2014). Origin and functions of tissue macrophages. *Immunity*, *41*(1), 21-35. https://doi.org/10.1016/j.immuni.2014.06.013
25. Mass, E., Nimmerjahn, F., Kierdorf, K., & Schlitzer, A. (2023). Tissue-specific macrophages: how they develop and choreograph tissue biology. *Nat Rev Immunol*, *23*(9), 563-579. https://doi.org/10.1038/s41577-023-00848-y
26. Chiao, Y. A., & Rabinovitch, P. S. (2015). The Aging Heart. *Cold Spring Harb Perspect Med*, *5*(9), a025148. https://doi.org/10.1101/cshperspect.a025148
27. Lopez-Otin, C., Blasco, M. A., Partridge, L., Serrano, M., & Kroemer, G. (2023). Hallmarks of aging: An expanding universe. *Cell*, *186*(2), 243-278. https://doi.org/10.1016/j.cell.2022.11.001
28. Obas, V., & Vasan, R. S. (2018). The aging heart. *Clin Sci (Lond)*, *132*(13), 1367-1382. https://doi.org/10.1042/CS20171156
29. Weinstein, J. R., & Anderson, S. (2010). The aging kidney: physiological changes. *Adv Chronic Kidney Dis*, *17*(4), 302-307. https://doi.org/10.1053/j.ackd.2010.05.002
30. Zaman, R., & Epelman, S. (2022). Resident cardiac macrophages: Heterogeneity and function in health and disease. *Immunity*, *55*(9), 1549-1563. https://doi.org/10.1016/j.immuni.2022.08.009
31. Rae, F., Woods, K., Sasmono, T., Campanale, N., Taylor, D., Ovchinnikov, D. A., Grimmond, S. M., Hume, D. A., Ricardo, S. D., & Little, M. H. (2007). Characterisation and trophic functions of murine embryonic macrophages based

upon the use of a Csf1r-EGFP transgene reporter. *Dev Biol*, *308*(1), 232-246. https://doi.org/10.1016/j.ydbio.2007.05.027
32. Kawakami, T., Lichtnekert, J., Thompson, L. J., Karna, P., Bouabe, H., Hohl, T. M., Heinecke, J. W., Ziegler, S. F., Nelson, P. J., & Duffield, J. S. (2013). Resident renal mononuclear phagocytes comprise five discrete populations with distinct phenotypes and functions. *J Immunol*, *191*(6), 3358-3372. https://doi.org/10.4049/jimmunol.1300342
33. Munro, D. A. D., & Hughes, J. (2017). The Origins and Functions of Tissue-Resident Macrophages in Kidney Development. *Front Physiol*, *8*, 837. https://doi.org/10.3389/fphys.2017.00837
34. Nguyen-Lefebvre, A. T., & Horuzsko, A. (2015). Kupffer Cell Metabolism and Function. *J Enzymol Metab*, *1*(1). https://www.ncbi.nlm.nih.gov/pubmed/26937490
35. Paolicelli, R. C., Sierra, A., Stevens, B., Tremblay, M. E., Aguzzi, A., Ajami, B., Amit, I., Audinat, E., Bechmann, I., Bennett, M., Bennett, F., Bessis, A., Biber, K., Bilbo, S., Blurton-Jones, M., Boddeke, E., Brites, D., Brône, B., Brown, G. C.,…Wyss-Coray, T. (2022). Microglia states and nomenclature: A field at its crossroads. In *Neuron* (Vol. 110, pp. 3458-3483): Cell Press.
36. Prinz, M., Jung, S., & Priller, J. (2019). Microglia Biology: One Century of Evolving Concepts. *Cell*, *179*(2), 292-311. https://doi.org/10.1016/j.cell.2019.08.053
37. Antignano, I., Liu, Y., Offermann, N., & Capasso, M. (2023). Aging microglia. *Cell Mol Life Sci*, *80*(5), 126. https://doi.org/10.1007/s00018-023-04775-y
38. Cuevas-Diaz Duran, R., Wei, H., & Wu, J. Q. (2017). Single-cell RNA-sequencing of the brain. In *Clinical and Translational Medicine* (Vol. 6, pp. 20): Wiley.
39. Kaikita, K., Hayasaki, T., Okuma, T., Kuziel, W. A., Ogawa, H., & Takeya, M. (2004). Targeted deletion of CC chemokine receptor 2 attenuates left ventricular remodeling after experimental myocardial infarction. *Am J Pathol*, *165*(2), 439-447. https://doi.org/10.1016/S0002-9440(10)63309-3
40. Kitagawa, K., Wada, T., Furuichi, K., Hashimoto, H., Ishiwata, Y., Asano, M., Takeya, M., Kuziel, W. A., Matsushima, K., Mukaida, N., & Yokoyama, H. (2004). Blockade of CCR2 ameliorates progressive fibrosis in kidney. *Am J Pathol*, *165*(1), 237-246. https://doi.org/10.1016/S0002-9440(10)63292-0
41. Nikolich-Zugich, J. (2018). The twilight of immunity: emerging concepts in aging of the immune system. *Nat Immunol*, *19*(1), 10-19. https://doi.org/10.1038/s41590-017-0006-x
42. López-Otín, C., Blasco, M. A., Partridge, L., Serrano, M., & Kroemer, G. (2013). The hallmarks of aging. In *Cell* (Vol. 153).
43. Schumacher, B., Pothof, J., Vijg, J., & Hoeijmakers, J. H. J. (2021). The central role of DNA damage in the ageing process. *Nature*, *592*(7856), 695-703. https://doi.org/10.1038/s41586-021-03307-7
44. Mah, L. J., El-Osta, A., & Karagiannis, T. C. (2010). γH2AX: a sensitive molecular marker of DNA damage and repair. In *Leukemia 2010 24:4* (Vol. 24, pp. 679-686): Nature Publishing Group.
45. Bouquet, F., Muller, C., & Salles, B. (2006). The loss of gammaH2AX signal is a marker of DNA double strand breaks repair only at low levels of DNA damage. *Cell Cycle*, *5*(10), 1116-1122. https://doi.org/10.4161/cc.5.10.2799
46. Sedelnikova, O. A., Pilch, D. R., Redon, C., & Bonner, W. M. (2003). Histone H2AX in DNA damage and repair. *Cancer Biol Ther*, *2*(3), 233-235. https://doi.org/10.4161/cbt.2.3.373

47. Krishnan, K. J., Reeve, A. K., Samuels, D. C., Chinnery, P. F., Blackwood, J. K., Taylor, R. W., Wanrooij, S., Spelbrink, J. N., Lightowlers, R. N., & Turnbull, D. M. (2008). What causes mitochondrial DNA deletions in human cells? *Nat Genet*, *40*(3), 275-279. https://doi.org/10.1038/ng.f.94
48. Nadalutti, C. A., Stefanick, D. F., Zhao, M. L., Horton, J. K., Prasad, R., Brooks, A. M., Griffith, J. D., & Wilson, S. H. (2020). Mitochondrial dysfunction and DNA damage accompany enhanced levels of formaldehyde in cultured primary human fibroblasts. *Sci Rep*, *10*(1), 5575. https://doi.org/10.1038/s41598-020-61477-2
49. Cao, K., Riley, J. S., Heilig, R., Montes-Gomez, A. E., Vringer, E., Berthenet, K., Cloix, C., Elmasry, Y., Spiller, D. G., Ichim, G., Campbell, K. J., Gilmore, A. P., & Tait, S. W. G. (2022). Mitochondrial dynamics regulate genome stability via control of caspase-dependent DNA damage. *Dev Cell*, *57*(10), 1211-1225 e1216. https://doi.org/10.1016/j.devcel.2022.03.019
50. Hayflick, L., & Moorhead, P. S. (1961). The serial cultivation of human diploid cell strains. *Exp Cell Res*, *25*, 585-621. https://doi.org/10.1016/0014-4827(61)90192-6
51. d'Adda di Fagagna, F., Reaper, P. M., Clay-Farrace, L., Fiegler, H., Carr, P., Von Zglinicki, T., Saretzki, G., Carter, N. P., & Jackson, S. P. (2003). A DNA damage checkpoint response in telomere-initiated senescence. *Nature*, *426*(6963), 194-198. https://doi.org/10.1038/nature02118
52. DiRocco, D. P., Bisi, J., Roberts, P., Strum, J., Wong, K. K., Sharpless, N., & Humphreys, B. D. (2014). CDK4/6 inhibition induces epithelial cell cycle arrest and ameliorates acute kidney injury. *Am J Physiol Renal Physiol*, *306*(4), F379-388. https://doi.org/10.1152/ajprenal.00475.2013
53. Kim, S. R., Puranik, A. S., Jiang, K., Chen, X., Zhu, X. Y., Taylor, I., Khodadadi-Jamayran, A., Lerman, A., Hickson, L. J., Childs, B. G., Textor, S. C., Tchkonia, T., Niewold, T. B., Kirkland, J. L., & Lerman, L. O. (2021). Progressive Cellular Senescence Mediates Renal Dysfunction in Ischemic Nephropathy. *J Am Soc Nephrol*, *32*(8), 1987-2004. https://doi.org/10.1681/ASN.2020091373
54. Cohn, R. L., Gasek, N. S., Kuchel, G. A., & Xu, M. (2023). The heterogeneity of cellular senescence: insights at the single-cell level. *Trends Cell Biol*, *33*(1), 9-17. https://doi.org/10.1016/j.tcb.2022.04.011
55. Dulic, V., Beney, G. E., Frebourg, G., Drullinger, L. F., & Stein, G. H. (2000). Uncoupling between phenotypic senescence and cell cycle arrest in aging p21-deficient fibroblasts. *Mol Cell Biol*, *20*(18), 6741-6754. https://doi.org/10.1128/MCB.20.18.6741-6754.2000
56. Stillman, J. M., Mendes Lopes, F., Lin, J. P., Hu, K., Reich, D. S., & Schafer, D. P. (2023). Lipofuscin-like autofluorescence within microglia and its impact on studying microglial engulfment. *Nat Commun*, *14*(1), 7060. https://doi.org/10.1038/s41467-023-42809-y
57. Coppe, J. P., Patil, C. K., Rodier, F., Sun, Y., Munoz, D. P., Goldstein, J., Nelson, P. S., Desprez, P. Y., & Campisi, J. (2008). Senescence-associated secretory phenotypes reveal cell-nonautonomous functions of oncogenic RAS and the p53 tumor suppressor. *PLoS Biol*, *6*(12), 2853-2868. https://doi.org/10.1371/journal.pbio.0060301
58. Campisi, J., & d'Adda di Fagagna, F. (2007). Cellular senescence: when bad things happen to good cells. *Nat Rev Mol Cell Biol*, *8*(9), 729-740. https://doi.org/10.1038/nrm2233
59. Artandi, S. E., & DePinho, R. A. (2000). A critical role for telomeres in suppressing and facilitating carcinogenesis. *Curr Opin Genet Dev*, *10*(1), 39-46. https://doi.org/10.1016/s0959-437x(99)00047-7

60. Chang, E., & Harley, C. B. (1995). Telomere length and replicative aging in human vascular tissues. *Proc Natl Acad Sci U S A*, *92*(24), 11190-11194. https://doi.org/10.1073/pnas.92.24.11190
61. Xu, M., Pirtskhalava, T., Farr, J. N., Weigand, B. M., Palmer, A. K., Weivoda, M. M., Inman, C. L., Ogrodnik, M. B., Hachfeld, C. M., Fraser, D. G., Onken, J. L., Johnson, K. O., Verzosa, G. C., Langhi, L. G. P., Weigl, M., Giorgadze, N., LeBrasseur, N. K., Miller, J. D., Jurk, D.,…Kirkland, J. L. (2018). Senolytics improve physical function and increase lifespan in old age. *Nat Med*, *24*(8), 1246-1256. https://doi.org/10.1038/s41591-018-0092-9
62. Yang, H., Wang, H., Ren, J., Chen, Q., & Chen, Z. J. (2017). cGAS is essential for cellular senescence. *Proc Natl Acad Sci U S A*, *114*(23), E4612-E4620. https://doi.org/10.1073/pnas.1705499114
63. Thompson, W. W., Shay, D. K., Weintraub, E., Brammer, L., Cox, N., Anderson, L. J., & Fukuda, K. (2003). Mortality associated with influenza and respiratory syncytial virus in the United States. *JAMA*, *289*(2), 179-186. https://doi.org/10.1001/jama.289.2.179
64. Fleming, D. M., & Elliot, A. J. (2005). The impact of influenza on the health and health care utilisation of elderly people. *Vaccine*, *23 Suppl 1*, S1-9. https://doi.org/10.1016/j.vaccine.2005.04.018
65. Geiger, H., & Van Zant, G. (2002). The aging of lympho-hematopoietic stem cells. *Nat Immunol*, *3*(4), 329-333. https://doi.org/10.1038/ni0402-329
66. Li, X., Li, C., Zhang, W., Wang, Y., Qian, P., & Huang, H. (2023). Inflammation and aging: signaling pathways and intervention therapies. *Signal Transduct Target Ther*, *8*(1), 239. https://doi.org/10.1038/s41392-023-01502-8
67. Davizon-Castillo, P., McMahon, B., Aguila, S., Bark, D., Ashworth, K., Allawzi, A., Campbell, R. A., Montenont, E., Nemkov, T., D'Alessandro, A., Clendenen, N., Shih, L., Sanders, N. A., Higa, K., Cox, A., Padilla-Romo, Z., Hernandez, G., Wartchow, E., Trahan, G. D.,…Di Paola, J. (2019). TNF-alpha-driven inflammation and mitochondrial dysfunction define the platelet hyperreactivity of aging. *Blood*, *134*(9), 727-740. https://doi.org/10.1182/blood.2019000200
68. Valletta, S., Thomas, A., Meng, Y., Ren, X., Drissen, R., Sengul, H., Di Genua, C., & Nerlov, C. (2020). Micro-environmental sensing by bone marrow stroma identifies IL-6 and TGFbeta1 as regulators of hematopoietic ageing. *Nat Commun*, *11*(1), 4075. https://doi.org/10.1038/s41467-020-17942-7
69. Della Bella, S., Bierti, L., Presicce, P., Arienti, R., Valenti, M., Saresella, M., Vergani, C., & Villa, M. L. (2007). Peripheral blood dendritic cells and monocytes are differently regulated in the elderly. *Clin Immunol*, *122*(2), 220-228. https://doi.org/10.1016/j.clim.2006.09.012
70. Shaw, A. C., Joshi, S., Greenwood, H., Panda, A., & Lord, J. M. (2010). Aging of the innate immune system. *Curr Opin Immunol*, *22*(4), 507-513. https://doi.org/10.1016/j.coi.2010.05.003
71. Montecino-Rodriguez, E., Berent-Maoz, B., & Dorshkind, K. (2013). Causes, consequences, and reversal of immune system aging. *J Clin Invest*, *123*(3), 958-965. https://doi.org/10.1172/JCI64096
72. Hirata, T., Arai, Y., Yuasa, S., Abe, Y., Takayama, M., Sasaki, T., Kunitomi, A., Inagaki, H., Endo, M., Morinaga, J., Yoshimura, K., Adachi, T., Oike, Y., Takebayashi, T., Okano, H., & Hirose, N. (2020). Associations of cardiovascular biomarkers and plasma albumin with exceptional survival to the highest ages. *Nat Commun*, *11*(1), 3820. https://doi.org/10.1038/s41467-020-17636-0

73. Sun, L., Wu, J., Du, F., Chen, X., & Chen, Z. J. (2013). Cyclic GMP-AMP synthase is a cytosolic DNA sensor that activates the type I interferon pathway. *Science*, *339*(6121), 786-791. https://doi.org/10.1126/science.1232458
74. Ishikawa, H., Ma, Z., & Barber, G. N. (2009). STING regulates intracellular DNA-mediated, type I interferon-dependent innate immunity. *Nature*, *461*(7265), 788-792. https://doi.org/10.1038/nature08476
75. Ishikawa, H., & Barber, G. N. (2008). STING is an endoplasmic reticulum adaptor that facilitates innate immune signalling. *Nature*, *455*(7213), 674-678. https://doi.org/10.1038/nature07317
76. Wu, J., Sun, L., Chen, X., Du, F., Shi, H., Chen, C., & Chen, Z. J. (2013). Cyclic GMP-AMP is an endogenous second messenger in innate immune signaling by cytosolic DNA. *Science*, *339*(6121), 826-830. https://doi.org/10.1126/science.1229963
77. Hussain, B., Xie, Y., Jabeen, U., Lu, D., Yang, B., Wu, C., & Shang, G. (2022). Activation of STING Based on Its Structural Features. *Front Immunol*, *13*, 808607. https://doi.org/10.3389/fimmu.2022.808607
78. Decout, A., Katz, J. D., Venkatraman, S., & Ablasser, A. (2021). The cGAS-STING pathway as a therapeutic target in inflammatory diseases. *Nat Rev Immunol*, *21*(9), 548-569. https://doi.org/10.1038/s41577-021-00524-z
79. Yang, H., Lee, W. S., Kong, S. J., Kim, C. G., Kim, J. H., Chang, S. K., Kim, S., Kim, G., Chon, H. J., & Kim, C. (2019). STING activation reprograms tumor vasculatures and synergizes with VEGFR2 blockade. *J Clin Invest*, *129*(10), 4350-4364. https://doi.org/10.1172/JCI125413
80. Motwani, M., Pesiridis, S., & Fitzgerald, K. A. (2019). DNA sensing by the cGAS-STING pathway in health and disease. *Nat Rev Genet*, *20*(11), 657-674. https://doi.org/10.1038/s41576-019-0151-1
81. Patel, S., & Jin, L. (2019). TMEM173 variants and potential importance to human biology and disease. *Genes Immun*, *20*(1), 82-89. https://doi.org/10.1038/s41435-018-0029-9
82. Yi, G., Brendel, V. P., Shu, C., Li, P., Palanathan, S., & Cheng Kao, C. (2013). Single nucleotide polymorphisms of human STING can affect innate immune response to cyclic dinucleotides. *PLoS One*, *8*(10), e77846. https://doi.org/10.1371/journal.pone.0077846
83. Kennedy, R. B., Haralambieva, I. H., Ovsyannikova, I. G., Voigt, E. A., Larrabee, B. R., Schaid, D. J., Zimmermann, M. T., Oberg, A. L., & Poland, G. A. (2020). Polymorphisms in STING Affect Human Innate Immune Responses to Poxviruses. *Front Immunol*, *11*, 567348. https://doi.org/10.3389/fimmu.2020.567348
84. Cerboni, S., Jeremiah, N., Gentili, M., Gehrmann, U., Conrad, C., Stolzenberg, M. C., Picard, C., Neven, B., Fischer, A., Amigorena, S., Rieux-Laucat, F., & Manel, N. (2017). Intrinsic antiproliferative activity of the innate sensor STING in T lymphocytes. *J Exp Med*, *214*(6), 1769-1785. https://doi.org/10.1084/jem.20161674
85. McNab, F., Mayer-Barber, K., Sher, A., Wack, A., & O'Garra, A. (2015). Type I interferons in infectious disease. *Nat Rev Immunol*, *15*(2), 87-103. https://doi.org/10.1038/nri3787
86. Baruch, K., Deczkowska, A., David, E., Castellano, J. M., Miller, O., Kertser, A., Berkutzki, T., Barnett-Itzhaki, Z., Bezalel, D., Wyss-Coray, T., Amit, I., & Schwartz, M. (2014). Aging. Aging-induced type I interferon response at the choroid plexus negatively affects brain function. In *Science* (Vol. 346, pp. 89-93).

87. Prinz, M., & Knobeloch, K. P. (2012). Type I interferons as ambiguous modulators of chronic inflammation in the central nervous system. In *Frontiers in Immunology* (Vol. 3, pp. 1-9).
88. Deczkowska, A., Baruch, K., & Schwartz, M. (2016). Type I/II Interferon Balance in the Regulation of Brain Physiology and Pathology. In *Trends in Immunology* (Vol. 37, pp. 181-192): Elsevier Ltd.
89. Ivashkiv, L. B., & Donlin, L. T. (2014). Regulation of type I interferon responses. *Nat Rev Immunol*, *14*(1), 36-49. https://doi.org/10.1038/nri3581
90. Ejlerskov, P., Hultberg, J. G., Wang, J. Y., Carlsson, R., Ambjørn, M., Kuss, M., Liu, Y., Porcu, G., Kolkova, K., Friis Rundsten, C., Ruscher, K., Pakkenberg, B., Goldmann, T., Loreth, D., Prinz, M., Rubinsztein, D. C., & Issazadeh-Navikas, S. (2015). Lack of Neuronal IFN-β-IFNAR Causes Lewy Body- and Parkinson's Disease-like Dementia. In *Cell* (Vol. 163, pp. 324-339).
91. Goldmann, T., Blank, T., & Prinz, M. (2016). Fine-tuning of type I IFN-signaling in microglia - implications for homeostasis, CNS autoimmunity and interferonopathies. In *Current Opinion in Neurobiology* (Vol. 36, pp. 38-42): Elsevier Ltd.
92. Yu, Q., Katlinskaya, Y. V., Carbone, C. J., Zhao, B., Katlinski, K. V., Zheng, H., Guha, M., Li, N., Chen, Q., Yang, T., Lengner, C. J., Greenberg, R. A., Johnson, F. B., & Fuchs, S. Y. (2015). DNA-Damage-Induced Type I Interferon Promotes Senescence and Inhibits Stem Cell Function. In *Cell Reports* (Vol. 11, pp. 785-797).
93. Wu, B., & Hur, S. (2015). How RIG-I like receptors activate MAVS. *Curr Opin Virol*, *12*, 91-98. https://doi.org/10.1016/j.coviro.2015.04.004
94. Kuriakose, T., & Kanneganti, T. D. (2018). ZBP1: Innate Sensor Regulating Cell Death and Inflammation. *Trends Immunol*, *39*(2), 123-134. https://doi.org/10.1016/j.it.2017.11.002
95. Taschuk, F., & Cherry, S. (2020). DEAD-Box Helicases: Sensors, Regulators, and Effectors for Antiviral Defense. *Viruses*, *12*(2). https://doi.org/10.3390/v12020181
96. Moreira, L. O., & Zamboni, D. S. (2012). NOD1 and NOD2 Signaling in Infection and Inflammation. *Front Immunol*, *3*, 328. https://doi.org/10.3389/fimmu.2012.00328
97. Gracias, D. T., Stelekati, E., Hope, J. L., Boesteanu, A. C., Doering, T. A., Norton, J., Mueller, Y. M., Fraietta, J. A., Wherry, E. J., Turner, M., & Katsikis, P. D. (2013). The microRNA miR-155 controls CD8(+) T cell responses by regulating interferon signaling. *Nat Immunol*, *14*(6), 593-602. https://doi.org/10.1038/ni.2576
98. Banks, W. A., & Kastin, A. J. (1996). Passage of peptides across the blood-brain barrier: pathophysiological perspectives. *Life Sci*, *59*(23), 1923-1943. https://doi.org/10.1016/s0024-3205(96)00380-3
99. Pan, W., Stone, K. P., Hsuchou, H., Manda, V. K., Zhang, Y., & Kastin, A. J. (2011). Cytokine signaling modulates blood-brain barrier function. *Curr Pharm Des*, *17*(33), 3729-3740. https://doi.org/10.2174/138161211798220918
100. DiSabato, D. J., Quan, N., & Godbout, J. P. (2016). Neuroinflammation: the devil is in the details. *J Neurochem*, *139 Suppl 2*(Suppl 2), 136-153. https://doi.org/10.1111/jnc.13607
101. Inflammatory Response in the CNS: Friend or Foe?, 54 Humana Press Inc. 8071-8089 (2017).

102. Mattson, M. P., & Arumugam, T. V. (2018). Hallmarks of Brain Aging: Adaptive and Pathological Modification by Metabolic States. *Cell Metab*, *27*(6), 1176-1199. https://doi.org/10.1016/j.cmet.2018.05.011
103. Stephan, A. H., Barres, B. A., & Stevens, B. (2012). The complement system: an unexpected role in synaptic pruning during development and disease. *Annu Rev Neurosci*, *35*, 369-389. https://doi.org/10.1146/annurev-neuro-061010-113810
104. Okun, E., Barak, B., Saada-Madar, R., Rothman, S. M., Griffioen, K. J., Roberts, N., Castro, K., Mughal, M. R., Pita, M. A., Stranahan, A. M., Arumugam, T. V., & Mattson, M. P. (2012). Evidence for a developmental role for TLR4 in learning and memory. *PLoS One*, *7*(10), e47522. https://doi.org/10.1371/journal.pone.0047522
105. Snow, W. M., Stoesz, B. M., Kelly, D. M., & Albensi, B. C. (2014). Roles for NF-kappaB and gene targets of NF-kappaB in synaptic plasticity, memory, and navigation. *Mol Neurobiol*, *49*(2), 757-770. https://doi.org/10.1007/s12035-013-8555-y
106. Montgomery, S. L., Mastrangelo, M. A., Habib, D., Narrow, W. C., Knowlden, S. A., Wright, T. W., & Bowers, W. J. (2011). Ablation of TNF-RI/RII expression in Alzheimer's disease mice leads to an unexpected enhancement of pathology: implications for chronic pan-TNF-alpha suppressive therapeutic strategies in the brain. *Am J Pathol*, *179*(4), 2053-2070. https://doi.org/10.1016/j.ajpath.2011.07.001
107. Sullivan, P. G., Bruce-Keller, A. J., Rabchevsky, A. G., Christakos, S., Clair, D. K., Mattson, M. P., & Scheff, S. W. (1999). Exacerbation of damage and altered NF-kappaB activation in mice lacking tumor necrosis factor receptors after traumatic brain injury. *J Neurosci*, *19*(15), 6248-6256. https://doi.org/10.1523/JNEUROSCI.19-15-06248.1999
108. Jovasevic, V., Wood, E. M., Cicvaric, A., Zhang, H., Petrovic, Z., Carboncino, A., Parker, K. K., Bassett, T. E., Moltesen, M., Yamawaki, N., Login, H., Kalucka, J., Sananbenesi, F., Zhang, X., Fischer, A., & Radulovic, J. (2024). Formation of memory assemblies through the DNA-sensing TLR9 pathway. *Nature*, *628*(8006), 145-153. https://doi.org/10.1038/s41586-024-07220-7
109. Escoubas, C. C., Dorman, L. C., Nguyen, P. T., Lagares-Linares, C., Nakajo, H., Anderson, S. R., Barron, J. J., Wade, S. D., Cuevas, B., Vainchtein, I. D., Silva, N. J., Guajardo, R., Xiao, Y., Lidsky, P. V., Wang, E. Y., Rivera, B. M., Taloma, S. E., Kim, D. K., Kaminskaya, E.,…Molofsky, A. V. (2024). Type-I-interferon-responsive microglia shape cortical development and behavior. *Cell*, *187*(8), 1936-1954 e1924. https://doi.org/10.1016/j.cell.2024.02.020
110. Pasciuto, E., Burton, O. T., Roca, C. P., Lagou, V., Rajan, W. D., Theys, T., Mancuso, R., Tito, R. Y., Kouser, L., Callaerts-Vegh, Z., de la Fuente, A. G., Prezzemolo, T., Mascali, L. G., Brajic, A., Whyte, C. E., Yshii, L., Martinez-Muriana, A., Naughton, M., Young, A.,…Liston, A. (2020). Microglia Require CD4 T Cells to Complete the Fetal-to-Adult Transition. *Cell*, *182*(3), 625-640 e624. https://doi.org/10.1016/j.cell.2020.06.026
111. Kiani Shabestari, S., Morabito, S., Danhash, E. P., McQuade, A., Sanchez, J. R., Miyoshi, E., Chadarevian, J. P., Claes, C., Coburn, M. A., Hasselmann, J., Hidalgo, J., Tran, K. N., Martini, A. C., Chang Rothermich, W., Pascual, J., Head, E., Hume, D. A., Pridans, C., Davtyan, H.,…Blurton-Jones, M. (2022). Absence of microglia promotes diverse pathologies and early lethality in Alzheimer's disease mice. *Cell Rep*, *39*(11), 110961. https://doi.org/10.1016/j.celrep.2022.110961

112. Bean, B. P. (2007). The action potential in mammalian central neurons. *Nat Rev Neurosci*, *8*(6), 451-465. https://doi.org/10.1038/nrn2148
113. Bradl, M., & Lassmann, H. (2010). Oligodendrocytes: biology and pathology. *Acta Neuropathol*, *119*(1), 37-53. https://doi.org/10.1007/s00401-009-0601-5
114. Araque, A., Parpura, V., Sanzgiri, R. P., & Haydon, P. G. (1999). Tripartite synapses: glia, the unacknowledged partner. *Trends Neurosci*, *22*(5), 208-215. https://doi.org/10.1016/s0166-2236(98)01349-6
115. Type I interferon pathway in CNS homeostasis and neurological disorders, 65 Wiley-Blackwell 1397-1406 (2017).
116. Colonna, M., & Butovsky, O. (2017). Microglia Function in the Central Nervous System During Health and Neurodegeneration. *Annu Rev Immunol*, *35*, 441-468. https://doi.org/10.1146/annurev-immunol-051116-052358
117. Castellani, G., Croese, T., Peralta Ramos, J. M., & Schwartz, M. (2023). Transforming the understanding of brain immunity. *Science*, *380*(6640), eabo7649. https://doi.org/10.1126/science.abo7649
118. Crotti, A., & Ransohoff, R. M. (2016). Microglial Physiology and Pathophysiology: Insights from Genome-wide Transcriptional Profiling. *Immunity*, *44*(3), 505-515. https://doi.org/10.1016/j.immuni.2016.02.013
119. Sikora, E., Bielak-Zmijewska, A., Dudkowska, M., Krzystyniak, A., Mosieniak, G., Wesierska, M., & Wlodarczyk, J. (2021). Cellular Senescence in Brain Aging. *Front Aging Neurosci*, *13*, 646924. https://doi.org/10.3389/fnagi.2021.646924
120. Pang, J. C., Aquino, K. M., Oldehinkel, M., Robinson, P. A., Fulcher, B. D., Breakspear, M., & Fornito, A. (2023). Geometric constraints on human brain function. *Nature*, *618*(7965), 566-574. https://doi.org/10.1038/s41586-023-06098-1
121. Jack, C. R., Jr., Shiung, M. M., Weigand, S. D., O'Brien, P. C., Gunter, J. L., Boeve, B. F., Knopman, D. S., Smith, G. E., Ivnik, R. J., Tangalos, E. G., & Petersen, R. C. (2005). Brain atrophy rates predict subsequent clinical conversion in normal elderly and amnestic MCI. *Neurology*, *65*(8), 1227-1231. https://doi.org/10.1212/01.wnl.0000180958.22678.91
122. Taylor, J. M., Minter, M. R., Newman, A. G., Zhang, M., Adlard, P. A., & Crack, P. J. (2014). Type-1 interferon signaling mediates neuro-inflammatory events in models of Alzheimer's disease. In *Neurobiology of Aging* (Vol. 35, pp. 1012-1023): Elsevier.
123. McGeer, P. L., & McGeer, E. G. (2004). *Inflammation and the degenerative diseases of aging*, New York Academy of Sciences.
124. Mendonca, G. V., Pezarat-Correia, P., Vaz, J. R., Silva, L., & Heffernan, K. S. (2017). Impact of Aging on Endurance and Neuromuscular Physical Performance: The Role of Vascular Senescence. *Sports Med*, *47*(4), 583-598. https://doi.org/10.1007/s40279-016-0596-8
125. Gluck, S., Guey, B., Gulen, M. F., Wolter, K., Kang, T. W., Schmacke, N. A., Bridgeman, A., Rehwinkel, J., Zender, L., & Ablasser, A. (2017). Innate immune sensing of cytosolic chromatin fragments through cGAS promotes senescence. *Nat Cell Biol*, *19*(9), 1061-1070. https://doi.org/10.1038/ncb3586
126. Gulen, M. F., Samson, N., Keller, A., Schwabenland, M., Liu, C., Gluck, S., Thacker, V. V., Favre, L., Mangeat, B., Kroese, L. J., Krimpenfort, P., Prinz, M., & Ablasser, A. (2023). cGAS-STING drives ageing-related inflammation and neurodegeneration. *Nature*, *620*(7973), 374-380. https://doi.org/10.1038/s41586-023-06373-1

127. Li, T., & Chen, Z. J. (2018). The cGAS-cGAMP-STING pathway connects DNA damage to inflammation, senescence, and cancer. *J Exp Med*, *215*(5), 1287-1299. https://doi.org/10.1084/jem.20180139
128. Lin, M. M., Liu, N., Qin, Z. H., & Wang, Y. (2022). Mitochondrial-derived damage-associated molecular patterns amplify neuroinflammation in neurodegenerative diseases. *Acta Pharmacol Sin*, *43*(10), 2439-2447. https://doi.org/10.1038/s41401-022-00879-6
129. Cao, W. (2024). In sickness and in health-Type I interferon and the brain. *Front Aging Neurosci*, *16*, 1403142. https://doi.org/10.3389/fnagi.2024.1403142
130. Filipi, M., & Jack, S. (2020). Interferons in the Treatment of Multiple Sclerosis: A Clinical Efficacy, Safety, and Tolerability Update. *Int J MS Care*, *22*(4), 165-172. https://doi.org/10.7224/1537-2073.2018-063
131. Ejlerskov, P., Hultberg, J. G., Wang, J., Carlsson, R., Ambjorn, M., Kuss, M., Liu, Y., Porcu, G., Kolkova, K., Friis Rundsten, C., Ruscher, K., Pakkenberg, B., Goldmann, T., Loreth, D., Prinz, M., Rubinsztein, D. C., & Issazadeh-Navikas, S. (2015). Lack of Neuronal IFN-beta-IFNAR Causes Lewy Body- and Parkinson's Disease-like Dementia. *Cell*, *163*(2), 324-339. https://doi.org/10.1016/j.cell.2015.08.069
132. Hosseini, S., Michaelsen-Preusse, K., Grigoryan, G., Chhatbar, C., Kalinke, U., & Korte, M. (2020). Type I Interferon Receptor Signaling in Astrocytes Regulates Hippocampal Synaptic Plasticity and Cognitive Function of the Healthy CNS. *Cell Rep*, *31*(7), 107666. https://doi.org/10.1016/j.celrep.2020.107666
133. Baruch, K., Deczkowska, A., David, E., Castellano, J. M., Miller, O., Kertser, A., Berkutzki, T., Barnett-Itzhaki, Z., Bezalel, D., Wyss-Coray, T., Amit, I., & Schwartz, M. (2014). Aging. Aging-induced type I interferon response at the choroid plexus negatively affects brain function. *Science*, *346*(6205), 89-93. https://doi.org/10.1126/science.1252945
134. Roy, E. R., Chiu, G., Li, S., Propson, N. E., Kanchi, R., Wang, B., Coarfa, C., Zheng, H., & Cao, W. (2022). Concerted type I interferon signaling in microglia and neural cells promotes memory impairment associated with amyloid beta plaques. *Immunity*, *55*(5), 879-894 e876. https://doi.org/10.1016/j.immuni.2022.03.018
135. Sanford, S. A. I., Miller, L. V. C., Vaysburd, M., Keeling, S., Tuck, B. J., Clark, J., Neumann, M., Syanda, V., James, L. C., & McEwan, W. A. (2024). The type-I interferon response potentiates seeded tau aggregation and exacerbates tau pathology. *Alzheimers Dement*, *20*(2), 1013-1025. https://doi.org/10.1002/alz.13493
136. Fabbri, E., Zoli, M., Gonzalez-Freire, M., Salive, M. E., Studenski, S. A., & Ferrucci, L. (2015). Aging and Multimorbidity: New Tasks, Priorities, and Frontiers for Integrated Gerontological and Clinical Research. *J Am Med Dir Assoc*, *16*(8), 640-647. https://doi.org/10.1016/j.jamda.2015.03.013
137. Schumacher, B., van der Pluijm, I., Moorhouse, M. J., Kosteas, T., Robinson, A. R., Suh, Y., Breit, T. M., van Steeg, H., Niedernhofer, L. J., van Ijcken, W., Bartke, A., Spindler, S. R., Hoeijmakers, J. H., van der Horst, G. T., & Garinis, G. A. (2008). Delayed and accelerated aging share common longevity assurance mechanisms. *PLoS Genet*, *4*(8), e1000161. https://doi.org/10.1371/journal.pgen.1000161
138. Sapieha, P., & Mallette, F. A. (2018). Cellular Senescence in Postmitotic Cells: Beyond Growth Arrest. *Trends Cell Biol*, *28*(8), 595-607. https://doi.org/10.1016/j.tcb.2018.03.003

139. Yu, Q., Katlinskaya, Y. V., Carbone, C. J., Zhao, B., Katlinski, K. V., Zheng, H., Guha, M., Li, N., Chen, Q., Yang, T., Lengner, C. J., Greenberg, R. A., Johnson, F. B., & Fuchs, S. Y. (2015). DNA-damage-induced type I interferon promotes senescence and inhibits stem cell function. *Cell Rep*, *11*(5), 785-797. https://doi.org/10.1016/j.celrep.2015.03.069
140. Eguchi, H., Fujiwara, N., Sakiyama, H., Yoshihara, D., & Suzuki, K. (2011). Hydrogen peroxide enhances LPS-induced nitric oxide production via the expression of interferon beta in BV-2 microglial cells. *Neurosci Lett*, *494*(1), 29-33. https://doi.org/10.1016/j.neulet.2011.02.047
141. Brouwers, F. P., Hillege, H. L., van Gilst, W. H., & van Veldhuisen, D. J. (2012). Comparing new onset heart failure with reduced ejection fraction and new onset heart failure with preserved ejection fraction: an epidemiologic perspective. *Curr Heart Fail Rep*, *9*(4), 363-368. https://doi.org/10.1007/s11897-012-0115-7
142. Lakatta, E. G. (2003). Arterial and cardiac aging: major shareholders in cardiovascular disease enterprises: Part III: cellular and molecular clues to heart and arterial aging. *Circulation*, *107*(3), 490-497. https://doi.org/10.1161/01.cir.0000048894.99865.02
143. Ma, Y., Mouton, A. J., & Lindsey, M. L. (2018). Cardiac macrophage biology in the steady-state heart, the aging heart, and following myocardial infarction. *Transl Res*, *191*, 15-28. https://doi.org/10.1016/j.trsl.2017.10.001
144. Sager, H. B., Hulsmans, M., Lavine, K. J., Moreira, M. B., Heidt, T., Courties, G., Sun, Y., Iwamoto, Y., Tricot, B., Khan, O. F., Dahlman, J. E., Borodovsky, A., Fitzgerald, K., Anderson, D. G., Weissleder, R., Libby, P., Swirski, F. K., & Nahrendorf, M. (2016). Proliferation and Recruitment Contribute to Myocardial Macrophage Expansion in Chronic Heart Failure. *Circ Res*, *119*(7), 853-864. https://doi.org/10.1161/CIRCRESAHA.116.309001
145. Smith, R. A., Hartley, R. C., Cocheme, H. M., & Murphy, M. P. (2012). Mitochondrial pharmacology. *Trends Pharmacol Sci*, *33*(6), 341-352. https://doi.org/10.1016/j.tips.2012.03.010
146. Wilkinson, J. E., Burmeister, L., Brooks, S. V., Chan, C. C., Friedline, S., Harrison, D. E., Hejtmancik, J. F., Nadon, N., Strong, R., Wood, L. K., Woodward, M. A., & Miller, R. A. (2012). Rapamycin slows aging in mice. *Aging Cell*, *11*(4), 675-682. https://doi.org/10.1111/j.1474-9726.2012.00832.x
147. Groban, L., Lindsey, S., Wang, H., Lin, M. S., Kassik, K. A., Machado, F. S., & Carter, C. S. (2012). Differential effects of late-life initiation of low-dose enalapril and losartan on diastolic function in senescent Fischer 344 x Brown Norway male rats. *Age (Dordr)*, *34*(4), 831-843. https://doi.org/10.1007/s11357-011-9283-8
148. Sanz, N., Diez-Fernandez, C., Alvarez, A. M., Fernandez-Simon, L., & Cascales, M. (1999). Age-related changes on parameters of experimentally-induced liver injury and regeneration. *Toxicol Appl Pharmacol*, *154*(1), 40-49. https://doi.org/10.1006/taap.1998.8541
149. Kim, I. H., Kisseleva, T., & Brenner, D. A. (2015). Aging and liver disease. *Curr Opin Gastroenterol*, *31*(3), 184-191. https://doi.org/10.1097/MOG.0000000000000176
150. Park, S. H., Jeon, W. K., Kim, S. H., Kim, H. J., Park, D. I., Cho, Y. K., Sung, I. K., Sohn, C. I., Keum, D. K., & Kim, B. I. (2006). Prevalence and risk factors of non-alcoholic fatty liver disease among Korean adults. *J Gastroenterol Hepatol*, *21*(1 Pt 1), 138-143. https://doi.org/10.1111/j.1440-1746.2005.04086.x
151. Verma, S., Tachtatzis, P., Penrhyn-Lowe, S., Scarpini, C., Jurk, D., Von Zglinicki, T., Coleman, N., & Alexander, G. J. (2012). Sustained telomere length in

hepatocytes and cholangiocytes with increasing age in normal liver. *Hepatology*, *56*(4), 1510-1520. https://doi.org/10.1002/hep.25787
152. Liu, P., Tang, Q., Chen, M., Chen, W., Lu, Y., Liu, Z., & He, Z. (2020). Hepatocellular Senescence: Immunosurveillance and Future Senescence-Induced Therapy in Hepatocellular Carcinoma. *Front Oncol*, *10*, 589908. https://doi.org/10.3389/fonc.2020.589908
153. Sanfeliu-Redondo, D., Gibert-Ramos, A., & Gracia-Sancho, J. (2024). Cell senescence in liver diseases: pathological mechanism and theranostic opportunity. *Nat Rev Gastroenterol Hepatol*, *21*(7), 477-492. https://doi.org/10.1038/s41575-024-00913-4
154. Kooman, J. P., Kotanko, P., Schols, A. M., Shiels, P. G., & Stenvinkel, P. (2014). Chronic kidney disease and premature ageing. *Nat Rev Nephrol*, *10*(12), 732-742. https://doi.org/10.1038/nrneph.2014.185
155. Hirst, J. A., Taal, M. W., Fraser, S. D., Mena, J. M. O., O'Callaghan, C. A., McManus, R. J., Taylor, C. J., Yang, Y., Ogburn, E., & Hobbs, F. R. (2022). Change in glomerular filtration rate over time in the Oxford Renal Cohort Study: observational study. *Br J Gen Pract*, *72*(717), e261-e268. https://doi.org/10.3399/BJGP.2021.0477
156. Shiels, P. G., McGuinness, D., Eriksson, M., Kooman, J. P., & Stenvinkel, P. (2017). The role of epigenetics in renal ageing. *Nat Rev Nephrol*, *13*(8), 471-482. https://doi.org/10.1038/nrneph.2017.78
157. Johmura, Y., Yamanaka, T., Omori, S., Wang, T. W., Sugiura, Y., Matsumoto, M., Suzuki, N., Kumamoto, S., Yamaguchi, K., Hatakeyama, S., Takami, T., Yamaguchi, R., Shimizu, E., Ikeda, K., Okahashi, N., Mikawa, R., Suematsu, M., Arita, M., Sugimoto, M.,…Nakanishi, M. (2021). Senolysis by glutaminolysis inhibition ameliorates various age-associated disorders. *Science*, *371*(6526), 265-270. https://doi.org/10.1126/science.abb5916
158. Yoshikawa, T., Oguchi, A., Toriu, N., Sato, Y., Kobayashi, T., Ogawa, O., Haga, H., Sakurai, S., Yamamoto, T., Murakawa, Y., & Yanagita, M. (2023). Tertiary Lymphoid Tissues Are Microenvironments with Intensive Interactions between Immune Cells and Proinflammatory Parenchymal Cells in Aged Kidneys. *J Am Soc Nephrol*, *34*(10), 1687-1708. https://doi.org/10.1681/ASN.0000000000000202
159. Tian, Y. E., Cropley, V., Maier, A. B., Lautenschlager, N. T., Breakspear, M., & Zalesky, A. (2023). Heterogeneous aging across multiple organ systems and prediction of chronic disease and mortality. *Nat Med*, *29*(5), 1221-1231. https://doi.org/10.1038/s41591-023-02296-6
160. Austad, S. N., & Fischer, K. E. (2016). Sex Differences in Lifespan. *Cell Metab*, *23*(6), 1022-1033. https://doi.org/10.1016/j.cmet.2016.05.019
161. Ullman-Cullere, M. H., & Foltz, C. J. (1999). Body condition scoring: a rapid and accurate method for assessing health status in mice. *Lab Anim Sci*, *49*(3), 319-323. https://www.ncbi.nlm.nih.gov/pubmed/10403450
162. Bankhead, P., Loughrey, M. B., Fernandez, J. A., Dombrowski, Y., McArt, D. G., Dunne, P. D., McQuaid, S., Gray, R. T., Murray, L. J., Coleman, H. G., James, J. A., Salto-Tellez, M., & Hamilton, P. W. (2017). QuPath: Open source software for digital pathology image analysis. *Sci Rep*, *7*(1), 16878. https://doi.org/10.1038/s41598-017-17204-5
163. Yang, L., Lin, W., Yan, X., & Zhang, Z. (2024). Comparative effects of lifelong moderate-intensity continuous training and high-intensity interval training on blood lipid levels and mental well-being in naturally ageing mice. *Exp Gerontol*, *194*, 112519. https://doi.org/10.1016/j.exger.2024.112519

164. Miedel, C. J., Patton, J. M., Miedel, A. N., Miedel, E. S., & Levenson, J. M. (2017). Assessment of Spontaneous Alternation, Novel Object Recognition and Limb Clasping in Transgenic Mouse Models of Amyloid-beta and Tau Neuropathology. *J Vis Exp*(123). https://doi.org/10.3791/55523
165. Baccin, C., Al-Sabah, J., Velten, L., Helbling, P. M., Grunschlager, F., Hernandez-Malmierca, P., Nombela-Arrieta, C., Steinmetz, L. M., Trumpp, A., & Haas, S. (2020). Combined single-cell and spatial transcriptomics reveal the molecular, cellular and spatial bone marrow niche organization. *Nat Cell Biol*, *22*(1), 38-48. https://doi.org/10.1038/s41556-019-0439-6
166. Deczkowska, A., Keren-Shaul, H., Weiner, A., Colonna, M., Schwartz, M., & Amit, I. (2018). Disease-Associated Microglia: A Universal Immune Sensor of Neurodegeneration. *Cell*, *173*(5), 1073-1081. https://doi.org/10.1016/j.cell.2018.05.003
167. Nazmi, A., Field, R. H., Griffin, E. W., Haugh, O., Hennessy, E., Cox, D., Reis, R., Tortorelli, L., Murray, C. L., Lopez-Rodriguez, A. B., Jin, L., Lavelle, E. C., Dunne, A., & Cunningham, C. (2019). Chronic neurodegeneration induces type I interferon synthesis via STING, shaping microglial phenotype and accelerating disease progression. In *Glia* (Vol. 67, pp. 1254-1276).
168. Mathur, V., Burai, R., Vest, R. T., Bonanno, L. N., Lehallier, B., Zardeneta, M. E., Mistry, K. N., Do, D., Marsh, S. E., Abud, E. M., Blurton-Jones, M., Li, L., Lashuel, H. A., & Wyss-Coray, T. (2017). Activation of the STING-Dependent Type I Interferon Response Reduces Microglial Reactivity and Neuroinflammation. *Neuron*, *96*(6), 1290-1302 e1296. https://doi.org/10.1016/j.neuron.2017.11.032
169. Lan, Y. Y., Heather, J. M., Eisenhaure, T., Garris, C. S., Lieb, D., Raychowdhury, R., & Hacohen, N. (2019). Extranuclear DNA accumulates in aged cells and contributes to senescence and inflammation. *Aging Cell*, *18*(2), e12901. https://doi.org/10.1111/acel.12901
170. Haag, S. M., Gulen, M. F., Reymond, L., Gibelin, A., Abrami, L., Decout, A., Heymann, M., van der Goot, F. G., Turcatti, G., Behrendt, R., & Ablasser, A. (2018). Targeting STING with covalent small-molecule inhibitors. *Nature*, *559*(7713), 269-273. https://doi.org/10.1038/s41586-018-0287-8
171. Xie, X., Ma, G., Li, X., Zhao, J., Zhao, Z., & Zeng, J. (2023). Activation of innate immune cGAS-STING pathway contributes to Alzheimer's pathogenesis in 5×FAD mice. In *Nature Aging 2023* (pp. 1-11): Nature Publishing Group.
172. Sladitschek-Martens, H. L., Guarnieri, A., Brumana, G., Zanconato, F., Battilana, G., Xiccato, R. L., Panciera, T., Forcato, M., Bicciato, S., Guzzardo, V., Fassan, M., Ulliana, L., Gandin, A., Tripodo, C., Foiani, M., Brusatin, G., Cordenonsi, M., & Piccolo, S. (2022). YAP/TAZ activity in stromal cells prevents ageing by controlling cGAS-STING. *Nature*, *607*(7920), 790-798. https://doi.org/10.1038/s41586-022-04924-6
173. Keren-Shaul, H., Spinrad, A., Weiner, A., Matcovitch-Natan, O., Dvir-Szternfeld, R., Ulland, T. K., David, E., Baruch, K., Lara-Astaiso, D., Toth, B., Itzkovitz, S., Colonna, M., Schwartz, M., & Amit, I. (2017). A Unique Microglia Type Associated with Restricting Development of Alzheimer's Disease. In *Cell* (Vol. 169, pp. 1276-1290.e1217): Elsevier.
174. Masuda, T., Sankowski, R., Staszewski, O., & Prinz, M. (2020). Microglia Heterogeneity in the Single-Cell Era. *Cell Rep*, *30*(5), 1271-1281. https://doi.org/10.1016/j.celrep.2020.01.010
175. Munro, D. A. D., Bestard-Cuche, N., McQuaid, C., Chagnot, A., Shabestari, S. K., Chadarevian, J. P., Maheshwari, U., Szymkowiak, S., Morris, K., Mohammad, M.,

Corsinotti, A., Bradford, B., Mabbott, N., Lennen, R. J., Jansen, M. A., Pridans, C., McColl, B. W., Keller, A., Blurton-Jones, M.,…Priller, J. (2024). Microglia protect against age-associated brain pathologies. *Neuron*. https://doi.org/10.1016/j.neuron.2024.05.018

176. Hahn, O., Foltz, A. G., Atkins, M., Kedir, B., Moran-Losada, P., Guldner, I. H., Munson, C., Kern, F., Palovics, R., Lu, N., Zhang, H., Kaur, A., Hull, J., Huguenard, J. R., Gronke, S., Lehallier, B., Partridge, L., Keller, A., & Wyss-Coray, T. (2023). Atlas of the aging mouse brain reveals white matter as vulnerable foci. *Cell*, *186*(19), 4117-4133 e4122. https://doi.org/10.1016/j.cell.2023.07.027
177. Merighi, A., Gionchiglia, N., Granato, A., & Lossi, L. (2021). The Phosphorylated Form of the Histone H2AX (gammaH2AX) in the Brain from Embryonic Life to Old Age. *Molecules*, *26*(23). https://doi.org/10.3390/molecules26237198
178. Taylor, E. N., Huang, N., Wisco, J., Wang, Y., Morgan, K. G., & Hamilton, J. A. (2020). The brains of aged mice are characterized by altered tissue diffusion properties and cerebral microbleeds. *J Transl Med*, *18*(1), 277. https://doi.org/10.1186/s12967-020-02441-6
179. Dileep, V., Boix, C. A., Mathys, H., Marco, A., Welch, G. M., Meharena, H. S., Loon, A., Jeloka, R., Peng, Z., Bennett, D. A., Kellis, M., & Tsai, L. H. (2023). Neuronal DNA double-strand breaks lead to genome structural variations and 3D genome disruption in neurodegeneration. *Cell*, *186*(20), 4404-4421 e4420. https://doi.org/10.1016/j.cell.2023.08.038
180. Gulen, M. F., Koch, U., Haag, S. M., Schuler, F., Apetoh, L., Villunger, A., Radtke, F., & Ablasser, A. (2017). Signalling strength determines proapoptotic functions of STING. *Nat Commun*, *8*(1), 427. https://doi.org/10.1038/s41467-017-00573-w
181. Moreno-Garcia, A., Kun, A., Calero, O., Medina, M., & Calero, M. (2018). An Overview of the Role of Lipofuscin in Age-Related Neurodegeneration. *Front Neurosci*, *12*, 464. https://doi.org/10.3389/fnins.2018.00464
182. Gray, D. A., & Woulfe, J. (2005). Lipofuscin and aging: a matter of toxic waste. *Sci Aging Knowledge Environ*, *2005*(5), re1. https://doi.org/10.1126/sageke.2005.5.re1
183. Campisi, M., Shin, Y., Osaki, T., Hajal, C., Chiono, V., & Kamm, R. D. (2018). 3D self-organized microvascular model of the human blood-brain barrier with endothelial cells, pericytes and astrocytes. *Biomaterials*, *180*, 117-129. https://doi.org/10.1016/j.biomaterials.2018.07.014
184. Saul, D., Kosinsky, R. L., Atkinson, E. J., Doolittle, M. L., Zhang, X., LeBrasseur, N. K., Pignolo, R. J., Robbins, P. D., Niedernhofer, L. J., Ikeno, Y., Jurk, D., Passos, J. F., Hickson, L. J., Xue, A., Monroe, D. G., Tchkonia, T., Kirkland, J. L., Farr, J. N., & Khosla, S. (2022). A new gene set identifies senescent cells and predicts senescence-associated pathways across tissues. *Nat Commun*, *13*(1), 4827. https://doi.org/10.1038/s41467-022-32552-1
185. Heng, T. S., Painter, M. W., & Immunological Genome Project, C. (2008). The Immunological Genome Project: networks of gene expression in immune cells. *Nat Immunol*, *9*(10), 1091-1094. https://doi.org/10.1038/ni1008-1091
186. Tay, T. L., Sagar, Dautzenberg, J., Grun, D., & Prinz, M. (2018). Unique microglia recovery population revealed by single-cell RNAseq following neurodegeneration. *Acta Neuropathol Commun*, *6*(1), 87. https://doi.org/10.1186/s40478-018-0584-3
187. Zhou, Y., Zhou, B., Pache, L., Chang, M., Khodabakhshi, A. H., Tanaseichuk, O., Benner, C., & Chanda, S. K. (2019). Metascape provides a biologist-oriented

resource for the analysis of systems-level datasets. *Nat Commun*, *10*(1), 1523. https://doi.org/10.1038/s41467-019-09234-6

188. Hammond, T. R., Dufort, C., Dissing-Olesen, L., Giera, S., Young, A., Wysoker, A., Walker, A. J., Gergits, F., Segel, M., Nemesh, J., Marsh, S. E., Saunders, A., Macosko, E., Ginhoux, F., Chen, J., Franklin, R. J. M., Piao, X., McCarroll, S. A., & Stevens, B. (2019). Single-Cell RNA Sequencing of Microglia throughout the Mouse Lifespan and in the Injured Brain Reveals Complex Cell-State Changes. *Immunity*, *50*(1), 253-271 e256. https://doi.org/10.1016/j.immuni.2018.11.004
189. Hammond, T. R., Dufort, C., Dissing-Olesen, L., Giera, S., Young, A., Wysoker, A., Walker, A. J., Gergits, F., Segel, M., Nemesh, J., Marsh, S. E., Saunders, A., Macosko, E., Ginhoux, F., Chen, J., Franklin, R. J. M., Piao, X., McCarroll, S. A., & Stevens, B. (2019). Single-Cell RNA Sequencing of Microglia throughout the Mouse Lifespan and in the Injured Brain Reveals Complex Cell-State Changes. In *Immunity* (Vol. 50, pp. 253-271.e256).
190. Fujioka, S., Niu, J., Schmidt, C., Sclabas, G. M., Peng, B., Uwagawa, T., Li, Z., Evans, D. B., Abbruzzese, J. L., & Chiao, P. J. (2004). NF-kappaB and AP-1 connection: mechanism of NF-kappaB-dependent regulation of AP-1 activity. *Mol Cell Biol*, *24*(17), 7806-7819. https://doi.org/10.1128/MCB.24.17.7806-7819.2004
191. Karakaslar, E. O., Katiyar, N., Hasham, M., Youn, A., Sharma, S., Chung, C. H., Marches, R., Korstanje, R., Banchereau, J., & Ucar, D. (2023). Transcriptional activation of Jun and Fos members of the AP-1 complex is a conserved signature of immune aging that contributes to inflammaging. *Aging Cell*, *22*(4), e13792. https://doi.org/10.1111/acel.13792
192. Wang, Y., Liu, L., Song, Y., Yu, X., & Deng, H. (2022). Unveiling E2F4, TEAD1 and AP-1 as regulatory transcription factors of the replicative senescence program by multi-omics analysis. *Protein Cell*, *13*(10), 742-759. https://doi.org/10.1007/s13238-021-00894-z
193. Wyss-Coray, T. (2016). Ageing, neurodegeneration and brain rejuvenation. *Nature*, *539*(7628), 180-186. https://doi.org/10.1038/nature20411
194. Allen, W. E., Blosser, T. R., Sullivan, Z. A., Dulac, C., & Zhuang, X. (2023). Molecular and spatial signatures of mouse brain aging at single-cell resolution. *Cell*, *186*(1), 194-208 e118. https://doi.org/10.1016/j.cell.2022.12.010
195. Castillo-Mariqueo, L., & Gimenez-Llort, L. (2022). Clasping, ledge-score coordination and early gait impairments as primary behavioural markers of functional impairment in Alzheimer's disease. *Behav Brain Res*, *435*, 114054. https://doi.org/10.1016/j.bbr.2022.114054
196. Suzuki, N., Oota-Ishigaki, A., Kaizuka, T., Itoh, M., Yamazaki, M., Natsume, R., Abe, M., Sakimura, K., Mishina, M., & Hayashi, T. (2024). Limb-Clasping Response in NMDA Receptor Palmitoylation-Deficient Mice. *Mol Neurobiol*. https://doi.org/10.1007/s12035-024-04166-9
197. Lalonde, R., & Strazielle, C. (2011). Brain regions and genes affecting limb-clasping responses. *Brain Res Rev*, *67*(1-2), 252-259. https://doi.org/10.1016/j.brainresrev.2011.02.005
198. Knox, E. G., Aburto, M. R., Clarke, G., Cryan, J. F., & O'Driscoll, C. M. (2022). The blood-brain barrier in aging and neurodegeneration. *Mol Psychiatry*, *27*(6), 2659-2673. https://doi.org/10.1038/s41380-022-01511-z
199. Salvador, E., Burek, M., Lohr, M., Nagai, M., Hagemann, C., & Forster, C. Y. (2021). Senescence and associated blood-brain barrier alterations in vitro. *Histochem Cell Biol*, *156*(3), 283-292. https://doi.org/10.1007/s00418-021-01992-z

200. Franke, M., Bieber, M., Stoll, G., & Schuhmann, M. K. (2021). Validity and Efficacy of Methods to Define Blood Brain Barrier Integrity in Experimental Ischemic Strokes: A Comparison of Albumin Western Blot, IgG Western Blot and Albumin Immunofluorescence. *Methods Protoc*, *4*(1). https://doi.org/10.3390/mps4010023
201. Wang, H. L., Zhang, C. L., Qiu, Y. M., Chen, A. Q., Li, Y. N., & Hu, B. (2021). Dysfunction of the Blood-brain Barrier in Cerebral Microbleeds: from Bedside to Bench. *Aging Dis*, *12*(8), 1898-1919. https://doi.org/10.14336/AD.2021.0514
202. Bedussi, B., van Lier, M. G., Bartstra, J. W., de Vos, J., Siebes, M., VanBavel, E., & Bakker, E. N. (2015). Clearance from the mouse brain by convection of interstitial fluid towards the ventricular system. *Fluids Barriers CNS*, *12*, 23. https://doi.org/10.1186/s12987-015-0019-5
203. Greiner, T., Manzhula, K., Baumann, L., Kaddatz, H., Runge, J., Keiler, J., Kipp, M., & Joost, S. (2022). Morphology of the murine choroid plexus: Attachment regions and spatial relation to the subarachnoid space. *Front Neuroanat*, *16*, 1046017. https://doi.org/10.3389/fnana.2022.1046017
204. Speir, M. L., Bhaduri, A., Markov, N. S., Moreno, P., Nowakowski, T. J., Papatheodorou, I., Pollen, A. A., Raney, B. J., Seninge, L., Kent, W. J., & Haeussler, M. (2021). UCSC Cell Browser: visualize your single-cell data. *Bioinformatics*, *37*(23), 4578-4580. https://doi.org/10.1093/bioinformatics/btab503
205. Haruwaka, K., Ikegami, A., Tachibana, Y., Ohno, N., Konishi, H., Hashimoto, A., Matsumoto, M., Kato, D., Ono, R., Kiyama, H., Moorhouse, A. J., Nabekura, J., & Wake, H. (2019). Dual microglia effects on blood brain barrier permeability induced by systemic inflammation. *Nat Commun*, *10*(1), 5816. https://doi.org/10.1038/s41467-019-13812-z
206. Lebrin, F., Goumans, M. J., Jonker, L., Carvalho, R. L., Valdimarsdottir, G., Thorikay, M., Mummery, C., Arthur, H. M., & ten Dijke, P. (2004). Endoglin promotes endothelial cell proliferation and TGF-beta/ALK1 signal transduction. *EMBO J*, *23*(20), 4018-4028. https://doi.org/10.1038/sj.emboj.7600386
207. Alvarez-Vergara, M. I., Rosales-Nieves, A. E., March-Diaz, R., Rodriguez-Perinan, G., Lara-Urena, N., Ortega-de San Luis, C., Sanchez-Garcia, M. A., Martin-Bornez, M., Gomez-Galvez, P., Vicente-Munuera, P., Fernandez-Gomez, B., Marchena, M. A., Bullones-Bolanos, A. S., Davila, J. C., Gonzalez-Martinez, R., Trillo-Contreras, J. L., Sanchez-Hidalgo, A. C., Del Toro, R., Scholl, F. G.,…Pascual, A. (2021). Non-productive angiogenesis disassembles Ass plaque-associated blood vessels. *Nat Commun*, *12*(1), 3098. https://doi.org/10.1038/s41467-021-23337-z
208. Xu, B., Wu, Y. Q., Huey, M., Arthur, H. M., Marchuk, D. A., Hashimoto, T., Young, W. L., & Yang, G. Y. (2004). Vascular endothelial growth factor induces abnormal microvasculature in the endoglin heterozygous mouse brain. *J Cereb Blood Flow Metab*, *24*(2), 237-244. https://doi.org/10.1097/01.WCB.0000107730.66603.51
209. Krasemann, S., Madore, C., Cialic, R., Baufeld, C., Calcagno, N., El Fatimy, R., Beckers, L., O'Loughlin, E., Xu, Y., Fanek, Z., Greco, D. J., Smith, S. T., Tweet, G., Humulock, Z., Zrzavy, T., Conde-Sanroman, P., Gacias, M., Weng, Z., Chen, H.,…Butovsky, O. (2017). The TREM2-APOE Pathway Drives the Transcriptional Phenotype of Dysfunctional Microglia in Neurodegenerative Diseases. *Immunity*, *47*(3), 566-581 e569. https://doi.org/10.1016/j.immuni.2017.08.008
210. Lund, H., Pieber, M., Parsa, R., Han, J., Grommisch, D., Ewing, E., Kular, L., Needhamsen, M., Espinosa, A., Nilsson, E., Overby, A. K., Butovsky, O., Jagodic, M., Zhang, X. M., & Harris, R. A. (2018). Competitive repopulation of an

empty microglial niche yields functionally distinct subsets of microglia-like cells. *Nat Commun*, *9*(1), 4845. https://doi.org/10.1038/s41467-018-07295-7
211. Getts, D. R., Terry, R. L., Getts, M. T., Muller, M., Rana, S., Shrestha, B., Radford, J., Van Rooijen, N., Campbell, I. L., & King, N. J. (2008). Ly6c+ "inflammatory monocytes" are microglial precursors recruited in a pathogenic manner in West Nile virus encephalitis. *J Exp Med*, *205*(10), 2319-2337. https://doi.org/10.1084/jem.20080421
212. Reinert, L. S., Lopusna, K., Winther, H., Sun, C., Thomsen, M. K., Nandakumar, R., Mogensen, T. H., Meyer, M., Vaegter, C., Nyengaard, J. R., Fitzgerald, K. A., & Paludan, S. R. (2016). Sensing of HSV-1 by the cGAS-STING pathway in microglia orchestrates antiviral defence in the CNS. *Nat Commun*, *7*, 13348. https://doi.org/10.1038/ncomms13348
213. Peng, Y., Zhuang, J., Ying, G., Zeng, H., Zhou, H., Cao, Y., Chen, H., Xu, C., Fu, X., Xu, H., Li, J., Cao, S., Chen, J., Gu, C., Yan, F., & Chen, G. (2020). Stimulator of IFN genes mediates neuroinflammatory injury by suppressing AMPK signal in experimental subarachnoid hemorrhage. *J Neuroinflammation*, *17*(1), 165. https://doi.org/10.1186/s12974-020-01830-4
214. MacLauchlan, S., Kushwaha, P., Tai, A., Chen, S., Manning, C., Swarnkar, G., Abu-Amer, Y., Fitzgerald, K. A., Sharma, S., & Gravallese, E. M. (2023). STING-dependent interferon signatures restrict osteoclast differentiation and bone loss in mice. *Proc Natl Acad Sci U S A*, *120*(15), e2210409120. https://doi.org/10.1073/pnas.2210409120
215. Larkin, B., Ilyukha, V., Sorokin, M., Buzdin, A., Vannier, E., & Poltorak, A. (2017). Cutting Edge: Activation of STING in T Cells Induces Type I IFN Responses and Cell Death. *J Immunol*, *199*(2), 397-402. https://doi.org/10.4049/jimmunol.1601999
216. Lang, F., & Cohen, P. (2001). Regulation and physiological roles of serum- and glucocorticoid-induced protein kinase isoforms. *Sci STKE*, *2001*(108), re17. https://doi.org/10.1126/stke.2001.108.re17
217. Kim, E. K., & Choi, E. J. (2010). Pathological roles of MAPK signaling pathways in human diseases. *Biochim Biophys Acta*, *1802*(4), 396-405. https://doi.org/10.1016/j.bbadis.2009.12.009
218. Krasemann, S., Madore, C., Cialic, R., Baufeld, C., Calcagno, N., El Fatimy, R., Beckers, L., O'Loughlin, E., Xu, Y., Fanek, Z., Greco, D. J., Smith, S. T., Tweet, G., Humulock, Z., Zrzavy, T., Conde-Sanroman, P., Gacias, M., Weng, Z., Chen, H.,…Correspondence, O. B. (2017). The TREM2-APOE Pathway Drives the Transcriptional Phenotype of Dysfunctional Microglia in Neurodegenerative Diseases. In *Immunity* (Vol. 47, pp. 566-581): Cell Press.
219. Microglia Heterogeneity in the Single-Cell Era, 30 Elsevier B.V. 1271-1281 (2020).
220. Kaya, T., Mattugini, N., Liu, L., Ji, H., Cantuti-Castelvetri, L., Wu, J., Schifferer, M., Groh, J., Martini, R., Besson-Girard, S., Kaji, S., Liesz, A., Gokce, O., & Simons, M. (2022). CD8(+) T cells induce interferon-responsive oligodendrocytes and microglia in white matter aging. *Nat Neurosci*, *25*(11), 1446-1457. https://doi.org/10.1038/s41593-022-01183-6
221. Ivashkiv, L. B., & Donlin, L. T. (2014). Regulation of type I interferon responses. In *Nature Reviews Immunology* (Vol. 14, pp. 36-49): Nature Publishing Group.
222. Deczkowska, A., Baruch, K., & Schwartz, M. (2016). Type I/II Interferon Balance in the Regulation of Brain Physiology and Pathology. *Trends Immunol*, *37*(3), 181-192. https://doi.org/10.1016/j.it.2016.01.006

223. Minter, M. R., Moore, Z., Zhang, M., Brody, K. M., Jones, N. C., Shultz, S. R., Taylor, J. M., & Crack, P. J. (2016). Deletion of the type-1 interferon receptor in APPSWE/PS1DeltaE9 mice preserves cognitive function and alters glial phenotype. *Acta Neuropathol Commun*, *4*(1), 72. https://doi.org/10.1186/s40478-016-0341-4
224. Taylor, J. M., Minter, M. R., Newman, A. G., Zhang, M., Adlard, P. A., & Crack, P. J. (2014). Type-1 interferon signaling mediates neuro-inflammatory events in models of Alzheimer's disease. *Neurobiol Aging*, *35*(5), 1012-1023. https://doi.org/10.1016/j.neurobiolaging.2013.10.089
225. Prinz, M., Schmidt, H., Mildner, A., Knobeloch, K. P., Hanisch, U. K., Raasch, J., Merkler, D., Detje, C., Gutcher, I., Mages, J., Lang, R., Martin, R., Gold, R., Becher, B., Brück, W., & Kalinke, U. (2008). Distinct and Nonredundant In Vivo Functions of IFNAR on Myeloid Cells Limit Autoimmunity in the Central Nervous System. In *Immunity* (Vol. 28, pp. 675-686).
226. Abdullah, A., Zhang, M., Frugier, T., Bedoui, S., Taylor, J. M., & Crack, P. J. (2018). STING-mediated type-I interferons contribute to the neuroinflammatory process and detrimental effects following traumatic brain injury. In *Journal of Neuroinflammation* (Vol. 15, pp. 323): BioMed Central.
227. Barrett, J. P., Knoblach, S. M., Bhattacharya, S., Gordish-Dressman, H., Stoica, B. A., & Loane, D. J. (2021). Traumatic Brain Injury Induces cGAS Activation and Type I Interferon Signaling in Aged Mice. In *Frontiers in Immunology* (Vol. 12, pp. 3396): Frontiers Media S.A.
228. Burnette, B. C., Liang, H., Lee, Y., Chlewicki, L., Khodarev, N. N., Weichselbaum, R. R., Fu, Y. X., & Auh, S. L. (2011). The efficacy of radiotherapy relies upon induction of type I interferon-dependent innate and adaptive immunity. In *Cancer Research* (Vol. 71, pp. 2488-2496).
229. Saravanan, S., Lewis, C. J., Dixit, B., O'Connor, M. S., Stolzing, A., & Boominathan, A. (2022). The Mitochondrial Genome in Aging and Disease and the Future of Mitochondrial Therapeutics. *Biomedicines*, *10*(2). https://doi.org/10.3390/biomedicines10020490
230. Yin, T., Yesiltepe, M., & D'Adamio, L. (2024). Functional BRI2-TREM2 interactions in microglia: implications for Alzheimer's and related dementias. *EMBO Rep*, *25*(3), 1326-1360. https://doi.org/10.1038/s44319-024-00077-x
231. Zhang, Z. H., & Song, G. L. (2021). Roles of Selenoproteins in Brain Function and the Potential Mechanism of Selenium in Alzheimer's Disease. *Front Neurosci*, *15*, 646518. https://doi.org/10.3389/fnins.2021.646518
232. Knox, K., Jeltema, D., Dobbs, N., Yang, K., Xing, C., Song, K., Tang, Z., Torres-Ramirez, G., Wang, J., Gao, S., Wu, T., Yao, C., Wang, J., & Yan, N. (2025). Dynamic STING repression orchestrates immune cell development and function. *Sci Immunol*, *10*(105), eado9933. https://doi.org/10.1126/sciimmunol.ado9933
233. Morita, M., Stamp, G., Robins, P., Dulic, A., Rosewell, I., Hrivnak, G., Daly, G., Lindahl, T., & Barnes, D. E. (2004). Gene-targeted mice lacking the Trex1 (DNase III) 3'-->5' DNA exonuclease develop inflammatory myocarditis. *Mol Cell Biol*, *24*(15), 6719-6727. https://doi.org/10.1128/MCB.24.15.6719-6727.2004
234. Bennion, B. G., Croft, C. A., Ai, T. L., Qian, W., Menos, A. M., Miner, C. A., Fremond, M. L., Doisne, J. M., Andhey, P. S., Platt, D. J., Bando, J. K., Wang, E. R., Luksch, H., Molina, T. J., Roberson, E. D. O., Artyomov, M. N., Rosen-Wolff, A., Colonna, M., Rieux-Laucat, F.,…Miner, J. J. (2020). STING Gain-of-Function Disrupts Lymph Node Organogenesis and Innate Lymphoid Cell Development in Mice. *Cell Rep*, *31*(11), 107771. https://doi.org/10.1016/j.celrep.2020.107771

235. Motwani, M., Pawaria, S., Bernier, J., Moses, S., Henry, K., Fang, T., Burkly, L., Marshak-Rothstein, A., & Fitzgerald, K. A. (2019). Hierarchy of clinical manifestations in SAVI N153S and V154M mouse models. *Proc Natl Acad Sci U S A*, *116*(16), 7941-7950. https://doi.org/10.1073/pnas.1818281116
236. Sharma, S., Campbell, A. M., Chan, J., Schattgen, S. A., Orlowski, G. M., Nayar, R., Huyler, A. H., Nundel, K., Mohan, C., Berg, L. J., Shlomchik, M. J., Marshak-Rothstein, A., & Fitzgerald, K. A. (2015). Suppression of systemic autoimmunity by the innate immune adaptor STING. *Proc Natl Acad Sci U S A*, *112*(7), E710-717. https://doi.org/10.1073/pnas.1420217112
237. Sharma, S., Campbell, A. M., Chan, J., Schattgen, S. A., Orlowski, G. M., Nayar, R., Huyler, A. H., Nündel, K., Mohan, C., Berg, L. J., Shlomchik, M. J., Marshak-Rothstein, A., & Fitzgerald, K. A. (2015). Suppression of systemic autoimmunity by the innate immune adaptor STING. In *Proceedings of the National Academy of Sciences of the United States of America* (Vol. 112, pp. E710-E717).
238. Narayanan, K., Reinier, K., Teodorescu, C., Uy-Evanado, A., Aleong, R., Chugh, H., Nichols, G. A., Gunson, K., London, B., Jui, J., & Chugh, S. S. (2014). Left ventricular diameter and risk stratification for sudden cardiac death. *J Am Heart Assoc*, *3*(5), e001193. https://doi.org/10.1161/JAHA.114.001193
239. Hunt, N. J., Kang, S. W. S., Lockwood, G. P., Le Couteur, D. G., & Cogger, V. C. (2019). Hallmarks of Aging in the Liver. *Comput Struct Biotechnol J*, *17*, 1151-1161. https://doi.org/10.1016/j.csbj.2019.07.021
240. Wilkinson, M. J., Selman, C., McLaughlin, L., Horan, L., Hamilton, L., Gilbert, C., Chadwick, C., & Flynn, J. N. (2020). Progressing the care, husbandry and management of ageing mice used in scientific studies. *Lab Anim*, *54*(3), 225-238. https://doi.org/10.1177/0023677219865291
241. Lessard-Beaudoin, M., Laroche, M., Demers, M. J., Grenier, G., & Graham, R. K. (2015). Characterization of age-associated changes in peripheral organ and brain region weights in C57BL/6 mice. *Exp Gerontol*, *63*, 27-34. https://doi.org/10.1016/j.exger.2015.01.003
242. Froechlich, G., Finizio, A., Napolano, A., Amiranda, S., De Chiara, A., Pagano, P., Mallardo, M., Leoni, G., Zambrano, N., & Sasso, E. (2023). The common H232 STING allele shows impaired activities in DNA sensing, susceptibility to viral infection, and in monocyte cell function, while the HAQ variant possesses wild-type properties. *Sci Rep*, *13*(1), 19541. https://doi.org/10.1038/s41598-023-46830-5
243. Hinkle, J. T., Patel, J., Panicker, N., Karuppagounder, S. S., Biswas, D., Belingon, B., Chen, R., Brahmachari, S., Pletnikova, O., Troncoso, J. C., Dawson, V. L., & Dawson, T. M. (2022). STING mediates neurodegeneration and neuroinflammation in nigrostriatal alpha-synucleinopathy. *Proc Natl Acad Sci U S A*, *119*(15), e2118819119. https://doi.org/10.1073/pnas.2118819119
244. Gui, X., Yang, H., Li, T., Tan, X., Shi, P., Li, M., Du, F., & Chen, Z. J. (2019). Autophagy induction via STING trafficking is a primordial function of the cGAS pathway. In *Nature* (Vol. 567, pp. 262-266): Nature Publishing Group.
245. Lv, B., Dion, W. A., Yang, H., Xun, J., Kim, D. K., Zhu, B., & Tan, J. X. (2024). A TBK1-independent primordial function of STING in lysosomal biogenesis. *Molecular Cell*, *84*. https://doi.org/10.1016/j.molcel.2024.08.026
246. Abdullah, A., Zhang, M., Frugier, T., Bedoui, S., Taylor, J. M., & Crack, P. J. (2018). STING-mediated type-I interferons contribute to the neuroinflammatory process and detrimental effects following traumatic brain injury. *J Neuroinflammation*, *15*(1), 323. https://doi.org/10.1186/s12974-018-1354-7

247. Li, Q., Wu, P., Du, Q., Hanif, U., Hu, H., & Li, K. (2024). cGAS-STING, an important signaling pathway in diseases and their therapy. *MedComm (2020)*, *5*(4), e511. https://doi.org/10.1002/mco2.511
248. Schoggins, J. W., MacDuff, D. A., Imanaka, N., Gainey, M. D., Shrestha, B., Eitson, J. L., Mar, K. B., Richardson, R. B., Ratushny, A. V., Litvak, V., Dabelic, R., Manicassamy, B., Aitchison, J. D., Aderem, A., Elliott, R. M., Garcia-Sastre, A., Racaniello, V., Snijder, E. J., Yokoyama, W. M.,…Rice, C. M. (2014). Pan-viral specificity of IFN-induced genes reveals new roles for cGAS in innate immunity. *Nature*, *505*(7485), 691-695. https://doi.org/10.1038/nature12862
249. Yum, S., Li, M., Fang, Y., & Chen, Z. J. (2021). TBK1 recruitment to STING activates both IRF3 and NF-kappaB that mediate immune defense against tumors and viral infections. *Proc Natl Acad Sci U S A*, *118*(14). https://doi.org/10.1073/pnas.2100225118
250. West, A. P., Khoury-Hanold, W., Staron, M., Tal, M. C., Pineda, C. M., Lang, S. M., Bestwick, M., Duguay, B. A., Raimundo, N., MacDuff, D. A., Kaech, S. M., Smiley, J. R., Means, R. E., Iwasaki, A., & Shadel, G. S. (2015). Mitochondrial DNA stress primes the antiviral innate immune response. In *Nature* (Vol. 520, pp. 553-557): Nature Publishing Group.
251. Payne, B. A., & Chinnery, P. F. (2015). Mitochondrial dysfunction in aging: Much progress but many unresolved questions. *Biochim Biophys Acta*, *1847*(11), 1347-1353. https://doi.org/10.1016/j.bbabio.2015.05.022
252. Shao, X., Shou, Q., Felix, K., Ojogho, B., Jiang, X., Gold, B. T., Herting, M. M., Goldwaser, E. L., Kochunov, P., Hong, L. E., Pappas, I., Braskie, M., Kim, H., Cen, S., Jann, K., & Wang, D. J. (2024). Age-Related Decline in Blood-Brain Barrier Function is More Pronounced in Males than Females in Parietal and Temporal Regions. *bioRxiv*. https://doi.org/10.1101/2024.01.12.575463
253. Ferecsko, A. S., Smallwood, M. J., Moore, A., Liddle, C., Newcombe, J., Holley, J., Whatmore, J., Gutowski, N. J., & Eggleton, P. (2023). STING-Triggered CNS Inflammation in Human Neurodegenerative Diseases. *Biomedicines*, *11*(5). https://doi.org/10.3390/biomedicines11051375
254. Byrns, C. N., Saikumar, J., & Bonini, N. M. (2021). Glial AP1 is activated with aging and accelerated by traumatic brain injury. *Nat Aging*, *1*(7), 585-597. https://doi.org/10.1038/s43587-021-00072-0
255. Liu, Y., Xu, P., Rivara, S., Liu, C., Ricci, J., Ren, X., Hurley, J. H., & Ablasser, A. (2022). Clathrin-associated AP-1 controls termination of STING signalling. *Nature*, *610*(7933), 761-767. https://doi.org/10.1038/s41586-022-05354-0
256. Robinson, M. S. (2004). Adaptable adaptors for coated vesicles. *Trends Cell Biol*, *14*(4), 167-174. https://doi.org/10.1016/j.tcb.2004.02.002
257. Jeyapalan, J. C., & Sedivy, J. M. (2008). Cellular senescence and organismal aging. *Mech Ageing Dev*, *129*(7-8), 467-474. https://doi.org/10.1016/j.mad.2008.04.001
258. Born, E., Lipskaia, L., Breau, M., Houssaini, A., Beaulieu, D., Marcos, E., Pierre, R., Do Cruzeiro, M., Lefevre, M., Derumeaux, G., Bulavin, D. V., Delcroix, M., Quarck, R., Reen, V., Gil, J., Bernard, D., Flaman, J. M., Adnot, S., & Abid, S. (2023). Eliminating Senescent Cells Can Promote Pulmonary Hypertension Development and Progression. *Circulation*, *147*(8), 650-666. https://doi.org/10.1161/CIRCULATIONAHA.122.058794
259. Barclay, K. M., Abduljawad, N., Cheng, Z., Kim, M. W., Zhou, L., Yang, J., Rustenhoven, J., Mazzitelli, J. A., Smyth, L. C. D., Kapadia, D., Brioschi, S., Beatty, W., Hou, J., Saligrama, N., Colonna, M., Yu, G., Kipnis, J., & Li, Q. (2024). An inducible genetic tool to track and manipulate specific microglial

states reveals their plasticity and roles in remyelination. *Immunity*, *57*(6), 1394-1412 e1398. https://doi.org/10.1016/j.immuni.2024.05.005
260. Chow, H. M., & Herrup, K. (2015). Genomic integrity and the ageing brain. *Nat Rev Neurosci*, *16*(11), 672-684. https://doi.org/10.1038/nrn4020
261. Welch, G., & Tsai, L. H. (2022). Mechanisms of DNA damage-mediated neurotoxicity in neurodegenerative disease. *EMBO Rep*, *23*(6), e54217. https://doi.org/10.15252/embr.202154217
262. Lan, Y. Y., Heather, J. M., Eisenhaure, T., Garris, C. S., Lieb, D., Raychowdhury, R., & Hacohen, N. (2019). Extranuclear DNA accumulates in aged cells and contributes to senescence and inflammation. In *Aging Cell* (Vol. 18, pp. e12901): John Wiley & Sons, Ltd (10.1111).
263. Ogrodnik, M., Evans, S. A., Fielder, E., Victorelli, S., Kruger, P., Salmonowicz, H., Weigand, B. M., Patel, A. D., Pirtskhalava, T., Inman, C. L., Johnson, K. O., Dickinson, S. L., Rocha, A., Schafer, M. J., Zhu, Y., Allison, D. B., von Zglinicki, T., LeBrasseur, N. K., Tchkonia, T.,…Jurk, D. (2021). Whole-body senescent cell clearance alleviates age-related brain inflammation and cognitive impairment in mice. *Aging Cell*, *20*(2), e13296. https://doi.org/10.1111/acel.13296
264. Bussian, T. J., Aziz, A., Meyer, C. F., Swenson, B. L., van Deursen, J. M., & Baker, D. J. (2018). Clearance of senescent glial cells prevents tau-dependent pathology and cognitive decline. *Nature*, *562*(7728), 578-582. https://doi.org/10.1038/s41586-018-0543-y
265. Chinta, S. J., Woods, G., Demaria, M., Rane, A., Zou, Y., McQuade, A., Rajagopalan, S., Limbad, C., Madden, D. T., Campisi, J., & Andersen, J. K. (2018). Cellular Senescence Is Induced by the Environmental Neurotoxin Paraquat and Contributes to Neuropathology Linked to Parkinson's Disease. *Cell Rep*, *22*(4), 930-940. https://doi.org/10.1016/j.celrep.2017.12.092
266. Crow, Y. J., & Stetson, D. B. (2022). The type I interferonopathies: 10 years on. *Nat Rev Immunol*, *22*(8), 471-483. https://doi.org/10.1038/s41577-021-00633-9
267. Riese, R. J., Mitchell, R. N., Villadangos, J. A., Shi, G. P., Palmer, J. T., Karp, E. R., De Sanctis, G. T., Ploegh, H. L., & Chapman, H. A. (1998). Cathepsin S activity regulates antigen presentation and immunity. *J Clin Invest*, *101*(11), 2351-2363. https://doi.org/10.1172/JCI1158
268. Lemere, C. A., Munger, J. S., Shi, G. P., Natkin, L., Haass, C., Chapman, H. A., & Selkoe, D. J. (1995). The lysosomal cysteine protease, cathepsin S, is increased in Alzheimer's disease and Down syndrome brain. An immunocytochemical study. *Am J Pathol*, *146*(4), 848-860. https://www.ncbi.nlm.nih.gov/pubmed/7717452
269. Wendt, W., Lubbert, H., & Stichel, C. C. (2008). Upregulation of cathepsin S in the aging and pathological nervous system of mice. *Brain Res*, *1232*, 7-20. https://doi.org/10.1016/j.brainres.2008.07.067
270. Chen, Y., Zhou, Y., Bai, Y., Jia, K., Zhang, H., Chen, Q., Song, M., Dai, Y., Shi, J., Chen, Z., Yan, X., & Shen, Y. (2025). Macrophage-derived CTSS drives the age-dependent disruption of the blood-CSF barrier. *Neuron*. https://doi.org/10.1016/j.neuron.2025.01.023
271. Wu, J., Wu, Z., He, A., Zhang, T., Zhang, P., Jin, J., Li, S., Li, G., Li, X., Liang, S., Pei, L., Liu, R., Tian, Q., He, X., Lu, Y., Tang, Z., & Li, H. (2021). Genome-Wide Screen and Validation of Microglia Pro-Inflammatory Mediators in Stroke. *Aging Dis*, *12*(3), 786-800. https://doi.org/10.14336/AD.2020.0926
272. Vig, M., & Kinet, J. P. (2009). Calcium signaling in immune cells. *Nat Immunol*, *10*(1), 21-27. https://doi.org/10.1038/ni.f.220

273. Staun-Ram, E., & Miller, A. (2011). Cathepsins (S and B) and their inhibitor Cystatin C in immune cells: modulation by interferon-beta and role played in cell migration. *J Neuroimmunol*, *232*(1-2), 200-206. https://doi.org/10.1016/j.jneuroim.2010.10.015
274. Nazmi, A., Field, R. H., Griffin, E. W., Haugh, O., Hennessy, E., Cox, D., Reis, R., Tortorelli, L., Murray, C. L., Lopez-Rodriguez, A. B., Jin, L., Lavelle, E. C., Dunne, A., & Cunningham, C. (2019). Chronic neurodegeneration induces type I interferon synthesis via STING, shaping microglial phenotype and accelerating disease progression. *Glia*, *67*(7), 1254-1276. https://doi.org/10.1002/glia.23592
275. Boda, A. R., Liu, A. J., Castro-Pando, S., Whitfield, B. T., Molldrem, J. J., Al-Atrash, G., Di Francesco, M. E., Jones, P., Ager, C. R., & Curran, M. A. (2024). Identification of Nonfunctional Alternatively Spliced Isoforms of STING in Human Acute Myeloid Leukemia. *Cancer Res Commun*, *4*(3), 911-918. https://doi.org/10.1158/2767-9764.CRC-24-0095
276. Balka, K. R., Venkatraman, R., Saunders, T. L., Shoppee, A., Pang, E. S., Magill, Z., Homman-Ludiye, J., Huang, C., Lane, R. M., York, H. M., Tan, P., Schittenhelm, R. B., Arumugam, S., Kile, B. T., O'Keeffe, M., & De Nardo, D. (2023). Termination of STING responses is mediated via ESCRT-dependent degradation. *EMBO J*, *42*(12), e112712. https://doi.org/10.15252/embj.2022112712
277. Khedr, S., Dissanayake, L. V., Alsheikh, A. J., Zietara, A., Spires, D. R., Kerketta, R., Mathison, A. J., Urrutia, R., Palygin, O., & Staruschenko, A. (2024). Role of cGAS/STING pathway in aging and sexual dimorphism in diabetic kidney disease. *JCI Insight*, *10*(1). https://doi.org/10.1172/jci.insight.174126